Viscoelastic Flows of PTT Fluid

Sibley, David

Award date:
2010

Awarding institution:
University of Bath

Viscoelastic Flows of PTT Fluids

submitted by

David N. Sibley

for the degree of Doctor of Philosophy

of the

University of Bath

Department of Mathematical Sciences

March 2010

Acknowledgements

During the writing of my PhD thesis, I realised there are a large number of people who are important to me. Firstly, I wish to thank my parents and grandparents for their love and support, and to apologise that I haven't pursued research in a subject involving more pictures - flicking through nearly 200 pages of this can't be all that fun!

I'm reminded of the first teachers who inspired my love of Mathematics - I would like to thank Mr Edwards and Mr MacLennan from Ysgol Pen-y-Bryn for the memories of learning about all things from adding fractions (and the desire to be the first to finish the exercises!) to having the first concept of air resistance and friction. The excitement and satisfaction of having a definite answer - and the resulting red tick - has stayed with me until this day.

I would also like to thank the many great teachers at Eirias High School who taught me in my secondary school and sixth form years. In particular my A-level teachers Mrs Bailey, Mr Parry and Mr Gerrard (who deserves special mention for giving up his lunch times to help me practice STEP papers), who encouraged and developed my ability and enjoyment of Maths. I'd also like to thank Mrs Dutton for her help applying to universities, and Dr Williams, Ms Taylor and Mr Robson for their Chemistry and Physics teaching - much of which is the extent to which I understand the science behind the models in this thesis!

My years of study would have been nowhere near as fun without the support of my friends. Tim for the intellectual arguments in coffee shops and pubs (more intellectual in the pubs!), Nick and Aidan for being great housemates, and Tristan, Sean, Maddy, Caro, Mark, Bjorn and all my other friends from Bath and back in Colwyn Bay.

In the Maths department I'd like to thank all the people who've put up with me in their office, Melina, Zhivko, Laura, Richard, Lisema, Clare, Simon, Steve and Robert, my internal examiner Ilia, Alastair for his role as the head of Postgraduate studies, and Carole, Eric, Mark and all the members of the support staff. I would also like to thank Prof. Stephen Wilson for acting as my external examiner.

Finally, and most importantly, I would like to recognise the wonderful work and time afforded to me by my supervisor, Dr Jonathan Evans. His enthusiasm for all I have done, giving me the opportunity to do this PhD and for all his encouragement to attend conferences and workshops have been crucial and allowed me to thoroughly enjoy my time in Bath. Thank you.

Summary

We consider the planar flow of Phan-Thien-Tanner (PTT) fluids in geometries where a singular stress is encountered. The main problem considered is flow around a sharp corner, with also preliminary results for sink flow in a wedge. Two distinct cases arise for the corner geometry, where the corner angle is denoted by π/α. For $1/2 \leq \alpha < 1$ we have a re-entrant corner, whilst for $1 < \alpha < \infty$ a so called salient corner occurs. These two regimes have markedly different flow behaviour. The model is considered in the absence of a solvent viscosity and the flow situation assumes complete flow around the corner with the absence of a lip vortex.

For the re-entrant corner problem a class of self-similar solutions has been identified with stress singularities of $O(r^{-2(1-\alpha)})$ and stream function behaviour $O(r^{(1+\alpha)\alpha})$ (r being the radial distance from the corner). These behaviours arise in a core flow region away from the walls and are shown to be solutions of the incompressible Euler equations. This region is reconciled with boundary layers at the upstream and downstream walls using the method of matched asymptotic expansions. The analysis benefits from the representation of the stress in both Cartesian and natural stress formulations, and is performed when the Weissenberg number (the dimensionless relaxation time) and the PTT model parameter κ (a dimensionless mobility factor) are both $O(1)$. The analysis is then extended for the various limits of these two parameters.

For the salient corner case the mathematically simpler Newtonian balance for the flow and stress fields are shown to dominate away from the walls. This gives a stream function behaviour of $O(r^{1+\lambda_0})$ and stress behaviour $O(r^{\lambda_0-1})$, where λ_0 is the Newtonian problem eigenvalue. This behaviour is again reconciled with boundary layers at the walls which recover viscometric behaviour.

Contents

List of Figures

List of Tables

Chapter 1

Introduction

This thesis is a study of viscoelastic flows of Phan-Thien-Tanner (PTT) fluids in specific geometries. To begin, this chapter introduces the field of viscoelasticity, including the motivation behind the governing equations of selected models and culminating in a description of the PTT model of interest in section 1.2. Following this, an overview of some industrial applications is given in 1.3, with an outline of the following chapters of the thesis and a review of the relevant literature in 1.4 upon which the main analysis of chapters 3–6 is based.

1.1 Introduction

Continuum mechanics is often split into the fields of solid mechanics and fluid mechanics, however many materials are not simply classified into one of these two groups. Rheology is the science of deformation and flow, and instead suggests that everything flows - provided the time-scale of the observation is long enough. The physical properties are now determined by the ratio of the experimental time-scale T and the time-scale of the material concerned τ. For example, consider granite at standard temperature and pressure. When the ratio τ/T is large granite behaves as a solid, but over geological time scales when the ratio τ/T is negligibly small, then granite may be seen to deform as a viscous fluid, [KSI78]. Typical fluid time-scales τ vary from 10^{-13}s for water, milliseconds for engine oil, minutes for polymer solutions, to hours for soft solids and melts (see [PT02] for example)[1].

Newtonian fluid mechanics is primarily an investigation of the interplay of inertial and viscous forces, and surface tension where applicable. As eluded to, many common or industrial fluids display more unusual behaviour due to their complex microstructure,

[1]Introductory information is primarily based on the excellent textbooks by Renardy [Ren00b], Phan-Thien [PT02], and Tanner [Tan00], all of which may be approached for further information.

from suspensions (e.g. bread dough or concrete), foams, granular media (such as sand or coal) to polymeric fluids like oils, molten plastics, paint, blood or egg white.

The models investigated in this thesis are primarily applied to flows of polymeric fluids, with their behaviour distinguished from Newtonian fluids due to the presence of long chain molecules. These molecules affect the flow behaviour by the way in which they align to the motion of the fluid, are then stretched out by the drag forces, and consequently want to retract back to their unstressed configuration in an elastic behaviour. The study of such fluids falls in the field of Viscoelasticity, termed due to the viscous and elastic behaviours displayed.

This thesis will concentrate on one of the many mathematical models used to describe viscoelastic fluids, the linear affine Phan-Thien-Tanner model without solvent viscosity (subsequently just Phan-Thien-Tanner, or PTT model unless specified), and will analyse the fluid flow behaviour in corner geometries primarily using matched asymptotic methods.

1.1.1 Balance Laws

All fluid motion is governed by the balance laws of conservation of mass, as well as linear and angular momentum. This is supplemented by a balance of energy if thermal effects are considered, although this is not investigated here. Another simplification made is that only incompressible fluids will be studied, a valid decision given that the fluids of interest are predominantly liquid at the temperatures they usually exist, and thus their compressibility is negligible.

For incompressible fluids the conservation of mass is simply

$$\nabla.\mathbf{v} = 0, \tag{1.1}$$

where $\mathbf{v}$ is the velocity of the fluid, and the balance of linear momentum gives

$$\rho\left(\frac{\partial \mathbf{v}}{\partial t} + (\mathbf{v}.\nabla)\mathbf{v}\right) = -\nabla p + \nabla.\mathbf{T}, \tag{1.2}$$

where ρ is the density, $\mathbf{T}$ is the extra stress tensor, and p is the pressure. The left hand side of this equation represents inertia, which will either be shown or assumed to be negligible in most of the flows we consider later. $\mathbf{T}$ represents the stress the fluid develops in response to the deformation, with the total stress tensor given by

$$\sigma = -p\mathbf{I} + \mathbf{T}, \qquad \sigma = \sigma^T, \tag{1.3}$$

where the conservation of angular momentum imposes that σ is a symmetric CT2

tensor as given above.

The derivation of these equations is given (for example) in chapter 6 of [Ach90]. The conservation equations above are not sufficient to determine all of the unknowns of the flow, so constitutive relations are introduced which relate the motion to the extra-stress tensor $\mathbf{T}$.

1.1.2 Constitutive relations

Newtonian Fluids

Firstly, it is useful to consider Newtonian fluids as this case occurs widely and has been studied in great detail. For a Newtonian viscous fluid, we have the constitutive relation

$$\mathbf{T} = 2\eta\mathbf{D}, \tag{1.4}$$

where η is the constant viscosity, and $\mathbf{D}$ is the rate of deformation tensor

$$\mathbf{D} = \frac{1}{2}\left(\nabla\mathbf{v} + (\nabla\mathbf{v})^T\right), \qquad \mathbf{v} = \begin{pmatrix} u(x,y) \\ v(x,y) \end{pmatrix}, \qquad \nabla\mathbf{v} = \begin{pmatrix} \frac{\partial u}{\partial x} & \frac{\partial u}{\partial y} \\ \frac{\partial v}{\partial x} & \frac{\partial v}{\partial y} \end{pmatrix}. \tag{1.5}$$

As an example the velocity $\mathbf{v}$ and the velocity gradient $\nabla\mathbf{v}$ have been represented in two-dimensional Cartesian components, with the velocity components $u(x,y)$ and $v(x,y)$ along the x and y axis respectively.

A viscous fluid is one in which the fluid resists forces exerted upon it through internal friction. Most fluids which have small molecules such as gases and water obey this model, however, as mentioned there are a number of fluids which exhibit other more complex behaviour. This thesis considers fluids which exhibit memory qualities, termed viscoelastic fluids, which can behave like elastic materials when deformed.

Viscoelastic Fluids

In viscoelastic fluids, the stresses depend not only on the current motion of the fluid (as in the Newtonian case), but also on the history of the motion. Although many methods of model derivation exist, the simplest as an introduction is to model the flows with mechanical analogues. Viscoelasticity can be considered as fluids consisting of both viscous elements and elastic elements. We can represent this as a combination of springs (for the elastic elements) and dashpots (for the viscous elements), see figure 1-1.

Maxwell's one-dimensional linear model is obtained with elements comprised of a spring and dashpot in series, as in (A) of figure 1-1. The spring, with spring constant

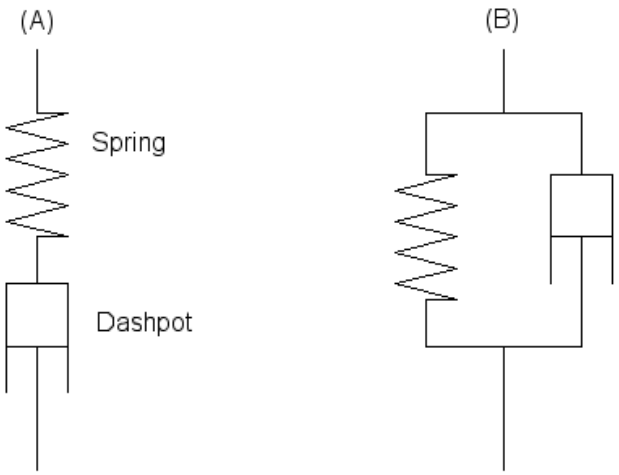

Figure 1-1: The spring and dashpot elements which together in various combinations model viscoelasticity. Two possible fluid elements are shown with (A) having the spring and dashpot elements arranged in series to create a Maxwell element, and (B) with the elements in parallel to give a Kelvin-Voigt element.

k, satisfies Hooke's law

$$\sigma_e = k\gamma_e, \tag{1.6}$$

where σ_e is the elastic stress and γ_e is the elastic strain. The dashpot then, as an ideal viscous element with viscosity η, extends at a rate proportional to the applied force, giving

$$\sigma_v = \eta\dot{\gamma}_v. \tag{1.7}$$

Since the spring and dashpot are connected in series, the total strain is the sum of the individual strains, hence

$$\gamma = \gamma_e + \gamma_v. \tag{1.8}$$

Differentiating with respect to time, substituting in equations (1.6) and (1.7), and noting that the stresses will be equal since the elements are connected in series (setting $\sigma = \sigma_e = \sigma_v$), we obtain

$$\sigma + \lambda\dot{\sigma} = \eta\dot{\gamma}. \tag{1.9}$$

with $\lambda = \frac{\eta}{k}$ being a relaxation time, which is roughly speaking a measure of the time for which the fluid remembers the flow history, see section 2.2 of [Ren00b]. Other combinations of springs and dashpots can also be considered, in particular, arranging one dashpot and one spring in parallel gives the Kelvin-Voigt model, the element shown

in (B) of figure 1-1. This is derived using similar arguments to the linear Maxwell model, but here, since the elements are connected in parallel we have that the total stress is the sum of the individual stresses, $\sigma = \sigma_e + \sigma_v$, and that the strains are all equal, $\gamma = \gamma_e = \gamma_v$. The model is then

$$\sigma = k\gamma + \eta\dot{\gamma}. \tag{1.10}$$

Neither of these models are yet in the tensor form of the governing equations (1.1)-(1.3). We consider the linear Maxwell model of (1.9) and (as described in chapter 1.5 of [Jos90]) we can make this a tensorial equation by declaring that σ is a symmetric tensor field (as in equation (1.3)) and that $\dot{\gamma}$ can be represented by $2\mathbf{D}$, where $\mathbf{D}$ stands for the symmetric part of $\nabla\mathbf{v}$ as before in (1.5). The constitutive equations of the rate type generalising (1.9) are thus (1.3) and

$$\mathbf{T} + \lambda\frac{\partial\mathbf{T}}{\partial t} = 2\eta\mathbf{D}. \tag{1.11}$$

Nonlinear models

The linear Maxwell model of equation (1.11) still requires further refinement. Oldroyd in his 1950 paper [Old50] set out the principles that a constitutive equation must be based upon, and they were put into a more elegant axiomatic form in the work of Noll in 1955 and 1958 (his textbook co-authored with Truesdell contains details, [TN65]). The conditions are

- The *principle of determinism of stress*, which states that the stress in a non-Newtonian body is determined by the history of the motion of that body.
- The *principle of local action*, which states that the stress at a material point is determined by the history of the deformation of an arbitrarily small neighbourhood around that material point.
- The *principle of coordinates invariance*, which states that the constitutive equation must be independent of the frame of reference used to describe them. This can be automatically satisfied if the equations are expressed in consistent tensorial form.
- The *principle of invariance under superimposed rigid body motion*, which states that the equations must have a significance which is independent of absolute motion in space, hence the stresses arising within the fluid should be in response to the material being deformed and not on the relative motion of the observer.

The fourth condition of frame indifference essentially says that if the material is rotated and then deformed the stress ought to be the same as without the rotation, and if the material is deformed then rotated then the stress tensor rotates with the material (explained in section 2.3 of [Ren00b]). All linear models apart from Newtonian fluids violate this frame indifference requirement, thus a nonlinear modification of the linear Maxwell model is necessary for all the principles to be satisfied. Possible modifications are written in the form

$$\mathbf{T} + \lambda \frac{D\mathbf{T}}{Dt} = 2\eta \mathbf{D}, \tag{1.12}$$

where the derivative $\frac{D\mathbf{T}}{Dt}$ can be defined in any way provided it is invariant. The most general derivative used to describe viscoelastic behaviour is the Gordon-Schowalter convected derivative

$$\frac{D\mathbf{T}}{Dt} = \frac{\partial \mathbf{T}}{\partial t} + \overset{\square}{\mathbf{T}}, \tag{1.13}$$

where

$$\overset{\square}{\mathbf{T}} = \mathbf{TW} - \mathbf{WT} - a(\mathbf{TD} + \mathbf{DT}), \qquad \mathbf{W} = \frac{1}{2}\left(\nabla \mathbf{v} - (\nabla \mathbf{v})^T\right), \tag{1.14}$$

with $\mathbf{W}$ being the the vorticity tensor as defined, and a a model parameter $a \in [-1, 1]$. There are a number of Maxwell models being specific cases of (1.12)–(1.13),

$$a = 1: \qquad \mathbf{T} + \lambda \left(\frac{\partial \mathbf{T}}{\partial t} + \overset{\triangledown}{\mathbf{T}} \right) = 2\eta \mathbf{D}, \quad \text{Upper convected Maxwell (UCM)}, \tag{1.15}$$

$$a = -1: \qquad \mathbf{T} + \lambda \left(\frac{\partial \mathbf{T}}{\partial t} + \overset{\triangle}{\mathbf{T}} \right) = 2\eta \mathbf{D}, \quad \text{Lower convected Maxwell (LCM)}, \tag{1.16}$$

$$a = 0: \qquad \mathbf{T} + \lambda \left(\frac{\partial \mathbf{T}}{\partial t} + \overset{\circ}{\mathbf{T}} \right) = 2\eta \mathbf{D}, \quad \text{Corotational Maxwell (COM)}. \tag{1.17}$$

The symbols $\triangledown$, $\triangle$, and $\circ$ above stand respectively for the upper-convected, lower-convected and corotational derivatives, and are defined[2] as

$$\overset{\triangledown}{\mathbf{T}} = (\mathbf{v}.\nabla)\mathbf{T} - (\nabla \mathbf{v})\mathbf{T} - \mathbf{T}(\nabla \mathbf{v})^T, \tag{1.18}$$

$$\overset{\triangle}{\mathbf{T}} = (\mathbf{v}.\nabla)\mathbf{T} + (\nabla \mathbf{v})^T\mathbf{T} + \mathbf{T}(\nabla \mathbf{v}), \qquad \text{and} \qquad \overset{\circ}{\mathbf{T}} = \frac{1}{2}\left(\overset{\triangledown}{\mathbf{T}} + \overset{\triangle}{\mathbf{T}} \right). \tag{1.19}$$

The constitutive equation (1.12) using the Gordon-Schowalter convected derivative (1.13)–(1.14) is named the Johnson-Segalman model, [JS77]. It is often written instead

[2]The problems later are all considered in steady flow and thus we have chosen to define the convected derivatives without the time derivative for easy comparison. The time derivative is thus written separately in the model equations where appropriate.

as a modification of the UCM model with the governing equations

$$\rho\left(\frac{\partial \mathbf{v}}{\partial t}+(\mathbf{v}.\nabla)\mathbf{v}\right)=-\nabla p+\nabla.\mathbf{T}, \qquad \nabla.\mathbf{v}=0,$$
$$\mathbf{T}+\lambda\left(\frac{\partial \mathbf{T}}{\partial t}+\overset{\triangledown}{\mathbf{T}}+\xi\left(\mathbf{TD}+\mathbf{DT}\right)\right)=2\eta\mathbf{D}, \tag{1.20}$$

where $\xi=(1-a)$ to agree with (1.14).

The UCM model is the most popular of the Maxwell models, the others being rarely mentioned in the literature. One reason for this is the accuracy of modelling the rheological properties of the normal stress differences, which are explained in section 2.3 with their definition in equation (2.44). Crucially UCM is preferred to the other Maxwell models since it gives the closest match to experimental data for $\frac{N_2}{N_1}$, the ratio of the second normal stress difference to the first normal stress difference. UCM gives $\frac{N_2}{N_1}=0$, LCM gives $\frac{N_2}{N_1}=-1$ and COM gives $\frac{N_2}{N_1}=-\frac{1}{2}$, whereas experimental data broadly suggests $\frac{N_2}{N_1}\approx -0.1$ for a range polymer solutions (for example see table 3.9 of [Tan00]).

Another reason is that the UCM model may be derived directly from considering the microstructure of the fluid, the theories of which we will consider next.

Constitutive models from microstructure theories

There are a vast number of constitutive models for viscoelastic behaviour, some improve on the accuracy of the UCM model to predict real world behaviour (at the expense of simplicity), with others adding specific features for particular fluids (and their individual behaviours).

The models presented here are not derived from the simple spring and dashpot idea mentioned thus far. Rather, a microstructural approach is considered where a model for the microstructure is postulated and then the consequences explored at the macrostructure level after appropriate averaging. There are broadly three approaches (see [Ren00b] section 2.4) to deriving the constitutive models from the polymer molecule behaviour:

- **Dilute solution theories:** These treat the polymer molecules individually, with each molecule modelled as a chain of beads and springs or beads and rods. The interaction with the flow is caused by the hydrodynamic drag exerted by the fluid on the beads. The UCM model can be derived in such a way, with good explanations in either section 2.4 of [Ren00b], or a more detailed description of dilute polymer solution modelling in chapter 7 of [PT02]. A particular model of

a molecule with two beads connected by a spring is the dumbbell model shown in figure 1-2.

- **Network theories:** The polymer is considered as a network of springs linked at junction points. Originally a method for model derivation of solid rubber with the junctions fixed, the method is altered to allow the junctions to form and decay following certain statistical laws. The interaction between the polymer and the flow occurs due to the motion of these junctions. The PTT model was originally derived using these network theories in the paper by Phan-Thien and Tanner [PTT77]. An example of this network theory model, based on the initial theories of Lodge and Yamamoto is shown in figure 1-3.

- **Reptation theories:** A middle ground between the two above extremes where the polymer molecules are treated individually, but to represent the interaction between other polymer molecules, each is constrained laterally by a 'tube'. A Doi-Edwards virtual tube is shown in figure 1-4.

Whilst the intricate details will not be presented here, chapter 5 of Engineering Rheology by Tanner, [Tan00], provides a thorough analysis of these different derivations and a wide variety of constitutive models, along with references for the original papers describing these theories.

The UCM model, as mentioned, may be derived from the dilute solution theory. This is achieved by modelling the polymer molecules individually as a linear elastic dumbbell, which localises the interactions between solvent and polymer at two beads at each end of the chain connected by a spring. This situation is shown in figure 1-2, and gives confidence that as this model had also been derived from continuum theory then models based on microstructure theories will be valid.

The Oldroyd-B model

The UCM model considers only the polymer contributed stresses. Combining these with the stresses of the solvent gives the Oldroyd-B model, [Old50], the linear superposition of the UCM model stress with a Newtonian contribution. These two stresses are often named the polymer stress, $\mathbf{T}^p$, satisfying (1.15) and solvent stress, $\mathbf{T}^s$, satisfying (1.4). The governing equations for Oldroyd-B are thus

$$\rho\left(\frac{\partial \mathbf{v}}{\partial t} + (\mathbf{v}.\nabla)\mathbf{v}\right) = -\nabla p + \nabla.\mathbf{T}, \quad \nabla.\mathbf{v} = 0,$$
$$\mathbf{T} = \mathbf{T}^s + \mathbf{T}^p, \quad \mathbf{T}^s = 2\eta_s\mathbf{D}, \quad \mathbf{T}^p + \lambda\left(\frac{\partial \mathbf{T}^p}{\partial t} + \overset{\triangledown}{\mathbf{T}^p}\right) = 2\eta_p\mathbf{D}, \tag{1.21}$$

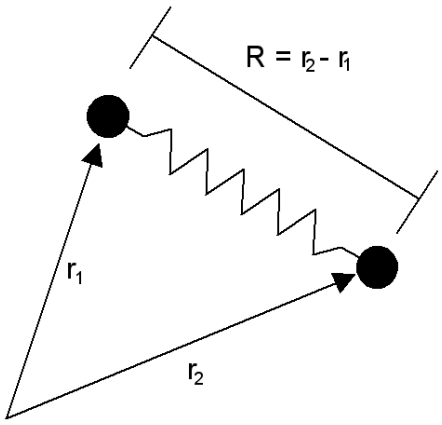

Figure 1-2: The elastic dumbbell of a polymer molecule. Represented are two beads connected by an elastic spring of which there would be many such molecules surrounded by a solvent.

where η_s and η_p are the solvent and polymer viscosities respectively. These equations may also be written in the other forms

$$\rho\left(\frac{\partial \mathbf{v}}{\partial t} + (\mathbf{v}.\nabla)\mathbf{v}\right) = -\nabla p + \nabla.\mathbf{T}^p + \eta_s\nabla^2\mathbf{v}, \quad \nabla.\mathbf{v} = 0,$$
$$\mathbf{T}^p + \lambda\left(\frac{\partial \mathbf{T}^p}{\partial t} + \overset{\triangledown}{\mathbf{T}}^p\right) = 2\eta_p\mathbf{D}, \tag{1.22}$$

by substituting the $\mathbf{T}$ equation into the momentum, or as

$$\rho\left(\frac{\partial \mathbf{v}}{\partial t} + (\mathbf{v}.\nabla)\mathbf{v}\right) = -\nabla p + \nabla.\mathbf{T}, \quad \nabla.\mathbf{v} = 0,$$
$$\mathbf{T} + \lambda\left(\frac{\partial \mathbf{T}}{\partial t} + \overset{\triangledown}{\mathbf{T}}\right) = 2\eta\left(\mathbf{D} + \lambda_R\left(\frac{\partial \mathbf{D}}{\partial t} + \overset{\triangledown}{\mathbf{D}}\right)\right), \tag{1.23}$$

by eliminating $\mathbf{T}^p$ from the constitutive equation using the $\mathbf{T}$ equation, where $\eta = \eta_s + \eta_p$ and $\lambda_R = \eta_s\lambda/\eta$. The Oldroyd-B model has been found to qualitatively describe many of the features of Boger fluids, which are dilute solutions of polymers in highly viscous solvents ([BB77]).

Dumbbells with limited extension

The UCM and Oldroyd-B models are both derived with the linear dumbbell model, which allows the dumbbell to be stretched infinitely. This leads to an issue of the models predicting infinite stress at finite strain rates for elongational flow (see section

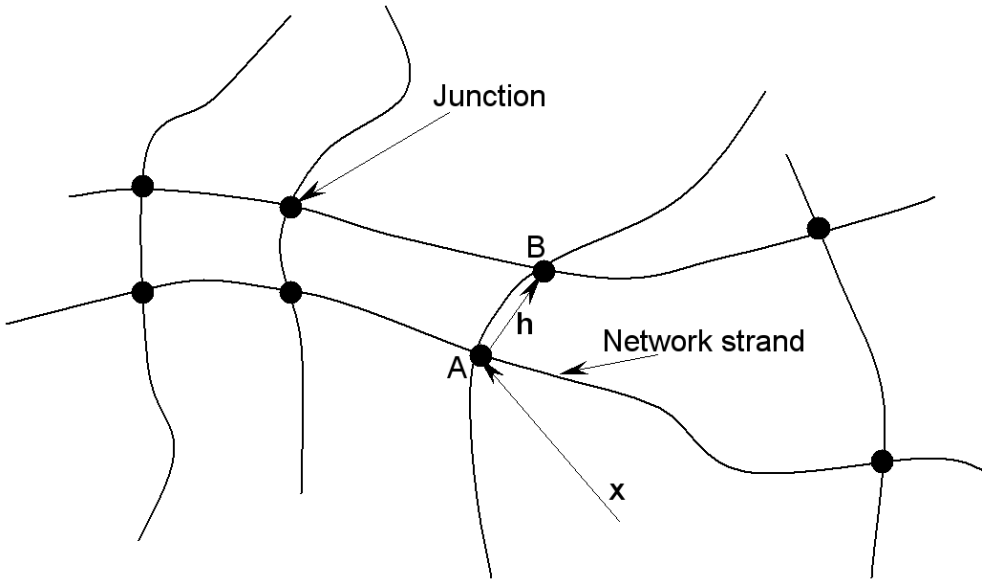

Figure 1-3: An example Lodge-Yamamoto network, from which the PTT ([PTT77]) model may be derived. The polymer liquid forms a network of molecules with temporary junctions (or entanglements). The element AB of the network is called a chain and is made up of N molecules with end-to-end vector $\mathbf{h}$.

4.3.1 of [Tan00]). This flow will not be described in this thesis as it is not required for the corner flow analysis, however, models have been produced to overcome this flaw by constraining the length of the dumbbell to a maximum allowable length. Models such as the Chilcott Rallison model [CR88], Giesekus model [Gie82], FENE-P [BW95] and FENE-L [LHJ$^+$98], may all be found from this dilute polymer dumbbell model with limited extension, with the PTT model of this thesis ([PTT77]) as previously mentioned derived from a non-dilute situation, assuming the polymer chains form a network.

It is possible (and given in [DPT04]) to write down the PTT model as a specific case of a larger set of equations representing the Chilcott-Rallison, FENE-P and Giesekus models along with UCM and Oldroyd-B models. This set of equations may be written

$$\nabla.\mathbf{v} = 0, \quad \rho\left(\frac{\partial \mathbf{v}}{\partial t} + (\mathbf{v}.\nabla)\mathbf{v}\right) = -\nabla p + \nabla.\mathbf{T}^p + \eta_s\nabla^2\mathbf{v}, \quad g = 1 + \frac{\kappa\lambda}{\eta_p}\text{tr }\mathbf{T},$$
$$g\mathbf{T}^p + \lambda\left(\frac{\partial}{\partial t}\left(\frac{\mathbf{T}^p}{f}\right) + \left(\frac{\overset{\triangledown}{\mathbf{T}^p}}{f}\right)\right) = 2\eta_p\mathbf{D} + \mathbf{Q}, \quad f = \left(1 - \frac{e}{L^2}\frac{3 + \frac{\lambda}{\eta_p}\text{tr}\mathbf{T}}{1 + \frac{\lambda}{\eta_p}\text{tr }\mathbf{T}/L^2}\right)^{-1}. \tag{1.24}$$

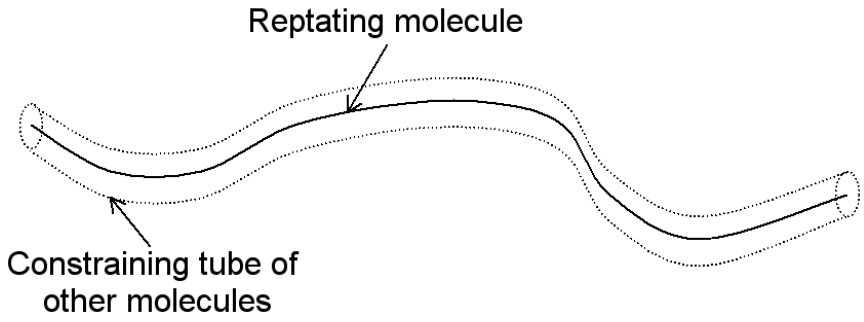

Figure 1-4: A visualisation of the Doi-Edwards reptating tube model. Here the high concentration of polymer molecules is modelled with each molecule being constrained in a virtual tube or cage (in reality formed by the proximity of the other molecules), with each chain moving through reptation - a random snakelike motion.

The additional parameters are κ, a model parameter of the PTT model, L, the maximum extension of the dumbbells, and e, a parameter included to select the model desired. For UCM, Oldroyd-B, PTT and Chilcott-Rallison then $\mathbf{Q} = 0$. Giesekus has $\mathbf{Q} = \alpha\mathbf{T}^2$ where α is a dimensionless 'mobility factor'. For the FENE-P model, then

$$\mathbf{Q} = -\eta_p \left(\frac{L^2+2}{L^2-1}\right)\left[(\mathbf{v}.\nabla)\left(\frac{\mathbf{I}}{f}\right) - \frac{2\mathbf{D}}{f}\right]. \tag{1.25}$$

The various models can be retrieved by appropriate choices of e, κ and η_s. For the PTT model, $e = 0$ and $\eta_s = 0$ (we will return to the exact specification of the PTT model in the following section). To then simplify to the UCM model set $\kappa = 0$. The Giesekus model has $e = 0$, $\kappa = 0$, and $\eta_s = 0$. Both Chilcott-Rallison and FENE-P have $e = 1$ and $\kappa = 0$, and it reduces to Oldroyd-B when $e = 0$ and $\kappa = 0$. Finally, a Newtonian fluid is recovered if $\lambda = 0$, with viscosity $\eta = \eta_s + \eta_p$.

There is a vast range of constitutive models available, with new ones appearing all the time - a more recent example (published in 2003) is the popular Rolie-Poly model [LG03], derived from the tube theory shown in figure 1-4. This model, like PTT, can be applied to flows of polymer melts but the added features and accuracy are at the expense of simplicity (as also seen with the FENE models), with a number of new parameters to be fixed.

1.2 The PTT Model

This thesis will focus on the Phan-Thien-Tanner, or PTT, model derived from the Lodge-Yamamoto network theory shown in figure 1-3 by Phan-Thien and Tanner in [PTT77]. The model is an extension of the Maxwell model (1.12) with the Gordon-Schowalter convected derivative of equations (1.13)–(1.14) to include a function dependent upon $\mathrm{tr}(\mathbf{T}^p)$, the trace of the polymer stress. The model may also include a solvent viscosity as in the Oldroyd-B model so that there is a contribution from both the polymer stress and a Newtonian (solvent) stress.

The governing equations for this PTT model, with the Gordon-Schowalter derivative written in the form of the Johnson-Segalman model (1.20), are

$$\begin{aligned}
&\rho\left(\frac{\partial \mathbf{v}}{\partial t}+(\mathbf{v}.\nabla)\mathbf{v}\right)=-\nabla p+\nabla.\mathbf{T}, \qquad \nabla.\mathbf{v}=0,\\
&\mathbf{T}=\mathbf{T}^s+\mathbf{T}^p, \qquad \mathbf{T}^s=2\eta_s\mathbf{D},\\
&f\left(\mathrm{tr}\ \mathbf{T}^p\right)\mathbf{T}^p+\lambda\left(\frac{\partial \mathbf{T}^p}{\partial t}+\overset{\triangledown}{\mathbf{T}}^p+\xi\left(\mathbf{T}^p\mathbf{D}+\mathbf{D}\mathbf{T}^p\right)\right)=2\eta_p\mathbf{D}.
\end{aligned} \tag{1.26}$$

There are three forms of the function $f\left(\mathrm{tr}\ \mathbf{T}^p\right)$ found in the literature

$$f\left(\mathrm{tr}\ \mathbf{T}^p\right)=\begin{cases}
1+\frac{\kappa\lambda}{\eta_p}\mathrm{tr}\ \mathbf{T}^p, & \text{Linear PTT},\\
1+\frac{\kappa\lambda}{\eta_p}\mathrm{tr}\ \mathbf{T}^p+\frac{1}{2}\left(\frac{\kappa\lambda}{\eta_p}\mathrm{tr}\ \mathbf{T}^p\right)^2, & \text{Quadratic PTT},\\
\exp\left(\frac{\kappa\lambda}{\eta_p}\mathrm{tr}\ \mathbf{T}^p\right), & \text{Exponential PTT},
\end{cases} \tag{1.27}$$

where $\kappa \in [0,1]$ is a model parameter. The linear and exponential forms of the PTT model are extensively used, and are the two forms mentioned in sections 5.6.5-5.6.6 of [Tan00] about the PTT model. The exponential model was first proposed by Phan-Thien [PT78] a year after the linear model of [PTT77]. The quadratic form is far less widely used or mentioned in the literature, but is used, for example, to model the wire-coating process in [NW02], where all three PTT forms are investigated.

Both affine ($\xi = 0$) and non-affine ($\xi \neq 0$) PTT models are found in the literature, but the simpler affine model is more prevalent in the study of contraction and re-entrant corner flows of which we are most interested (e.g. the numerical analysis of Alves et. al. [AOP03] and the analytical work of Renardy [Ren97b]). It is also the simplest extension to the UCM model, which has been studied in detail for the re-entrant corner problem by Hinch and Renardy, with Evans completing the solution and analytical work ([Hin93], [Ren95], [Eva05b], for example). Details of the previous work will be described in section 1.4. The PTT model improves on the UCM model

for modelling polymeric fluids since the UCM model over predicts stresses at large deformation rates, along with obtaining a closer fit to the real world normal stress differences (defined and explained in section 2.3).

Additionally, we mainly consider the PTT model in the limit of vanishing solvent viscosity. It is expected that this model will display flow behaviour markedly different to the Newtonian model, being an extension to the simple UCM model before adding the complicating effects of solvent stresses. Comment is made on the model with solvent viscosity in appendix A.

The model equations to be studied are thus (1.26) with the linear function from (1.27) and

$$\xi = 0, \quad \text{and} \quad \eta_s = 0, \qquad \text{implying} \qquad \mathbf{T}^s = 0, \quad \mathbf{T} = \mathbf{T}^p. \tag{1.28}$$

Given that there is only a polymer stress contribution, we subsequently drop the superscript p from the equations, and to progress towards solving problems we next nondimensionalise our PTT governing equations.

Nondimensionalisation

In the problems of the following chapters we consider the PTT equations in steady state. In dimensional form the equations to consider are

$$\begin{aligned} &\rho(\mathbf{v}.\nabla)\mathbf{v} = -\nabla p + \nabla.\mathbf{T}, \qquad \nabla.\mathbf{v} = 0, \\ &\mathbf{T} + \lambda \overset{\triangledown}{\mathbf{T}} + \frac{\kappa\lambda}{\eta}\,(\text{tr }\mathbf{T})\,\mathbf{T} = 2\eta\mathbf{D}, \end{aligned} \tag{1.29}$$

which are the momentum, continuity and constitutive equations respectively. We nondimensionalise by scaling the parameters with respective nondimensional length, stress and velocity scalings using

$$x = L\bar{x}, \quad y = L\bar{y}, \quad \mathbf{T} = t_0\bar{\mathbf{T}}, \quad \mathbf{v} = U\bar{\mathbf{v}}, \quad p = t_0\bar{p}, \tag{1.30}$$

which (after re-arrangement) give

$$\begin{aligned} &\bar{\nabla}.\bar{\mathbf{v}} = 0, \qquad \frac{\rho U^2}{t_0}(\bar{\mathbf{v}}.\bar{\nabla})\bar{\mathbf{v}} = -\bar{\nabla}\bar{p} + \bar{\nabla}.\bar{\mathbf{T}}, \\ &\frac{Lt_0}{U\eta}\bar{\mathbf{T}} + \frac{L\lambda}{U\eta}\left(\frac{Ut_0}{L}\,\overset{\triangledown}{\bar{\mathbf{T}}} + \frac{\kappa t_0^2}{\eta}(\text{tr }\bar{\mathbf{T}})\bar{\mathbf{T}}\right) = 2\bar{\mathbf{D}}, \end{aligned} \tag{1.31}$$

where $\bar{\mathbf{D}}$ is defined in terms of $\bar{\mathbf{v}}$. Letting $t_0 = (U\eta)/L$ and dropping bars from the variables subsequently for clarity gives

$$\text{Re } (\mathbf{v}.\nabla)\mathbf{v} = -\nabla p + \nabla.\mathbf{T}, \tag{1.32}$$

$$\nabla.\mathbf{v} = 0, \tag{1.33}$$

$$\mathbf{T} + \text{We}\left(\overset{\triangledown}{\mathbf{T}} + \kappa\,(\text{tr}\mathbf{T})\,\mathbf{T}\right) = 2\mathbf{D}, \tag{1.34}$$

where

$$\text{Re } = \frac{\rho U L}{\eta}, \qquad \text{We } = \frac{\lambda U}{L}, \tag{1.35}$$

and it can be verified that these parameters along with the PTT model parameter κ are all nondimensional. Here Re is the Reynolds number and We is the Weissenberg number, a comparison of the elastic forces to the viscous effects. In all subsequent sections all variables are now non-dimensional.

Clearly both Weissenberg and Reynolds numbers depend on the typical length and velocity scales. Inertial terms are assumed to be negligible for most flows considered in this thesis (or are shown to be if $\text{Re} = O(1)$), and given the possibility of a wide range of Weissenberg numbers, we will consider the cases of both large and small Weissenberg number as well as $\text{We} = O(1)$. For the PTT model parameter κ, values lie in the range $\kappa \in [0, 1]$, with values approaching 1 being unrealistically large.

In [AGAK96a], Azaiez et. al. simulate the flow of a viscoelastic polymer solution (specifically a 5 wt.% polyisobutylene (PIB) in tetradecane) through a planar 4:1 contraction, comparing and fitting the PTT model to data from the literature. In their work, they fitted both a one mode and a four mode PTT model to the experimental data, and using our notation the values are given in table 1.1. Of particular interest is the value of $\kappa = 0.25$.

Another paper [SSP$^+$98] investigates stagnation flow of a 2.5% polyisobutylene solution both experimentally and numerically, fitting the PTT model well with the model parameter $\kappa = 0.8$. Further typical values of κ are given in [Tan00] when describing the PTT model in section 5.6.6. Two typical values are suggested of $\kappa = 0.02$ for dilute solution behaviour and $\kappa = 0.25$ for high density polyethylene (HDPE) melts.

1.3 Industrial Applications

The study of viscoelasticity is relatively new - seminal work by J.G. Oldroyd was published in 1950, [Old50] and the PTT model was created and published in 1977 [PTT77]. Much of the initial work has been performed by chemical engineers who have

	4-mode PTT model				1-mode PTT model
Mode number	1	2	3	4	
κ	0.25	0.25	0.25	0.25	0.25
η	0.0400	0.2324	0.5664	0.5850	1.422
λ	0.6855	0.1396	0.0389	0.0059	0.04
We	15.94	3.25	0.90	0.14	0.93
Re	0.27	0.27	0.27	0.27	0.27

Table 1.1: Table showing the parameters for a 5 wt.% polyisobutylene (PIB) in tetradecane, from [AGAK96a].

used experimental data to derive models and predict more complex behaviour. One of the best known applications of work in this area was solving a problem of disposing 'red mud' (the waste product of the processing of bauxite to alumina). This research, carried out by Nguyen and Boger, has been implemented successfully by Alcoa of Australia, an aluminium mining company, to reduce both costs and environmental impact of their waste disposal system, [NB98]. These techniques have since been used to examine pipeline transportation to dispose of clay-based coal tailings from the Hunter Valley coal mine in New South Wales, also described in [NB98]. Boger has also applied his work to the oil industry, developing pipeline designs such that the fluidity of high wax content crude oils is maintained, [WB91]. This work also has applications to the behaviour of drops of fluids, and is linked to applications in atomisation, inkjet printing, delivery of agricultural chemicals, and with intelligent gels, [CB00].

Materials exhibiting viscoelastic behaviour also appear in biology. There has been recent work by numerous people to investigate the behaviour of internal organs, applications of which are as diverse as providing equations to model organ movement accurately for use in surgical simulations to understanding internal trauma during car crashes (see [NBFT04]). The work by Nasseria, Bilston, Fasheun and Tanner in [NBFT04] is particularly interesting as it predicts behaviour of soft tissue (pig liver) and bread dough under various compressions using the Phan-Thien-Tanner model studied in this thesis.

Another biological application is in human and veterinary ophthalmology, where a viscoelastic fluid - most commonly sodium hyaluronate, is used during surgery to fill and maintain the anterior chamber, reposition the iris and to coat and protect the corneal endothelium, [WW99]. It is clear that viscoelastic materials occur in many diverse and critical situations and, as such, accurate modelling of such fluids is of great interest.

More applications specific to the Phan-Thien-Tanner model include the modelling of plastics such as PET resins, which are used in, for example, film casting, [HHVC97].

It has also been used in many publications to simulate the process of wire-coating, such as in [NW02]. The latter paper is of further interest as it considers the models shortcomings, and investigates extensions to the linear PTT model (as mentioned in section 1.2 here).

1.4 Previous work and outline of thesis

We now discuss the previous work applicable to the following chapters of this thesis, the structure of which will provide a natural way to order the literature review. Chapter 2 contains preliminary analysis of the PTT model by classifying the type of the equations, followed by a description of two formulations of the governing equations - those of the Cartesian and the natural stress basis (see section 2.2 for details). Finally simple shear flow is investigated, which gives the viscometric behaviour expected for flow near a solid wall. Chapters 3-5 contain analysis of the specific problems. In particular re-entrant corner flow (with $\kappa = O(1)$, $\mathrm{We} = O(1)$) is studied in chapter 3, re-entrant corner flow in small and high parameter regimes in chapter 4, and salient corner flow in chapter 5.

Chapter 3: Early re-entrant corner work

As mentioned chapter 3 considers re-entrant corner flow of the PTT fluid with $\kappa = O(1)$, $\mathrm{We} = O(1)$. The PTT model shares many features with the UCM and Oldroyd-B models, and thus previous analysis involving these models is also of vital importance for the understanding of the PTT problem.

To make initial progress, Renardy [Ren93] focused on investigating the stresses of the UCM model with an assumed Newtonian velocity field. It was found that the upper convected derivative dominates in the constitutive equation away from the walls, and the solution of this implied that the stress would be dominated by its component in the flow direction $\mathbf{T} \sim g(\psi)\mathbf{v}\mathbf{v}^T$, with $g(\psi)$ an arbitrary function of the stream function. Whilst it was known that the Newtonian velocity field assumption was incorrect, it still allowed the main features of the flow to be studied, in particular that the core flow would not recover viscometric behaviour thus determining the presence of boundary layers near the walls, found to be of thickness $\theta \sim r^{1-\lambda_0}$ (where r is the radial distance from the corner, θ is the angle made with the upstream wall, and $\lambda_0 \approx 0.5445$ for the corner angle of 270^o. More details of the geometry are given in section 3.1.2). Another interesting feature found was the instability downstream of the corner when attempting to integrate the stresses, leading to large amplification of numerical errors at the downstream wall. The prescribed Newtonian velocity field behaves as $\psi \sim r^{1+\lambda_0}$, with the stresses as $\mathbf{T}^p \sim r^{-0.74}$ (contrasting with $\mathbf{T}^p \sim r^{-0.91}$ at the walls from the

viscometric behaviour using the Newtonian shear rate).

Following this work Renardy suggested a method to overcome the downstream instability in [Ren94]. The method was to represent the stresses in a natural stress basis aligned along the streamlines (more specific details are contained in section 2.2.2). This basis represents the stresses in three components of vastly different orders of magnitude, with the 'dangerous' mode ν decoupled from the other variables and avoiding the instability. This feature of the natural stress basis proves crucial to our analysis. This idea of transforming the stress variables to align them with the streamlines had been previously exploited in numerical situations by Keiller [Kei93] and Dupont et al. [DMC85], but [Ren94] was the first to realise its importance to the re-entrant corner problem.

The full re-entrant corner problem of the UCM (and/or Oldroyd-B) fluid without the Newtonian flow field assumption was initially considered in three papers, firstly in 1993 by Davies and Devlin [DD93] and Hinch [Hin93], and later in 1995 by Renardy [Ren95]. In [DD93] the Oldroyd-B fluid is considered as a singular perturbation series, whereas the approach of both Hinch and Renardy was to use matched asymptotics (and it is this approach that we use here). The analysis of both Hinch and Renardy is given for the specific corner angle of 270^o.

As mentioned, [Hin93] is the first paper upon which the analysis of chapter 3 is based and motivated. It contains the correct balance of the upper convected stress derivative dominating in the core region away from the walls and consequently the Euler equations apply and can be solved by a potential flow solution. For the 270^o corner angle Hinch finds a velocity behaviour of $\mathbf{v} \sim r^{5/9}$ and stresses of $\mathbf{T}^p \sim r^{-2/3}$. At the walls however, Hinch could not match the stream function to the expected viscometric behaviour of $\psi \sim \theta^2$, instead finding a stream function behaviour of $\psi \sim \theta^{7/3}$.

Renardy illustrated the derivation of the Hinch core solution more clearly in [Ren95], along with showing that the boundary layer equations have a similarity solution which may be matched to Hinch's potential flow solution in the core and to viscometric behaviour $\psi = O(\theta^2)$ at the walls. He also determined the boundary layer thickness to be $\theta \sim r^{1/3}$. Outstanding from these works is the complete solution to the problem to include matching to the downstream boundary layer.

Further work of interest was published by Renardy in 1997. [Ren97a] concentrates on high Weissenberg boundary layers (not around a corner) of the UCM fluid. It is of interest since the relation between natural stress and Cartesian bases within this high Weissenberg boundary layer are given and will apply to the Weissenberg $O(1)$ regime considered around a re-entrant corner. Following this, [Ren97c] contains details of how the equations governing UCM flow in a high Weissenberg number limit can be reduced

to the (compressible) Euler equations, with solutions generated by potential flow. The other area of interest within the paper is a brief discussion of the PTT model. This discussion includes a comment that for many flows the term $\mathrm{tr}(\mathbf{T})\mathbf{T}$ must be of a lower order than the upper convected derivative terms, providing warning when considering the possible core balances for our problem.

Also in 1997, two papers concerning the PTT fluid were published by Renardy [Ren97b] and Hagen and Renardy [HR97]. The first of these considers integration of the constitutive equations of the PTT fluid near a 270^o re-entrant corner in a Newtonian velocity field. This is the first major analytical work published which considers the PTT fluid, and in fact provides the solution to the case of the PTT flow with a solvent viscosity, explained in appendix A, which includes a detailed analysis of the results of [Ren97b]. The analysis performed shares much in common with the earlier paper for UCM corner flow [Ren93] as once again the numerical results are obtained with the velocity field assumed to be Newtonian. It is this assumption that is relaxed here in order to provide the solution to our PTT problem (see chapter 3). Renardy found the same stream function behaviour of $r^{1+\lambda_0}$, with $\lambda_0 \approx 0.5445$ for the 270^o corner, but with less singular stresses of $r^{-0.329}$ and thinner boundary layers $\theta \sim r^{(1-\lambda_0)/3}$ compared to the UCM model in a Newtonian velocity field.

[HR97] finds the boundary layer equations for high Weissenberg number flows of the PTT fluid in a similar way to [Ren97a]. This paper shows derivation of the viscometric behaviour of PTT fluids (which is detailed here in section 2.3.1), and also considers the case of κ being small, specifically when κ is related to the Weissenberg number by $\kappa = O(\mathrm{We}^{-2})$. The small κ limit for re-entrant corner flow is considered here in chapter 4.

Complete descriptions of the re-entrant corner problem

The first papers published resolving the downstream boundary layer to complete the re-entrant corner solution were published by Rallison and Hinch [RH04] for the Oldroyd-B fluid, and by Evans [Eva05b] for the UCM fluid. Both papers extend the earlier work of Renardy and Hinch on the re-entrant corner geometry, and both agree that for UCM and Oldroyd-B fluids the stream function vanishes as $\psi \sim r^{(3-\alpha)\alpha}$, with a stress singularity of $O(r^{-2(1-\alpha)})$ and boundary layer thicknesses $\theta \sim r^{1-\alpha}$ where α is related to the corner angle θ by $\theta = \pi/\alpha$. These values agree for the 270^o corner angle ($\alpha = 2/3$) with the previous results of Hinch and Renardy. [Eva05b] provides analytical work in the Cartesian basis to solve the problem using similarity solutions with matching performed to recover viscoelastic behaviour uniformly. The downstream boundary layer issue is resolved through an expansion of the core flow behaviour to

recover the critical higher order terms required to pose the downstream boundary value problem numerically. In contrast, [RH04] uses the natural stress basis from [Ren94] avoiding the need for such an expansion. [Eva05b] also includes work on a double boundary layer structure possibly present, with a further structure to include reverse flow in lip vortices in [Eva05a]. These structures are certainly of interest given that vortices appear experimentally in contraction flows (where 270^o re-entrant corners are present). Other than in this paper, all other analysis assumes complete flow around the corner with no reverse flow, and this is an assumption made throughout the analysis of this thesis. Reverse flow and the presence of a separating streamline is very much an open question and further work would be of interest in this area.

Most recently the papers published in 2008 upon which the analysis of this thesis is most closely related are those by Evans [Eva08a] and [Eva08b]. These two connected papers complete the analysis of the re-entrant corner flow of the UCM fluid (with the assumption of complete flow around the corner) in the Cartesian and natural stress bases. These papers clarify the analysis of [Eva05b] and display the exact interplay between these two bases with the benefits of both shown.

Two papers are currently published from the work of this thesis, [ES08] and [ES09], together describing the work of chapter 3 here. Published in the same volume as [ES08] was work by Atalik [Ata08] who considers the slightly different approach of using Lie group theory to obtain the similarity solutions of the boundary layer equations. This paper investigates the corner flow of both PTT and UCM models, with numerics presented for the upstream boundary layer and agrees with the analysis of [Eva08a] and [ES08].

Chapters 4 and 5

Chapter 4 contains analysis of the re-entrant corner problem in the three parameter regimes of $\kappa \to 0$ with $\mathrm{We} = O(1)$, and the small and high Weissenberg number limits with $\kappa = O(1)$. Directly applicable is the work of Evans [Eva06], where the small and high limits of the Weissenberg number for the re-entrant corner flow of the UCM model are considered.

Chapter 5 focuses on salient corner flow. Crucial for this analysis is the understanding of corner flows involving the Newtonian fluid. The problem was initially examined by Rayleigh in 1920 (referenced in the later papers [DM49] and [Mof64]), but contained an assumption about the stream function behaviour later shown to be too restrictive by Dean and Montagnon, [DM49]. Further work to improve the solution and to consider many complex flow scenarios around the corner including symmetrical flows and flows with eddies was published in 1964 by Moffatt [Mof64]. The Newtonian solution is of use

in the non-Newtonian cases of low Weissenberg number (in most viscoelastic models, setting $\mathrm{We} = 0$ recovers the Newtonian governing equations), and also in salient corner flow (flow with corners of angle less than 180^o). For the re-entrant corner flow (with corner angle greater than 180^o), the Newtonian solution is no longer relevant and quite different behaviour is found.

Chapter 2

Preliminary analysis

This chapter introduces the main mathematical preliminaries to be used in chapters 3–6. It begins with an analysis of the type of the PTT governing equations in section 2.1, followed by the representation of the equations in the Cartesian and natural stress formulations in 2.2. The chapter is then concluded by considering the steady shear flow and viscometric behaviour of the PTT fluid in section 2.3, with descriptions of the important rheological properties of the viscosity and normal stresses.

2.1 Classification of type

The dimensionless governing equations for steady planar flow for a Phan-Thien-Tanner viscoelastic fluid are given in (1.32)–(1.34). Although the intention of this thesis is to solve specific problems rather than to analyse the possible existence and uniqueness issues relating to the way the problems are posed, it is still of interest to be able to classify this system of PDEs.

There are numerous good sources discussing classification of PDEs, for instance chapter 2 of [RR04], with the classification of viscoelastic models of Maxwell type discussed in particular by Joseph et. al. in [JRS85] and then furthered by Gerritsma and Phillips [GP01], [GP08].

Whilst detailed analysis exists for the classification and subsequent description of how to obtain a well-posed problem for the UCM model has been performed in the above, the PTT model appears to have not been investigated. Given that the PTT model only extends the UCM model with a nonlinear stress term, it is likely that the classification will produce the same result as for UCM, however we discuss the details here following a similar method to that of Gerritsma and Phillips in [GP08].

The steady planar PTT governing equations (1.32)-(1.34) form a system of 6 quasi-

linear equations. They can be written in the form

$$L\mathbf{q} = \mathbf{A}_1 \frac{\partial \mathbf{q}}{\partial x} + \mathbf{A}_2 \frac{\partial \mathbf{q}}{\partial y} + \mathbf{S}\mathbf{q} = \mathbf{0}, \tag{2.1}$$

where $\mathbf{q} = (p, u, v, T_{11}, T_{12}, T_{22})^T$. p, u, and v are the pressure and velocity components in the x and y Cartesian directions as defined in the introduction, T_{11} and T_{22} are the normal stresses in the x and y directions respectively, and T_{12} is the shear stress. The matrices in (2.1) are then

$$\mathbf{A}_1 = \begin{pmatrix} 0 & 1 & 0 & 0 & 0 & 0 \\ 1 & \text{Re } u & 0 & -1 & 0 & 0 \\ 0 & 0 & \text{Re } u & 0 & -1 & 0 \\ 0 & -2\text{We } T_{11} - 2 & 0 & \text{We } u & 0 & 0 \\ 0 & 0 & -2\text{We } T_{12} & 0 & 0 & \text{We } u \\ 0 & 0 & -\text{We } T_{11} - 1 & 0 & \text{We } u & 0 \end{pmatrix},$$

$$\mathbf{A}_2 = \begin{pmatrix} 0 & 0 & 1 & 0 & 0 & 0 \\ 0 & \text{Re } v & 0 & 0 & -1 & 0 \\ 1 & 0 & \text{Re } v & 0 & 0 & -1 \\ 0 & -2\text{We } T_{12} & 0 & \text{We } v & 0 & 0 \\ 0 & 0 & -2\text{We } T_{22} - 2 & 0 & 0 & \text{We } v \\ 0 & -\text{We } T_{22} - 1 & 0 & 0 & \text{We } v & 0 \end{pmatrix},$$

$$\mathbf{S} = (1 + \text{We } \kappa\,(T_{11} + T_{22})) \begin{pmatrix} 0 & 0 & 0 & 0 & 0 & 0 \\ 0 & 0 & 0 & 0 & 0 & 0 \\ 0 & 0 & 0 & 0 & 0 & 0 \\ 0 & 0 & 0 & 1 & 0 & 0 \\ 0 & 0 & 0 & 0 & 0 & 1 \\ 0 & 0 & 0 & 0 & 1 & 0 \end{pmatrix}. \tag{2.2}$$

Following [GP08], we use the approach to the classification of this system of studying the stability of short waves. Gerritsma and Phillips consider the UCM equations in unsteady planar flow, and hence our analysis changes to remove the time dependence, along with differences in the PTT governing equations and our notation. We first calculate the symbol of the differential operator, defined as follows:

Consider the linear differential operator

$$P\left(\mathbf{x}, \frac{\partial}{\partial x}, \frac{\partial}{\partial y}\right), \tag{2.3}$$

where $\mathbf{x} = (x, y)$ are the space coordinates. Then the symbol of P is

$$\text{Symbol of } P \ = P\left(\mathbf{x}, i\xi_1, i\xi_2\right). \tag{2.4}$$

After this, we compute the determinant of this symbol, followed by the zeros of the principal part (the terms of highest order in ξ_i) of this polynomial expression.

We consider a plane wave solution of (2.1) propagating in the ξ-direction of the form

$$\mathbf{q}(\mathbf{x}, t) = \mathbf{q}_0 e^{i\xi.\mathbf{x}}, \tag{2.5}$$

where $\xi = \xi_1\mathbf{e}_x + \xi_2\mathbf{e}_y$ is a wave vector (and $\mathbf{e}_x$, $\mathbf{e}_y$ are the unit vectors in the x and y directions respectively), with wave numbers ξ_1 and ξ_2, and $|\xi| = \sqrt{\xi_1^2 + \xi_2^2}$. Substituting this into our governing equations (2.1) yields

$$i(\xi_1\mathbf{A}_1 + \xi_2\mathbf{A}_2)\mathbf{q}_0 + \mathbf{S}\mathbf{q}_0 = \mathbf{0}, \tag{2.6}$$

which will have a non-trivial solution $\mathbf{q}_0$ if

$$\det\ (\xi_1\mathbf{A}_1 + \xi_2\mathbf{A}_2 - i\mathbf{S}) = 0. \tag{2.7}$$

As mentioned in [GP08], the symbol of the differential operator defined by (2.1) is the response of the system to a solution of the form (2.5). Therefore the symbol $P(\mathbf{q}, i, \xi)$ for the PTT model is

$$P(\mathbf{q}, i, \xi) = i(\xi_1\mathbf{A}_1 + \xi_2\mathbf{A}_2 - i\mathbf{S}). \tag{2.8}$$

The requirement that $\det\left(P(\mathbf{q}, i, \xi)\right) = 0$, leads to the polynomial equation

$$(\xi_1^2 + \xi_2^2)\left(\mathrm{We}\left(\mathbf{v}.\xi\right) - i[\kappa]\right)^2\left(\xi^T(\mathrm{We}\ \mathbf{T} + \mathbf{I})\xi - \mathrm{Re}\left(\mathbf{v}.\xi\right)\left(\mathrm{We}\left(\mathbf{v}.\xi\right) - i[\kappa]\right)\right) = 0, \tag{2.9}$$

where $[\kappa] = \mathrm{We}\ \kappa\left(T_{11} + T_{22}\right) + 1$ has been introduced for simplicity. This polynomial equation in ξ_1 and ξ_2 is analogous to (16) in [GP08] for the UCM model, with the main difference that $\kappa = 0$ for UCM, causing $[\kappa] = 1$, removing the tr$\mathbf{T}$ term from $[\kappa]$. The principal part of this polynomial, which as mentioned is the terms of highest degree in ξ_i, is

$$P^p = \mathrm{We}^2(\xi_1^2 + \xi_2^2)(\mathbf{v}.\xi)^2\left(\xi^T(\mathrm{We}\ \mathbf{T} + \mathbf{I})\xi - \mathrm{ReWe}\left(\mathbf{v}.\xi\right)^2\right), \tag{2.10}$$

which is identical to the steady UCM model principal part of the symbol (when written in the same notation). The additional PTT terms involving tr$\mathbf{T}$ do not contribute to the principal part of the symbol, which is used to classify the original governing equations.

To make conclusions about the type of the PTT equations, we note from [RR04]

the classification of the general second-order PDE in two spacial dimensions

$$Lu = a(x,y)\frac{\partial^2 u}{\partial x^2} + b(x,y)\frac{\partial^2 u}{\partial x \partial y} + c(x,y)\frac{\partial^2 u}{\partial y^2} + d(x,y)\frac{\partial u}{\partial x} + e(x,y)\frac{\partial u}{\partial y} + f(x,y)u + g(x,y) = 0. \tag{2.11}$$

Here the principal part of the symbol L is

$$L^p = -a(x,y)\xi_1^2 - b(x,y)\xi_1\xi_2 - c(x,y)\xi_2^2 = (\xi_1, \xi_2)\begin{pmatrix} -a & -\frac{1}{2}b \\ -\frac{1}{2}b & -c \end{pmatrix}\begin{pmatrix} \xi_1 \\ \xi_2 \end{pmatrix} = \xi^T \mathbf{A} \xi, \tag{2.12}$$

and is classified as:

- Elliptic - if the symmetric matrix $\mathbf{A}$ is (positive or negative) definite,
- Hyperbolic - if $\mathbf{A}$ has eigenvalues of both signs,
- Parabolic - if $\mathbf{A}$ is singular (i.e. it has at least one zero eigenvalue).

We now consider the factors of P^p in (2.10) using the above and with reference to the previous papers [JRS85], [GP01], and [GP08] (since they include classification of the type of the UCM equations, which as mentioned has the same principal part) to conclude:

- Firstly, the factor $(\mathbf{v}.\xi)^2$ demonstrates that there are two real characteristics $(\mathbf{v}.\xi) = 0$, and corresponds to two pieces of information that are convected along streamlines. As such the system always has at least two linearly independent eigenvectors associated with this factor, giving the system a hyperbolic character.
- Next we consider the factor $(\xi_1^2 + \xi_2^2) = \xi^T \mathbf{A} \xi$ with $\mathbf{A} = \mathbf{I}$. The eigenvalues of $\mathbf{I}$ are both $+1$, so $\mathbf{I}$ is positive definite, and the factor is elliptic. This factor in fact corresponds to the symbol of the Laplace operator resulting from the incompressibility constraint - specifically from the divergence of the velocity field and gradient of the pressure.
- Finally, the factor

$$\xi^T(\mathrm{We}\ \mathbf{T} + \mathbf{I})\xi - \mathrm{ReWe}\,(\mathbf{v}.\xi)^2 = \mathrm{We}\ \xi^T\left(\mathbf{T} + \frac{1}{\mathrm{We}}\mathbf{I} - \mathrm{Re}\ \mathbf{v}\mathbf{v}^T\right)\xi,$$

  which is associated by Joseph [JRS85] to the vorticity. This factor is more

complicated and can change type depending on the eigenvalues of the tensor $\mathbf{A} = \left(\mathbf{T} + \frac{1}{\mathrm{We}}\mathbf{I} - \mathrm{Re}\ \mathbf{v}\mathbf{v}^T\right)$ as suggested above for the general second-order PDE.

From this we conclude that the system of partial differential equations for the steady PTT model (regardless of the type of the final factor) is of mixed elliptic-hyperbolic type.

2.2 Formulations of the governing equations

2.2.1 Cartesian stress basis equations

The governing equations for the PTT fluid are given in equations (1.32)–(1.34). Written in Cartesian component form for the steady planar case the momentum and constitutive equations are

$$\mathrm{Re}\ (\mathbf{v}.\nabla)u = -\frac{\partial p}{\partial x} + \frac{\partial T_{11}}{\partial x} + \frac{\partial T_{12}}{\partial y}, \tag{2.13}$$

$$\mathrm{Re}\ (\mathbf{v}.\nabla)v = -\frac{\partial p}{\partial y} + \frac{\partial T_{12}}{\partial x} + \frac{\partial T_{22}}{\partial y}, \tag{2.14}$$

and

$$T_{11} + \left(u\frac{\partial T_{11}}{\partial x} + v\frac{\partial T_{11}}{\partial y} - 2\frac{\partial u}{\partial y}T_{12} - 2\frac{\partial u}{\partial x}T_{11} + \kappa(T_{11}+T_{22})T_{11}\right) = 2\frac{\partial u}{\partial x}, \tag{2.15}$$

$$T_{22} + \left(u\frac{\partial T_{22}}{\partial x} + v\frac{\partial T_{22}}{\partial y} - 2\frac{\partial v}{\partial x}T_{12} - 2\frac{\partial v}{\partial y}T_{22} + \kappa(T_{11}+T_{22})T_{22}\right) = 2\frac{\partial v}{\partial y}, \tag{2.16}$$

$$T_{12} + \left(u\frac{\partial T_{12}}{\partial x} + v\frac{\partial T_{12}}{\partial y} - \frac{\partial v}{\partial x}T_{11} - \frac{\partial u}{\partial y}T_{22} + \kappa(T_{11}+T_{22})T_{12}\right) = \frac{\partial u}{\partial y} + \frac{\partial v}{\partial x}, \tag{2.17}$$

where the Weissenberg number, We, has been set to unity as it may be removed via the scalings

$$r \mapsto \frac{r}{\mathrm{We}^{1/2}}, \qquad \mathbf{v} \mapsto \mathrm{We}^{1/2}\mathbf{v}, \qquad \mathbf{T} \mapsto \mathrm{We}\ \mathbf{T}, \qquad p \mapsto \mathrm{We}\ p, \qquad \kappa \mapsto \kappa, \tag{2.18}$$

similarly to remark 2 in [Eva08a]. Clearly these scalings break down in the low and high Weissenberg limits $\mathrm{We} \to 0^+$, and $\mathrm{We} \to +\infty$, and these limits are analysed in chapter 4. Here also the PTT model parameter κ is taken in the range $[0, 1]$, although the values at the upper end of this range would be considered unrealistically large, as mentioned in the introduction. In chapter 3, it is assumed that $\kappa = O(1)$ where a distinct behaviour from the UCM model is expected. The UCM limit of $\kappa \to 0$ is

considered in chapter 4. The velocity field in planar flow can be represented by

$$\mathbf{v} = \begin{pmatrix} u \\ v \end{pmatrix} = \begin{pmatrix} \frac{\partial \psi}{\partial y} \\ -\frac{\partial \psi}{\partial x} \end{pmatrix}, \tag{2.19}$$

where ψ is the usual stream function, and thus causing the continuity equation (1.33) to be immediately satisfied. The governing equations in terms of the stream function can thus be written as

$$T_{11} + \left(\frac{\partial \psi}{\partial y}\frac{\partial T_{11}}{\partial x} - \frac{\partial \psi}{\partial x}\frac{\partial T_{11}}{\partial y} - 2\frac{\partial^2 \psi}{\partial y^2}T_{12} - 2\frac{\partial^2 \psi}{\partial x \partial y}T_{11} + \kappa(T_{11}+T_{22})T_{11} \right) = 2\frac{\partial^2 \psi}{\partial x \partial y}, \tag{2.20}$$

$$T_{22} + \left(\frac{\partial \psi}{\partial y}\frac{\partial T_{22}}{\partial x} - \frac{\partial \psi}{\partial x}\frac{\partial T_{22}}{\partial y} + 2\frac{\partial^2 \psi}{\partial x^2}T_{12} + 2\frac{\partial^2 \psi}{\partial x \partial y}T_{22} + \kappa(T_{11}+T_{22})T_{22} \right) = -2\frac{\partial^2 \psi}{\partial x \partial y}, \tag{2.21}$$

$$T_{12} + \left(\frac{\partial \psi}{\partial y}\frac{\partial T_{12}}{\partial x} - \frac{\partial \psi}{\partial x}\frac{\partial T_{12}}{\partial y} + \frac{\partial^2 \psi}{\partial x^2}T_{11} - \frac{\partial^2 \psi}{\partial y^2}T_{22} + \kappa(T_{11}+T_{22})T_{12} \right) = \frac{\partial^2 \psi}{\partial y^2} - \frac{\partial^2 \psi}{\partial x^2}, \tag{2.22}$$

and

$$\mathrm{Re}\ \left(\frac{\partial \psi}{\partial y}\frac{\partial^2 \psi}{\partial x \partial y} - \frac{\partial \psi}{\partial x}\frac{\partial^2 \psi}{\partial y^2} \right) = -\frac{\partial p}{\partial x} + \frac{\partial T_{11}}{\partial x} + \frac{\partial T_{12}}{\partial y}, \tag{2.23}$$

$$\mathrm{Re}\ \left(-\frac{\partial \psi}{\partial y}\frac{\partial^2 \psi}{\partial x^2} + \frac{\partial \psi}{\partial x}\frac{\partial^2 \psi}{\partial x \partial y} \right) = -\frac{\partial p}{\partial y} + \frac{\partial T_{12}}{\partial x} + \frac{\partial T_{22}}{\partial y}. \tag{2.24}$$

This is a system of 5 coupled, nonlinear, partial differential equations of 2nd order in ψ, which are mixed elliptic-hyperbolic in nature, as shown in section 2.1.

Determinant relationship

It will also be useful to have a relation between the determinant $\det(\mathbf{T}+\mathbf{I})$ and ψ as in [Eva08a]. We have that the symmetric matrix $(\mathbf{T}+\mathbf{I})$ is given by

$$(\mathbf{T}+\mathbf{I}) = \begin{pmatrix} T_{11}+1 & T_{12} \\ T_{12} & T_{22}+1 \end{pmatrix} \quad \text{hence} \quad \begin{aligned} &\det(\mathbf{T}+\mathbf{I}) = (T_{11}+1)(T_{22}+1) - T_{12}^2, \\ &\mathrm{tr}(\mathbf{T}+\mathbf{I}) = T_{11}+T_{22}+2, \end{aligned} \tag{2.25}$$

and a rearrangement of the PTT model (with We scaled out) gives

$$(\mathbf{v}.\nabla)\mathbf{T} = (\nabla \mathbf{v})(\mathbf{T}+\mathbf{I}) + (\mathbf{T}+\mathbf{I})(\nabla \mathbf{v})^{\mathrm{T}} - (\kappa(\mathrm{tr}\mathbf{T})+1)\mathbf{T}. \tag{2.26}$$

Computing the matrix multiplication and applying the continuity equation gives the three equations

$$\begin{aligned}(\mathbf{v}.\nabla)T_{11} &= 2(T_{11}+1)u_x + 2T_{12}u_y - (\kappa(T_{11}+T_{22})+1)T_{11},\\ (\mathbf{v}.\nabla)T_{12} &= (T_{11}+1)v_x + (T_{22}+1)u_y - (\kappa(T_{11}+T_{22})+1)T_{12},\\ (\mathbf{v}.\nabla)T_{22} &= 2(T_{22}+1)v_y + 2T_{12}v_x - (\kappa(T_{11}+T_{22})+1)T_{22}. \end{aligned} \tag{2.27}$$

Combining (2.25) and (2.27), and again using continuity where appropriate gives that

$$\begin{aligned}(\mathbf{v}.\nabla)\det(\mathbf{T}+\mathbf{I}) &= (\mathbf{v}.\nabla)(T_{11}T_{12}+T_{11}+T_{22}+1-T_{12}^2)\\ &= (T_{11}+1)(\mathbf{v}.\nabla)T_{22} + (T_{22}+1)(\mathbf{v}.\nabla)T_{11} - 2T_{12}(\mathbf{v}.\nabla)T_{12}\\ &= -\left(\kappa(T_{11}+T_{22})+1\right)\left((T_{11}+1)T_{22}+(T_{22}+1)T_{11}-2T_{12}^2\right)\\ &= \left(\kappa(T_{11}+T_{22})+1\right)\left(\mathrm{tr}(\mathbf{T}+\mathbf{I}) - 2\det(\mathbf{T}+\mathbf{I})\right). \end{aligned} \tag{2.28}$$

Thus in summary

$$(\mathbf{v}.\nabla)\det(\mathbf{T}+\mathbf{I}) = \left(\kappa \mathrm{tr}\left(\mathbf{T}\right)+1\right)\left(\mathrm{tr}\left(\mathbf{T}+\mathbf{I}\right) - 2\det\left(\mathbf{T}+\mathbf{I}\right)\right), \tag{2.29}$$

and we will later show that

$$\det(\mathbf{T}+\mathbf{I}) = \Delta_0\left(\frac{\psi}{C_0}\right)^{\frac{2(\alpha-1)}{n}}, \tag{2.30}$$

holds in the core region, with the constant Δ_0 and n able to be determined by matching to the upstream boundary layer. The analysis using this determinant relationship is contained in appendix B.

2.2.2 The natural stress basis equations

In addition to formulating the problem in a Cartesian system, we can use a natural basis aligned along streamlines, first proposed for application to problems of this kind by Renardy [Ren94]. This will be of benefit to further the analysis of the Cartesian basis to complete the description of the downstream boundary layer. We introduce the vector $\mathbf{w}$ given by

$$\mathbf{w} = (w_1, w_2)^{\mathrm{T}} = \left(-\frac{v}{u^2+v^2}, \frac{u}{u^2+v^2}\right)^{\mathrm{T}}, \tag{2.31}$$

which is orthogonal to $\mathbf{v}$ and satisfies $|\,\mathbf{v}\times\mathbf{w}\,| = 1$.

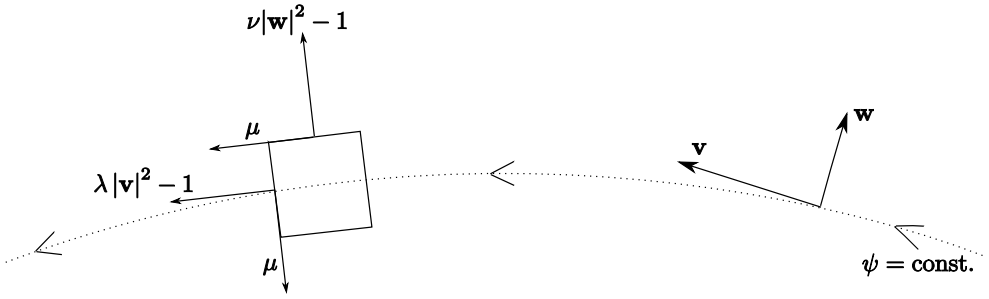

Figure 2-1: An illustration of a representative streamline along with an element traveling along the streamline. Shown are the basis vectors $\mathbf{v}$ and $\mathbf{w}$ of the natural stress formulation, where $\mathbf{v}$ is the fluid velocity, and $\mathbf{w}$ is a vector perpendicular to $\mathbf{v}$ as defined in (2.31). Also shown are the actions of the natural stress variables on a representative element.

The extra-stress tensor $\mathbf{T}$ can then be represented as

$$\mathbf{T} = -\mathbf{I} + \lambda \mathbf{v}\mathbf{v}^T + \mu(\mathbf{v}\mathbf{w}^T + \mathbf{w}\mathbf{v}^T) + \nu \mathbf{w}\mathbf{w}^T, \tag{2.32}$$

where $\lambda(x, y)$, $\mu(x, y)$, and $\nu(x, y)$ are the natural stress variables[3]. $\lambda(x, y)$ and $\nu(x, y)$ represent normal stresses along and perpendicular to the streamline, with $\mu(x, y)$ a shear stress. The vectors $\mathbf{v}$ and $\mathbf{w}$, along with the action of the natural stress variables on a representative element traveling along are streamline are shown in figure 2-1.

The relations between the Cartesian and natural stress bases are then

$$T_{11} = -1 + \lambda u^2 - \frac{2\mu uv}{|\mathbf{v}|^2} + \frac{\nu v^2}{|\mathbf{v}|^4}, \tag{2.33}$$

$$T_{12} = \lambda uv + \frac{\mu(u^2 - v^2)}{|\mathbf{v}|^2} - \frac{\nu uv}{|\mathbf{v}|^4}, \tag{2.34}$$

$$T_{22} = -1 + \lambda v^2 + \frac{2\mu uv}{|\mathbf{v}|^2} + \frac{\nu u^2}{|\mathbf{v}|^4}, \tag{2.35}$$

where $|\mathbf{v}|^2 = u^2 + v^2$, noting that $|\mathbf{w}|^2 = 1/|\mathbf{v}|^2$, and also (for future reference)

$$\det(\mathbf{T} + \mathbf{I}) = \lambda\nu - \mu^2. \tag{2.36}$$

[3]It may be also of interest to note that $\mathbf{w} = \frac{\nabla\psi}{|\mathbf{v}|^2}$, and that $\mathbf{v} = \nabla \times (\psi \mathbf{k})$.

Using these, our constitutive equations (2.15)-(2.17) become

$$\lambda + (\mathbf{v}.\nabla)\lambda + 2\mu\nabla.\mathbf{w} + \kappa\left(\lambda\left|\mathbf{v}\right|^2 - 2 + \frac{\nu}{\left|\mathbf{v}\right|^2}\right)\left(\lambda - \frac{1}{\left|\mathbf{v}\right|^2}\right) = \frac{1}{\left|\mathbf{v}\right|^2}, \tag{2.37}$$

$$\mu + (\mathbf{v}.\nabla)\mu + \nu\nabla.\mathbf{w} + \kappa\left(\lambda\left|\mathbf{v}\right|^2 - 2 + \frac{\nu}{\left|\mathbf{v}\right|^2}\right)\mu = 0, \tag{2.38}$$

$$\nu + (\mathbf{v}.\nabla)\nu + \kappa\left(\lambda\left|\mathbf{v}\right|^2 - 2 + \frac{\nu}{\left|\mathbf{v}\right|^2}\right)\left(\nu - \left|\mathbf{v}\right|^2\right) = \left|\mathbf{v}\right|^2, \tag{2.39}$$

where

$$\nabla.\mathbf{w} = \frac{1}{\left|\mathbf{v}\right|^4}\left((v^2 - u^2)\left(\frac{\partial v}{\partial x} + \frac{\partial u}{\partial y}\right) + 4uv\frac{\partial u}{\partial x}\right), \tag{2.40}$$

and the momentum equations (2.13)-(2.14) become

$$\text{Re}\ (\mathbf{v}.\nabla)u = -\frac{\partial p}{\partial x} + (\mathbf{v}.\nabla)(\lambda u) + \nabla.\left(\mu u\mathbf{w} + (\mu\mathbf{v} + \nu\mathbf{w})w_1\right), \tag{2.41}$$

$$\text{Re}\ (\mathbf{v}.\nabla)v = -\frac{\partial p}{\partial y} + (\mathbf{v}.\nabla)(\lambda v) + \nabla.\left(\mu v\mathbf{w} + (\mu\mathbf{v} + \nu\mathbf{w})w_2\right). \tag{2.42}$$

It is worth noting for comparison to the UCM model that

$$\begin{aligned}\kappa\ \text{tr}(\mathbf{T}) &= -2\kappa + \kappa\lambda(u^2 + v^2) + \frac{\kappa\nu(u^2 + v^2)}{\left|\mathbf{v}\right|^4} \\ &= \kappa\left(\lambda\left|\mathbf{v}\right|^2 - 2 + \frac{\nu}{\left|\mathbf{v}\right|^2}\right).\end{aligned} \tag{2.43}$$

2.3 Simple shear flow

An important flow to consider both to display some of the properties of the PTT fluid, and for use in the more complicated geometries of later sections is that of steady simple shear. It is with this flow that the crucial rheological property of viscosity can be understood clearly. In this situation, and for the flows considered in this thesis, viscosity will refer to shear-rate dependent viscosity and is defined as the ratio of the shear stress to the shear rate.

There is a thorough discussion in Chapter 3.1 of [Ren00b] of steady simple shear flow for the UCM, PTT, and other non-Newtonian fluids. Here we concentrate on the PTT fluid with reference to the results of other fluids for comparison.

In steady simple shear flow, the flow is purely two dimensional with the velocity a function of y solely in the x direction, i.e. $\mathbf{v} = (u(y), 0, 0)^T$. The quantities of interest will be the shear rate $\dot{\gamma} = \frac{du}{dy}$, the shear stress T_{12}, and the viscosity $\eta = \frac{T_{12}}{\dot{\gamma}}$, as well

as the first and second normal stress differences N_1 and N_2 defined as

$$N_1 = T_{11} - T_{22} \qquad \text{and} \qquad N_2 = T_{22} - T_{33}. \tag{2.44}$$

In a Newtonian fluid when sheared, the fluid resists the motion by developing the frictional force of viscosity. In a polymeric fluid, the polymer chains align with the flow, and hence this causes a tension force in the flow direction referred to as a 'normal stress'. There are a number of interesting effects associated with these non-zero normal stresses N_1 and N_2, such as the Weissenberg effect when a fluid may climb up a rotating rod, rather than the normal dip near the rod seen with a Newtonian fluid. More of these unusual effects and photos of the experiments may be found in [BW93].

As the flow profile is uniform in both x and z directions, the stresses in this flow regime are all functions of y, hence $T_{ij} = T_{ij}(y)$, and $T_{13} = T_{23} = 0$.

Substituting these quantities into the PTT constitutive equations (1.34) gives

$$\begin{aligned}
T_{11}\,(1 + \mathrm{We}\ \kappa(T_{11} + T_{22} + T_{33})) &= 2\mathrm{We}\ \dot{\gamma} T_{12},\\
T_{12}\,(1 + \mathrm{We}\ \kappa(T_{11} + T_{22} + T_{33})) &= \mathrm{We}\ \dot{\gamma} T_{22} + \dot{\gamma},\\
T_{22}\,(1 + \mathrm{We}\ \kappa(T_{11} + T_{22} + T_{33})) &= 0,\\
T_{33}\,(1 + \mathrm{We}\ \kappa(T_{11} + T_{22} + T_{33})) &= 0,
\end{aligned} \tag{2.45}$$

with the final two equations thus implying $T_{22} = T_{33} = 0$[4] (we consider $\kappa = O(1)$, $\mathrm{We} = O(1)$ here for comparison to UCM and Newtonian flow). This leaves

$$\begin{aligned}
T_{11}\,(1 + \mathrm{We}\ \kappa T_{11}) &= 2\mathrm{We}\ \dot{\gamma} T_{12},\\
T_{12}\,(1 + \mathrm{We}\ \kappa T_{11}) &= \dot{\gamma},
\end{aligned} \tag{2.47}$$

which upon eliminating T_{11} from the first of these using the second gives the equation for the shear stress as

$$2\mathrm{We}^2 \kappa T_{12}^3 + T_{12} = \dot{\gamma}. \tag{2.48}$$

Equation (2.48) shows that for small shear rates $T_{12} \sim \dot{\gamma}$ whereas for large shear rates $T_{12} \sim \left(\frac{\dot{\gamma}}{2\mathrm{We}^{\,2}\kappa}\right)^{\frac{1}{3}}$. From this we can determine the viscosity of the PTT model, which is recorded in table 2.1 along with the viscosities of the Newtonian and UCM models

[4]The final two equations in (2.45) could instead imply $\mathrm{We}\ \kappa(T_{11} + T_{22} + T_{33}) = -1$, leading to

$$T_{11} = \frac{\kappa - 1}{\mathrm{We}\ \kappa} - T_{33}, \qquad T_{12} = 0, \qquad T_{22} = -\frac{1}{\mathrm{We}}. \tag{2.46}$$

Significantly T_{12}, the shear stress, is zero and hence a physically unrealistic result for shear flow.

for comparison. It is clear from table 2.1 that the viscosity of the PTT model decreases as the shear rate is increased. This is the property of shear thinning, and a property the UCM model does not capture.

		Newtonian	UCM	PTT
η	Small $\dot{\gamma}$	1	1	~ 1
η	Large $\dot{\gamma}$	1	1	$\sim \left(\left(\frac{1}{2\mathrm{We}^2\kappa} \right)^{\frac{1}{3}} \dot{\gamma}^{-\frac{2}{3}} \right)$

Table 2.1: Table showing the (non-dimensionalised) viscosities of various fluid models.

The result that the UCM model has a constant viscosity may be surprising in that it is supposed to be a non-Newtonian model. The non-Newtonian nature only becomes apparent when comparing the normal stress differences. For a Newtonian fluid in shear flow, the normal stress differences $N_1 = N_2 = 0$, however, for a UCM fluid $N_1 = \frac{2\dot{\gamma}^2}{\mathrm{We}}$ and $N_2 = 0$. For the PTT fluid since $T_{22} = T_{33} = 0$, we again have $N_2 = 0$, but from the first equation in (2.47) we can see that for small shear rates N_1 is proportional to $\dot{\gamma}^2$, but proportional to $\dot{\gamma}^{\frac{2}{3}}$ at high shear rates.

Engineering Rheology [Tan00], section 3.8, contains experimental data from various authors. A large amount of excellent data is from [Mei75], figure 7 in particular showing clearly the shear thinning behaviour of three low density polyethylene samples - examples of polymer melts (reproduced in [Tan00] in Fig. 3.17). Table 3.9 of [Tan00] gives values of N_2/N_1 for a range of fluids from various sources, confirming the credentials of the PTT equations for modelling these fluids.

2.3.1 Viscometric behaviour

The main use of simple shear flow behaviour in this thesis is that it is expected that the flow near the walls in the geometries considered later will satisfy similar behaviour. The stream function will be expected to vanish as $\psi \sim O(y^2)$ as $y \to 0$ (y being a Cartesian coordinate away from the wall), thus satisfying both no slip and no normal velocity, and this, with the resulting stresses is termed viscometric behaviour. We consider the governing equations in two dimensions with the velocities represented in the usual stream function form (2.19), and assume the stream function behaviour

$$\psi \sim \frac{1}{2}\dot{\gamma}y^2, \qquad \text{as} \qquad y \to 0, \tag{2.49}$$

still with $T_{ij} = T_{ij}(y)$. Substituting these into the constitutive relations (1.34) we obtain

$$\begin{aligned} T_{11}\left(1 + \text{We }\kappa(T_{11}+T_{22})\right) - 2\text{We }\dot{\gamma}T_{12} &= 0, \\ T_{22}\left(1 + \text{We }\kappa(T_{11}+T_{22})\right) &= 0, \\ T_{12}\left(1 + \text{We }\kappa(T_{11}+T_{22})\right) - \text{We }\dot{\gamma}T_{22} &= \dot{\gamma}, \end{aligned} \tag{2.50}$$

with the T_{22} equation implying $T_{22} = 0$ (and once again we ignore unphysical solution of We $\kappa(T_{11} + T_{22}) = -1$, commented on in footnote 4). Simplifying equations (2.50) we find

$$T_{22} = 0, \qquad T_{11} + \text{We }\kappa T_{11}^2 = 2\text{We }\dot{\gamma}T_{12}, \qquad \text{and} \qquad T_{12} + \text{We }\kappa T_{11}T_{12} = \dot{\gamma}, \tag{2.51}$$

which imply that

$$T_{22} = 0, \qquad \dot{\gamma} - T_{12} = 2\text{We}^2\kappa T_{12}^3, \qquad \text{and} \qquad T_{11} = 2\text{We }T_{12}^2, \tag{2.52}$$

as found in [HR97]. The behaviour takes different forms depending on the shear rate. When the shear rate is large, $\dot{\gamma} \gg 1$, the viscometric behaviour satisfies

$$\psi \sim \frac{1}{2}\dot{\gamma}y^2, \qquad T_{11} \sim 2\text{We }\left(\frac{\dot{\gamma}}{2\text{We}^2\kappa}\right)^{2/3}, \qquad T_{12} \sim \left(\frac{\dot{\gamma}}{2\text{We}^2\kappa}\right)^{1/3}, \qquad T_{22} = 0, \tag{2.53}$$

and when $\dot{\gamma} \ll 1$ the behaviour is instead

$$\psi \sim \frac{1}{2}\dot{\gamma}y^2, \qquad T_{11} \sim 2\text{We }\dot{\gamma}^2, \qquad T_{12} \sim \dot{\gamma}, \qquad T_{22} = 0, \tag{2.54}$$

which is in fact the same as the viscometric behaviour found for the UCM model.

The above viscometric behaviours apply when $\kappa = O(1)$ and We $= O(1)$, with high shear rate, $\dot{\gamma} \gg 1$, applicable to re-entrant corner flow and low shear rate, $\dot{\gamma} \ll 1$, applicable to salient corner flow (these geometries are defined at the start of chapter 3). Chapter 4 however contains analysis for re-entrant corner flow in the parameter regimes of small κ (with We $= O(1)$), and low and high We, (with $\kappa = O(1)$). There is a complex relationship in the second equation of (2.52) between T_{12}, κ and We in these large and small parameter limits, to determine the applicable viscometric behaviour. We consider the behaviour for re-entrant corner flow such that all behaviours occur with $\dot{\gamma} \gg 1$, and are summarised in table 2.2, where two further forms of viscometric behaviour (in addition to (2.53) and (2.54)) are found to be relevant. This table is of interest as it predicts the critical length scales of the asymptotic structures in chapter

4. Firstly a possible behaviour in the small κ limit is

$$\psi \sim \frac{1}{2}\dot{\gamma}y^2, \quad T_{11} \sim \frac{2}{\kappa}\mathrm{We}\ b^2, \quad T_{12} \sim \frac{b}{\kappa^{1/2}}, \quad T_{22} = 0, \quad \text{where} \quad \dot{\gamma} = \frac{b + 2\mathrm{We}^2 b^3}{\kappa^{1/2}}, \tag{2.55}$$

and secondly, a possible behaviour for the small We limit is

$$\psi \sim \frac{1}{2}\dot{\gamma}y^2, \quad T_{11} \sim \frac{2}{\mathrm{We}}b^2, \quad T_{12} \sim \frac{b}{\mathrm{We}}, \quad T_{22} = 0, \quad \text{where} \quad \dot{\gamma} = \frac{b + 2\kappa b^3}{\mathrm{We}}, \tag{2.56}$$

the full conditions for when these apply are given in table 2.2. The viscometric behaviour of the multiple limits ($\mathrm{We} \ll 1, \kappa = o(1)$) and ($\mathrm{We} \gg 1, \kappa = o(1)$) are not included as the full analysis in these situations are left as open problems.

Parameter Regime	T_{12} condition	Viscometric behaviour form
$\mathrm{We} = O(1)$, $\kappa \ll 1$	$1 \ll T_{12} \ll \kappa^{-1/2}$	$T_{11} \sim 2\mathrm{We}\frac{\partial^2\psi}{\partial y^2}T_{12}$, $T_{12} \sim \frac{\partial^2\psi}{\partial y^2}$, see (2.54)
$\mathrm{We} = O(1)$, $\kappa \ll 1$	$T_{12} = O\left(\kappa^{-1/2}\right)$	$T_{11} \sim 2\mathrm{We}\frac{\partial^2\psi}{\partial y^2}T_{12} - \mathrm{We}\kappa T_{11}^2$, $T_{12} \sim \frac{\partial^2\psi}{\partial y^2} - \mathrm{We}\kappa T_{11}T_{12}$, see (2.55)
$\mathrm{We} = O(1)$, $\kappa \ll 1$	$1 \ll \kappa^{-1/2} \ll T_{12}$	$\kappa T_{11}^2 \sim 2\frac{\partial^2\psi}{\partial y^2}T_{12}$, $\mathrm{We}\kappa T_{11}T_{12} \sim \frac{\partial^2\psi}{\partial y^2}$, see (2.53)
$\mathrm{We} \ll 1$, $\kappa = O(1)$	$1 \ll T_{12} \ll \mathrm{We}^{-1}$	$T_{11} \sim 2\mathrm{We}\frac{\partial^2\psi}{\partial y^2}T_{12}$, $T_{12} \sim \frac{\partial^2\psi}{\partial y^2}$, see (2.54)
$\mathrm{We} \ll 1$, $\kappa = O(1)$	$T_{12} = O\left(\mathrm{We}^{-1}\right)$	$T_{11} \sim 2\mathrm{We}\frac{\partial^2\psi}{\partial y^2}T_{12} - \mathrm{We}\kappa T_{11}^2$, $T_{12} \sim \frac{\partial^2\psi}{\partial y^2} - \mathrm{We}\kappa T_{11}T_{12}$, see (2.56)
$\mathrm{We} \ll 1$, $\kappa = O(1)$	$1 \ll \mathrm{We}^{-1} \ll T_{12}$	$\kappa T_{11}^2 \sim 2\frac{\partial^2\psi}{\partial y^2}T_{12}$, $\mathrm{We}\kappa T_{11}T_{12} \sim \frac{\partial^2\psi}{\partial y^2}$, see (2.53)
$\mathrm{We} \gg 1$, $\kappa = O(1)$	$1 \ll T_{12}$	$\kappa T_{11}^2 \sim 2\frac{\partial^2\psi}{\partial y^2}T_{12}$, $\mathrm{We}\kappa T_{11}T_{12} \sim \frac{\partial^2\psi}{\partial y^2}$, see (2.53)

Table 2.2: Table showing the expected viscometric behaviour as $y \to 0$ for various parameter regimes. In all cases the shear rate is taken to be large, $\dot{\gamma} \gg 1$, for application to the re-entrant corner geometry. The terms of the constitutive equations which contribute are listed in the final column (with additionally, in all cases $T_{22} = 0$ for viscometric behaviour), along with a reference to the equation containing the appropriate behaviour.

Irrespective of the form of the viscometric behaviour, the form of the stream function (equation (2.49)) and stresses being $T_{ij} = T_{ij}(y)$ with $T_{22} = 0$ for all forms, then the momentum equations immediately imply that the pressure must be independent of y, or equivalently

$$p = p(\dot{\gamma}). \tag{2.57}$$

When imposing viscometric behaviour as a boundary condition at a wall, the leading order behaviour implied by the above equations will be required. In re-entrant corner flow (in the initial $\kappa = O(1)$, We $= O(1)$ problem) a high shear rate at the wall is expected, and thus the behaviour is expected to come from equation (2.53) with We $= 1$ from the scaling mentioned in (2.18). It follows that the expected viscometric behaviour is

$$\psi \sim \kappa a^3 y^2, \qquad T_{11} \sim 2a^2, \qquad T_{12} \sim a, \qquad T_{22} = 0, \tag{2.58}$$

after setting $\dot{\gamma} = 2\kappa a^3$. Viscometric behaviour in natural stress can be found using (2.52) and the relationship equations (2.33)-(2.35), giving

$$\lambda = \frac{1 + 2\mu^2}{\dot{\gamma}^2 y^2}, \qquad \mu = \dot{\gamma} - 2\kappa\mu^3, \qquad \nu = \dot{\gamma}^2 y^2, \tag{2.59}$$

so clearly λ is unbounded at the boundary $y = 0$. Setting $\dot{\gamma} = 2\kappa a^3$ once again and considering the leading order behaviour we have

$$\lambda \sim \frac{1 + 2a^2}{4\kappa^2 a^6 y^2}, \qquad \mu \sim a, \qquad \nu \sim 4\kappa^2 a^6 y^2, \tag{2.60}$$

and if $1 \ll 2a^2$ then this finally reduces to

$$\lambda \sim \frac{1}{2\kappa^2 a^4 y^2}, \qquad \mu \sim a, \qquad \nu \sim 4\kappa^2 a^6 y^2. \tag{2.61}$$

These behaviours (2.58) and (2.61) are expected to be the relevant behaviours for the re-entrant corner flow of chapter 3.

2.3.2 An extension to viscometric behaviour

Having found a leading order solution at the wall where $\psi \sim \frac{1}{2}\dot{\gamma} y^2$, it is now of interest to consider a ψ behaviour with an arbitrary power of y. This could apply either in the limit of $\dot{\gamma} \to 0$, where we would expect $\psi = O(y^n)$ with $n > 2$, or when investigating a more general stream function away from the walls.

Substituting

$$\psi \sim a y^n, \tag{2.62}$$

and $T_{ij} = T_{ij}(y)$ into the constitutive equations (1.34) we obtain

$$T_{11} + \text{We } \left(-2an(n-1)y^{n-2}T_{12} + \kappa(T_{11}+T_{22})T_{11}\right) = 0, \tag{2.63}$$

$$T_{22} + \text{We } \left(\kappa(T_{11}+T_{22})T_{22}\right) = 0, \tag{2.64}$$

$$T_{12} + \text{We } \left(-an(n-1)y^{n-2}T_{22} + \kappa(T_{11}+T_{22})T_{12}\right) = an(n-1)y^{n-2}. \tag{2.65}$$

The y exponent, n, could be any number provided that $\psi = \frac{\partial \psi}{\partial y} = 0$ on $y = 0$ to satisfy the no-slip and no normal velocity conditions, i.e. $n > 1$. The second equation above, (2.64), implies that

$$T_{22}\left(1 + \text{We } \kappa(T_{11}+T_{22})\right) = 0, \tag{2.66}$$

and hence

$$\text{We } \kappa(T_{11}+T_{22}) = -1, \qquad \text{or} \qquad T_{22} = 0. \tag{2.67}$$

Case (a), $\text{We}\,\kappa(T_{11}+T_{22}) = -1$

Equations (2.63) and (2.65) become

$$T_{11} - \text{We } \left(2an(n-1)y^{n-2}T_{12}\right) - T_{11} = 0, \tag{2.68}$$

$$T_{12} - \text{We } \left(an(n-1)y^{n-2}T_{22}\right) - T_{12} = an(n-1)y^{n-2}. \tag{2.69}$$

which thus implies that

$$T_{12} = 0, \qquad T_{22} = -\frac{1}{\text{We}}, \qquad \text{and} \qquad T_{11} = \frac{1}{\text{We}}\left(1 - \frac{1}{\kappa}\right). \tag{2.70}$$

As before in footnote 4, this behaviour is unrealistic as in shear flow the shear stress would not be expected to be zero.

Case (b), $T_{22} = 0$

Equations (2.63) and (2.65) become

$$T_{11} + \text{We } \left(-2an(n-1)y^{n-2}T_{12} + \kappa T_{11}^2\right) = 0, \tag{2.71}$$

$$T_{12} + \text{We } \kappa T_{11}T_{12} = an(n-1)y^{n-2}, \tag{2.72}$$

which can be simplified to

$$T_{12} = an(n-1)y^{n-2} - 2\text{We}^2\kappa T_{12}^3, \qquad T_{11} = 2\text{We } T_{12}^2. \tag{2.73}$$

As previously in the standard viscometric case, we consider a both large and small. When $a \ll 1$ the behaviours become

$$T_{22} = 0, \qquad T_{12} \sim an(n-1)y^{n-2}, \qquad T_{11} \sim 2\mathrm{We}\ \left(an(n-1)\right)^2 y^{2n-4}, \tag{2.74}$$

whereas when $a \gg 1$ the behaviours become

$$T_{22} = 0, \qquad T_{12} \sim \left(\frac{an(n-1)}{2\mathrm{We}^2\kappa}\right)^{\frac{1}{3}} y^{\frac{1}{3}(n-2)}, \qquad T_{11} \sim 2\mathrm{We}\ \left(\frac{(an(n-1))^2}{4\mathrm{We}^2\kappa^2}\right)^{\frac{1}{3}} y^{\frac{2}{3}(n-2)}, \tag{2.75}$$

and can be simplified by setting

$$\tilde{a} = \left(\frac{an(n-1)}{2\mathrm{We}^2\kappa}\right)^{\frac{1}{3}}, \tag{2.76}$$

hence

$$T_{22} = 0, \qquad T_{12} \sim \tilde{a} y^{\frac{1}{3}(n-2)}, \qquad T_{11} \sim 2\mathrm{We}\ \tilde{a}^2 y^{\frac{2}{3}(n-2)}. \tag{2.77}$$

It can be seen from these equations that integer powers of y will occur when $n = 2+3k$ for $k \in \mathbf{N}$, the first two occurring when $\psi \sim ay^2$ and $\psi \sim ay^5$. When the limit $\dot{\gamma} \to 0$ is considered for the re-entrant corner problem in section 3.2.3 later, the $n = 5$ case is shown to be relevant.

Chapter 3

Re-entrant corner flow $\kappa = O(1)$, $\mathrm{We} = O(1)$

The central problem of this thesis is that of the re-entrant corner flow of the PTT fluid when both the Weissenberg number and the PTT model parameter κ are both $O(1)$ quantities. The preceding chapters have provided a general introduction and contain some preliminary results, with the later chapters relying on the analysis contained here. We define two types of sharp corner. A salient corner has an angle of less than 180°, whereas a re-entrant corner is greater than 180°[5].

Section 3.1 gives a further introduction specific to the corner, and contains the fundamental results upon which the analysis of this chapter will be based. We begin by motivating the analysis of this corner geometry before defining the problem precisely in sections 3.1.1-3.1.2. Following this the solution for core flow, the solution away from the walls, is found in sections 3.1.3-3.1.4.

Analytical work to find the asymptotic structure, the balances appropriate in each region, and how to correctly define and set up the boundary layer problem is all contained in section 3.2. Given its comparative complexity, a detailed explanation of how the analysis is undertaken and structured may be found at the beginning of the section. Also of note is that the analysis will proceed simultaneously in both Cartesian and natural stress bases (see section 2.2 for the description of these bases).

The boundary layer equations found in section 3.2 have to be solved numerically. In section 3.3 we detail how our numerical scheme is implemented followed by the numerical results and analysis. Section 3.3.1 solves the upstream boundary layer using

[5]There is some discussion by Tanner in chapter 8 of Engineering Rheology, [Tan00], on the naming of these corners. Here the widely adopted names from the literature (in particular in the papers discussed in section 1.4) have been used, with the description re-entrant referring to the corner protruding into the fluid.

the Cartesian formulation, with section 3.3.2 completing the analysis in the natural stress basis by providing results for both upstream and downstream boundary layers.

This chapter concludes with a discussion of the results. Of particular interest is the comparison to the re-entrant corner flow of the UCM fluid, along with the surprising result that the analysis is found to hold only for corner angles between 180^o and 270^o.

3.1 Introduction and preliminary analysis

3.1.1 Motivation

The mathematical modelling of fluid flow in or around a sharp corner is of vital importance to modelling flow in a variety of situations. In particular, contraction and extrusion flows (a contraction shown in figure 3-1), where both salient and re-entrant corner flows occur.

A contraction can occur when fluid flows between two pipes of different diameters, and in this case the re-entrant corner has a 270° angle. The singularities produced by the corner cause difficulties in numerical simulation, and hence a detailed mathematical model of the situation is required so that accurate predictions of the stresses created can be made. We investigate two dimensional planar flows, which have direct application to the contraction and extrusion flows with both rectangular and axisymmetric channels, all of which are standard benchmark problems for numerical schemes.

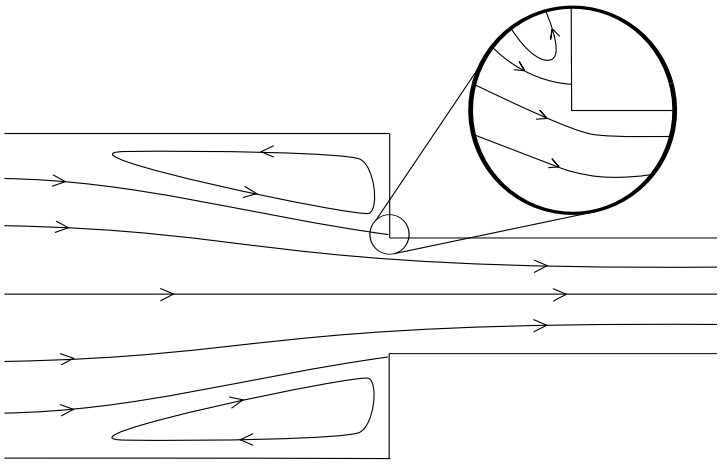

Figure 3-1: Diagram showing a contraction. Clearly shown are regions of recirculation in the salient corners, with inset the region close to one of the re-entrant corners displaying complete flow around the corner. Numerical simulations of contraction flows show this region of recirculation reaching the re-entrant corners on some occasions or show the presence of upstream lip vortices. Our analysis will however assume complete flow around the corner as in the situation shown.

3.1.2 Problem statement

Figure 3-2 shows the re-entrant corner geometry. We consider the two dimensional sector $0 < r < \infty$, $0 \leq \theta \leq \pi/\alpha$, with $\theta = 0$ representing the upstream wall and $\theta = \pi/\alpha$ the downstream wall (so that $1/2 \leq \alpha < 1$). Here (r, θ) are polar coordinates centred on the corner. Cartesian axes will be taken with the x-axis along the upstream wall and the y-axis along the ray $\theta = \pi/2$. On both solid walls both no-slip and no normal velocity boundary conditions apply ($\mathbf{v}=\mathbf{0}$ on the walls), in our case we prefer to write

$$\psi = \frac{\partial \psi}{\partial \theta} = 0, \qquad \text{on} \quad \theta = 0, \ \frac{\pi}{\alpha}. \tag{3.1}$$

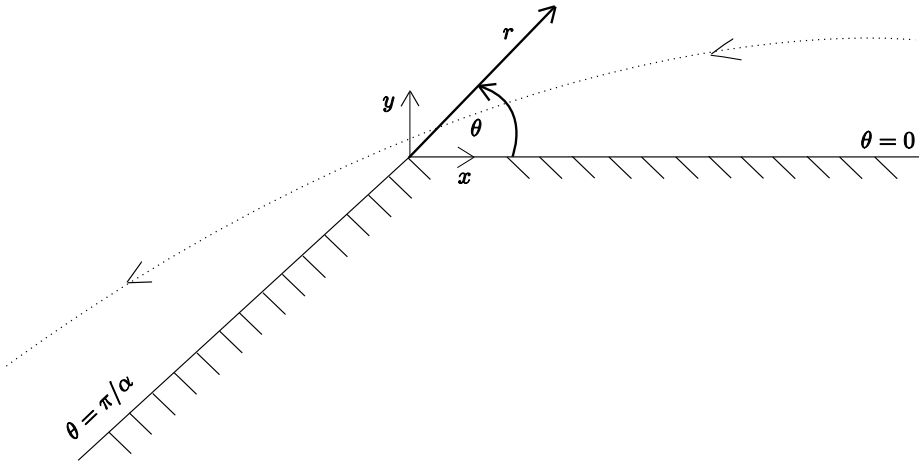

Figure 3-2: An illustration of the re-entrant corner geometry, showing clearly both Cartesian and polar axes centered on the corner, with the flow direction from right to left. On the walls both no-slip and no normal velocity boundary conditions apply.

To progress, we consider the flow away from the walls in a core (outer) region, and attempt to find a dominant balance in the constitutive equations (1.34).

3.1.3 The core balance

Crucial to the analysis of the re-entrant corner flow with $\kappa = O(1)$, We $= O(1)$ is that the upper convected stress derivative is assumed to dominate in the outer region, i.e.

$$\overset{\triangledown}{\mathbf{T}} + o(1) = 0, \qquad \text{as } r \to 0. \tag{3.2}$$

This assumption can be intuitively justified by considering the orders of magnitude of the terms in the PTT constitutive equation (1.34). Setting $\psi = O(r^k)$ and $\mathbf{T} = O(r^{-m})$

for unknown k, m, with $m > 0$ due to the assumed stress singularity at the corner, the terms in (1.34) are then

$$\mathbf{T} = O(r^{-m}), \quad \overset{\triangledown}{\mathbf{T}} = O(r^{k-2-m}), \quad (\mathrm{tr}\mathbf{T})\,\mathbf{T} = O(r^{-2m}), \quad \mathbf{D} = O(r^{k-2}). \tag{3.3}$$

The upper convected stress derivative dominates over the rate of strain terms $\mathbf{D}$ since $m > 0$, and over the stress terms $\mathbf{T}$ assuming $k < 2$. This assumption is physically realistic as the fluid is expected to accelerate around a re-entrant corner, becoming infinite as $r \to 0$ (the opposite being true for the salient corner geometry, where the fluid becomes stagnant at the corner). Finally $\overset{\triangledown}{\mathbf{T}} \gg (\mathrm{tr}\mathbf{T})\,\mathbf{T}$ if $k < 2 - m$. From this analysis, the two possible balances are

$$\overset{\triangledown}{\mathbf{T}} + o(1) = 0, \qquad \text{or} \quad \overset{\triangledown}{\mathbf{T}} + \kappa\,(\mathrm{tr}\mathbf{T})\,\mathbf{T} + o(1) = 0, \qquad \text{as } r \to 0, \tag{3.4}$$

however the second of these has been discussed briefly by Renardy in [Ren97c] with the conclusion that it is physically unrealistic.

Renardy's argument benefits from the use of the natural stress formulation, with a modification of equation (2.32) due to the fact that in this core region $\mathbf{T}$ is expected to dominate over $\mathbf{I}$, the identity matrix, as seen by $\mathbf{T} = O(r^{-m})$ with $m > 0$ mentioned above. Thus the transformation takes the form

$$\mathbf{T} = \lambda \mathbf{v}\mathbf{v}^T + \mu(\mathbf{v}\mathbf{w}^T + \mathbf{w}\mathbf{v}^T) + \nu \mathbf{w}\mathbf{w}^T, \tag{3.5}$$

in the core region with the second balance in (3.4) becoming

$$\left.\begin{aligned} (\mathbf{v}.\nabla)\lambda + 2\mu\nabla.\mathbf{w} + \kappa\,(\mathrm{tr}\mathbf{T})\,\lambda = 0, \\ (\mathbf{v}.\nabla)\mu + \nu\nabla.\mathbf{w} + \kappa\,(\mathrm{tr}\mathbf{T})\,\mu = 0, \\ (\mathbf{v}.\nabla)\nu + \kappa\,(\mathrm{tr}\mathbf{T})\,\nu = 0, \end{aligned}\right\} \quad \text{where} \quad \mathrm{tr}\mathbf{T} = \lambda\,|\mathbf{v}|^2 + \frac{\nu}{|\mathbf{v}|^2}. \tag{3.6}$$

The argument in [Ren97c] asserts that tr$\mathbf{T}$ should be positive[6], and thus the last equation determines that ν decreases monotonically along streamlines. In our corner situation, this prevents matching between upstream and downstream boundary layers, as the information from the upstream cannot be communicated through the core unchanged. The possibility of $\nu = 0$ then produces recursive arguments that $\mu = \lambda = 0$ similarly, with the conclusion then that the tr$\mathbf{T}$ terms must be of lower order and the

[6] In corner flow, in the core region away from the walls, the stress component along streamlines $\lambda\mathbf{v}\mathbf{v}^T$ will be far larger than the component perpendicular, $\nu\mathbf{w}\mathbf{w}^T$. λ will also be uniformly positive, as the fluid is being stretched around the corner. Using these observations it is clear that $\mathrm{tr}\mathbf{T} = \lambda\,|\mathbf{v}|^2 + \frac{\nu}{|\mathbf{v}|^2} > 0$.

first balance in (3.4) holds.

Further work to analyse the second balance in (3.4) would certainly be of interest however, especially as it appears to be the correct core balance for the PTT fluid in a wedge geometry (see initial results in appendix C). The previous argument does not apply in the wedge geometry as in either sink or source wedge flows there is no need to communicate information between boundary layers, being equivalent to upstream boundary layers in sink flow, and downstream boundary layers in source flow.

The analysis here will concentrate on the balance in (3.2) with the upper convected stress derivative dominating. The solution to this balance $\mathbf{T} = \lambda(\psi)\mathbf{v}\mathbf{v}^T$, discussed in section 3.1.4, is physically realistic as near the corner (away from the walls) the velocity gradients are high, and thus comparing the natural stress formulation of the stress in equation (2.32), the $\lambda\mathbf{v}\mathbf{v}^T$ would indeed be expected to dominate.

3.1.4 The core solution

Away from the boundaries in the outer (core flow) region we expect the upper convected stress derivative terms to dominate as in (3.2) with the momentum and continuity equations still applicable. As mentioned in section 3.1.3 this has a solution of the form

$$\mathbf{T} = \lambda(\psi)\mathbf{v}\mathbf{v}^T, \tag{3.7}$$

or in component form $T_{ij} = \lambda(\psi)v_i v_j$, which is physically realistic as in this region we expect the fluid to advect and deform affinely - there is no slip of the polymer in the solvent, and thus the stresses occur along streamlines in the $\mathbf{v}\mathbf{v}^T$ direction (see for example [Hin93], [Ren93]). The momentum equation becomes

$$\begin{aligned}
&\text{Re } v_k \frac{\partial}{\partial x_k} v_i = -\frac{\partial p}{\partial x_i} + \frac{\partial T_{ik}}{\partial x_k} \\
\Rightarrow \quad &\text{Re } v_k \frac{\partial v_i}{\partial x_k} = -\frac{\partial p}{\partial x_i} + \frac{\partial}{\partial x_k}\lambda(\psi)v_i v_k + \lambda(\psi)\left(\frac{\partial v_i}{\partial x_k}v_k + \frac{\partial v_k}{\partial x_k}v_i\right) \\
\Rightarrow \quad &\text{Re } v_k \frac{\partial v_i}{\partial x_k} = -\frac{\partial p}{\partial x_i} + v_i v_k \frac{\partial \lambda(\psi)}{\partial x_k} + \lambda(\psi)v_k \frac{\partial v_i}{\partial x_k} + \lambda(\psi)\frac{\partial v_k}{\partial x_k} \\
\Rightarrow \quad &(\text{Re } - \lambda(\psi))\, \mathbf{v}.\nabla v_i = -\frac{\partial p}{\partial x_i} + v_i \mathbf{v}.\nabla\lambda(\psi) + \lambda(\psi)v_i \nabla.\mathbf{v} \\
\Rightarrow \quad &(\text{Re } - \lambda(\psi))\, \mathbf{v}.\nabla v_i = -\frac{\partial p}{\partial x_i},
\end{aligned} \tag{3.8}$$

which is a form of the Euler equations. Assuming that $\lambda(\psi) \gg$ Re since the inertia terms are expected to be subdominant to the pressure and stress terms in the momen-

tum equation, we may now consider the equation

$$\lambda(\psi)\mathbf{v}.\nabla\mathbf{v} - \nabla p = 0. \tag{3.9}$$

Before attempting to find a solution for both the stream function and $\lambda(\psi)$, we re-write equation (3.9) along streamlines as a modified form of Bernoulli's equation to solve for the pressure. Considering a streamline parameter s, such that along a streamline $x = x(s)$, $y = y(s)$, then (3.9) becomes[7]

$$\lambda(\psi)\frac{d\mathbf{v}}{ds} = \begin{pmatrix} \frac{1}{u}\left(\frac{dp}{ds} - v\frac{\partial p}{\partial y}\right) \\ \frac{1}{v}\left(\frac{dp}{ds} - u\frac{\partial p}{\partial x}\right) \end{pmatrix}. \tag{3.12}$$

Adding the two equations of (3.12), this simplifies to

$$\frac{d}{ds}\left(p - \left(\frac{1}{2}\lambda\left|\mathbf{v}\right|^2\right)\right) = 0, \qquad \text{thus} \qquad p = P_0(\psi) + \frac{1}{2}\lambda\left|\mathbf{v}\right|^2, \tag{3.13}$$

where $P_0(\psi)$ is an arbitrary function of the stream function appearing from the integration. To derive this result we have used information from footnote 7, and that $\lambda(\psi)$ is constant along a streamline.

Returning to equation (3.9), we progress by introducing the vector $\mathbf{u} = \lambda^{\frac{1}{2}}\mathbf{v}$ simplifying (3.9) to

$$\mathbf{u}.\nabla\mathbf{u} - \nabla p = 0. \tag{3.14}$$

The vector $\mathbf{u}$ still satisfies the continuity equation since

$$\nabla.\mathbf{u} = \nabla.(\lambda^{\frac{1}{2}}\mathbf{v}) = \mathbf{v}.\nabla\lambda^{\frac{1}{2}} + \lambda^{\frac{1}{2}}\nabla.\mathbf{v} = 0. \tag{3.15}$$

It is also noteworthy that equation (3.14) may also be derived from the natural stress momentum equations using the same form for $\mathbf{u}$. Continuing with this equation

$$\nabla p = \mathbf{u}.\nabla\mathbf{u} = (\nabla\times\mathbf{u})\times\mathbf{u} + \nabla\left(\frac{1}{2}\left|\mathbf{u}\right|^2\right) = \mathbf{\Omega}\times\mathbf{u} + \nabla\left(\frac{1}{2}\left|\mathbf{u}\right|^2\right), \tag{3.16}$$

[7] The chain rule implies that

$$\frac{d}{ds} = \frac{dx}{ds}\frac{\partial}{\partial x} + \frac{dy}{ds}\frac{\partial}{\partial y} = \left(\frac{dx}{ds}, \frac{dy}{ds}\right)^T.\nabla, \tag{3.10}$$

where $\frac{d}{ds}$ is the rate of change along a streamline (i.e. in the direction of the velocity $\mathbf{v}$). Thus we also have

$$\frac{d}{ds} = \mathbf{v}.\nabla, \qquad \text{implying that} \qquad u = \frac{dx}{ds}, \quad v = \frac{dy}{ds}. \tag{3.11}$$

and taking the curl of both sides (to simplify since the curl of a gradient is zero) then gives

$$\mathbf{0} = \nabla \times (\mathbf{\Omega} \times \mathbf{u}) = (\mathbf{u}.\nabla)\,\mathbf{\Omega} - (\mathbf{\Omega}.\nabla)\,\mathbf{u} + \mathbf{\Omega}\,(\nabla.\mathbf{u}) - \mathbf{u}\,(\nabla.\mathbf{\Omega}) = (\mathbf{u}.\nabla)\,\mathbf{\Omega}. \tag{3.17}$$

Now since $\mathbf{\Omega}$ is the two-dimensional vorticity,

$$\mathbf{\Omega} = \left(\frac{\partial \tilde{v}}{\partial x} - \frac{\partial \tilde{u}}{\partial y}\right)\mathbf{k} = \left(-\frac{\partial^2 \tilde{\psi}}{\partial x^2} - \frac{\partial^2 \tilde{\psi}}{\partial y^2}\right)\mathbf{k} = -\left(\nabla^2 \tilde{\psi}\right)\mathbf{k} = \Omega\mathbf{k}. \tag{3.18}$$

Thus by solving $0 = (\mathbf{u}.\nabla)\,\Omega$ as $\Omega = -f(\tilde{\psi})$, where $f(\tilde{\psi})$ is an arbitrary function of $\tilde{\psi}$, then

$$\nabla^2 \tilde{\psi} = f(\tilde{\psi}). \tag{3.19}$$

This in addition has to satisfy the boundary conditions

$$\tilde{\psi} = 0, \qquad \text{on } \theta = 0,\ \frac{\pi}{\alpha}, \tag{3.20}$$

as $\mathbf{u}$ is parallel to $\mathbf{v}$.

In all previous work in the literature (in particular [Hin93], [Ren93], [Ren95], [Eva05b], [Eva08a], [RH04]) the solution pursued is the homogeneous solution of the Poisson equation (3.19), thus making the assumption that $f(\tilde{\psi}) = 0$. A brief reasoning for this case being the physically realistic solution to investigate is given in section 7.2 of [Ren00b]. From the order of magnitude estimates for the core balance in section 3.1.3, then as $\psi = O(r^k)$ where $k < 2$, the function f would satisfy $f = O(r^{k/n-2})$ if a balance with the Laplacian term in (3.19) is made (This is explained in (3.24) where $\psi = O(\tilde{\psi}^n)$, and n is found to satisfy $n > 1$). This implies that the f is singular as $r \to 0$, which would lead to singular behaviour of the stream function and as such it is unlikely that such a situation is physically relevant. It is interesting to analyse this case, if only as it has not been considered in the literature, to investigate the possible alternative stream function solutions. Analysis to include the forcing term f at leading order is contained in appendix D.

Continuing here with the solution of the homogeneous equation (3.19), Laplace's equation in two-dimensional polar coordinates is

$$\frac{1}{r}\frac{\partial}{\partial r}\left(r\frac{\partial \tilde{\psi}}{\partial r}\right) + \frac{1}{r^2}\frac{\partial^2 \tilde{\psi}}{\partial \theta^2} = 0. \tag{3.21}$$

Using separation of variables, this can be solved to give the solutions

$$\begin{aligned} \tilde{\psi} &= \left(A_j r^j + \tfrac{B_j}{r^j}\right)\left(C_j \cos(j\theta) + D_j \sin(j\theta)\right), && \text{for } j \in \mathbb{C}\backslash\{0\}, \\ \tilde{\psi} &= A_c + A_0 \log r + B_0\theta, && \text{for } j = 0, \end{aligned} \tag{3.22}$$

where A_j, B_j, C_j, D_j, A_c, A_0, and B_0, are all arbitrary constants. We require a real stream function solution that satisfies $\tilde{\psi} = 0$ on $\theta = 0$, $\frac{\pi}{\alpha}$, and that has nonsingular behaviour as $r \to 0$, then $j > 0 \in \mathbb{R}$. The first j to satisfy these requirements, giving the dominant solution as $r \to 0$ is

$$\tilde{\psi} = A_h r^\alpha \sin(\alpha\theta), \tag{3.23}$$

where $A_h \in \mathbb{R}$ is an arbitrary constant. $\tilde{\psi}$ is the stream function for $\mathbf{u}$, not the true velocity field $\mathbf{v}$, but as they are parallel and thus have the same streamlines, then the true stream function ψ must be a function of $\tilde{\psi}$. Making the assumption that

$$\psi = g(\tilde{\psi}) = \tilde{c}_1 \tilde{\psi}^n, \tag{3.24}$$

where $\tilde{c}_1$ and n are constants, then

$$\frac{\partial \tilde{\psi}}{\partial y} = \lambda^{1/2}\frac{\partial \psi}{\partial y} = n\tilde{c}_1 \lambda^{1/2}\tilde{\psi}^{n-1}\frac{\partial \tilde{\psi}}{\partial y}. \tag{3.25}$$

Therefore we may determine

$$\lambda(\psi) = \left(n\tilde{c}_1^{\frac{1}{n}}\right)^{-2} \psi^{\frac{2(1-n)}{n}} = \bar{c}_1 \psi^{\frac{2(1-n)}{n}}. \tag{3.26}$$

Here, we are effectively assuming a form for the (currently arbitrary) function $\lambda(\psi)$. Interestingly, this is not a simple power law form as $n > 0$ to allow ψ to satisfy the boundary conditions. Hence the form of λ is in fact assumed to be $\lambda = \bar{c}_1 \psi^{n_l}$, where $-2 < n_l < \infty$. To summarise

$$\psi = c_0 r^{n\alpha} \sin^n(\alpha\theta), \tag{3.27}$$

$$\lambda(\psi) = c_1 \left(\frac{\psi}{c_0 \alpha^n}\right)^{\frac{2(1-n)}{n}}, \tag{3.28}$$

where c_0 and c_1 are arbitrary constants (combinations of $\bar{c}_1$ and n combined for clarity), and n is an undetermined exponent.

The solution for the pressure p in the core was determined in equation (3.13). This can be simplified by using the stream function in polar coordinates, in particular that

$|\mathbf{v}|^2 = \left(\frac{1}{r}\frac{\partial\psi}{\partial\theta}\right)^2 + \left(\frac{\partial\psi}{\partial r}\right)^2$, and (3.27)–(3.28) to find

$$p = P_0(\psi) + \frac{1}{2}c_1 c_0^2 n^2 \alpha^{2n} r^{-2(1-\alpha)} = P_0(\psi) + p_0 r^{-2(1-\alpha)}. \tag{3.29}$$

The pressure near the upstream wall must satisfy (2.57) which is the viscometric behaviour of the pressure. Thus at leading order p must be a function of x only (where $r \sim x$ for small θ, explained later in footnote 9), and as such $P_0(\psi)$ must be subdominant. Thus in the core region as $r \to 0$ at leading order

$$p = p_0 r^{-2(1-\alpha)}, \tag{3.30}$$

where $p_0 = \frac{1}{2}c_1 c_0^2 n^2 \alpha^{2n}$ is another constant.

For completeness, we are now able to note the form of the constants in (3.23) and (3.24) in terms of the new constants introduced.

$$\tilde{c}_1 = \frac{c_0 \alpha^n}{(c_0^2 c_1 n^2 \alpha^{2n})^{n/2}} = \frac{c_0 \alpha^n}{(2p_0)^{n/2}}, \tag{3.31}$$

hence

$$\psi = g(\tilde{\psi}) = \frac{c_0 \alpha^n}{(2p_0)^{n/2}}\tilde{\psi}^n, \qquad \tilde{\psi} = \left(\frac{c_0}{\tilde{c}_1}\right)^{1/n} r^\alpha \sin(\alpha\theta) = \frac{(2p_0)^{1/2}}{\alpha} r^\alpha \sin(\alpha\theta). \tag{3.32}$$

The core flow has thus been determined subject to the two arbitrary constants c_0 and p_0 (c_1 being determined by the other two constants), the exponent n which will be determined through matching to the wall boundary layers, and the known parameter α, set by the corner angle of interest.

The asymptotic structure of the corner is based upon this solution behaviour, with the solution determining that

$$\psi = O(r^{n\alpha}), \quad \mathbf{T} = O(r^{-2(1-\alpha)}), \quad \lambda = O(r^{2\alpha(1-n)}), \quad p = O(r^{-2(1-\alpha)}), \quad \text{as } r \to 0, \tag{3.33}$$

and being fundamental to the following analysis.

3.2 Asymptotic Analysis

With the knowledge obtained in the previous section, we now begin to solve the re-entrant corner problem itself by determining the main asymptotic regions and the solution behaviour occurring in each. As suggested in section 2.2, there are two representations of the stress tensor which will be beneficial, those of the Cartesian and natural stress bases.

When considering the problem, analysis may be performed using either formulation without recourse to the other and indeed the papers published from this work [ES08] and [ES09] use the Cartesian and natural stress bases respectively. It will become apparent that the Cartesian stress basis is ideal to provide an initial investigation of the problem and determine the regions, as well as allowing easier interpretation of the results. The natural stress basis is required however as it is able to complete the problem to match the solution from the upstream to the downstream boundary layer (a feat not possible in the Cartesian basis due to the key pieces of information transferred being at high order in an asymptotic expansion of the core behaviour and thus too susceptible to numerical error).

In contrast to the papers mentioned, the asymptotic analysis here will proceed by considering both stress formulations simultaneously to provide a succinct analysis whilst highlighting the benefit of each stress basis.

The three main asymptotic regions local to the corner are shown in figure 3-3, comprising the outer (core) flow region away from the boundaries, and the inner (boundary) layers at the upstream and downstream walls. Shown is the case where no lip vortex is present, an assumption made for the analysis in this chapter, although commented on in the discussion. The distances from the corner are of $O(\epsilon)$ and are assumed small, with the boundary layer thickness found to be $O(\epsilon^{2-\alpha})$ on these length scales.

This section will proceed as follows. First in section 3.2.1 we use the core solution behaviour of section 3.1.4 to motivate core scalings for the variables, and verify the core balance assumed. As this leading order self-similar solution is not consistent with the viscometric behaviour of section 2.3.1 we match the core solution into stress boundary layers in section 3.2.2. The leading order boundary layer equations of section 3.2.2 admit a self-similar form in both stress formulations, which have to be solved numerically. The wall behaviour of the similarity solution equations is considered in 3.2.3, the far-field behaviour then in 3.2.4. This determines that the upstream problem may be solved as an initial value problem provided both the upstream wall shear rate and the pressure are given, and the downstream problem is then solved as a boundary value problem determining the downstream wall shear rate.

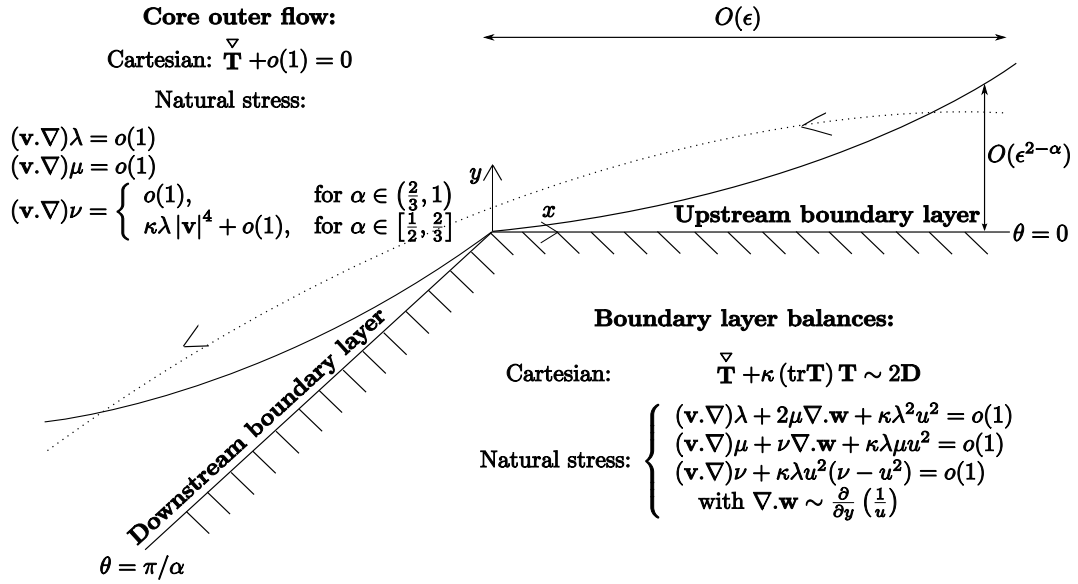

Figure 3-3: A schematic illustration of the main asymptotic regions local to the corner for self-similar solutions of PTT fluids when $\kappa = O(1)$ and We $= O(1)$. Distances to the corner are of $O(\epsilon)$ and assumed small. The upper convective stress derivative is assumed to dominate in the core flow and self-similar solutions of the form $\psi = c_0 r^{n\alpha}\sin^n(\alpha\theta)$, $\mathbf{T} = \lambda(\psi)\mathbf{v}\mathbf{v}^T$ can be matched to both upstream and downstream boundary layers which form symmetrically at the walls. Flow remains parallel within the boundary layers, with the fluid originating near the upstream wall flowing fully around the corner. A lip vortex is implicitly assumed to be absent, so that the situation of reverse flow at the upstream wall is not considered. The boundary layers described here are single layer structures occurring for the critical value of $n = 1 + \alpha$ which arises in the self-similar solution of the core. These boundary layers have a wall viscometric behaviour associated with the PTT high Weissenberg number boundary layer equations [HR97]. The shown dominant balances for the constitutive equations conveniently summarise the terms that contribute to the leading order equations in their respective regions (although not all components of each term necessarily appear). The leading order balances using the natural stress formulation are also shown for the respective regions.

3.2.1 The core region

The analysis of the re-entrant corner geometry takes place in a region close to the corner, so it is convenient to rescale r by $r = \epsilon R^*$, where ϵ is an artificial small parameter, thus the scalings we introduce are

$$r = \epsilon R^*, \qquad x = \epsilon X^*, \qquad y = \epsilon Y^*, \tag{3.34}$$

where $0 < \epsilon \ll 1$, and $R^* = O(1)$. The outer region is defined as being away from the walls and for which $X^* = O(1)$, $Y^* = O(1)$. Using the order of magnitudes given in

(3.33), and the velocity field (2.19) we may then find the scalings

$$\psi = \epsilon^{n\alpha}\Psi^*, \quad \mathbf{v} = \epsilon^{n\alpha-1}\mathbf{v}^*, \quad \mathbf{w} = \epsilon^{1-n\alpha}\mathbf{w}^*, \quad p = \epsilon^{-2(1-\alpha)}p^*, \quad \mathbf{T} = \epsilon^{-2(1-\alpha)}\mathbf{T}^*,$$
$$\lambda = \epsilon^{2\alpha(1-n)}\lambda^*, \quad \mu = \theta_2\mu^*, \quad \nu = \theta_3\nu^*, \tag{3.35}$$

where the scalings for the natural stress variables μ and ν are as yet undetermined and denoted by the gauges $\theta_2(\epsilon)$ and $\theta_3(\epsilon)$. These gauges will be found after matching into the boundary layer. For completeness we note then that

$$\Psi^* = c_0 R^{*n\alpha}\sin^n(\alpha\theta), \quad \mathbf{v}^* = \begin{pmatrix} \frac{\partial\Psi^*}{\partial Y^*} \\ -\frac{\partial\Psi^*}{\partial X^*} \end{pmatrix}, \quad \mathbf{T}^* = \lambda(\Psi^*)\mathbf{v}^*\mathbf{v}^{*T}. \tag{3.36}$$

We now write the governing equations in both Cartesian and natural stress formulae in the outer (starred) variables. The momentum equations (1.32) in Cartesian form are

$$\text{Re }\epsilon^{2\alpha(n-1)}(\mathbf{v}^*.\nabla^*)\mathbf{v}^* = -\nabla^* p^* + \nabla^*.\mathbf{T}^*, \tag{3.37}$$

and in the natural stress basis (2.41) and (2.42) become

$$\text{Re }\epsilon^{2\alpha(n-1)}(\mathbf{v}^*.\nabla^*)u^* = -\frac{\partial p^*}{\partial X^*} + (\mathbf{v}^*.\nabla^*)(\lambda^* u^*) + \delta_2\nabla^*.(\mu^* u^*\mathbf{w}^* + \mu^*\mathbf{v}^* w_1^*)$$
$$+\delta_3\nabla^*.(\nu^*\mathbf{w}^* w_1^*), \tag{3.38}$$
$$\text{Re }\epsilon^{2\alpha(n-1)}(\mathbf{v}^*.\nabla^*)v^* = -\frac{\partial p^*}{\partial Y^*} + (\mathbf{v}^*.\nabla^*)(\lambda^* v^*) + \delta_2\nabla^*.(\mu^* v^*\mathbf{w}^* + \mu^*\mathbf{v}^* w_2^*)$$
$$+\delta_3\nabla^*.(\nu^*\mathbf{w}^* w_2^*), \tag{3.39}$$

where we have set

$$\delta_2 = \theta_2\epsilon^{2(1-\alpha)}, \quad \text{and} \quad \delta_3 = \theta_3\epsilon^{2(2-\alpha(1+n))}, \tag{3.40}$$

for convenience. In either formulation it is clear that we require $2\alpha(n-1) > 0 \Rightarrow n > 1$ for the inertia terms to be subdominant. Introducing the scalings into the constitutive equation (1.34) in the Cartesian basis gives

$$\epsilon^{2-\alpha n}\mathbf{T}^* + \overset{\triangledown}{\mathbf{T}}^* + \kappa\epsilon^{\alpha(2-n)}(\text{tr}\mathbf{T}^*)\mathbf{T}^* = 2\epsilon^{2(1-\alpha)}\mathbf{D}^*, \tag{3.41}$$

and so $\overset{\triangledown}{\mathbf{T}}^*$ dominates at leading-order if

$$2 - \alpha n > 0 \quad \Rightarrow \quad n < \frac{2}{\alpha} \tag{3.42}$$

$$\alpha(2 - n) > 0 \quad \Rightarrow \quad n < 2 \tag{3.43}$$

$$2 - 2\alpha > 0 \quad \Rightarrow \quad \alpha < 1. \tag{3.44}$$

As the geometry dictates that $\frac{1}{2} \leq \alpha < 1$, then these restrictions imply that $n < 2$, hence we now have

$$1 < n < 2. \tag{3.45}$$

When $n = 2$ the upper convected stress derivative is balanced by the quadratic stress terms and the solution (3.27) is no longer applies for $\kappa = O(1)$. In the case of (3.45) the stress scaling is fully determined by the angle of the corner and independent of n. In the following section, n will be shown to be $1 + \alpha$, which falls within this range of validity.

Now the corresponding core constitutive equations in the natural stress variables (from (2.37)-(2.39)) are

$$(\mathbf{v}^*.\nabla^*)\lambda^* + \epsilon^{2-n\alpha}\lambda^* + \delta_2 2\mu^*\nabla^*.\mathbf{w}^* + \kappa \ \mathrm{tr}(\mathbf{T}^*)\left(\lambda^* - \frac{\epsilon^{2(1-\alpha)}}{|\mathbf{v}^*|^2}\right) = \frac{\epsilon^{4-\alpha(n+2)}}{|\mathbf{v}^*|^2}, \tag{3.46}$$

$$(\mathbf{v}^*.\nabla^*)\mu^* + \epsilon^{2-n\alpha}\mu^* + \frac{\delta_3}{\delta_2}\nu^*\nabla^*.\mathbf{w}^* + \kappa \ \mathrm{tr}(\mathbf{T}^*)\mu^* = 0, \tag{3.47}$$

$$(\mathbf{v}^*.\nabla^*)\nu^* + \epsilon^{2-n\alpha}\nu^* + \kappa \ \mathrm{tr}(\mathbf{T}^*)\left(\nu^* - \frac{\epsilon^{2(1-\alpha)}}{\delta_3}|\mathbf{v}^*|^2\right) = \frac{\epsilon^{4-\alpha(n+2)}}{\delta_3}|\mathbf{v}^*|^2, \tag{3.48}$$

where we have defined

$$\mathrm{tr}(\mathbf{T}^*) = \epsilon^{\alpha(2-n)}\lambda^*|\mathbf{v}^*|^2 - 2\epsilon^{2-n\alpha} + \delta_3\epsilon^{\alpha(2-n)}\frac{\nu^*}{|\mathbf{v}^*|^2}. \tag{3.49}$$

It is also possible to relate the two formulations using (2.33)-(2.35), the expressions becoming

$$T_{11}^* = -\epsilon^{2(1-\alpha)} + \lambda^* u^{*2} - \delta_2\frac{2\mu^* u^* v^*}{|\mathbf{v}^*|^2} + \delta_3\frac{\nu^* v^{*2}}{|\mathbf{v}^*|^4}, \tag{3.50}$$

$$T_{12}^* = \lambda^* u^* v^* + \delta_2\frac{\mu^*(u^{*2} - v^{*2})}{|\mathbf{v}^*|^2} - \delta_3\frac{\nu^* u^* v^*}{|\mathbf{v}^*|^4}, \tag{3.51}$$

$$T_{22}^* = -\epsilon^{2(1-\alpha)} + \lambda^* v^{*2} + \delta_2\frac{2\mu^* u^* v^*}{|\mathbf{v}^*|^2} + \delta_3\frac{\nu^* u^{*2}}{|\mathbf{v}^*|^4}. \tag{3.52}$$

We now pose the expansions

$$\Psi^* = \Psi^{*(0)} + o(1), \quad \mathbf{T}^* = \mathbf{T}^{*(0)} + o(1), \quad p^* = p^{*(0)} + o(1),$$
$$\lambda^* = \lambda^{*(0)} + o(1), \quad \mu^* = \mu^{*(0)} + o(1), \quad \nu^* = \nu^{*(0)} + o(1), \qquad \text{as } \epsilon \to 0, \tag{3.53}$$

and for the natural stress equations make the assumptions

$$\delta_2 \ll 1, \quad \delta_3 \ll 1, \quad 1 < n < 2,$$
$$\frac{\delta_3}{\delta_2} \ll 1, \quad \delta_3 \epsilon^{\alpha(2-n)} \ll 1, \quad \frac{\epsilon^{4-\alpha(n+2)}}{\delta_3} \ll 1, \quad \frac{\epsilon^{2-n\alpha}}{\delta_3} \ll 1, \tag{3.54}$$

which need to be verified a posteriori once n and the gauges θ_2, θ_3 are determined. This then gives the leading order problem

$$\nabla^* p^{*(0)} = \nabla^* . \mathbf{T}^{*(0)} = \left(\mathbf{v}^{*(0)} . \nabla^*\right) \left(\lambda^{*(0)} \mathbf{v}^{*(0)}\right), \quad \overset{\triangledown}{\mathbf{T}}{}^{*(0)} = 0,$$
$$\left(\mathbf{v}^{*(0)} . \nabla^*\right) \lambda^{*(0)} = 0, \quad \left(\mathbf{v}^{*(0)} . \nabla^*\right) \mu^{*(0)} = 0, \quad \left(\mathbf{v}^{*(0)} . \nabla^*\right) \nu^{*(0)} = 0, \tag{3.55}$$

in the core region[8]. These equations may be solved in the same way as in section 3.1.4, giving

$$\Psi^{*(0)} = c_0 R^{*n\alpha} \sin^n(\alpha\theta), \quad \lambda^{*(0)} = c_1 \left(\frac{\Psi^{*(0)}}{c_0 \alpha^n}\right)^{\frac{2(1-n)}{n}}, \quad p^{*(0)} = p_0 R^{*-2(1-\alpha)}, \tag{3.57}$$

where the stream function satisfies $\Psi^{*(0)} = 0$ on $\theta = 0$ and $\theta = \pi/\alpha$, and the constants c_0 and p_0 are arbitrary (the constant c_1 being determined by the other constants as in (3.29)).The stress components in the Cartesian basis are

$$T_{11}^{*(0)} = c_1 \left(\frac{\Psi^{*(0)}}{c_0 \alpha^n}\right)^{\frac{2}{n}-2} \left(\frac{\partial \Psi^{*(0)}}{\partial Y^*}\right)^2, \quad T_{12}^{*(0)} = -c_1 \left(\frac{\Psi^{*(0)}}{c_0 \alpha^n}\right)^{\frac{2}{n}-2} \left(\frac{\partial \Psi^{*(0)}}{\partial X^*} \frac{\partial \Psi^{*(0)}}{\partial Y^*}\right),$$
$$T_{22}^{*(0)} = c_1 \left(\frac{\Psi^{*(0)}}{c_0 \alpha^n}\right)^{\frac{2}{n}-2} \left(\frac{\partial \Psi^{*(0)}}{\partial X^*}\right)^2, \tag{3.58}$$

[8] There is another possible core balance in the $\nu^{*(0)}$ natural stress variable equation where a positive forcing term intrudes from the quadratic stress term, that of

$$\left(\mathbf{v}^{*(0)} . \nabla^*\right) \nu^{*(0)} = \kappa \lambda^{*(0)} \left|\mathbf{v}^{*(0)}\right|^4, \tag{3.56}$$

which changes the final assumption in (3.54). Here we would have $\delta_3 = \epsilon^{2-n\alpha}$. This balance is found to be appropriate when $1/2 \leq \alpha \leq 2/3$ in (3.119)-(3.120), and is analysed further in appendix E.

and finally we note that $\mu^{*(0)}$, and $\nu^{*(0)}$ are functions of $\Psi^{*(0)}$. We assume a power law form for these variables, and then the general solution to their equations is

$$\mu^{*(0)} = d_2 \left(\frac{\Psi^{*(0)}}{c_0 \alpha^n} \right)^{n_2}, \quad \nu^{*(0)} = d_3 \left(\frac{\Psi^{*(0)}}{c_0 \alpha^n} \right)^{n_3}, \tag{3.59}$$

for arbitrary constants d_2, d_3, and exponents n_2 and n_3. An important observation here is that $\lambda^{*(0)}$, $\mu^{*(0)}$, and $\nu^{*(0)}$ are constant along leading order streamlines, with the information received from the upstream boundary layer being unchanged through the core region and then delivered to the downstream layer thus linking the two boundary layers together.

To match with the upstream boundary layer we consider the behaviour as $Y^* \to 0$, which corresponds to $\theta \to 0$. By considering the expansions of $\sin(\theta)$ and $\cos(\theta)$ for small θ then $R^* \sim X^*$ and $\theta \sim Y^*/X^*$ at leading order[9]. Then from (3.57) we derive the matching conditions as

$$\Psi^{*(0)} \sim c_0 X^{*n\alpha} \alpha^n \left(\frac{Y^*}{X^*} \right)^n = C_0 X^{*n(\alpha-1)} Y^{*n}, \qquad p^{*(0)} \sim p_0 X^{*2\alpha-2}, \tag{3.64}$$

[9]Firstly, we record the expansions for $\sin(\theta)$, $\cos(\theta)$ and the relationships between (r, θ) and (x, y).

$$\sin(\theta) = \theta - \frac{\theta^3}{3!} + ..., \qquad \cos(\theta) = 1 - \frac{\theta^2}{2!} + \frac{\theta^4}{4!} - ...,$$
$$x = r\cos\theta, \quad y = r\sin\theta, \quad r^2 = x^2 + y^2, \quad \tan(\theta) = \frac{y}{x}. \tag{3.60}$$

We can also note that

$$\begin{array}{cccc} f(z) = \tan^{-1}(z) & f'(z) = \frac{1}{1+z^2} & f''(z) = \frac{-2z}{(1+z^2)^2} & f'''(z) = \frac{2(3z^2-1)}{(1+z^2)^3} \\ f(0) = 0 & f'(0) = 1 & f''(0) = 0 & f'''(0) = -2 \end{array} \tag{3.61}$$

such that

$$\theta = \tan^{-1}\left(\frac{y}{x}\right) = \frac{y}{x} - \frac{1}{3}\left(\frac{y}{x}\right)^3 + ... \tag{3.62}$$

Using $r^2 = x^2 + y^2$ and performing a Taylor series expansion we have

$$r = x + \frac{1}{2}\frac{y^2}{x} + ..., \tag{3.63}$$

so the second terms for both r and θ are $\left(\frac{y}{x}\right)^2$ smaller than the leading order terms.

from (3.58) we can see that

$$\begin{aligned} T_{11}^{*(0)} &\sim c_1 \left(\frac{C_0}{c_0 \alpha^n} X^{*n(\alpha-1)} Y^{*n} \right)^{\frac{2}{n}(1-n)} C_0^2 X^{2(\alpha-1)n} n^2 Y^{*2(n-1)} \\ &= C_1 X^{*(2\alpha-2)}, \qquad (3.65) \\ T_{12}^{*(0)} &\sim -c_1 \left(\frac{C_0}{c_0 \alpha^n} X^{*n(\alpha-1)} Y^{*n} \right)^{\frac{2}{n}(1-n)} C_0^2 n(\alpha-1) X^{*n(\alpha-1)-1} Y^{*n} n X^{n(\alpha-1)} Y^{n-1} \\ &= C_1 (1-\alpha) X^{*(2\alpha-3)} Y^*, \qquad (3.66) \\ T_{22}^{*(0)} &\sim c_1 \left(\frac{C_0}{c_0 \alpha^n} X^{*n(\alpha-1)} Y^{*n} \right)^{\frac{2}{n}(1-n)} C_0^2 n^2 (\alpha-1)^2 X^{*2n(\alpha-1)-2} Y^{*2n} \\ &= C_1 (1-\alpha)^2 X^{*(2\alpha-4)} Y^{*2}, \qquad (3.67) \end{aligned}$$

and from (3.57) and (3.59) the natural stress variables have the limiting behaviour

$$\lambda^{*(0)} \sim c_1 X^{*2(\alpha-1)(1-n)} Y^{*2(1-n)}, \qquad \mu^{*(0)} \sim d_2 X^{*n(\alpha-1)n_2} Y^{*nn_2},$$
$$\nu^{*(0)} \sim d_3 X^{*n(\alpha-1)n_3} Y^{*nn_3}, \qquad (3.68)$$

where the constants

$$C_0 = c_0 \alpha^n, \quad C_1 = c_1 n^2 C_0^2, \quad p_0 = \frac{1}{2} C_1, \qquad (3.69)$$

have been introduced for convenience. Similar expressions can be deduced for the behaviour at the downstream wall, the way the two are related is given at the start of the following section. However, since neither upstream nor downstream behaviours capture the viscometric behaviour (in (2.58)) this leads to consideration of wall boundary layers.

3.2.2 Wall boundary layer structures

The governing equations hold in both the upstream and downstream regions. The natural choice of Cartesian axes for the downstream region is with the x-axis along the downstream wall $\theta = \pi/\alpha$ and the y-axis orthogonal along the ray $\theta = \pi/\alpha + \pi/2$ into the wall. Comparing then the upstream and downstream regions the transformation relating the two is

$$\psi \mapsto -\psi, \qquad y \mapsto -y, \qquad T_{12} \mapsto -T_{12}, \qquad \mu \mapsto -\mu. \qquad (3.70)$$

leaving the governing equations invariant. This is analogous to remark 3 of [Eva08a]. Inner regions are now sought at both walls, and the boundary layer equations will be found to be the same as those noted by [HR97] for the high Weissenberg number limit.

The upstream wall is considered without loss of generality, since the re-orientation of axes from (3.70) allows the downstream wall to be similarly considered. To move into the upstream boundary layer we need only to rescale the y variable, since rescaling x would only bring us even closer to the corner. Hence the scalings are

$$X^* = \bar{X}, \quad Y^* = \delta(\epsilon)\bar{Y}, \quad \Psi^* = \gamma(\epsilon)\bar{\Psi}. \tag{3.71}$$

Using the matching conditions (3.64)-(3.68), we can determine $\gamma = \delta^n$, and the scalings for the other variables become

$$\begin{aligned} T_{11}^* = \bar{T}_{11}, \quad T_{12}^* = \delta\bar{T}_{12}, \quad T_{22}^* = \delta^2\bar{T}_{22}, \quad p^* = \bar{p}, \\ u^* = \delta^{n-1}\bar{u}, \quad v^* = \delta^n\bar{v}, \quad w_1^* = \delta^{2-n}\bar{w}_1, \\ w_2^* = \delta^{1-n}\bar{w}_2, \quad \lambda^* = \delta^{2(1-n)}\bar{\lambda}, \quad \mu^* = \delta^{nn_2}\bar{\mu}, \quad \nu^* = \delta^{nn_3}\bar{\nu}, \end{aligned} \tag{3.72}$$

where

$$\bar{u} = \frac{\partial\bar{\Psi}}{\partial\bar{Y}}, \quad \bar{v} = -\frac{\partial\bar{\Psi}}{\partial\bar{X}}, \quad \bar{w}_1 = -\frac{\bar{v}}{\bar{u}^2 + \delta^2\bar{v}^2}, \quad \bar{w}_2 = \frac{\bar{u}}{\bar{u}^2 + \delta^2\bar{v}^2}, \tag{3.73}$$

and the gauge $\delta = \delta(\epsilon)$ is to be determined, but is presumed small in order for this region to be thin i.e. a boundary layer. To scale our equations in the boundary layer it is useful to note

$$\nabla^*.\mathbf{w}^* = \frac{\partial w_1^*}{\partial X^*} + \frac{\partial w_2^*}{\partial Y^*} = \delta^{-n}\left(\frac{\partial\bar{w}_2}{\partial\bar{Y}} + \delta^2\frac{\partial\bar{w}_1}{\partial\bar{X}}\right) = \delta^{-n}\bar{\nabla}.\bar{\mathbf{w}}, \tag{3.74}$$

$$(\mathbf{v}^*.\nabla^*) = \left(u^*\frac{\partial}{\partial X^*} + v^*\frac{\partial}{\partial Y^*}\right) = \delta^{n-1}\left(\bar{u}\frac{\partial}{\partial\bar{X}} + \bar{v}\frac{\partial}{\partial\bar{Y}}\right) = \delta^{n-1}(\bar{\mathbf{v}}.\bar{\nabla}). \tag{3.75}$$

For the inner region $\bar{X} = O(1)$, $\bar{Y} = O(1)$ these give the constitutive equations in the Cartesian stress basis as

$$\frac{\epsilon^{2-n\alpha}}{\delta^{n-1}}\bar{T}_{11} + \left(\frac{\partial\bar{\Psi}}{\partial\bar{Y}}\frac{\partial\bar{T}_{11}}{\partial\bar{X}} - \frac{\partial\bar{\Psi}}{\partial\bar{X}}\frac{\partial\bar{T}_{11}}{\partial\bar{Y}} - 2\frac{\partial^2\bar{\Psi}}{\partial\bar{Y}^2}\bar{T}_{12} - 2\frac{\partial^2\bar{\Psi}}{\partial\bar{X}\partial\bar{Y}}\bar{T}_{11}\right) + \frac{\epsilon^{\alpha(2-n)}}{\delta^{n-1}}\kappa(\bar{T}_{11} + \delta^2\bar{T}_{22})\bar{T}_{11} = 2\epsilon^{2(1-\alpha)}\frac{\partial^2\bar{\Psi}}{\partial\bar{X}\partial\bar{Y}}, \tag{3.76}$$

$$\frac{\epsilon^{2-n\alpha}}{\delta^{n-1}}\bar{T}_{22} + \left(\frac{\partial\bar{\Psi}}{\partial\bar{Y}}\frac{\partial\bar{T}_{22}}{\partial\bar{X}} - \frac{\partial\bar{\Psi}}{\partial\bar{X}}\frac{\partial\bar{T}_{22}}{\partial\bar{Y}} + 2\frac{\partial^2\bar{\Psi}}{\partial\bar{X}^2}\bar{T}_{12} + 2\frac{\partial^2\bar{\Psi}}{\partial\bar{X}\partial\bar{Y}}\bar{T}_{22}\right) + \frac{\epsilon^{\alpha(2-n)}}{\delta^{n-1}}\kappa(\bar{T}_{11} + \delta^2\bar{T}_{22})\bar{T}_{22} = -2\frac{\epsilon^{2(1-\alpha)}}{\delta^2}\frac{\partial^2\bar{\Psi}}{\partial\bar{X}\partial\bar{Y}}, \tag{3.77}$$

$$\frac{\epsilon^{2-n\alpha}}{\delta^{n-1}}\bar{T}_{12} + \left(\frac{\partial\bar{\Psi}}{\partial\bar{Y}}\frac{\partial\bar{T}_{12}}{\partial\bar{X}} - \frac{\partial\bar{\Psi}}{\partial\bar{X}}\frac{\partial\bar{T}_{12}}{\partial\bar{Y}} + \frac{\partial^2\bar{\Psi}}{\partial\bar{X}^2}\bar{T}_{11} - \frac{\partial^2\bar{\Psi}}{\partial\bar{Y}^2}\bar{T}_{22}\right) + \frac{\epsilon^{\alpha(2-n)}}{\delta^{n-1}}\kappa(\bar{T}_{11} + \delta^2\bar{T}_{22})\bar{T}_{12} = \frac{\epsilon^{2(1-\alpha)}}{\delta^2}\left(\frac{\partial^2\bar{\Psi}}{\partial\bar{Y}^2} - \delta^2\frac{\partial^2\bar{\Psi}}{\partial\bar{X}^2}\right), \tag{3.78}$$

and using natural stress variables

$$(\bar{\mathbf{v}}.\bar{\nabla})\bar{\lambda} + \left(\frac{\epsilon^{2-n\alpha}}{\delta^{n-1}}\right)\bar{\lambda} + \left(\frac{\delta_2\delta^{nn_2}}{\delta}\right)2\bar{\mu}\bar{\nabla}.\bar{\mathbf{w}} + \kappa\ \mathrm{tr}(\bar{\mathbf{T}})\left(\bar{\lambda} - \frac{\epsilon^{2(1-\alpha)}}{\bar{u}^2 + \delta^2\bar{v}^2}\right) = \left(\frac{\epsilon^{4-\alpha(n+2)}}{\delta^{n-1}}\right)\frac{1}{\bar{u}^2 + \delta^2\bar{v}^2}, \tag{3.79}$$

$$(\bar{\mathbf{v}}.\bar{\nabla})\bar{\mu} + \left(\frac{\epsilon^{2-n\alpha}}{\delta^{n-1}}\right)\bar{\mu} + \left(\frac{\delta_3\delta^{nn_3+1}}{\delta_2\delta^{n(n_2+2)}}\right)\bar{\nu}\bar{\nabla}.\bar{\mathbf{w}} + \kappa\ \mathrm{tr}(\bar{\mathbf{T}})\bar{\mu} = 0, \tag{3.80}$$

$$(\bar{\mathbf{v}}.\bar{\nabla})\bar{\nu} + \left(\frac{\epsilon^{2-n\alpha}}{\delta^{n-1}}\right)\bar{\nu} + \kappa\ \mathrm{tr}(\bar{\mathbf{T}})\left(\bar{\nu} - \frac{\epsilon^{2(1-\alpha)}\delta^{2(n-1)}}{\delta_3\delta^{nn_3}}\left(\bar{u}^2 + \delta^2\bar{v}^2\right)\right) = \left(\frac{\epsilon^{4-\alpha(n+2)}}{\delta^{1-n+nn_3}\delta_3}\right)\left(\bar{u}^2 + \delta^2\bar{v}^2\right), \tag{3.81}$$

where

$$\bar{\nabla}.\bar{\mathbf{w}} = \frac{\partial}{\partial\bar{Y}}\left(\frac{\bar{u}}{\bar{u}^2 + \delta^2\bar{v}^2}\right) - \delta^2\frac{\partial}{\partial\bar{X}}\left(\frac{\bar{v}}{\bar{u}^2 + \delta^2\bar{v}^2}\right) = \frac{\partial}{\partial\bar{Y}}\left(\frac{1}{\bar{u}}\right) + O(\delta^2), \tag{3.82}$$

and we define

$$\mathrm{tr}(\bar{\mathbf{T}}) = \frac{\epsilon^{\alpha(2-n)}}{\delta^{n-1}}\left(\bar{\lambda}\left(\bar{u}^2 + \delta^2\bar{v}^2\right) - 2\epsilon^{2(1-\alpha)} + \frac{\delta_3}{\delta^{2(n-1)-nn_3}}\left(\frac{\bar{v}}{\bar{u}^2 + \delta^2\bar{v}^2}\right)\right). \tag{3.83}$$

The momentum equations are then

$$\text{Re } \epsilon^{2\alpha(n-1)}\delta^{2(n-1)}\left(\frac{\partial\bar{\Psi}}{\partial\bar{Y}}\frac{\partial^2\bar{\Psi}}{\partial\bar{X}\partial\bar{Y}} - \frac{\partial\bar{\Psi}}{\partial\bar{X}}\frac{\partial^2\bar{\Psi}}{\partial\bar{Y}^2}\right) = -\frac{\partial\bar{p}}{\partial\bar{X}} + \frac{\partial\bar{T}_{11}}{\partial\bar{X}} + \frac{\partial\bar{T}_{12}}{\partial\bar{Y}}, \tag{3.84}$$

$$\text{Re } \epsilon^{2\alpha(n-1)}\delta^{2n}\left(-\frac{\partial\bar{\Psi}}{\partial\bar{Y}}\frac{\partial^2\bar{\Psi}}{\partial\bar{X}^2} + \frac{\partial\bar{\Psi}}{\partial\bar{X}}\frac{\partial^2\bar{\Psi}}{\partial\bar{X}\partial\bar{Y}}\right) = -\frac{\partial\bar{p}}{\partial\bar{Y}} + \delta^2\left(\frac{\partial\bar{T}_{12}}{\partial\bar{X}} + \frac{\partial\bar{T}_{22}}{\partial\bar{Y}}\right), \tag{3.85}$$

and

$$\begin{aligned}\text{Re } \delta^{2(n-1)}\epsilon^{2\alpha(n-1)}(\bar{\mathbf{v}}.\bar{\nabla})\bar{u} = &-\frac{\partial\bar{p}}{\partial\bar{X}} + (\bar{\mathbf{v}}.\bar{\nabla})(\bar{\lambda}\bar{u}) \\ &+ \delta_2\delta^{nn_2-1}\left\{\frac{\partial}{\partial\bar{Y}}\left(\bar{\mu}\bar{u}\bar{w}_2 + \delta^2\bar{\mu}\bar{v}\bar{w}_1\right) + \delta^2\frac{\partial}{\partial\bar{X}}\left(2\bar{\mu}\bar{u}\bar{w}_1\right)\right\} \\ &+ \delta_3\delta^{nn_3+2-2n}\left\{\frac{\partial}{\partial\bar{Y}}\left(\bar{\nu}\bar{w}_2\bar{w}_1\right) + \delta^2\frac{\partial}{\partial\bar{X}}\left(\bar{\nu}{\bar{w}_1}^2\right)\right\},\end{aligned} \tag{3.86}$$

$$\begin{aligned}\text{Re } \delta^{2n-1}\epsilon^{2\alpha(n-1)}(\bar{\mathbf{v}}.\bar{\nabla})\bar{v} = &-\delta^{-1}\frac{\partial\bar{p}}{\partial\bar{Y}} + \delta(\bar{\mathbf{v}}.\bar{\nabla})(\bar{\lambda}\bar{v}) \\ &+ \delta_2\delta^{nn_2}\left\{\frac{\partial}{\partial\bar{Y}}\left(2\bar{\mu}\bar{v}\bar{w}_2\right) + \frac{\partial}{\partial\bar{X}}\left(\bar{\mu}\bar{u}\bar{w}_2 + \delta^2\bar{\mu}\bar{v}\bar{w}_1\right)\right\} \\ &+ \delta_3\delta^{nn_3+1-2n}\left\{\frac{\partial}{\partial\bar{Y}}\left(\bar{\nu}{\bar{w}_2}^2\right) + \delta^2\frac{\partial}{\partial\bar{X}}\left(\bar{\nu}\bar{w}_1\bar{w}_2\right)\right\}.\end{aligned} \tag{3.87}$$

Dominant balance in equations (3.76)-(3.78) that retains quadratic stress and rate of strain terms occurs when $\delta^{n-1} = \epsilon^{\alpha(2-n)}$ and $\delta^2 = \epsilon^{2(1-\alpha)}$, which determines

$$\delta = \epsilon^{1-\alpha}, \qquad \text{and} \qquad n = 1 + \alpha, \tag{3.88}$$

with dominant balance in (3.79)-(3.81) requiring

$$\frac{\delta_2\delta^{nn_2}}{\delta} = 1, \quad \frac{\epsilon^{\alpha(2-n)}}{\delta^{n-1}} = 1, \quad \left(\frac{\delta_3\delta^{nn_3+1}}{\delta_2\delta^{n(n_2+2)}}\right) = 1, \quad \frac{\epsilon^{2(1-\alpha)}\delta^{2(n-1)}}{\delta_3\delta^{nn_3}} = 1, \tag{3.89}$$

which give additionally

$$\delta_2\delta^{nn_2} = \epsilon^{1-\alpha}, \quad \delta_3\delta^{nn_3} = \epsilon^{2(1-\alpha^2)}, \quad \text{i.e.} \quad \theta_2\delta^{nn_2} = \epsilon^{\alpha-1}, \quad \theta_3\delta^{nn_3} = \epsilon^{2(2\alpha-1)}. \tag{3.90}$$

For clarity in the natural stress variable equations, we note the equations in the boundary layer are now

$$\text{Re } \epsilon^{2\alpha}(\bar{\mathbf{v}}.\bar{\nabla})\bar{u} = -\frac{\partial\bar{p}}{\partial\bar{X}} + (\bar{\mathbf{v}}.\bar{\nabla})(\bar{\lambda}\bar{u}) + \frac{\partial}{\partial\bar{Y}}\left(\bar{\mu}\bar{u}\bar{w}_2\right) + O(\delta^2), \tag{3.91}$$

$$\text{Re } \epsilon^{2}(\bar{\mathbf{v}}.\bar{\nabla})\bar{v} = -\frac{\partial\bar{p}}{\partial\bar{Y}} + O(\delta^2), \tag{3.92}$$

and

$$(\bar{\mathbf{v}}.\bar{\nabla})\bar{\lambda} + \epsilon^{2(1-\alpha)}\bar{\lambda} + 2\bar{\mu}\bar{\nabla}.\bar{\mathbf{w}} + \kappa\ \mathrm{tr}(\bar{\mathbf{T}})\left(\bar{\lambda} - O(\epsilon^{2(1-\alpha)})\right) = O(\epsilon^{4(1-\alpha)}), \tag{3.93}$$

$$(\bar{\mathbf{v}}.\bar{\nabla})\bar{\mu} + \epsilon^{2(1-\alpha)}\bar{\mu} + \bar{\nu}\bar{\nabla}.\bar{\mathbf{w}} + \kappa\ \mathrm{tr}(\bar{\mathbf{T}})\bar{\mu} = 0, \tag{3.94}$$

$$(\bar{\mathbf{v}}.\bar{\nabla})\bar{\nu} + \epsilon^{2(1-\alpha)}\bar{\nu} + \kappa\ \mathrm{tr}(\bar{\mathbf{T}})\left(\bar{\nu} - \bar{u}^2 + O(\delta^2)\right) = O(\epsilon^{2(1-\alpha)}), \tag{3.95}$$

with

$$\mathrm{tr}(\bar{\mathbf{T}}) = \bar{\lambda}\left(\bar{u}^2 + O(\delta^2)\right) - 2\epsilon^{2(1-\alpha)} + O(\epsilon^{2(1-\alpha)}). \tag{3.96}$$

Considering $\bar{X} = O(1)$, $\bar{Y} = O(1)$, noting that $\delta = \epsilon^{1-\alpha}$ is small and thus that at leading order $\bar{w}_1 = -\frac{\bar{v}}{\bar{u}^2}$, $\bar{w}_2 = \frac{1}{\bar{u}}$, and also $\bar{\nabla}.\bar{w} = -\frac{1}{\bar{u}^2}\frac{\partial \bar{u}}{\partial \bar{Y}}$, then the leading order boundary layer equations are

$$\left(\frac{\partial\bar{\Psi}}{\partial\bar{Y}}\frac{\partial\bar{T}_{11}}{\partial\bar{X}} - \frac{\partial\bar{\Psi}}{\partial\bar{X}}\frac{\partial\bar{T}_{11}}{\partial\bar{Y}} - 2\frac{\partial^2\bar{\Psi}}{\partial\bar{Y}^2}\bar{T}_{12} - 2\frac{\partial^2\bar{\Psi}}{\partial\bar{X}\partial\bar{Y}}\bar{T}_{11}\right) + \kappa\bar{T}_{11}^2 = 0, \tag{3.97}$$

$$\left(\frac{\partial\bar{\Psi}}{\partial\bar{Y}}\frac{\partial\bar{T}_{22}}{\partial\bar{X}} - \frac{\partial\bar{\Psi}}{\partial\bar{X}}\frac{\partial\bar{T}_{22}}{\partial\bar{Y}} + 2\frac{\partial^2\bar{\Psi}}{\partial\bar{X}^2}\bar{T}_{12} + 2\frac{\partial^2\bar{\Psi}}{\partial\bar{X}\partial\bar{Y}}\bar{T}_{22}\right) + \kappa\bar{T}_{11}\bar{T}_{22} = -2\frac{\partial^2\bar{\Psi}}{\partial\bar{X}\partial\bar{Y}}, \tag{3.98}$$

$$\left(\frac{\partial\bar{\Psi}}{\partial\bar{Y}}\frac{\partial\bar{T}_{12}}{\partial\bar{X}} - \frac{\partial\bar{\Psi}}{\partial\bar{X}}\frac{\partial\bar{T}_{12}}{\partial\bar{Y}} + \frac{\partial^2\bar{\Psi}}{\partial\bar{X}^2}\bar{T}_{11} - \frac{\partial^2\bar{\Psi}}{\partial\bar{Y}^2}\bar{T}_{22}\right) + \kappa\bar{T}_{11}\bar{T}_{12} = \frac{\partial^2\bar{\Psi}}{\partial\bar{Y}^2}, \tag{3.99}$$

with equation (3.85) implying that $0 = -\frac{\partial\bar{p}}{\partial\bar{Y}}$. This gives $\bar{p} = \bar{p}(\bar{X})$, and hence (3.84) at leading order gives

$$0 = -\frac{d\bar{p}}{d\bar{X}} + \frac{\partial\bar{T}_{11}}{\partial\bar{X}} + \frac{\partial\bar{T}_{12}}{\partial\bar{Y}}, \tag{3.100}$$

where we note that the linear stress terms are subdominant in (3.97)-(3.99) being of $O(\epsilon^{2(1-\alpha)})$ relative to the terms retained. The natural stress boundary layer equations at leading order are

$$\begin{aligned}
0 &= -\frac{d\bar{p}}{d\bar{X}} + (\bar{\mathbf{v}}.\bar{\nabla})(\bar{\lambda}\bar{u}) + \frac{\partial\bar{\mu}}{\partial\bar{Y}} \\
&(\bar{\mathbf{v}}.\bar{\nabla})\bar{\lambda} - \frac{2\bar{\mu}}{\bar{u}^2}\frac{\partial\bar{u}}{\partial\bar{Y}} + \kappa\bar{\lambda}^2\bar{u}^2 = 0, \\
&(\bar{\mathbf{v}}.\bar{\nabla})\bar{\mu} - \frac{\bar{\nu}}{\bar{u}^2}\frac{\partial\bar{u}}{\partial\bar{Y}} + \kappa\bar{\lambda}\bar{\mu}\bar{u}^2 = 0, \\
&(\bar{\mathbf{v}}.\bar{\nabla})\bar{\nu} + \kappa\bar{\lambda}\bar{u}^2\left(\bar{\nu} - \bar{u}^2\right) = 0,
\end{aligned} \tag{3.101}$$

where $\bar{p} = \bar{p}(\bar{X})$ is confirmed from the second momentum equation (3.92). These are equivalent to the boundary layer equations in the high Weissenberg number situation by Hagen and Renardy [HR97]. They are also related to those stated in Cartesian

stress components in (3.97)-(3.100), using the change of variables

$$\bar{T}_{11} = \bar{\lambda}\bar{u}^2, \qquad \bar{T}_{12} = \bar{\lambda}\bar{u}\bar{v} + \bar{\mu}, \qquad \bar{T}_{22} = -1 + \bar{\lambda}\bar{v}^2 + \left(\frac{2\bar{\mu}\bar{v}}{\bar{u}}\right) + \left(\frac{\bar{\nu}}{\bar{u}^2}\right), \quad (3.102)$$

which follow from

$$\bar{T}_{11} = -\delta^2 + \bar{\lambda}\bar{u}^2 - \delta^2\left(\frac{2\bar{\mu}\bar{u}\bar{v}}{\bar{z}}\right) + \delta^4\left(\frac{\bar{\nu}\bar{v}^2}{\bar{z}^2}\right), \quad (3.103)$$

$$\bar{T}_{12} = \bar{\lambda}\bar{u}\bar{v} + \frac{\bar{\mu}}{\bar{z}}\left(\bar{u}^2 - \delta^2\bar{v}^2\right) - \delta^2\left(\frac{\bar{\nu}\bar{u}\bar{v}}{\bar{z}^2}\right), \quad (3.104)$$

$$\bar{T}_{22} = -1 + \bar{\lambda}\bar{v}^2 + \left(\frac{2\bar{\mu}\bar{u}\bar{v}}{\bar{z}}\right) + \left(\frac{\bar{\nu}\bar{u}^2}{\bar{z}^2}\right), \quad (3.105)$$

at leading order. These equations are precisely the relationships derived by Renardy [Ren97a] in the context of the high Weissenberg number boundary layers, and can be written using the stream function as

$$\bar{T}_{11} = \bar{\lambda}\left(\frac{\partial\bar{\Psi}}{\partial\bar{Y}}\right)^2, \quad (3.106)$$

$$\bar{T}_{12} = \bar{\mu} - \bar{\lambda}\left(\frac{\partial\bar{\Psi}}{\partial\bar{Y}}\right)\left(\frac{\partial\bar{\Psi}}{\partial\bar{X}}\right), \quad (3.107)$$

$$\left(\frac{\partial\bar{\Psi}}{\partial\bar{Y}}\right)^2\bar{T}_{22} = \left(\frac{\partial\bar{\Psi}}{\partial\bar{Y}}\right)^2\left\{-1 + \bar{\lambda}\left(\frac{\partial\bar{\Psi}}{\partial\bar{X}}\right)^2\right\} - 2\bar{\mu}\left(\frac{\partial\bar{\Psi}}{\partial\bar{X}}\right)\left(\frac{\partial\bar{\Psi}}{\partial\bar{Y}}\right) + \bar{\nu}. \quad (3.108)$$

The leading order boundary layer equations (3.101) may also be stated in terms of the stream function

$$-\frac{d\bar{p}}{d\bar{X}} + \left(\frac{\partial\bar{\Psi}}{\partial\bar{Y}}\right)\frac{\partial}{\partial\bar{X}}\left(\bar{\lambda}\frac{\partial\bar{\Psi}}{\partial\bar{Y}}\right) - \left(\frac{\partial\bar{\Psi}}{\partial\bar{X}}\right)\frac{\partial}{\partial\bar{Y}}\left(\bar{\lambda}\frac{\partial\bar{\Psi}}{\partial\bar{Y}}\right) + \frac{\partial\bar{\mu}}{\partial\bar{Y}} = 0, \quad (3.109)$$

$$\left(\frac{\partial\bar{\Psi}}{\partial\bar{Y}}\right)^2\left\{\frac{\partial\bar{\Psi}}{\partial\bar{Y}}\frac{\partial\bar{\lambda}}{\partial\bar{X}} - \frac{\partial\bar{\Psi}}{\partial\bar{X}}\frac{\partial\bar{\lambda}}{\partial\bar{Y}} + \kappa\bar{\lambda}^2\left(\frac{\partial\bar{\Psi}}{\partial\bar{Y}}\right)^2\right\} - 2\bar{\mu}\frac{\partial^2\bar{\Psi}}{\partial\bar{Y}^2} = 0, \quad (3.110)$$

$$\left(\frac{\partial\bar{\Psi}}{\partial\bar{Y}}\right)^2\left\{\frac{\partial\bar{\Psi}}{\partial\bar{Y}}\frac{\partial\bar{\mu}}{\partial\bar{X}} - \frac{\partial\bar{\Psi}}{\partial\bar{X}}\frac{\partial\bar{\mu}}{\partial\bar{Y}} + \kappa\bar{\lambda}\bar{\mu}\left(\frac{\partial\bar{\Psi}}{\partial\bar{Y}}\right)^2\right\} - \bar{\nu}\frac{\partial^2\bar{\Psi}}{\partial\bar{Y}^2} = 0, \quad (3.111)$$

$$\frac{\partial\bar{\Psi}}{\partial\bar{Y}}\frac{\partial\bar{\nu}}{\partial\bar{X}} - \frac{\partial\bar{\Psi}}{\partial\bar{X}}\frac{\partial\bar{\nu}}{\partial\bar{Y}} + \kappa\bar{\lambda}\left(\frac{\partial\bar{\Psi}}{\partial\bar{Y}}\right)^2\left\{\bar{\nu} - \left(\frac{\partial\bar{\Psi}}{\partial\bar{Y}}\right)^2\right\} = 0. \quad (3.112)$$

These leading order boundary layer equations (in either basis) represent the leading order problem in this inner region and the problem can be solved without the need to

proceed to the higher order terms. They are completed with the matching conditions

$$\begin{aligned}\text{as } \bar{Y} \to \infty: \quad & \bar{\Psi} \sim C_0 \bar{X}^{n(\alpha-1)} \bar{Y}^n, \qquad \bar{T}_{11} \sim C_1 \bar{X}^{(2\alpha-2)}, \\ & \bar{T}_{12} \sim C_1(1-\alpha)\bar{X}^{(2\alpha-3)}\bar{Y}, \qquad \bar{T}_{22} \sim C_1(1-\alpha)^2 \bar{X}^{(2\alpha-4)}\bar{Y}^2, \\ & \bar{\lambda} \sim c_1 \bar{X}^{2(\alpha-1)(1-n)}\bar{Y}^{2(1-n)}, \qquad \bar{\mu} \sim d_2 \bar{X}^{(\alpha-1)nn_2}\bar{Y}^{nn_2}, \\ & \bar{\nu} \sim d_3 \bar{X}^{(\alpha-1)nn_3}\bar{Y}^{nn_3}, \qquad \bar{p} \sim p_0 \bar{X}^{2(\alpha-1)}, \end{aligned} \tag{3.113}$$

from (3.64)-(3.68), where $n = 1+\alpha$, and $c_1 = \frac{2p_0}{(1+\alpha)^2 C_0^2}$, as well as viscometric behaviour at the walls arising from the solid boundary and no slip conditions

$$\text{at } \bar{Y} = 0, \quad \bar{\Psi} = \frac{\partial \bar{\Psi}}{\partial \bar{Y}} = 0. \tag{3.114}$$

As mentioned at the start of this section the problem statement for the downstream layer is exactly the same and may be deduced using the transformation given in (3.70) which leave the boundary layer (and full governing equations) invariant. Consequently the above equations (3.97)-(3.114) pertain for the downstream boundary layer, the only difference being a change in sign of the coefficient C_0.

For analysis of the boundary layer equations, attention will focus upon similarity solutions. The one parameter scaling group

$$\begin{aligned}&\bar{X} = \hat{\alpha}\hat{X}, \quad \bar{Y} = \hat{\alpha}^{2-\alpha}\hat{Y}, \quad \bar{\Psi} = \hat{\alpha}^{1+\alpha}\hat{\Psi}, \quad \bar{T}_{11} = \hat{\alpha}^{2\alpha-2}\hat{T}_{11}, \quad \bar{T}_{12} = \hat{\alpha}^{\alpha-1}\hat{T}_{12}, \\ &\bar{T}_{22} = \hat{T}_{22}, \quad \bar{p} = \hat{\alpha}^{2\alpha-2}\hat{p}, \quad \bar{\lambda} = \hat{\alpha}^{-2\alpha}\hat{\lambda}, \quad \bar{\mu} = \hat{\alpha}^{\alpha-1}\hat{\mu}, \quad \bar{\nu} = \hat{\alpha}^{2(2\alpha-1)}\hat{\nu}, \end{aligned} \tag{3.115}$$

for real $\hat{\alpha}$, leaves the problem (3.97)-(3.100) and (3.109)-(3.114) invariant. This also determines the values

$$n_2 = \frac{\alpha-1}{n} = -\frac{1-\alpha}{1+\alpha}, \qquad n_3 = \frac{2(2\alpha-1)}{n} = \frac{2(2\alpha-1)}{1+\alpha}, \tag{3.116}$$

which gives the gauges θ_2, θ_3, using (3.90) as

$$\theta_2 = \epsilon^{\alpha(\alpha-1)}, \qquad \theta_3 = \epsilon^{2\alpha(2\alpha-1)}. \tag{3.117}$$

The assumptions in (3.54) leading to the dominant balances become

$$\begin{aligned}
&\delta_2 = \epsilon^{(1-\alpha)(2-\alpha)} \ll 1, \quad \delta_3 = \epsilon^{2(1-\alpha)(2-\alpha)} \ll 1, \quad 1 < 1+\alpha < 2, \\
&\frac{\delta_3}{\delta_2} = \epsilon^{(1-\alpha)(2-\alpha)} \ll 1, \quad \delta_3 \epsilon^{\alpha(2-n)} = \epsilon^{(1-\alpha)(4-\alpha)} \ll 1, \\
&\frac{\epsilon^{4-\alpha(n+2)}}{\delta_3} = \epsilon^{3\alpha(1-\alpha)} \ll 1, \quad \frac{\epsilon^{2-n\alpha}}{\delta_3} = \epsilon^{(3\alpha-2)(1-\alpha)} \ll 1,
\end{aligned} \tag{3.118}$$

which can all be verified except the final one, which is only small when $2/3 < \alpha < 1$. This contradiction implies that the assumption made was only correct for this α range, and instead that for $1/2 \leq \alpha \leq 2/3$ the assumption should be that

$$\delta_3 = \epsilon^{2-n\alpha}, \quad \text{thus} \quad \theta_3 = \epsilon^{n\alpha+2\alpha-2} = \epsilon^{\alpha^2+3\alpha-2}. \tag{3.119}$$

The balance that changes in the core region is in the $\nu^{*(0)}$ equation, where now

$$\left(\mathbf{v}^{*(0)}.\nabla^*\right)\nu^{*(0)} = \kappa\lambda^{*(0)}\left|\mathbf{v}^{*(0)}\right|^4, \tag{3.120}$$

as already mentioned in (3.56) in footnote 8. Details of this situation (which is in fact found to consist of the two cases $1/2 \leq \alpha < 2/3$ and $\alpha = 2/3$) can be found in appendix E.

In Cartesian and all three natural stress cases $1/2 \leq \alpha < 2/3$, $\alpha = 2/3$ and $2/3 < \alpha < 1$, the governing equations and wall and matching conditions are invariant under the one parameter scaling group given in (3.115). This scaling group suggests the similarity solution

$$\begin{aligned}
\xi = \frac{\bar{Y}}{\bar{X}^{2-\alpha}}, \quad \bar{\Psi} = \kappa\bar{X}^{1+\alpha}f(\xi), \quad \bar{p} = p_0\bar{X}^{-2(1-\alpha)}, \\
\bar{T}_{11} = \bar{X}^{2\alpha-2}t_{11}(\xi), \quad \bar{T}_{12} = \bar{X}^{\alpha-1}t_{12}(\xi), \quad \bar{T}_{22} = t_{22}(\xi), \\
\bar{\lambda} = \frac{1}{\kappa^2}\bar{X}^{-2\alpha}\tilde{\lambda}(\xi), \quad \bar{\mu} = \bar{X}^{\alpha-1}\tilde{\mu}(\xi), \quad \bar{\nu} = \kappa^2\bar{X}^{2(2\alpha-1)}\tilde{\nu}(\xi),
\end{aligned} \tag{3.121}$$

where the opportunity to scale out the (order one) parameter κ has been taken[10]. The

[10]It is also possible to scale with p_0 as well, since it is common to all three regions (core and both boundary layers). This option will be exploited later before considering the numerics in section 3.2.5.

leading order boundary layer equations become

$$2(\alpha-1)(t_{11}-p_0)-(2-\alpha)\xi t_{11}'+t_{12}'=0, \tag{3.122}$$

$$-(1+\alpha)ft_{11}'+2t_{11}\left[-\alpha f'+(2-\alpha)\xi f''\right]-2f''t_{12}+t_{11}^2=0, \tag{3.123}$$

$$\begin{aligned}-(1+\alpha)ft_{22}'+2t_{12}\left[\alpha(1+\alpha)f-(2-\alpha)(3\alpha-1)\xi f'+(2-\alpha)^2\xi^2 f''\right]\\ +2(1+t_{22})\left[(2\alpha-1)f'-(2-\alpha)\xi f''\right]+t_{11}t_{22}=0,\end{aligned} \tag{3.124}$$

$$\begin{aligned}-(1+\alpha)ft_{12}'+\left[\alpha(1+\alpha)f-(2-\alpha)(3\alpha-1)\xi f'+(2-\alpha)^2\xi^2 f''\right]t_{11}\\ -(1-\alpha)f't_{12}-(1+t_{22})f''+t_{11}t_{12}=0,\end{aligned} \tag{3.125}$$

where $'$ denotes $d/d\xi$, or in natural stress variables

$$f(1+\alpha)\left(\tilde{\lambda}f''+\tilde{\lambda}'f'\right)+\tilde{\lambda}f'^2-2(1-\alpha)p_0-\tilde{\mu}'=0, \tag{3.126}$$

$$2\tilde{\mu}f''-\left(\tilde{\lambda}^2f'^2-2\alpha\tilde{\lambda}f'-f\tilde{\lambda}'(1+\alpha)\right)f'^2=0, \tag{3.127}$$

$$\tilde{\nu}f''-\left(\tilde{\mu}\tilde{\lambda}f'^2-\tilde{\mu}f'(1-\alpha)-\tilde{\mu}'f(1+\alpha)\right)f'^2=0, \tag{3.128}$$

$$\tilde{\lambda}f'^2\left(f'^2-\tilde{\nu}\right)+2(1-2\alpha)\tilde{\nu}f'+\tilde{\nu}'f(1+\alpha)=0. \tag{3.129}$$

In either formulation these represent a fifth order system of four coupled ODEs, and require the boundary and matching conditions

$$\text{at } \xi=0: \qquad f=f'=0, \tag{3.130}$$

$$\text{as } \xi\to\infty: \qquad f\sim\frac{C_0}{\kappa}\xi^{1+\alpha},\quad t_{11}\sim C_1,\quad t_{12}\sim C_1(1-\alpha)\xi,\quad t_{22}\sim C_1(1-\alpha)^2\xi^2. \tag{3.131}$$

For the natural stress equations the matching conditions to the core flow instead are

$$\begin{aligned}\text{as } \xi\to\infty: \qquad & f\sim\frac{C_0}{\kappa}\xi^{1+\alpha},\quad \tilde{\lambda}\sim\frac{2p_0\kappa^2}{(1+\alpha)^2C_0^2}\xi^{-2\alpha},\quad \tilde{\mu}\sim d_2\xi^{\alpha-1},\\ & \tilde{\nu}\sim\begin{cases}\frac{d_3}{\kappa^2}\xi^{2(2\alpha-1)}, & \text{for } \frac{2}{3}<\alpha<1,\\ -\frac{10p_0C_0}{3\kappa}\xi^{\frac{2}{3}}\log(\xi), & \text{for } \alpha=\frac{2}{3},\\ -\frac{2p_0(1+\alpha)C_0}{(2-3\alpha)\kappa}\xi^{\alpha}, & \text{for } \frac{1}{2}\le\alpha<\frac{2}{3}.\end{cases}\end{aligned} \tag{3.132}$$

The $\alpha = 2/3$ and $1/2 \le \alpha < 2/3$ $\tilde{\nu}$ matching conditions being detailed in appendix E. Since the points $\xi = 0$ and $\xi = \infty$ are both singular for the system of equations,

further analysis of the asymptotic behaviour near such points is required.

The similarity form of the boundary layer equations (3.126)-(3.129) are related to the Cartesian formulation (3.122)-(3.125) through the relationships

$$\tilde{\lambda} = \frac{t_{11}}{f'^2}, \tag{3.133}$$

$$\tilde{\mu} = t_{12} + \frac{t_{11}}{f'} \left\{ (1+\alpha) f - (2-\alpha)\xi f' \right\}, \tag{3.134}$$

$$\tilde{\nu} = (1+t_{22}) f'^2 + t_{11} \left\{ (1+\alpha) f - (2-\alpha)\xi f' \right\}^2 + 2t_{12} f' \left\{ (1+\alpha) f - (2-\alpha)\xi f' \right\}, \tag{3.135}$$

which follows from (3.106)-(3.108).

3.2.3 Behaviour at the wall

At the wall, we are interested in viscometric behaviour for the equations (3.122)-(3.125), and equations (3.126)-(3.129). Consequently, we consider a power series expansion about $\xi = 0$ which yields for (3.122)-(3.125) the behaviour

$$f(\xi) = a^3\xi^2 + a^4 b\xi^3 + \frac{1}{4!} f''''(0)\xi^4 + O(\xi^5), \tag{3.136}$$

$$t_{11}(\xi) = 2a^2 + 2((1-\alpha) + 2b)a^3\xi + ((1-\alpha)(11\alpha - 17) + 2b(b-\alpha))a^4\xi^2 + O(\xi^3), \tag{3.137}$$

$$t_{12}(\xi) = a + (6(1-\alpha) + b)a^2\xi + (4 - 3\alpha)(1 - \alpha + 2b)a^3\xi^2 + O(\xi^3), \tag{3.138}$$

$$t_{22}(\xi) = 6(1-\alpha)a\xi + 3((7-6\alpha)(1-\alpha) + b)a^2\xi^2 + \left(2(1-2\alpha)b^2 + (1-\alpha)\left((13-2\alpha)b + \frac{2}{3}(34\alpha^2 - 83\alpha + 42) \right) \right) a^3\xi^3 + O(\xi^4), \tag{3.139}$$

and for the natural stress equations (3.126)-(3.129) the behaviour

$$f(\xi) = a^3\xi^2 + a^4 b\xi^3 + \frac{1}{4!} f''''(0)\xi^4 + O(\xi^5), \tag{3.140}$$

$$\tilde{\lambda}(\xi) = \frac{1}{2a^4}\xi^{-2} + \frac{(1-\alpha) - b}{2a^3}\xi^{-1} + O(1), \tag{3.141}$$

$$\tilde{\mu}(\xi) = a + \{3(1-\alpha) + b\}\, a^2\xi + O(\xi^2), \tag{3.142}$$

$$\tilde{\nu}(\xi) = 4a^6\xi^2 + 12\,\{(1-\alpha) + b\}\, a^7\xi^3 + O(\xi^4), \tag{3.143}$$

where we have that

$$p_0 = -a^2 \left(1 + \frac{b}{2(1-\alpha)} \right), \tag{3.144}$$

and

$$f''''(0) = 2((1-\alpha)(17\alpha - 33) + 6b(b-1))a^5. \tag{3.145}$$

It can be seen that (3.136)-(3.139) reproduces viscometric behaviour as $\xi \to 0$ by using the leading order terms for f and t_{ij} and seeing that they are consistent with the equations (2.58) found in section 2.3.1 (with $\kappa = 1$ as it has been scaled out of the equations here). Equivalently the expansions (3.140)-(3.143) again satisfy viscometric behaviour as $\xi \to 0$, as the leading order terms are consistent with the equations (2.61), which hold provided $1 \ll 2a^2$ (again κ has been scaled out here). The constants a and b are related to $f''(0)$ and $f'''(0)$ by

$$f''(0) = 2a^3, \qquad f'''(0) = 6a^4 b. \tag{3.146}$$

The expansions above involve two independent parameters (a, p_0), where the parameter b has been introduced for convenience and is given in terms of the other two via (3.144). Imposing the asymptotic behaviour (3.136)-(3.139) upon the system (3.122)-(3.125), or equivalently imposing (3.140)-(3.143) on (3.126)-(3.129), furnishes a different boundary condition count according to the sign of the parameter a. This is crucial as $a < 0$ and $a > 0$ represent flow towards and away from the corner respectively (as it determines the sign of f, see equation (3.136) for example).

Cartesian wall analysis

To determine the number of degrees of freedom contained within the asymptotic behaviours (3.136)-(3.143) we perform an eigenmode analysis and consider the perturbation

$$(f(\xi), t_{ij}(\xi)) = \left(f_0(\xi), t^0_{ij}(\xi)\right) + \hat{\delta}\left(\hat{f}(\xi), \hat{t}_{ij}(\xi)\right), \quad \text{as } \xi \to \infty \tag{3.147}$$

where $f_0(\xi), t^0_{ij}(\xi)$ represent the regular power series expansion terms given in (3.136)-(3.139), and $\hat{\delta} \ll 1$ is a small artificial gauge. Keeping terms of $O(\hat{\delta})$, we record the

linearised equations satisfied by $\hat{f}(\xi)$, $\hat{t}_{ij}(\xi)$ in the Cartesian basis

$$0 = \xi\,(-2+\alpha)\,\hat{t}'_{11} - 2\,\hat{t}_{11} + \hat{t}'_{12} + 2\,\hat{t}_{11}\alpha, \tag{3.148}$$

$$\begin{aligned}0 = {} & \left((4\,\xi - 2\,\xi\,\alpha)\,\hat{t}_{11} - 2\,\hat{t}_{12}\right) f^{(0)\prime\prime} + \left((4\,\xi - 2\,\xi\,\alpha)\,t_{11}^{(0)} - 2\,t_{12}^{(0)}\right)\hat{f}'' + \hat{f}\,(-1-\alpha)\,t_{11}^{(0)\prime} \\ & + f^{(0)}\,(-1-\alpha)\,\hat{t}'_{11} - 2\,\hat{t}_{11} f^{(0)\prime}\alpha - 2\,t_{11}^{(0)}\left(\hat{f}'\,\alpha - \hat{t}_{11}\right),\end{aligned} \tag{3.149}$$

$$\begin{aligned}0 = {} & 2\left(\xi\,(-2+\alpha)\,t_{12}^{(0)} + 1 + t_{22}^{(0)}\right)(-2+\alpha)\,\xi\,\hat{f}'' + 2\,(-2+\alpha)\,\xi\,\left(\xi\,(-2+\alpha)\,\hat{t}_{12}\right. \\ & \left. + \hat{t}_{22}\right) f^{(0)\prime\prime} + \left(\left(4\,\xi + 6\,\xi\,\alpha^2 - 14\,\xi\,\alpha\right)t_{12}^{(0)} + (-2+4\,\alpha)\,t_{22}^{(0)} - 2 + 4\,\alpha\right)\hat{f}' \\ & + \left(\left(4\,\xi + 6\,\xi\,\alpha^2 - 14\,\xi\,\alpha\right)\hat{t}_{12} + (-2+4\,\alpha)\,\hat{t}_{22}\right) f^{(0)\prime} + \hat{f}\,(-1-\alpha)\,t_{22}^{(0)\prime} \\ & + f^{(0)}\,(-1-\alpha)\,\hat{t}'_{22} + 2\,\alpha\,\hat{f}\,(1+\alpha)\,t_{12}^{(0)} + 2\,\alpha\,f^{(0)}\,(1+\alpha)\,\hat{t}_{12} + \left(\hat{t}_{11}t_{22}^{(0)} + t_{11}^{(0)}\hat{t}_{22}\right),\end{aligned} \tag{3.150}$$

$$\begin{aligned}0 = {} & \left(\xi^2\,(-2+\alpha)^2\,t_{11}^{(0)} - t_{22}^{(0)} - 1\right)\hat{f}'' + \left(\xi^2\,(-2+\alpha)^2\,\hat{t}_{11} - \hat{t}_{22}\right) f^{(0)\prime\prime} \\ & + \left(\left(3\,\xi\,\alpha^2 - 7\,\xi\,\alpha + 2\,\xi\right)\hat{t}_{11} + \hat{t}_{12}\,(\alpha - 1)\right) f^{(0)\prime} + \left(\left(3\,\xi\,\alpha^2 - 7\,\xi\,\alpha + 2\,\xi\right)t_{11}^{(0)}\right. \\ & \left. + t_{12}^{(0)}\,(\alpha-1)\right)\hat{f}' + \hat{f}\,(-1-\alpha)\,t_{12}^{(0)\prime} + f^{(0)}\,(-1-\alpha)\,\hat{t}'_{12} + \left(\left(\alpha+\alpha^2\right)\hat{f} + \hat{t}_{12}\right)t_{11}^{(0)} \\ & + \hat{t}_{11}\left(\left(\alpha+\alpha^2\right)f^{(0)} + t_{12}^{(0)}\right).\end{aligned} \tag{3.151}$$

We can then substitute in the behaviour (3.136)-(3.139), and find the five asymptotic behaviours as $\xi \to 0$ (there will be five behaviours as we are considering a fifth order system). Three behaviours can be found with power series approximations in ξ for the functions $\hat{f}$ and $\hat{t}_{ij}$. They are

$$\left.\begin{array}{c}\hat{f} \sim 1 \\ \hat{t}_{11} \sim -\frac{(1+\alpha)(17\,\alpha - 3\,b - 13)a}{3} \\ \hat{t}_{12} \sim -\frac{(1+\alpha)(31\,\alpha - 23)}{6} \\ \hat{t}_{22} \sim -\frac{(1+\alpha)(4\alpha-3)}{a}\end{array}\right\}, \quad \left.\begin{array}{c}\hat{f} \sim \xi \\ \hat{t}_{11} \sim 1-\alpha \\ \hat{t}_{12} \sim \frac{1-2\,\alpha}{a} \\ \hat{t}_{22} \sim \frac{1-2\,\alpha}{a^2}\end{array}\right\}, \quad \left.\begin{array}{c}\hat{f} \sim \xi^2 \\ \hat{t}_{11} \sim \frac{4}{3a} \\ \hat{t}_{12} \sim \frac{1}{3a^2} \\ \hat{t}_{22} \sim \frac{2(1-\alpha)}{a^2}\xi\end{array}\right\}, \tag{3.152}$$

The final two behaviours are found by considering an exponential rather than power series form, being

$$\left.\begin{array}{l}\hat{f} = \xi^q \exp\left(-\frac{2}{a(1+\alpha)\xi} \pm \frac{4\sqrt{2a(1-2\alpha)}}{a(1+\alpha)\xi^{1/2}} + O(\xi^{1/2})\right) \\ \hat{t}_{11} = \frac{4}{(1+\alpha)^2 a^3}\xi^{q-4}\exp\left(-\frac{2}{a(1+\alpha)\xi} \pm \frac{4\sqrt{2a(1-2\alpha)}}{a(1+\alpha)\xi^{1/2}} + O(\xi^{1/2})\right) \\ \hat{t}_{12} = \frac{4(2-\alpha)}{(1+\alpha)^2 a^3}\xi^{q-3}\exp\left(-\frac{2}{a(1+\alpha)\xi} \pm \frac{4\sqrt{2a(1-2\alpha)}}{a(1+\alpha)\xi^{1/2}} + O(\xi^{1/2})\right) \\ \hat{t}_{22} = \mp\frac{2\sqrt{2a(1-2\alpha)}}{a^5(1+\alpha)^2}\xi^{q-7/2}\exp\left(-\frac{2}{a(1+\alpha)\xi} \pm \frac{4\sqrt{2a(1-2\alpha)}}{a(1+\alpha)\xi^{1/2}} + O(\xi^{1/2})\right)\end{array}\right\}, \tag{3.153}$$

where

$$q = \frac{27\alpha + 11 + 8b}{4(1+\alpha)}.$$

In the particular case $\alpha = 1/2$, the last two modes become

$$\left.\begin{array}{l} \hat{f} = \xi^q \exp\left(-\frac{2}{a(1+\alpha)\xi}\right) \\ \hat{t}_{11} = \frac{16}{9a^3}\xi^{q-4}\exp\left(-\frac{2}{a(1+\alpha)\xi}\right) \\ \hat{t}_{12} = \frac{8}{3a^3}\xi^{q-3}\exp\left(-\frac{2}{a(1+\alpha)\xi}\right) \\ \hat{t}_{22} = \frac{8(4b+10-3q)}{3a^4(4b-1-3q)}\xi^{q-3}\exp\left(-\frac{2}{a(1+\alpha)\xi}\right) \end{array}\right\}, \tag{3.154}$$

where

$$q = \frac{1}{6}\left(8b + 23 \pm \sqrt{97}\right).$$

For the exponential eigenmodes, sufficient terms in the expansions are needed to obtain the correction terms beyond the controlling factor. We note that the third algebraic mode in (3.152) corresponds to changes in the free parameter a and that its sign also determines the sign of the controlling factors in the exponential modes. Thus, the consistency of these eigenmodes with the wall behaviour (3.136)-(3.139) depends upon the sign of the parameter a and whether it is specified or not. Before drawing conclusions from this analysis, we note that a similar procedure can be undertaken to find the natural stress wall eigenmodes.

Natural stress wall analysis

Similarly to determine the number of degrees of freedom contained within the asymptotic behaviours (3.140)-(3.143) we perform an eigenmode analysis and consider the perturbation

$$\left(f(\xi), \tilde{\lambda}(\xi), \tilde{\mu}(\xi), \tilde{\nu}(\xi)\right) = (f_0(\xi), \lambda_0(\xi), \mu_0(\xi), \nu_0(\xi)) + \hat{\delta}\left(\hat{f}(\xi), \hat{\lambda}(\xi), \hat{\mu}(\xi), \hat{\nu}(\xi)\right), \quad \text{as } \xi \to \infty \tag{3.155}$$

where $f_0(\xi)$, $\lambda_0(\xi)$, $\mu_0(\xi)$, $\nu_0(\xi)$ represent the regular power series expansion terms given in (3.140)-(3.143). The natural stress wall eigenmodes are thus

$$\left.\begin{array}{c} \hat{f} \sim 1 \\ \hat{\lambda} \sim -\frac{(1+\alpha)(5\alpha-3)}{6a^5}\xi^{-2} \\ \hat{\mu} \sim \frac{1+\alpha}{a}\xi^{-1} \\ \hat{\nu} \sim 4a^4(1+\alpha)\xi \end{array}\right\}, \quad \left.\begin{array}{c} \hat{f} \sim \xi \\ \hat{\lambda} \sim -\frac{1}{2a^7}\xi^{-3} \\ \hat{\mu} \sim \frac{25(1-\alpha)}{6a} \\ \hat{\nu} \sim 4a^3\xi \end{array}\right\}, \quad \left.\begin{array}{c} \hat{f} \sim \xi^2 \\ \hat{\lambda} \sim -\frac{2}{3a^7}\xi^{-2} \\ \hat{\mu} \sim \frac{1}{3a^2} \\ \hat{\nu} \sim 8a^3\xi^2 \end{array}\right\}, \tag{3.156}$$

and

$$\left.\begin{aligned}
\hat{f} &\sim \xi^q \exp\left(-\tfrac{2}{a(1+\alpha)\xi} \pm \tfrac{4\sqrt{2a(1-2\alpha)}}{a(1+\alpha)\xi^{1/2}} + O(\xi^{1/2})\right) \\
\hat{\lambda} &\sim \tfrac{1}{(1+\alpha)^2 a^9}\xi^{q-6}\exp\left(-\tfrac{2}{a(1+\alpha)\xi} \pm \tfrac{4\sqrt{2a(1-2\alpha)}}{a(1+\alpha)\xi^{1/2}} + O(\xi^{1/2})\right) \\
\hat{\mu} &\sim \tfrac{2(3-\alpha)}{(1+\alpha)^2 a^3}\xi^{q-3}\exp\left(-\tfrac{2}{a(1+\alpha)\xi} \pm \tfrac{4\sqrt{2a(1-2\alpha)}}{a(1+\alpha)\xi^{1/2}} + O(\xi^{1/2})\right) \\
\hat{\nu} &\sim \mp\tfrac{8a\sqrt{2a(1-2\alpha)}}{(1+\alpha)^2}\xi^{q-3/2}\exp\left(-\tfrac{2}{a(1+\alpha)\xi} \pm \tfrac{4\sqrt{2a(1-2\alpha)}}{a(1+\alpha)\xi^{1/2}} + O(\xi^{1/2})\right)
\end{aligned}\right\},$$

$$\text{where} \quad q = \frac{27\alpha + 11 + 8b}{4(1+\alpha)}. \tag{3.157}$$

The third eigenmode corresponds to changes in the parameter a. In the particular case $\alpha = 1/2$, the last two modes become

$$\left.\begin{aligned}
\hat{f} &\sim \xi^q \exp\left(-\tfrac{2}{a(1+\alpha)\xi}\right) \\
\hat{\lambda} &\sim \tfrac{4}{9a^9}\xi^{q-6}\exp\left(-\tfrac{2}{a(1+\alpha)\xi}\right) \\
\hat{\mu} &\sim \tfrac{8(2+\alpha)}{9a^3}\xi^{q-3}\exp\left(-\tfrac{2}{a(1+\alpha)\xi}\right) \\
\hat{\nu} &\sim \tfrac{32(3q-4b-10)}{3(3q-4b+1)}\xi^{q-1}\exp\left(-\tfrac{2}{a(1+\alpha)\xi}\right)
\end{aligned}\right\}, \quad \text{where} \quad q = \frac{1}{6}\left(8b + 23 \pm \sqrt{97}\right). \tag{3.158}$$

Wall behaviour conclusions

The conclusions from the Cartesian eigenmode analysis (also holding from the natural stress analysis) are thus

- The case $a < 0$ represents flow towards the corner singularity and is relevant to the upstream boundary layer. Specifying a (and p_0) in (3.136)-(3.139) means that such an expansion imposes five conditions on the system (3.122)-(3.125) since all modes are now inconsistent. Consequently the upstream boundary layer problem may be posed as an initial value problem, the complete wall expansion being analytic in this case.

- The case $a > 0$ is relevant to the downstream boundary layer, where the usual situation is for a to be left unspecified and determined as part of the solution. The expansion (3.136)-(3.139) now imposes only two conditions on (3.122)-(3.125). Consequently the downstream boundary layer needs to be posed as a boundary value problem, where the far-field matching conditions need to supply three boundary conditions (i.e. three linearly independent pieces of information need to come from the solution in the core outer region). The wall expansion is no

longer analytic but now contains an essential singularities manifested through two sets of linearly independent exponentially small terms.

The degenerate case of zero shear rate $a = 0$ needs care and is not straightforward for the expansion (3.136)-(3.139), we consider this in the Cartesian basis as an illustration of the issue. Performing the same substitutions as at the beginning of this section, but assuming that the power series of f starts at ξ^3 then the wall expansion now takes the form

$$f(\xi) = \frac{4}{5}(\alpha-1)^3 p_0^3 \xi^5 + \frac{8}{21}(\alpha-1)^4 p_0^4 (2\alpha-3)\xi^7 + O(\xi^8), \tag{3.159}$$

$$t_{11}(\xi) = 8(\alpha-1)^2 p_0^2 \xi^2 + \frac{56}{15}(\alpha-1)^3 p_0^3 (2\alpha-3)\xi^4 + O(\xi^5), \tag{3.160}$$

$$t_{12}(\xi) = 2(\alpha-1)p_0\xi - \frac{16}{3}(\alpha-1)^2 p_0^2 (2\alpha-3)\xi^3 + O(\xi^5), \tag{3.161}$$

$$t_{22}(\xi) = -3(\alpha-1)p_0(2\alpha-3)\xi^2 + \frac{1}{15}(\alpha-1)^2 p_0^2 (115\alpha-167)(2\alpha-3)\xi^4 + O(\xi^5), \tag{3.162}$$

which cannot be obtained simply by taking the limit $a \to 0$ in (3.136)-(3.139). The leading order terms do agree however with those found in section 2.3.2, where a more general expansion than viscometric behaviour has been investigated. To relate these coefficients to equation (2.77) we set

$$n = 5, \qquad \tilde{a} = -2(1-\alpha)p_0, \qquad \text{and} \qquad \mathrm{We} = 1. \tag{3.163}$$

To find out how this relates to the nonzero a case we consider the pressure, p_0. With a nonzero the pressure is given in (3.144), and thus for the pressure to be nonzero and finite in the $a \to 0$ case, we require $b \to \infty$ with $b = O(a^{-2})$. Such a behaviour eventually causes certain coefficients in each variable in (3.136)-(3.139) to become singular (note the third term for $t_{22}(\xi)$, see (3.139), whilst it occurs for latter terms in the expansion for the other variables). Consequently the double limit $(a, \xi) \to 0$ appears to be non-uniform, in contrast to that of the UCM model. Another observation is that since $p_0 > 0$, the expansion (3.159)-(3.162) appears only to be relevant to the upstream boundary layer due to the stream function f being negative close to the wall. In other words, the equations do not seem to allow parallel (as oppose to reverse) flows with zero shear rate to form at the downstream wall.

These issues with the $a \to 0$ limit are possibly expected. The form of the viscometric behaviour (2.58) which arises from the expansions (3.136)-(3.139) from the boundary layer equations $\overset{\triangledown}{\mathbf{T}} + \kappa\,(\mathrm{tr}\mathbf{T})\,\mathbf{T} = 2\mathbf{D}$ is actually the form for when the shear rate is large (see section 2.3.1, equation (2.53)). The $a \to 0$ limit is the limit of zero shear,

and thus the viscometric behaviour from section 2.3.1 would be of the UCM form of (2.54). This suggests that in the $a \to 0$ limit there is a complex relationship between the sizes of ξ and ϵ causing a different balance in the boundary layer equations.

3.2.4 The far-field behaviour

Knowing the conditions supplied by imposing behaviour at the upstream and downstream walls, we now investigate the behaviour in the far-field.

Cartesian far-field analysis

Since we know the asymptotic behaviour as $\xi \to \infty$ of our functions (from (3.131)), we can perturb a small amount $\hat{\delta}$ away:

$$\begin{aligned} f &\sim \frac{C_0}{\kappa}\xi^{(1+\alpha)}(1+\hat{\delta}\hat{f}), \qquad t_{11} \sim C_1(1+\hat{\delta}\hat{t}_{11}), \\ t_{12} &\sim C_1(1-\alpha)\xi(1+\hat{\delta}\hat{t}_{12}), \qquad t_{22} \sim C_1(1-\alpha)^2\xi^2(1+\hat{\delta}\hat{t}_{22}), \end{aligned} \tag{3.164}$$

For the Cartesian modes, substituting $\hat{f} = \xi^m$ and $\hat{t}_{ij} = A_{ij}\xi^m$ and linearising the equations gives values of m of

$$m = 0, -2(1-\alpha), -1, -(2-\alpha), -2(2-\alpha) \tag{3.165}$$

and thus the asymptotic behaviours for the eigenmodes are

$$\left.\begin{aligned} \hat{f} &\sim 1 \\ \hat{t}_{11} &\sim 0 \\ \hat{t}_{12} &\sim 0 \\ \hat{t}_{22} &\sim 0 \end{aligned}\right\}, \quad \left.\begin{aligned} \hat{f} &\sim \xi^{-2(1-\alpha)} \\ \hat{t}_{11} &\sim \tfrac{4\alpha-2}{1+\alpha}\xi^{-2(1-\alpha)} \\ \hat{t}_{12} &\sim \tfrac{4\alpha-4}{1+\alpha}\xi^{-2(1-\alpha)} \\ \hat{t}_{22} &\sim \tfrac{4\alpha-6}{1+\alpha}\xi^{-2(1-\alpha)} \end{aligned}\right\}, \quad \left.\begin{aligned} \hat{f} &\sim \xi^{-1} \\ \hat{t}_{11} &\sim 0 \\ \hat{t}_{12} &\sim \tfrac{-1}{1-\alpha^2}\xi^{-1} \\ \hat{t}_{22} &\sim \tfrac{-2}{1-\alpha^2}\xi^{-1} \end{aligned}\right\}, \tag{3.166}$$

$$\left.\begin{aligned} \hat{f} &\sim \xi^{-(2-\alpha)} \\ \hat{t}_{11} &\sim \tfrac{2(2-\alpha)(2\alpha-1)(1-\alpha)}{(1+\alpha)(\alpha^2-5\alpha+2)}\xi^{-(2-\alpha)} \\ \hat{t}_{12} &\sim \tfrac{2(2-\alpha)(2\alpha-1)(\alpha^2-2\alpha+2)}{(1-\alpha)(1+\alpha)(\alpha^2-5\alpha+2)}\xi^{-(2-\alpha)} \\ \hat{t}_{22} &\sim \tfrac{2(2-\alpha)(2\alpha-1)(\alpha^2-2\alpha+3)}{(1-\alpha)(1+\alpha)(\alpha^2-5\alpha+2)}\xi^{-(2-\alpha)} \end{aligned}\right\}, \tag{3.167}$$

$$\left.\begin{aligned} \hat{f} &\sim \xi^{-2(2-\alpha)} \\ \hat{t}_{11} &\sim \tfrac{6(1-\alpha)(2-\alpha)(2\alpha-3)}{(1+\alpha)(3\alpha^2-10\alpha+6)}\xi^{-2(2-\alpha)} \\ \hat{t}_{12} &\sim \tfrac{12(-2+\alpha)(\alpha^2-3\alpha+3)}{(1+\alpha)(3\alpha^2-10\alpha+6)}\xi^{-2(2-\alpha)} \\ \hat{t}_{22} &\sim \tfrac{2(-2+\alpha)(6\alpha^5-33\alpha^4+75\alpha^3-73\alpha^2+20\alpha+6)}{\alpha(1-\alpha)^2(1+\alpha)(3\alpha^2-10\alpha+6)}\xi^{-2(2-\alpha)} \end{aligned}\right\}. \tag{3.168}$$

It should be noted that the coefficients involved in the fourth eigenmode are singular at $\alpha = \frac{5-\sqrt{7}}{3} \approx 0.785$, indicating that such terms require modifying at this isolated value of the corner angle.

Full far-field description

To continue the work in the far-field using the Cartesian basis, we need to determine higher order terms in the asymptotic expansion (not just the leading order terms in (3.131)), to have a correct specification of the problem. This will include homogeneous terms which can be determined from the eigenmodes above, and the forcing terms which were neglected in the linearised equations. It would be expected that the expansion contain five free constants $(C_0, C_2, C_3, C_4, C_5)$, with each eigenmode corresponding to small changes in these constants, as was found by Evans for the UCM model in [Eva08a]. C_1 is fixed by equation (3.69) and it has been assumed that p_0 is also fixed in our analysis.

The expressions found are significantly larger than the UCM equivalent, and thus are recorded in appendix F. Here we note simply the forms of the expansions, being

$$\begin{aligned} f(\xi) \sim & \frac{C_0}{\kappa}\xi^{1+\alpha}\Big(1 + C_2\xi^{-2+2\alpha} + C_3\xi^{-1} + C_4\xi^{-2+\alpha} \\ & + C_5\xi^{-4+2\alpha} + \left[\frac{2(2\alpha-1)\kappa p_0}{\alpha(1-\alpha)(3\alpha-2)C_0}\xi^{-\alpha} + \text{additional forcing terms}\right]\Big), \end{aligned} \tag{3.169}$$

$$\begin{aligned} t_{11}(\xi) \sim & C_1\left(1 + \frac{2(2\alpha-1)C_2}{1+\alpha}\xi^{-2+2\alpha} + \left(\frac{2(1-\alpha)(2\alpha-1)(2-\alpha)C_4}{(1+\alpha)(\alpha^2-5\alpha+2)}\right)\xi^{-2+\alpha}\right. \\ & + \frac{6(2\alpha-3)(1-\alpha)(2-\alpha)C_5}{(1+\alpha)(3\alpha^2-10\alpha+6)}\xi^{-4+2\alpha} + \left[\frac{\kappa C_1}{C_0(1+\alpha)(3\alpha-2)}\xi^{-\alpha}\right. \\ & \left.\left. + \text{additional forcing terms}\right]\right), \end{aligned} \tag{3.170}$$

$$\begin{aligned} t_{12}(\xi) \sim & C_1(1-\alpha)\xi\left(1 - \frac{4(1-\alpha)C_2}{1+\alpha}\xi^{-2+2\alpha} - \frac{C_3}{(1-\alpha)(1+\alpha)}\xi^{-1}\right. \\ & + \frac{2(\alpha^2-2\alpha+2)(2\alpha-1)(2-\alpha)C_4}{(1+\alpha)(\alpha^2-5\alpha+2)(1-\alpha)}\xi^{-2+\alpha} \\ & + \frac{12(\alpha^2-3\alpha+3)(-2+\alpha)C_5}{(1+\alpha)(3\alpha^2-10\alpha+6)}\xi^{-4+2\alpha} \\ & \left. + \left[\frac{\kappa C_1(\alpha^2-4\alpha+2)}{C_0(1+\alpha)(3\alpha-2)(1-\alpha)^2}\xi^{-\alpha} + \text{ additional forcing terms}\right]\right), \end{aligned} \tag{3.171}$$

$$\begin{aligned} t_{22}(\xi) \sim & C_1(1-\alpha)^2\xi^2\left(1+\frac{2(2\alpha-3)C_2}{1+\alpha}\xi^{-2+2\alpha}-\frac{2C_3}{(1-\alpha)(1+\alpha)}\xi^{-1}\right. \\ & +\frac{2C_4(2-\alpha)(2\alpha-1)(\alpha^2-2\alpha+3)}{(1-\alpha)(1+\alpha)(\alpha^2-5\alpha+2)}\xi^{-2+\alpha} \\ & +\frac{2C_5(-2+\alpha)(6\alpha^5-33\alpha^4+75\alpha^3-73\alpha^2+20\alpha+6)}{\alpha(1+\alpha)(1-\alpha)^2(3\alpha^2-10\alpha+6)}\xi^{-4+2\alpha} \\ & \left.+\left[\frac{(\alpha^2-6\alpha+3)\kappa C_1}{(1+\alpha)(3\alpha-2)(1-\alpha)^2C_0}\xi^{-\alpha}+\text{ additional forcing terms}\right]\right). \end{aligned} \tag{3.172}$$

It should be noted that the expansions recorded in appendix F are for both $\alpha \neq 2/3$ and $\alpha = 2/3$, the second case arising as the coefficients of the leading order forced terms are singular at $\alpha = 2/3$. It is also important to note that the forcing terms intrude in the expansion between the unforced terms, the terms of $O(\xi^{-\alpha})$ shown indeed occur before the unforced terms of $O(\xi^{-2+2\alpha})$ for $1/2 < \alpha < 2/3$. Using the relationship between the two bases, (3.133)-(3.135), we can now use these full far-field expansions to find the asymptotic behaviour of the natural stress variables in terms of the Cartesian free constants as

$$\tilde{\lambda} \sim \frac{\kappa^2 C_1}{(1+\alpha)^2 C_0^2}\xi^{-2\alpha}, \tag{3.173}$$

$$\tilde{\mu} \sim \begin{cases} -\left(\frac{C_1C_4\alpha(1-\alpha)(2-\alpha)}{(\alpha^2-5\alpha+2)(1+\alpha)}\right)\xi^{-1+\alpha}, & \text{for } \alpha \neq \frac{2}{3}, \\ -\left(\frac{3969C_1^3\kappa^2}{320C_0^2}-\frac{C_1C_4}{5}\right)\xi^{-1/3}, & \text{for } \alpha = \frac{2}{3}, \end{cases} \tag{3.174}$$

$$\tilde{\nu} \sim \begin{cases} \frac{C_0^2(2-\alpha)^2}{243\kappa^2C_1\alpha(3\alpha^2-10\alpha+6)}\left(-\frac{(3\alpha^5-16\alpha^4+15\alpha^3+15\alpha^2-21\alpha+6)C_4^2}{2(\alpha^2-5\alpha+2)}\right. & \\ \qquad \left.+C_5(2\alpha-3)(1+\alpha)\right)\xi^{4\alpha-2}+\frac{C_1C_0(1+\alpha)}{\kappa(3\alpha-2)}\xi^{\alpha}, & \text{for } \alpha \neq \frac{2}{3}, \\ -\frac{5C_0C_1}{3\kappa}\xi^{2/3}\log(\xi) & \\ \qquad +\left(-\frac{C_1C_0}{24\kappa}+\frac{9741079971}{5120000}\frac{C_1^5\kappa^2}{C_0^2}+\frac{310511}{4800}C_1^3C_4\right. & \\ \qquad\qquad \left.+\frac{14C_0^2C_1C_4^2}{9\kappa^2}-\frac{200C_0^2C_1C_5}{9\kappa^2}\right)\xi^{2/3} & \text{for } \alpha = \frac{2}{3}, \end{cases} \tag{3.175}$$

as $\xi \to \infty$.

Natural stress far-field analysis

In the natural stress basis we know the asymptotic behaviour as $\xi \to \infty$ of our functions from (3.132). We thus perturb by $\hat{\delta}$ similarly to the Cartesian analysis:

$$f \sim \frac{C_0}{\kappa}\xi^{(1+\alpha)}(1+\hat{\delta}\hat{f}), \qquad \tilde{\lambda} \sim \frac{2p_0\kappa^2}{(1+\alpha)^2C_0^2}\xi^{-2\alpha}(1+\hat{\delta}\hat{\lambda}), \qquad \tilde{\mu} \sim d_2\xi^{\alpha-1}(1+\hat{\delta}\hat{\mu}),$$
$$\tilde{\nu} \sim \begin{cases} \frac{d_3}{\kappa^2}\xi^{2(2\alpha-1)}(1+\hat{\delta}\hat{\nu}), & \text{for } \frac{2}{3} < \alpha < 1, \\ -\frac{5C_0C_1}{3\kappa}\xi^{2/3}\log(\xi)(1+\hat{\delta}\hat{\nu}), & \text{for } \alpha = \frac{2}{3}, \\ \frac{d_1C_0^3n^3}{\kappa(3\alpha-2)}\xi^{\alpha}(1+\hat{\delta}\hat{\nu}), & \text{for } \frac{1}{2} \le \alpha < \frac{2}{3}. \end{cases} \tag{3.176}$$

To find the eigenmodes we linearise by keeping only the $O(\hat{\delta})$ terms. Retaining only the leading order we obtain

$$\begin{aligned} 2\alpha\hat{f}' + \hat{\lambda}'(1+\alpha) &= 0, \\ (1-\alpha)\hat{f}' + \hat{\mu}'(1+\alpha) &= 0, \\ \xi^2\hat{f}'' + \xi(1+\alpha)\hat{\lambda}' + 4\xi\hat{f}' + (1+\alpha)(1-\alpha)(2\hat{f}+\hat{\lambda}) &= 0, \end{aligned} \tag{3.177}$$

with either

$$2(1-2\alpha)\hat{f}' + \hat{\nu}'(1+\alpha) = 0, \tag{3.178}$$

when $\frac{2}{3} \le \alpha < 1$, or when $\frac{1}{2} \le \alpha < \frac{2}{3}$ the $\hat{\nu}$ equation is

$$(3\alpha-2)(1+\alpha)(3\hat{f}+\hat{\lambda}-\hat{\nu}) + \xi\left((1+\alpha)\hat{\nu}' + 2(4\alpha-3)\hat{f}'\right) = 0. \tag{3.179}$$

The far-field eigenmodes are found from the above equations for $\frac{2}{3} < \alpha < 1$ as

$$\left.\begin{array}{c} \hat{f} \sim 1 \\ \hat{\lambda} \sim -2 \\ \hat{\mu} \sim 0 \\ \hat{\nu} \sim 0 \end{array}\right\}, \quad \left.\begin{array}{c} \hat{f} \sim 0 \\ \hat{\lambda} \sim 0 \\ \hat{\mu} \sim 1 \\ \hat{\nu} \sim 0 \end{array}\right\}, \quad \left.\begin{array}{c} \hat{f} \sim 0 \\ \hat{\lambda} \sim 0 \\ \hat{\mu} \sim 0 \\ \hat{\nu} \sim 1 \end{array}\right\},$$

$$\left.\begin{array}{c} \hat{f} \sim \xi^{-1} \\ \hat{\lambda} \sim -\frac{2\alpha}{1+\alpha}\xi^{-1} \\ \hat{\mu} \sim -\frac{1-\alpha}{1+\alpha}\xi^{-1} \\ \hat{\nu} \sim -\frac{2(1-2\alpha)}{1+\alpha}\xi^{-1} \end{array}\right\}, \quad \left.\begin{array}{c} \hat{f} \sim \xi^{-2(1-\alpha)} \\ \hat{\lambda} \sim -\frac{2\alpha}{1+\alpha}\xi^{-2(1-\alpha)} \\ \hat{\mu} \sim -\frac{1-\alpha}{1+\alpha}\xi^{-2(1-\alpha)} \\ \hat{\nu} \sim -\frac{2(1-2\alpha)}{1+\alpha}\xi^{-2(1-\alpha)} \end{array}\right\}, \tag{3.180}$$

for $\frac{1}{2} \leq \alpha < \frac{2}{3}$ as

$$\left.\begin{array}{c}\hat{f}\sim 1\\ \hat{\lambda}\sim -2\\ \hat{\mu}\sim 0\\ \hat{\nu}\sim 1\end{array}\right\},\quad \left.\begin{array}{c}\hat{f}\sim 0\\ \hat{\lambda}\sim 0\\ \hat{\mu}\sim 1\\ \hat{\nu}\sim 0\end{array}\right\},\quad \left.\begin{array}{c}\hat{f}\sim 0\\ \hat{\lambda}\sim 0\\ \hat{\mu}\sim 0\\ \hat{\nu}\sim \xi^{3\alpha-2}\end{array}\right\},$$

$$\left.\begin{array}{c}\hat{f}\sim \xi^{-1}\\ \hat{\lambda}\sim -\frac{2\alpha}{1+\alpha}\xi^{-1}\\ \hat{\mu}\sim -\frac{1-\alpha}{1+\alpha}\xi^{-1}\\ \hat{\nu}\sim \frac{\alpha}{1+\alpha}\xi^{-1}\end{array}\right\},\quad \left.\begin{array}{c}\hat{f}\sim \xi^{-2(1-\alpha)}\\ \hat{\lambda}\sim -\frac{2\alpha}{1+\alpha}\xi^{-2(1-\alpha)}\\ \hat{\mu}\sim -\frac{1-\alpha}{1+\alpha}\xi^{-2(1-\alpha)}\\ \hat{\nu}\sim \frac{19\alpha^2-21\alpha+6}{\alpha(1+\alpha)}\xi^{-2(1-\alpha)}\end{array}\right\}, \tag{3.181}$$

and finally

$$\left.\begin{array}{c}\hat{f}\sim 1\\ \hat{\lambda}\sim -2\\ \hat{\mu}\sim 0\\ \hat{\nu}\sim 1\end{array}\right\},\quad \left.\begin{array}{c}\hat{f}\sim 0\\ \hat{\lambda}\sim 0\\ \hat{\mu}\sim 1\\ \hat{\nu}\sim 0\end{array}\right\},\quad \left.\begin{array}{c}\hat{f}\sim 0\\ \hat{\lambda}\sim 0\\ \hat{\mu}\sim 0\\ \hat{\nu}\sim 1/\log(\xi)\end{array}\right\},$$

$$\left.\begin{array}{c}\hat{f}\sim \xi^{-1}\\ \hat{\lambda}\sim -\frac{4}{5}\xi^{-1}\\ \hat{\mu}\sim -\frac{1}{5}\xi^{-1}\\ \hat{\nu}\sim \frac{2}{5}\xi^{-1}\end{array}\right\},\quad \left.\begin{array}{c}\hat{f}\sim \xi^{-2/3}\\ \hat{\lambda}\sim -\frac{4}{5}\xi^{-2/3}\\ \hat{\mu}\sim -\frac{1}{5}\xi^{-2/3}\\ \hat{\nu}\sim \frac{2}{5}\xi^{-2/3}\end{array}\right\}, \tag{3.182}$$

for $\alpha = 2/3$. We are now in a position to write a full far-field expansion of the natural stress variables, with it being

$$\begin{aligned} f &\sim \frac{C_0}{\kappa}\xi^{1+\alpha}, \qquad \tilde{\lambda} \sim \frac{2p_0\kappa^2}{(1+\alpha)^2 C_0^2}\xi^{-2\alpha}, \qquad \tilde{\mu} \sim d_2\xi^{-1+\alpha},\\ \tilde{\nu} &\sim \begin{cases} \frac{d_3}{\kappa^2}\xi^{4\alpha-2} + \frac{C_1C_0(1+\alpha)}{\kappa(3\alpha-2)}\xi^{\alpha}, & \text{for } \alpha \neq \frac{2}{3}\\ -\frac{5C_0C_1}{3\kappa}\xi^{2/3}\log(\xi) + \frac{d_3}{\kappa}\xi^{2/3} & \text{for } \alpha = \frac{2}{3}, \end{cases} \end{aligned} \tag{3.183}$$

The two terms in the $\tilde{\nu}$ expansion change their relative order depending on the value of α. This shows where the free constant d_3 appears for $\frac{1}{2} \leq \alpha < \frac{2}{3}$, and that as α reaches and then exceeds $\frac{2}{3}$ the term involving d_3 dominates.

Boundary layer analysis summary

We summarise the findings from the wall and far-field analysis.

- The case $a < 0$ is relevant to the upstream layer, where the Cartesian system (3.122)-(3.125), or the natural stress system (3.126)-(3.129) with the appropriate expansions from (3.136)-(3.143) can be posed as an IVP to attain the far-field

behaviours (F.1)-(F.8) or (3.183). The coefficients a and p_0 need to be specified and the wall expansion may be expressed as a power series in ξ.

- The case $a > 0$ applies to the downstream layer, where (3.122)-(3.125) with (3.136)-(3.139) and (F.1)-(F.8), or the natural stress system (3.126)-(3.129) with (3.140)-(3.143) and (3.183) is a two-point BVP. Imposing the wall behaviour furnishes two conditions with the remaining three from prescribing C_0, d_2 and d_3 in the natural stress formulation, or any three from C_0, C_2, C_3, C_4, C_5, in the Cartesian formulation. The coefficient a is now to be determined (p_0 still needs to be specified) and the wall expansion in addition to the power series contains exponentially small terms (see the two sets of exponential wall eigenmodes in either basis).

Considering the natural stress formulation, the first two terms in the far-field behaviour for $\tilde{\nu}$ (3.183) are of relevance. We note that when $1/2 \leq \alpha \leq 2/3$, the homogeneous terms $O(\xi^{2(2\alpha-1)})$ match into corresponding higher order homogeneous outer solution terms of size $O(\delta^{3\alpha-2}) = O(\epsilon^{(1-\alpha)(3\alpha-2)})$ relative to $\nu^{*(0)}$. This is precisely the relative difference in the two scalings for θ_3, which were

$$\begin{aligned} &\theta_3 = \epsilon^{2\alpha(2\alpha-1)}, \quad n_3 = \tfrac{2(2\alpha-1)}{1+\alpha}, \quad \text{for } 2/3 < \alpha < 1, \\ &\theta_3 = \epsilon^{\alpha^2+3\alpha-2}, \quad n_3 = \tfrac{\alpha}{1+\alpha}, \qquad \text{for } 1/2 \leq \alpha \leq 2/3, \end{aligned} \tag{3.184}$$

where we have included the different values of n_3 for reference also. These values are continuous at $\alpha = 2/3$.

As stated, both (3.122)-(3.125) and (3.126)-(3.129) are fifth-order implicit systems. They can be rearranged to form an explicit system, which we demonstrate for the natural stress equations. Using (3.127) and (3.128) in (3.126), we may obtain the expression

$$f'' = f'^2 \frac{2p_0(1-\alpha^2)f + \tilde{\mu}f'(\tilde{\lambda}f' + \alpha - 1) - (1+\alpha)ff'^2\tilde{\lambda}(\tilde{\lambda}f' + 1 - 2\alpha)}{(1+\alpha)^2 f^2 f'^2 \tilde{\lambda} - 2(1+\alpha)ff'\tilde{\mu} + \tilde{\nu}}. \tag{3.185}$$

As a result, (3.185) with (3.127)-(3.129) allow an explicit statement of the system involving f, f', $\tilde{\lambda}$, $\tilde{\mu}$, $\tilde{\nu}$, which is more convenient for numerical implementation.

3.2.5 Solution parameter dependence

Considering the Cartesian system, the continuous scaling group

$$\xi = \beta\bar{\xi}, \quad f = \frac{1}{\beta}\bar{f}, \quad t_{11} = \frac{1}{\beta^2}\bar{t}_{11}, \quad t_{12} = \frac{1}{\beta}\bar{t}_{12}, \quad t_{22} = \bar{t}_{22}, \quad p_0 = \frac{1}{\beta^2}\bar{p}_0,$$
$$a = \frac{1}{\beta}\bar{a}, \quad b = \bar{b}, \quad C_0 = \frac{1}{\beta^{2+\alpha}}\bar{C}_0 \quad C_1 = \frac{1}{\beta^2}\bar{C}_1, \quad C_2 = \beta^{2(1-\alpha)}\bar{C}_2,$$
$$C_3 = \beta\bar{C}_3, \quad C_4 = \beta^{2-\alpha}\bar{C}_4, \quad C_5 = \beta^{2(2-\alpha)}\bar{C}_5, \tag{3.186}$$

leaves the equations (3.122)–(3.125), the wall expansions (3.136)–(3.139) and the far-field behaviours (F.1)–(F.8) invariant for β real. Such an invariance may be exploited to reduce the solution parameter dependence as follows. Since the pressure gradient coefficient p_0 is common to all three asymptotic regions, we choose to normalise its value to unity by using $\beta = p_0^{-1/2}$ in the above scalings. Consequently, if we have the parameter values $(a, p_0, C_0, C_2, C_3, C_4, C_5) = (\bar{a}, \bar{p}_0, \bar{C}_0, \bar{C}_2, \bar{C}_3, \bar{C}_4, \bar{C}_5)$ in the case $\bar{p}_0 = 1$ (where b is fixed through (3.144)), then we can obtain their values for general $p_0 > 0$ via the relationships

$$a = p_0^{1/2}\bar{a}, \quad C_0 = p_0^{1+(\alpha/2)}\bar{C}_0 \quad C_2 = p_0^{\alpha-1}\bar{C}_2, \quad C_3 = p_0^{-(1/2)}\bar{C}_3,$$
$$C_4 = p_0^{-1+(\alpha/2)}\bar{C}_4, \quad C_5 = p_0^{\alpha-2}\bar{C}_5. \tag{3.187}$$

Similarly, the parameter p_0 can be removed from the equations (3.126)-(3.129) through the scalings

$$\xi = p_0^{-1/2}\hat{\xi}, \quad f = p_0^{1/2}\hat{f}, \quad \tilde{\lambda} = p_0^{-1}\hat{\lambda}, \quad \tilde{\mu} = p_0^{1/2}\hat{\mu}, \quad \tilde{\nu} = p_0^2\hat{\nu}, \tag{3.188}$$

allowing the wall and far-field behaviours ((3.140)-(3.143) and (3.183) respectively) to be expressed in terms of the similarity parameters

$$\frac{a}{p_0^{1/2}}, \quad \frac{C_0}{\kappa p_0^{1+(\alpha/2)}}, \quad \frac{d_2}{p_0^{\alpha/2}}, \quad \frac{d_3}{\kappa^2 p_0^{1+2\alpha}}, \tag{3.189}$$

this last parameter (associated with the far-field behaviour of $\tilde{\nu}$) needing modification in the case $\alpha = 2/3$ to

$$\frac{d_3}{\kappa^2 p_0^{7/3}} + \frac{5}{3}\frac{C_0}{\kappa p_0^{4/3}}\log(p_0). \tag{3.190}$$

As such, the boundary layer solution can be described without explicit prescription of the parameters p_0 and κ.

3.3 Numerical analysis

To complete the solution, we provide numerical results for the upstream and downstream boundary layers. Initially we will consider the Cartesian formulation, for which we can give numerical results for the upstream boundary layer followed by results using the natural stress formulation for both upstream and downstream boundary layers.

3.3.1 Cartesian numerical results for the upstream boundary layer

Here we use the Cartesian system of equations applied to the upstream wall boundary layer. We are interested in solving the fifth order system (3.122)-(3.125) subject to wall expansions (3.136)-(3.139) in the case where $a < 0$ in which flow is towards the singularity. Imposing (3.136)-(3.139) gives us the five boundary conditions needed to be able to solve this system numerically as an initial value problem using MATLAB's stiff solver ode15s, which is a variable-order, multi-step solver based on numerical differentiation formulas. The equations (3.122)-(3.125) as stated are implicit, but can be made explicit by using (3.123) and (3.125) in (3.122) to obtain an equation for $f''(\xi)$ and consequently can be expressed as a system of first-order equations involving $f, f', t_{11}, t_{12}, t_{22}$. Tight solver tolerances of $RelTol = 10^{-13}$ and $AbsTol = 10^{-13}$ were used and the numerical domain taken as $[\xi_0, \xi_\infty]$ with $\xi_0 > 0$ and ξ_∞ being suitably small and large, respectively. As initial data, two terms of the expansions (3.136)-(3.139) were used at $\xi = \xi_0$.

Figure 3-4 illustrates the numerical solution in the case of a 270^o corner for parameter values $\alpha = 2/3$, $a = -1$, $p_0 = 1$, $\xi_0 = 10^{-6}$. Figure 3-4(B) shows convergence to the far-field behaviour (3.131), and at $\xi_\infty = 10^{30}$ it produces the estimates

$$\begin{aligned}
&\frac{f}{\xi_\infty^{1+\alpha}} \simeq -4.14563377595242, \\
&t_{11} \simeq 2.00000000001192, \qquad t_{11} = C_1 = 2, \\
&\frac{t_{12}}{\xi_\infty} \simeq 0.66666666667468, \qquad \frac{t_{12}}{\xi_\infty} = C_1(1-\alpha) = \frac{2}{3} = 0.\dot{6}, \\
&\frac{t_{22}}{\xi_\infty^2} \simeq 0.22222222222624, \qquad \frac{t_{22}}{\xi_\infty^2} = C_1(1-\alpha)^2 = \frac{2}{9} = 0.\dot{2},
\end{aligned} \tag{3.191}$$

which agree well with the leading order approximations (agreement to 10 decimal places), shown on the right, where $C_1 = 2p_0$ has been used from (3.69).

We may use the leading order asymptotic behaviour for the similarity stream func-

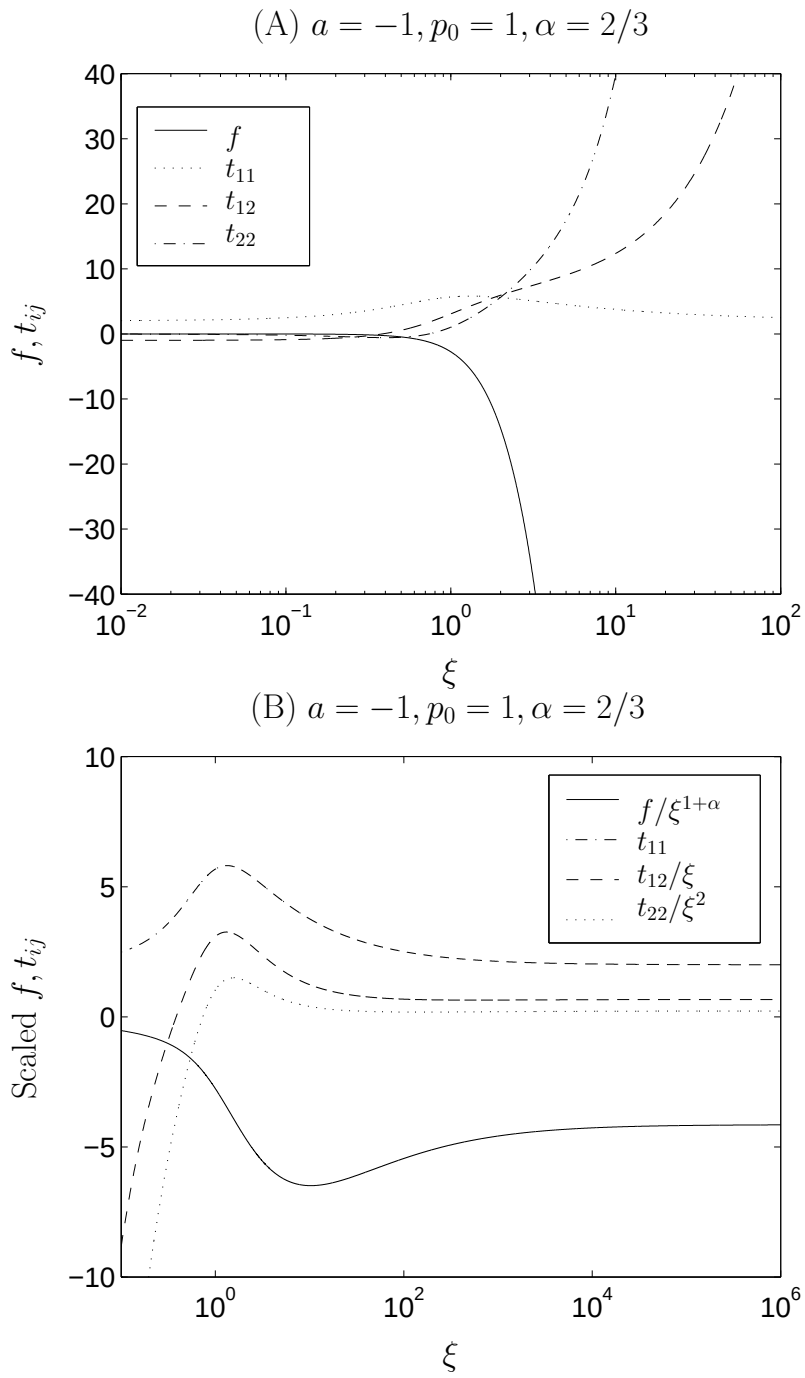

Figure 3-4: Illustration of the numerical solution to (3.122)-(3.125) as an initial value problem and relevant to the upstream case of a 270^o corner. Parameter values are $\alpha = 2/3$, $a = -1$, $p_0 = 1$, $\xi_0 = 10^{-6}$ with (A) and (B) showing the solution for small and large ξ respectively.

tion variable f in (3.131) to give estimates of C_0/κ, denoted by C_0^e/κ, as follows

$$C_0^e/\kappa = f(\xi_\infty)\xi_\infty^{-(1+\alpha)}. \tag{3.192}$$

Figure 3-5 shows such estimates with varying upstream wall shear rate coefficient a in the case $p_0 = 1$ for selected α. For a fixed corner angle parameter α, the profiles are monotonic decreasing as $-a$ increases with maximum values occurring in the limit of vanishing wall shear rate. The curves in Figure 3-5(A) suggest a limiting value in this latter case, which we denote by k_0. The variation of

$$k_0 = \lim_{a\to 0}\left(-C_0/\kappa\right), \tag{3.193}$$

with corner angle parameter α is shown in Figure 3-5(B) for $p_0 = 1$.

In table 3.1, sensitivity of these estimates for C_0^e/κ are given as the domain end points ξ_0, ξ_∞ are varied, illustrating convergence for the specific case of $p_0 = 1$, $\alpha = 2/3$ and selected a. As $|a|$ increases, smaller ξ_0 and larger ξ_∞ values are needed in order to obtain a specified accuracy. The convergence rate to the far-field behaviour appears slower for these PTT equations than in the corresponding UCM equations.

As the eigenmode analysis in section 3.2.4 displayed, to complete the solution description with the downstream boundary layer, at least three of the constants (C_0, C_2, C_3, C_4, C_5) need to be known to be passed to the downstream boundary value problem. To determine estimates for the next constant in the far-field expressions, C_2, we consider the simplest case when $\alpha > 2/3$ (the other cases arising due to the non-uniform ordering of the terms in the far-field expansions). The possible approximations found from the full far field expansions of the stress variables ((F.1)–(F.4)) are

$$\begin{aligned}
C_2^{(11)e} &= \left(\frac{t_{11}(\xi_\infty)}{C_1} - 1\right)\frac{(1+\alpha)}{(4\alpha-2)}\xi_\infty^{2-2\alpha},\\
C_2^{(12)e} &= \left(\frac{t_{12}(\xi_\infty)}{C_1(1-\alpha)\xi_\infty} - 1\right)\frac{(1+\alpha)}{(4\alpha-4)}\xi_\infty^{2-2\alpha},\\
C_2^{(22)e} &= \left(\frac{t_{22}(\xi_\infty)}{C_1(1-\alpha)^2\xi_\infty^2} - 1\right)\frac{(1+\alpha)}{(4\alpha-6)}\xi_\infty^{2-2\alpha}.
\end{aligned} \tag{3.194}$$

Figure 3-6 illustrates the convergence to the constant C_2 using these three estimates, with (A) showing the whole data range and (B) plotted on restricted axes to show the converging region more closely. These plots show the numerical instability for large ξ values clearly. When using looser tolerances, this instability occurs at smaller ξ values, so we know that it is a problem with the numerical method. Unfortunately, without a reliable approximation for C_2, the other constants cannot be found and hence a

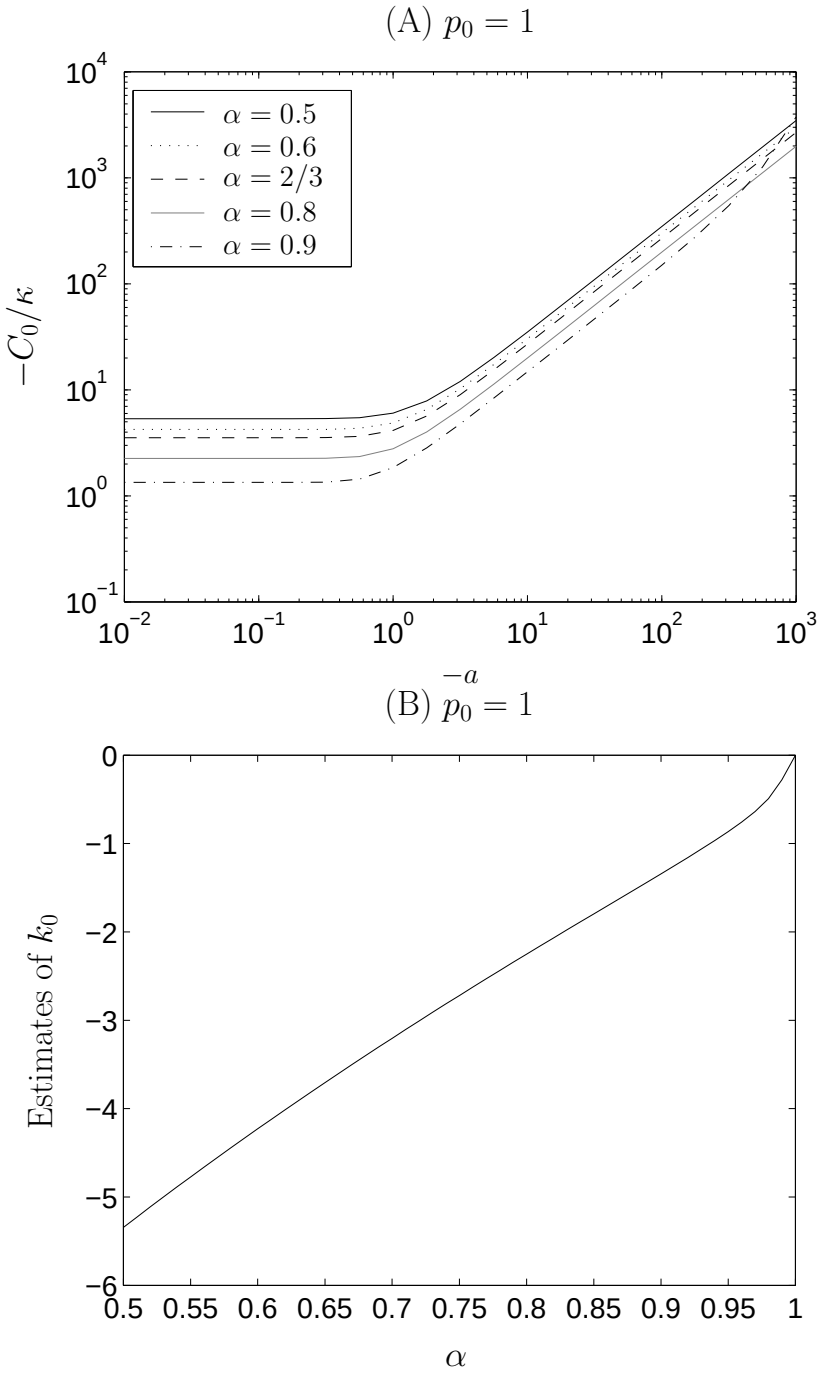

Figure 3-5: Estimates of the far-field parameter C_0/κ in the case $p_0 = 1$. (A) shows estimates using (3.192) with varying a for selected α. The choice $\xi_0 = 10^{-6}$ was used for $|a| < 1$ and $\xi_0 = 10^{-6}/(-a)^{3/2}$ for $|a| > 1$. The estimate (3.192) was evaluated at $\xi_\infty = 10^{30}$. (B) gives the values of k_0, the limiting value of C_0/κ, with α. The estimates were evaluated at $a = -10^{-2}$ using $\xi_0 = 10^{-6}$, $\xi_\infty = 10^{30}$.

(A) $a = -10^{-2}$

	$\xi_0 = 10^{-2}$	$\xi_0 = 10^{-4}$	$\xi_0 = 10^{-6}$	$\xi_0 = 10^{-8}$
ξ_∞	C_0^e/κ			
10^5	−3.56050322	−3.56050320	−3.56050320	−3.56050320
10^{10}	−3.53646547	−3.53646545	−3.53646545	−3.53646545
10^{15}	−3.53644628	−3.53644626	−3.53644626	−3.53644626
10^{20}	−3.53644627	−3.53644625	−3.53644625	−3.53644625

(B) $a = -1$

	$\xi_0 = 10^{-2}$	$\xi_0 = 10^{-4}$	$\xi_0 = 10^{-6}$	$\xi_0 = 10^{-8}$
ξ_∞	C_0^e/κ			
10^5	−4.17776182	−4.17699266	−4.17699259	−4.17699259
10^{10}	−4.14641455	−4.14565670	−4.14565662	−4.14565663
10^{15}	−4.14639171	−4.14563386	−4.14563379	−4.14563379
10^{20}	−4.14639170	−4.14563385	−4.14563378	−4.14563378

(C) $a = -10^2$

	$\xi_0 = 10^{-2}$	$\xi_0 = 10^{-4}$	$\xi_0 = 10^{-6}$	$\xi_0 = 10^{-8}$
ξ_∞	C_0^e/κ			
10^5	−2958.68348598	−1735.93922309	−1735.18925647	−1735.18918253
10^{10}	−270.83875830	−271.79638196	−271.74017753	−271.74017199
10^{15}	−264.11415047	−269.01239218	−268.95783487	−268.95782949
10^{20}	−264.11059066	−269.01098681	−268.95643035	−268.95642497
10^{25}	−264.11058899	−269.01098614	−268.95642968	−268.95642430
10^{30}	−264.11058898	−269.01098613	−268.95642967	−268.95642429

Table 3.1: Estimates of the upstream boundary layer far-field constant C_0^e/κ in the case $p_0 = 1$, $\alpha = 2/3$ for selected a. The estimates use (3.192) evaluated at $\xi = \xi_\infty$. Sensitivity of these estimates to the initial starting value ξ_0 and the interval end point ξ_∞ are shown in each table (A)-(C). Convergence is illustrated for both decreasing ξ_0 and increasing ξ_∞ as well as the necessity for taking smaller ξ_0 and larger ξ_∞ as $|a|$ increases.

scheme for the downstream layer cannot be numerically implemented. We see clearly here the deficiency with the analysis in the Cartesian basis - the natural stress basis rearranges the equations to have the information carrying constants at leading order in the far field expansion and hence avoid complications arising with the C_2 and C_3 constants. Numerical analysis using the natural stress basis will be pursued in the following sections.

3.3.2 The case $2/3 < \alpha < 1$ in the natural stress basis

In the Cartesian formulation access to the far field constants required to furnish the downstream boundary problem with the required number of boundary conditions was prevented through numerical inaccuracy. As we have seen, the natural stress formulation can help to unpick the complex Cartesian full far field descriptions (F.1)–(F.8), allowing enough independent constants for the downstream problem to be found at leading order in the natural stress variables.

For the case $2/3 < \alpha < 1$, numerical solutions can be obtained for the upstream and downstream boundary layers linked through a well behaved outer solution. The numerical approach we adopt is similar to that used in the UCM case [Eva08b].

The upstream boundary layer

The IVP for the upstream layer is to solve (3.127)-(3.129) with (3.185) for a given value of α over the truncated interval $[\xi_0, \xi_\infty]$. The wall behaviour (3.140)-(3.143) is imposed at $\xi = \xi_0$ and the far-field behaviour (3.183) is to be attained. The interval end points ξ_0 and ξ_∞ are taken sufficiently small and large respectively in order to obtain convergence to the far-field behaviour to within specified accuracy (their values determined by numerical experiment). For clarity we label the parameters in the wall and far-field behaviours with a subscript u to identify them as upstream parameters. For numerical implementation it is convenient to use the scaled stress variables

$$l(\xi) = \xi^2 \tilde{\lambda}(\xi), \qquad m(\xi) = \tilde{\mu}(\xi), \qquad n(\xi) = \frac{\tilde{\nu}(\xi)}{\xi^2}, \tag{3.195}$$

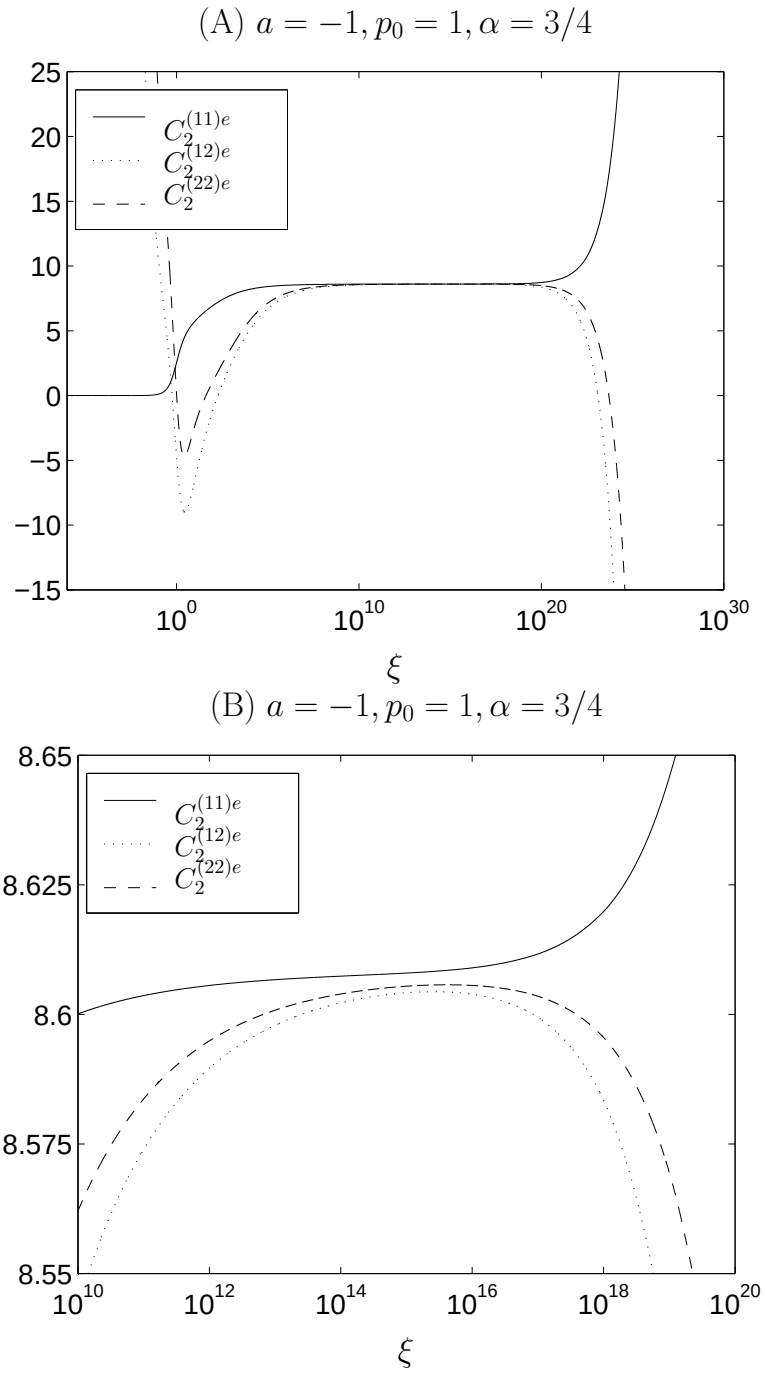

Figure 3-6: Illustration of the convergence to C_2 using the three estimates $C_2^{(ij)e}$ from (3.194). Parameter values are $\alpha = 3/4$, $a = -1$, $p_0 = 1$, $\xi_0 = 10^{-6}$ with (A) and (B) showing the same data but with (B) using restricted axes to show the converging region more closely.

for which the wall behaviour is now finite, and using (3.140)-(3.143) gives us the initial conditions

$$\text{at } \xi = \xi_0 \qquad f = a_u^3\xi_0^2 + a_u^4 b_u \xi_0^3, \tag{3.196}$$

$$l = \frac{1}{2a_u^4} + \frac{(1-\alpha) - b_u}{2a_u^3}\xi_0, \tag{3.197}$$

$$m = a_u + \{3(1-\alpha) + b_u\}\, a_u^2 \xi_0, \tag{3.198}$$

$$n = 4a_u^6 + 12\,\{(1-\alpha) + b_u\}\, a_u^7 \xi_0, \tag{3.199}$$

where b_u and C_{1u} are found from the relationships

$$p_{0u} = -a_u^2\left(1 + \frac{b_u}{2(1-\alpha)}\right), \qquad C_{1u} = 2p_{0u}. \tag{3.200}$$

The following results were obtained using MATLABs ode15s solver with error tolerances $RelTol = AbsTol = 10^{-13}$. Illustrative solution profiles are shown in figure 3-7 in the parameter case $a_u = -1$, $p_{0u} = 1$, $\alpha = 0.75$ with $\xi_0 = 10^{-15}$, $\xi_\infty = 10^{30}$. Figure 3-8 shows estimates of the far-field similarity parameters

$$C_{0u}^{sp} = \frac{C_{0u}}{\kappa p_{0u}^{1+(\alpha/2)}}, \qquad d_{2u}^{sp} = \frac{d_{2u}}{p_{0u}^{\alpha/2}}, \qquad d_{3u}^{sp} = \frac{d_{3u}}{\kappa^2 p_{0u}^{1+2\alpha}}, \tag{3.201}$$

as the upstream wall similarity parameter $a_u^{sp} = \frac{a_u}{p_{0u}^{1/2}}$ is varied for selected values of α. The scalings (3.188) have been employed. Noteworthy in figure 3-8 is the suggestion of the limiting behaviours

$$\frac{C_{0u}}{\kappa p_{0u}^{1+(\alpha/2)}} \sim k_0, \quad \frac{d_{2u}}{p_{0u}^{\alpha/2}} \sim k_2, \quad \frac{d_{3u}}{\kappa^2 p_{0u}^{1+2\alpha}} \sim k_3, \quad \text{as} \quad \frac{a_u}{p_{0u}^{1/2}} \to 0^-, \tag{3.202}$$

where the parameters k_0, k_2, k_3 vary with α. These provide explicit parameter dependencies for the limits of small upstream wall shear rate or large upstream wall pressure coefficient.

The downstream boundary layer

For the downstream boundary layer, where flow is away from the corner and $a > 0$, we need to solve (3.127)-(3.129) with (3.185) for fixed α as a two-point BVP over the truncated interval $[\xi_0, \xi_\infty]$. The wall expansions (3.140)-(3.143) supply two conditions with the far-field behaviour (3.183) supplying the three remaining conditions. These behaviours will be imposed at the interval end points. For clarity we label parameters with a subscript d to identify them as belonging to the downstream problem. Allowing

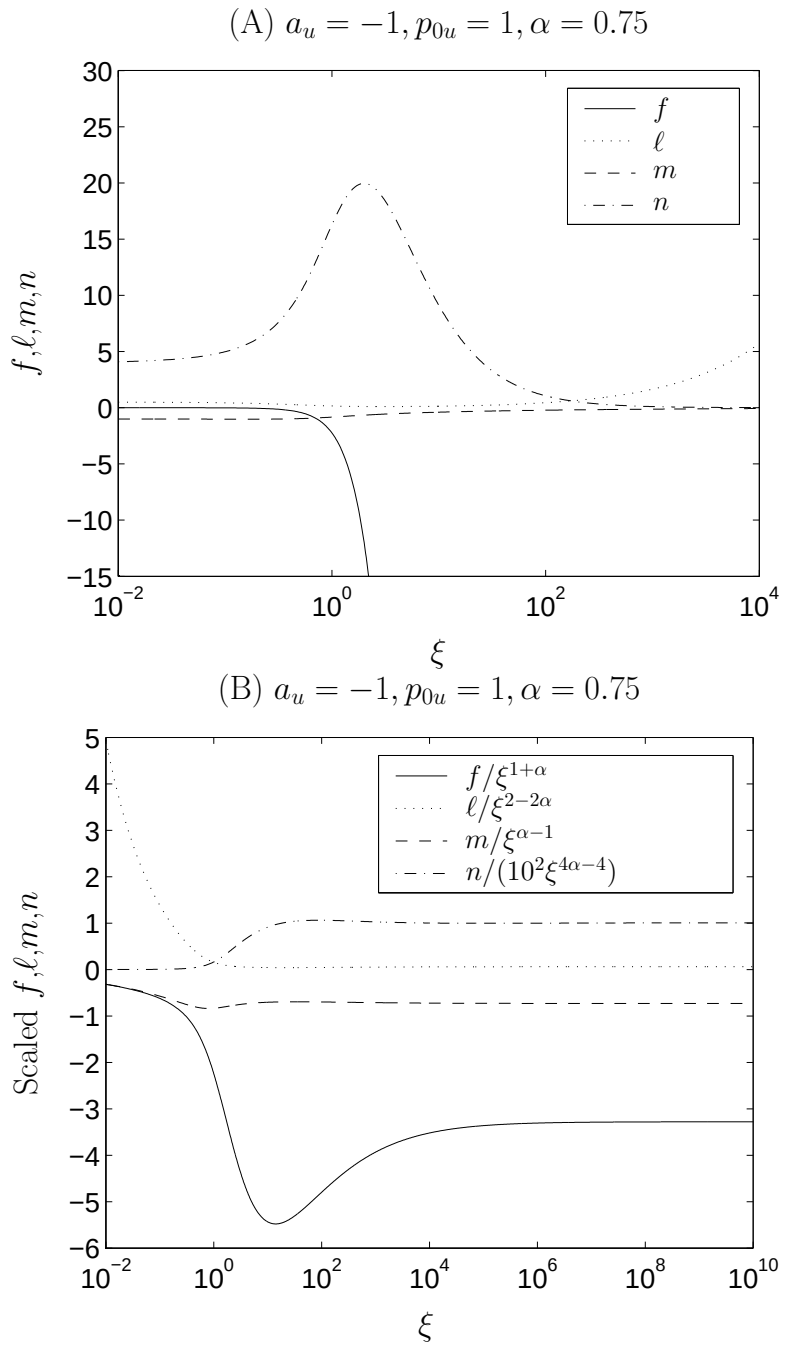

Figure 3-7: Solution profiles of the upstream boundary layer. Parameters values used were $a_u = -1$, $p_{0u} = 1$, $\alpha = 0.75$ with range end points $\xi_0 = 10^{-15}$, $\xi_\infty = 10^{30}$. (A) The stream function and related natural stress variables ℓ, m, n (as defined in (3.195)). (B) Convergence to the far-field behaviours given in (3.183), with n further scaled with the factor 10^2.

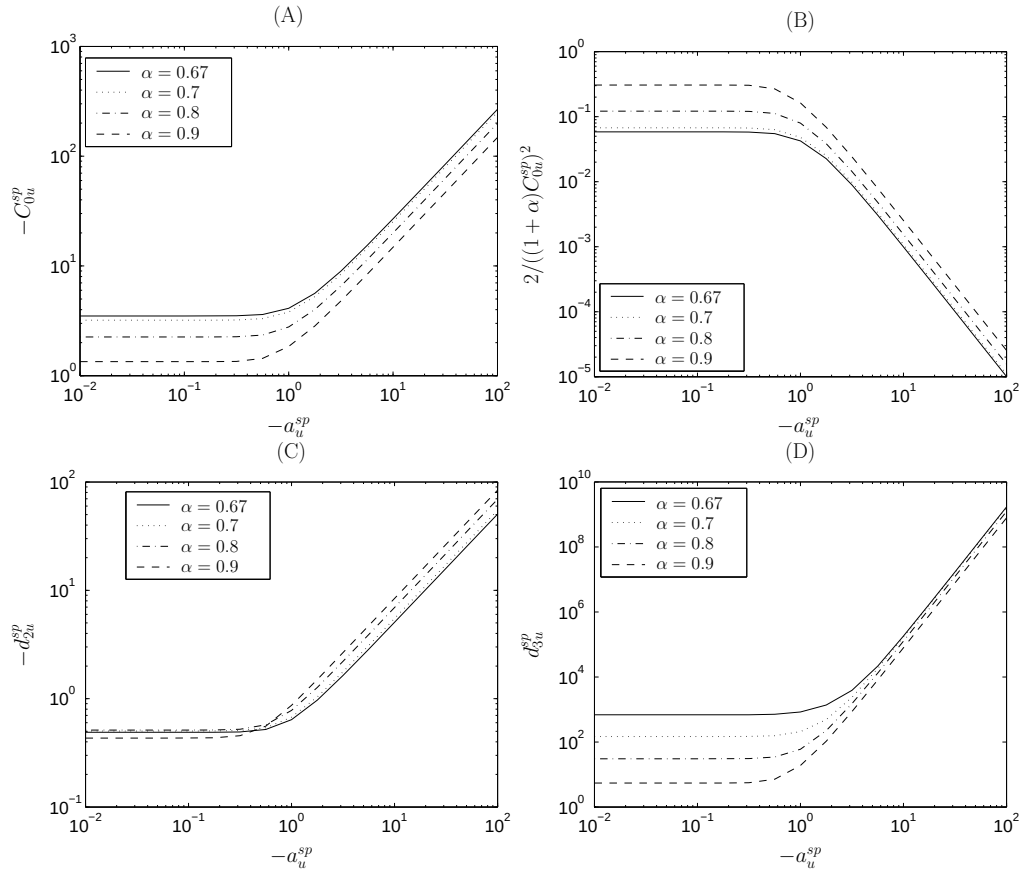

Figure 3-8: Estimates of the upstream far-field similarity parameters (3.201) with variation of the upstream wall similarity parameter $a_u^{sp} = \frac{a_u}{p_{0u}^{1/2}}$ for selected corner angle values α. The IVP was solved with interval end points $\xi_0 = 10^{-8}$, $\xi_\infty = 10^{34}$. (B) consistent behaviour for the coefficient of $\tilde{\lambda}$.

for a suitable change of sign for axes orientation, the upstream and downstream layer far-field parameters are linked through the outer solution via

$$p_{0d} = p_{0u}, \qquad C_{0d} = -C_{0u}, \qquad d_{2d} = -d_{2d}, \qquad d_{3d} = d_{3u}. \tag{3.203}$$

This problem is significantly more difficult to solve numerically than that of the corresponding UCM case in [Eva08b]. One approach is to use continuation to deform the UCM downstream layer equations into those that we have here for PTT.

The constitutive equations in inner variables were recorded in equations (3.79)-(3.81), with the dominant balance occurring when $n = 1 + \alpha$. However, for the UCM model in [Eva08b], then the dominant balance changes, and gives $n = 3 - \alpha$. We thus create a combined model where both UCM and PTT can be recovered dependent upon a new artificial parameter s. UCM occurs when $s = 1$, and PTT when $s = 0$, with our suggestion of

$$\hat{n} = (1 + 2s) + \alpha(1 - 2s), \tag{3.204}$$

creating a straightforward interpolation of the two model equations.

The hybrid similarity solution equations from this interpolation are

$$f'' = \frac{f'^2}{\hat{n}^2 f^2 f'^2 \tilde{\lambda} - 2\hat{n} f f' \tilde{\mu} + \tilde{\nu}} \Big(2(1-\alpha)\hat{n} p_0 f + \tilde{\mu} f' ((1-s)\tilde{\lambda} f' + \alpha - 1) + s(\tilde{\mu} - \hat{n}\tilde{\lambda} f f') - \hat{n} f f'^2 \tilde{\lambda} ((1-s)\tilde{\lambda} f' + 2 - \alpha - \hat{n}) \Big), \tag{3.205}$$

$$2\tilde{\mu} f'' - \Big((1-s)\tilde{\lambda}^2 f'^2 + (2 - 2\hat{n})\tilde{\lambda} f' - \hat{n} f \tilde{\lambda}' + s\tilde{\lambda} \Big) f'^2 = 0, \tag{3.206}$$

$$\tilde{\nu} f'' - \Big((1-s)\tilde{\mu}\tilde{\lambda} f'^2 - \tilde{\mu} f' (1-\alpha) - \hat{n}\tilde{\mu}' f + s\tilde{\mu} \Big) f'^2 = 0, \tag{3.207}$$

$$\hat{n} f \tilde{\nu}' + (1-s) \Big(2(1-2\alpha)\tilde{\nu} f' + \tilde{\lambda} f'^2 (f'^2 - \tilde{\nu}) \Big) + s \left(f'^2 - (1 + 2f')\tilde{\nu} \right) = 0. \tag{3.208}$$

The eigenmode analysis of sections 3.2.3-3.2.4 found that downstream two conditions are applied by the wall behaviour and thus three conditions must be applied in the far-field (by fixing the three independent constants C_0, d_2 and d_3 from the upstream), and this is also the same for the UCM equations.

For the upstream hybrid BVP we take the wall and matching conditions

$$\text{at } \xi = \xi_0, \qquad f = \left(a_u^3 (1-s) + \frac{s a_u}{2} \right) \xi_0^2, \qquad \tilde{\lambda} = \left(\frac{(1-s)}{2a_u^4} + 2s \right) \xi_0^{-2},$$
$$\tilde{\mu} = a_u, \qquad \tilde{\nu} = \left(4a_u^6 (1-s) + s a_u^2 \right) \xi_0^2, \tag{3.209}$$

and use

$$\text{at } \xi = \xi_\infty, \qquad f = \left(\frac{C_{0u}}{\kappa}\right)^h \xi_\infty^{\hat{n}}, \quad \tilde{\mu} = (d_{2u})^h \xi_\infty^{\alpha-1}, \quad \tilde{\nu} = \left(\frac{d_{3u}}{\kappa^2}\right)^h \xi_\infty^{2s+2(1-s)(2\alpha-1)}, \tag{3.210}$$

to obtain estimates of the upstream far-field hybrid parameters denoted with a superscript h.

For the downstream hybrid BVP we take the wall and matching conditions

$$\text{at } \xi = \xi_0, \quad f = \left(\tilde{\mu}^3(1-s) + \frac{s\tilde{\mu}}{2}\right)\xi_0^2, \quad \tilde{\nu} = \left(4\tilde{\mu}^6(1-s) + s\tilde{\mu}^2\right)\xi_0^2, \tag{3.211}$$

$$\text{at } \xi = \xi_\infty, \quad f = -\left(\frac{C_{0u}}{\kappa}\right)^h \xi_\infty^{\hat{n}}, \quad \tilde{\mu} = -(d_{2u})^h \xi_\infty^{\alpha-1}, \quad \tilde{\nu} = \left(\frac{d_{3u}}{\kappa^2}\right)^h \xi_\infty^{2s+2(1-s)(2\alpha-1)}. \tag{3.212}$$

The scheme proceeds as follows for given values of the upstream parameters (a_u, p_{0u}) and corner angle parameter α:

- At each step in s, the hybrid equations (3.205)–(3.208) are solved as an IVP subject to (3.209) with (3.210) used to obtain estimates of the far-field parameters.
- MATLABs ode15s is used with error tolerances $RelTol = AbsTol = 10^{-7}$ and interval end points $\xi_0 = 10^{-10}$, $\xi_\infty = 10^{30}$.
- These far-field parameter estimates are used in the downstream hybrid problem (using relation (3.203)), where (3.205)–(3.208) with (3.211)–(3.212) are solved on a truncated domain with $\xi_0 = 10^{-1}$, $\xi_\infty = 10^1$ using MATLABs bvp4c solver with relaxed error tolerances $RelTol = AbsTol = 10^{-1}$.
- The solution at the previous s value is used as the initial guess.
- This iteration in s continues from $s = 1$ to $s = 0$ (typically in steps of 10^{-2}) after which the downstream domain is extended to $\xi_0 = 10^{-4.1}$, $\xi_\infty = 10^{4.1}$ and error tolerances tightened to $RelTol = 10^{-3}$, $AbsTol = 10^{-6}$.
- At the start $s = 1$, an initial guess solution for the downstream equations can be obtained from solving the upstream hybrid IVP with $s = 1$ on the truncated domain $\xi_0 = 10^{-1}$, $\xi_\infty = 10^1$ and using these profiles with a change of sign for f and $\tilde{\mu}$.
- The scheme benefits from use of the transformed stress variables (3.195).

Figure 3-9 illustrates downstream profiles in the parameter case $\alpha = 0.75$, $a_u = -1$, $p_{0u} = p_{0d} = 1$, as well as convergence of estimates for the downstream wall parameter a_d. A parameter plot of the downstream wall similarity parameter $a_d^{sp} = a_d/p_{0d}^{1/2}$ against the corresponding upstream parameter is shown in figure 3-10 for selected corner angle values of α. These numerical results suggest the limiting behaviour

$$\frac{a_d}{p_{0d}^{1/2}} \sim k_d, \qquad \text{as} \qquad \frac{a_u}{p_{0u}^{1/2}} \to 0^-, \tag{3.213}$$

where the parameter k_d varies with α.

3.4 Discussion

The asymptotic structure local to re-entrant corners has been described for a class of self-similar solutions of the PTT equations in the model parameter regime $\kappa = O(1)$, and with We $= O(1)$. Rather surprisingly these solutions appear restricted to the corner angle parameter range $2/3 < \alpha < 1$ (i.e. re-entrant corners angles in the range $(180^o, 270^o)$) in the situation of complete flow around the corner. We make remarks about the remaining range $1/2 \leq \alpha \leq 2/3$ (i.e. angles in the interval $[270^o, 360^o]$) where the outer solutions as constructed here are unable to match into the downstream boundary layer (the analysis having been performed in appendix E).

The case $1/2 \leq \alpha \leq 2/3$

For this parameter range, the outer solution for $\nu^{*(0)}$ can no longer be matched into the downstream boundary layer. The difficulty arises since the outer solution (E.7) increases monotonically in θ along streamlines (and becomes unbounded as $\theta \to \pi/\alpha$ for $1/2 < \alpha \leq 2/3$). It cannot then be reconciled with the required behaviour (E.17) or (E.22), which must equally hold for the downstream layer (allowing for suitable sign changes associated with axes orientation).

Specifically it is certainly possible to compute the upstream behaviour in the same way as for $2/3 < \alpha < 1$, obtaining the far-field constants using (3.183), but these constants cannot then be used for the downstream analysis, d_3 in particular, as through the core it has increased monotonically becoming unbounded.

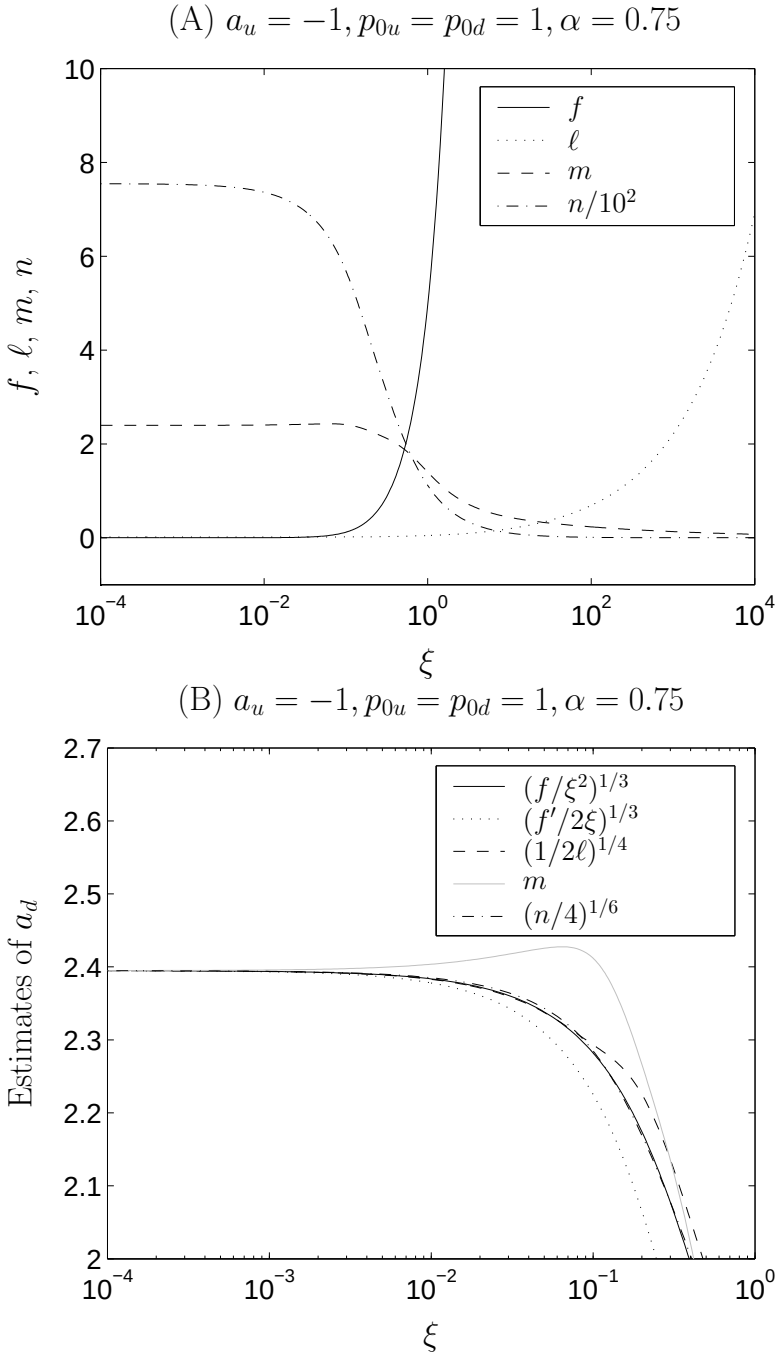

Figure 3-9: Illustration of the solution profile and estimates of a_d in the case $\alpha = 0.75$, $a_u = -1$, $p_{0u} = p_{0d} = 1$. The maximum residual is 1.7×10^{-4}. (A) shows the solution profiles and (B) the behaviour for small ξ of the variables $(f/\xi^2)^{1/3}$, $(f'/2\xi)^{1/3}$, $(1/2\ell)^{1/4}$, m, and $(n/4)^{1/6}$, all of which give estimates of a_d (agreeing to 4d.p. at $\xi_0 = 10^{-4.1}$).

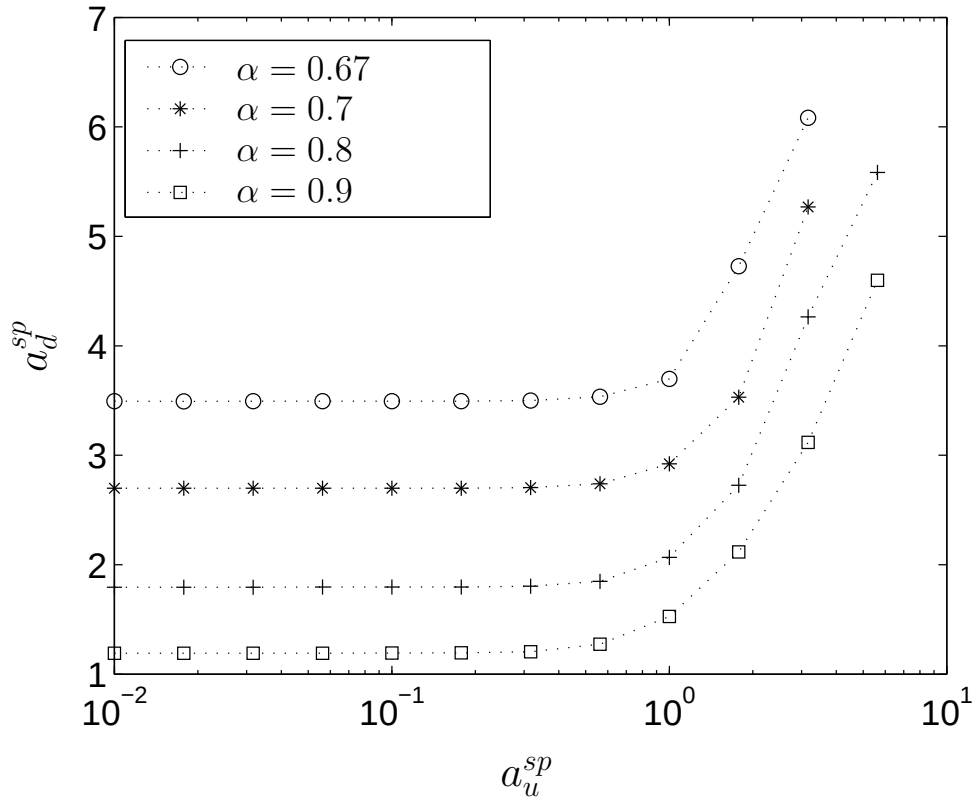

Figure 3-10: A plot to show the variation of downstream wall similarity parameter $a_d^{sp} = a_d/p_{0d}^{1/2}$ with $a_u^{sp} = a_u/p_{0u}^{1/2}$ for selected α. Estimates for a_d were taken from $(f/\xi^2)^{1/3}$ evaluated at $\xi_0 = 10^{-4.1}$. Maximum residual for results shown was 5.7×10^{-4}. The scheme encountered convergence difficulties for values of $a_u^{sp} = a_u/p_{0u}^{1/2}$ outside those shown.

As such we are unable to construct solutions for the asymptotic structure presented here in the range $1/2 \leq \alpha \leq 2/3$. It thus remains an open question as to whether the PTT model has an attached flow at the downstream wall for these corner angles.[11]

The consideration of alternative flow structures now arises, particularly those involving the presence of a separating streamline from the corner (upstream or downstream or even both). Two such situations are depicted in figure 3-11 which are worth briefly remarking upon. Figure 3-11(A) shows an upstream separating streamline taken at $\theta = 0$, with the upstream wall at $\theta = -\theta_0$. The outer and downstream boundary layer solutions of the earlier sections should be applicable, except that we would anticipate a greater combination of values for the outer solution coefficients (C_0, d_2, d_3) (than those given by the upstream boundary layer solution). Alternatively, figure 3-11(B) shows the situation of a downstream separating streamline now taken at $\theta = \pi/\alpha$, with the downstream wall at $\theta = \pi/\alpha + \theta_0$. The upstream boundary layer and outer solutions as constructed earlier may be expected to apply. In both cases $2/3 < \alpha < 1$ and we mention that the total corner angle $\pi/\alpha + \theta_0$ need not be restricted to being 270^o or greater and may also occur for total corner angles down to 180^o.

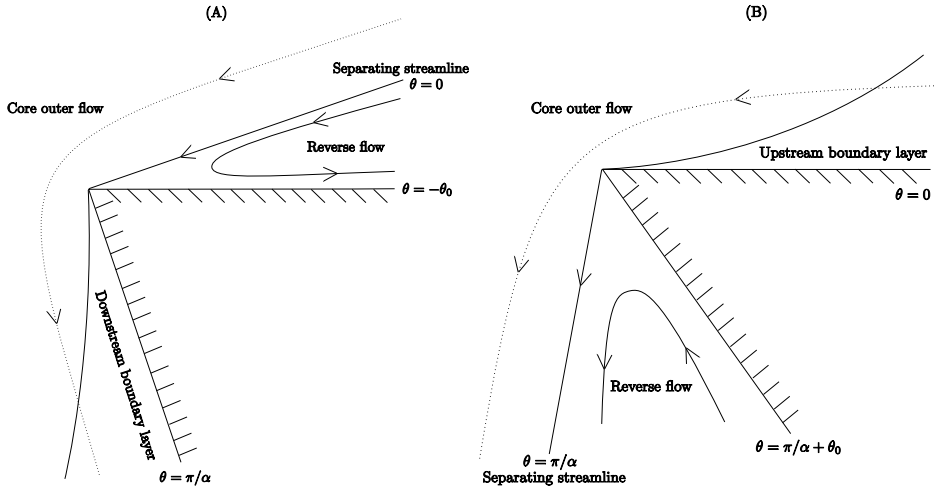

Figure 3-11: Schematic illustration of two possible flow scenarios involving a separating streamline, where the solutions of this chapter may be partially relevant. We have the restricted range $\alpha \in (2/3, 1)$, although the total corner angle $\pi/\alpha + \theta_0$ may exceed 270^o. The outer and downstream boundary layer regions may occur in (A), while the outer and upstream boundary layer regions may apply to (B). This assumes that the separating streamline in both instances can be locally straightened near the corner.

[11] If such solutions do exist, then either a different self-similar solution dominates (for example, one controlled by global considerations rather than local) or it is no longer of self-similar form. In respect of the former case, it is worth noting here the presence of logarithmic terms at the critical angle $\alpha = 2/3$. This is suggestive of a possible transition between first and second kind self-similar solutions (see the illustrative model problem in section 6.5.3 of [OHLM99]).

Solutions for reverse flow regions have yet to be constructed, but would certainly be interesting and important for future work. It is worth noting that in full numerical simulations (performed by an anonymous referee of the paper [ES09]), the situation of figure 3-11(A) appears to be the one of preference for all re-entrant corner angles. The lip vortex intensity increases with both increasing corner angle and Deborah number (in our notation, this is our Weissenberg number, with the typical length and velocity scales being based on the exit channel half-width and velocity). We may here note that there has been good numerical work for the PTT model published in contraction flows (for example [AGAK96b], [AGAK96a], and [AOP03]). All three papers use the numerically simpler PTT model with solvent viscosity, so do not apply to this case. The recent (2003) work of Alves et. al. [AOP03] agrees well with the analytical results of Renardy [Ren97b], whose application to the solvent viscosity model is described in appendix A.

The case $2/3 < \alpha < 1$ and final remarks

The class of solutions for this parameter regime is associated with the balance (3.2), which holds away from the walls in a core flow outer region and give a stress singularity of $O\left(r^{-2(1-\alpha)}\right)$. The stream function vanishes as $O\left(r^{n\alpha}\right)$, the index $n = 1 + \alpha$ in (3.27) being determined by matching such solutions into wall boundary layers. The wall boundary layers are needed to recover viscometric behaviour and it is noted that the leading order equations are the same as those obtained in the high Weissenberg limit, where the linear stress terms are uniformly subdominant. Thus the asymptotic structure, stress singularity and boundary layer thicknesses are the same as those obtained for the UCM model, the difference for the PTT equations being the slower vanishing of the stream function in the core (equivalently slower far-field growth in the boundary layers) compared to $O\left(r^{\alpha(3-\alpha)}\right)$ for the UCM model. The solution structure has been shown to depend upon two parameters, the upstream pressure coefficient p_{0u} and wall shear rate a_u, in terms of which the amplitudes of the outer core stream function and stresses have been determined (part analytically and part numerically).

These two coefficients are set by incoming flow behaviour to the corner and may be conveniently combined into the similarity combination $a_u/p_{0u}^{1/2}$.

An important comment is that the amplitudes of the velocity and stress fields C_0 and C_1 appear to be genuinely independent and that this local analysis does not impose a relationship between them. This is correlated to the independence of the upstream pressure coefficient p_{0u} and wall shear rate a_u. Any dependence between these parameters appears to require global information from the full flow fields away from the corner.

Chapter 4

Re-entrant corner flows in low and high parameter regimes

The previous chapter has identified a similarity solution for the flow of the PTT fluid around a re-entrant corner when the Weissenberg number and the PTT model parameter κ are both $O(1)$. Here we investigate the flow in the physically relevant limits of low and high Weissenberg number, and firstly of small κ.

The analysis for re-entrant corner flows of the UCM fluid in the two limits of low ($\mathrm{We} \to 0$) and high ($\mathrm{We} \to \infty$) Weissenberg number are given by Evans in [Eva06]. These limits are also of interest with the PTT model equations (1.32)–(1.34), with $\kappa = O(1)$. The double limits of $(\mathrm{We}, \kappa) \to (0, 0)$, and $(\mathrm{We}, \kappa) \to (\infty, 0)$ are left as an open problem (although the regions found in the analysis of this chapter would likely be present in more complicated asymptotic structures).

4.1 The UCM limit of the PTT equations, $\kappa \to 0$, $\mathrm{We} = O(1)$

4.1.1 Introduction

To extend the analysis of the previous chapter, we now describe the local asymptotic structure at re-entrant corners of the PTT model in the limit of vanishing model parameter κ. The same situation of steady planar flow is taken and the PTT model is again considered in the absence of any solvent viscosity. In the case $\kappa = 0$, the PTT model reduces to that of the Upper Convected Maxwell (UCM) model for which an analogous similarity solution (sharing the same stress singularity and wall boundary layer thicknesses) has been constructed in [Eva08a], [Eva08b]. Our intention then is to

understand the transition between these two cases which occurs in the model parameter limit $\kappa \to 0$. The setup of the problem will be the same as the previous chapter, and hence will not be repeated here.

The dimensionless governing equations are

$$0 = -\nabla p + \nabla.\mathbf{T}, \qquad \nabla.\mathbf{v} = 0, \qquad \mathbf{T} + \overset{\triangledown}{\mathbf{T}} + \kappa\,(\mathrm{tr}\mathbf{T})\,\mathbf{T} = 2\mathbf{D}. \tag{4.1}$$

The only dimensionless parameter is the model parameter κ which will be assumed small. The inertia terms have been neglected in the momentum equations (the analysis has been performed including them, but they play no role at leading order in any of the regions and are thus excluded for conciseness. Neglecting inertia terms is common in the literature, e.g. [Hin93], [Ren95]) and the dimensionless relaxation time (the Weissenberg number) taken as unity, possible through the scalings (2.18). The x, y axes are aligned at the upstream wall as before and the usual stream function ψ used to represent the velocity field, which satisfies the no-slip condition on the walls. The situation with the main asymptotic regions is shown in figure 4-1.

The downstream boundary layer equations can be obtained from the upstream boundary layers through the transformation (3.70), and hence upstream and downstream are labeled together.

4.1.2 The main length scale $r = O(\kappa^{\frac{1}{2(1-\alpha)}})$

We begin by determining the length scale on which fullest balance is obtained in the constitutive equations, where both the linear and quadratic stress terms are retained in the boundary layer. This is the expected balance as it would contain all the terms contained in both the UCM ($\kappa = 0$) and PTT with $\kappa = O(1)$ boundary layer equations. We thus consider distances from the corner of $O(\epsilon)$, with the gauge $\epsilon(\kappa)$ being a small parameter whose dependency on κ is to be found. In the outer region away from the walls we consider the scalings

$$r = \epsilon R^*, \quad x = \epsilon X^*, \quad y = \epsilon Y^*, \quad \psi = \epsilon^q \Psi^*, \quad \mathbf{v} = \epsilon^{q-1}\mathbf{v}^*,$$
$$\mathbf{T} = \epsilon^{2(\alpha-1)}\mathbf{T}^*, \quad p = \epsilon^{2(\alpha-1)}p^*, \tag{4.2}$$

where we anticipate that the stress scaling will not change from the $\kappa = O(1)$ and $\kappa = 0$ cases (it being the same for both) and the velocity scaling left arbitrary for the

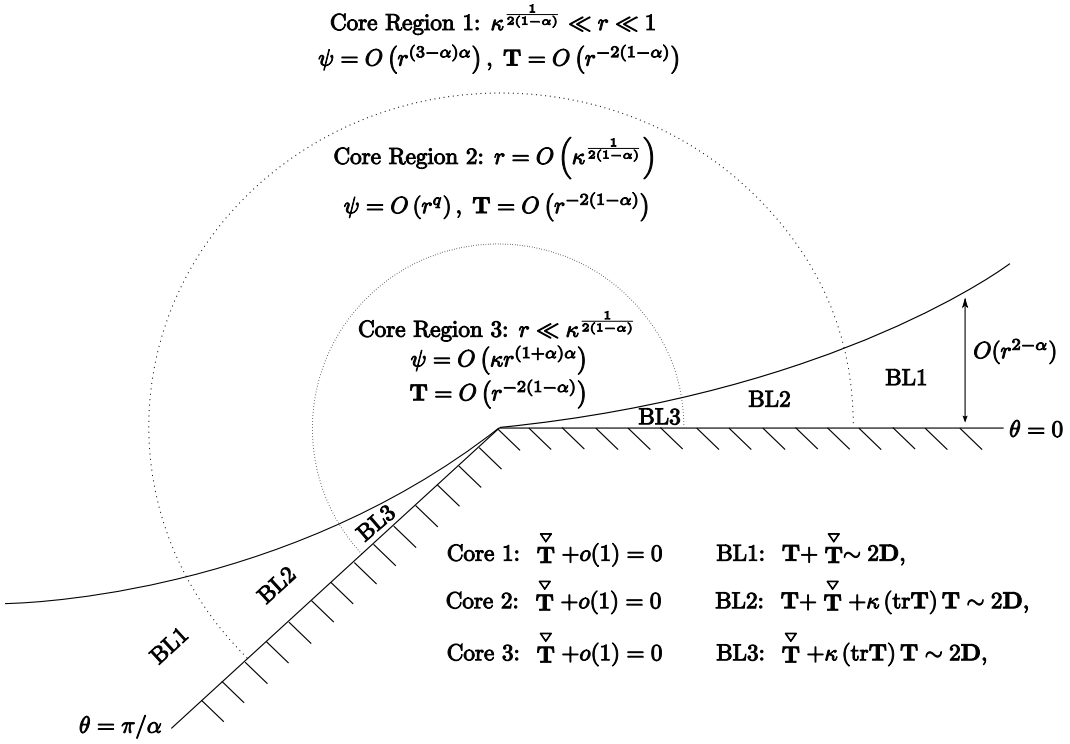

Figure 4-1: A schematic illustration of the asymptotic regions local to the re-entrant corner for the PTT model when $\kappa = o(1)$. The structure is composed of nine regions based on three length scales. The exterior regions occur for $\kappa^{\frac{1}{2(1-\alpha)}} \ll r \ll 1$, which comprise core region 1 and boundary layers (BL 1, upstream and downstream) in which the UCM problem is obtained at leading order. The intermediate regions occur for $r = O(\kappa^{\frac{1}{2(1-\alpha)}})$, comprising core region 2 and boundary layers BL 2. Finally for $r \ll \kappa^{\frac{1}{2(1-\alpha)}}$ we have core region 3 and boundary layers BL 3, in which we have the PTT $\kappa = O(1)$ problem. The boundary layer thicknesses are $O(r^{2-\alpha})$, with the upstream wall structures repeated at the downstream wall. The three boundary layer balances are those associated with the high Weissenberg number limit for the PTT model identified in [HR97] and UCM in [Ren97a]. The stress singularity $O(r^{-2(1-\alpha)})$ is also common to the three core regions. The scaling for the stream function in core region 2 varies with radial distance, with q taking values in the range stated in (4.6).

moment through the index q. The momentum and constitutive equations become

$$0 = -\nabla^* p^* + \nabla^* . \mathbf{T}^*, \tag{4.3}$$

$$\epsilon^{2-q}\mathbf{T}^* + \overset{\triangledown}{\mathbf{T}}^* + \kappa\epsilon^{2\alpha-q}(\mathrm{tr}\mathbf{T}^*)\mathbf{T}^* = 2\epsilon^{2(1-\alpha)}\mathbf{D}^*. \tag{4.4}$$

The upper convected stress derivative dominates if

$$q < 2 \qquad \text{and} \qquad \kappa\epsilon^{2\alpha-q} \ll 1. \tag{4.5}$$

The first restriction on q holds for $\alpha \in [1/2, 1)$ since we show later when we consider the intermediate regions in section 4.1.3 that q lies in the range

$$(3-\alpha)\alpha \leq q \leq \alpha^2 - \alpha + 2 = (3-\alpha)\alpha + 2(1-\alpha)^2, \tag{4.6}$$

the lower limit being associated with the velocity scaling for UCM case $\kappa = 0$ and the upper limit for the PTT $\kappa = O(1)$ case. In this outer region, the value of q is not fixed, but actually changes between these limits according to the radial distance, this being a consequence of the stream function not being self-similar (separable).

In the wall boundary layers we adopt the scalings

$$\begin{aligned} X^* = \bar{X}, \quad Y^* = \epsilon^{1-\alpha}\bar{Y}, \quad \Psi^* = \epsilon^{\bar{q}}\bar{\Psi}, \\ T_{11}^* = \bar{T}_{11}, \quad T_{12}^* = \epsilon^{1-\alpha}\bar{T}_{12}, \quad T_{22}^* = \epsilon^{2(1-\alpha)}\bar{T}_{22}, \quad p^* = \bar{p}, \end{aligned} \tag{4.7}$$

where the scalings for T_{ij}^* and p^* are assumed to be the same as the scalings in both $\kappa = 0$ and $\kappa = O(1)$ cases, the scaling for Y^* follows from the retention of the rate of strain terms D_{12} and D_{22} (again as in the $\kappa = 0$ and $\kappa = O(1)$ cases), and the scaling for the stream function is left general and to be found. The momentum equations become

$$0 = -\frac{\partial \bar{p}}{\partial \bar{X}} + \frac{\partial \bar{T}_{11}}{\partial \bar{X}} + \frac{\partial \bar{T}_{12}}{\partial \bar{Y}}, \quad 0 = -\frac{\partial \bar{p}}{\partial \bar{Y}} + \epsilon^{2(1-\alpha)}\left(\frac{\partial \bar{T}_{12}}{\partial \bar{X}} + \frac{\partial \bar{T}_{22}}{\partial \bar{Y}}\right), \tag{4.8}$$

and we have the constitutive equations

$$\begin{aligned} &\epsilon^{3-q-\alpha-\bar{q}}\bar{T}_{11} + \left(\frac{\partial \bar{\Psi}}{\partial \bar{Y}}\frac{\partial \bar{T}_{11}}{\partial \bar{X}} - \frac{\partial \bar{\Psi}}{\partial \bar{X}}\frac{\partial \bar{T}_{11}}{\partial \bar{Y}} - 2\frac{\partial^2 \bar{\Psi}}{\partial \bar{Y}^2}\bar{T}_{12} - 2\frac{\partial^2 \bar{\Psi}}{\partial \bar{X}\partial \bar{Y}}\bar{T}_{11}\right) \\ &\qquad + \kappa\epsilon^{1+\alpha-q-\bar{q}}(\bar{T}_{11} + \epsilon^{2(1-\alpha)}\bar{T}_{22})\bar{T}_{11} = 2\epsilon^{2(1-\alpha)}\frac{\partial^2 \bar{\Psi}}{\partial \bar{X}\partial \bar{Y}}, \end{aligned} \tag{4.9}$$

$$\begin{aligned} &\epsilon^{3-q-\alpha-\bar{q}}\bar{T}_{22} + \left(\frac{\partial \bar{\Psi}}{\partial \bar{Y}}\frac{\partial \bar{T}_{22}}{\partial \bar{X}} - \frac{\partial \bar{\Psi}}{\partial \bar{X}}\frac{\partial \bar{T}_{22}}{\partial \bar{Y}} + 2\frac{\partial^2 \bar{\Psi}}{\partial \bar{X}^2}\bar{T}_{12} + 2\frac{\partial^2 \bar{\Psi}}{\partial \bar{X}\partial \bar{Y}}\bar{T}_{22}\right) \\ &\qquad + \kappa\epsilon^{1+\alpha-q-\bar{q}}(\bar{T}_{11} + \epsilon^{2(1-\alpha)}\bar{T}_{22})\bar{T}_{22} = -2\frac{\partial^2 \bar{\Psi}}{\partial \bar{X}\partial \bar{Y}}, \end{aligned} \tag{4.10}$$

$$\begin{aligned} &\epsilon^{3-q-\alpha-\bar{q}}\bar{T}_{12} + \left(\frac{\partial \bar{\Psi}}{\partial \bar{Y}}\frac{\partial \bar{T}_{12}}{\partial \bar{X}} - \frac{\partial \bar{\Psi}}{\partial \bar{X}}\frac{\partial \bar{T}_{12}}{\partial \bar{Y}} + \frac{\partial^2 \bar{\Psi}}{\partial \bar{X}^2}\bar{T}_{11} - \frac{\partial^2 \bar{\Psi}}{\partial \bar{Y}^2}\bar{T}_{22}\right) \\ &\qquad + \kappa\epsilon^{1+\alpha-q-\bar{q}}(\bar{T}_{11} + \epsilon^{2(1-\alpha)}\bar{T}_{22})\bar{T}_{12} = \frac{\partial^2 \bar{\Psi}}{\partial \bar{Y}^2} - \epsilon^{2(1-\alpha)}\frac{\partial^2 \bar{\Psi}}{\partial \bar{X}^2}, \end{aligned} \tag{4.11}$$

and so the linear stress terms are retained when $\bar{q} = 3 - q - \alpha$, giving

$$\bar{\mathbf{T}} + \overset{\triangledown}{\bar{\mathbf{T}}} + \kappa\epsilon^{2(\alpha-1)}(\mathrm{tr}\bar{\mathbf{T}})\bar{\mathbf{T}} = 2\bar{\mathbf{D}}, \tag{4.12}$$

where

$$\begin{aligned}(\mathrm{tr}\bar{\mathbf{T}}) = \bar{T}_{11} + \epsilon^{2(1-\alpha)}\bar{T}_{22}, \qquad \bar{D}_{11} = 2\epsilon^{2(1-\alpha)}\frac{\partial^2\bar{\Psi}}{\partial\bar{X}\partial\bar{Y}},\\ \bar{D}_{12} = \frac{\partial^2\bar{\Psi}}{\partial\bar{Y}^2} - \epsilon^{2(1-\alpha)}\frac{\partial^2\bar{\Psi}}{\partial\bar{X}^2}, \qquad \bar{D}_{22} = -2\frac{\partial^2\bar{\Psi}}{\partial\bar{X}\partial\bar{Y}}.\end{aligned} \tag{4.13}$$

The quadratic stress terms are thus retained when

$$\epsilon = \kappa^{\frac{1}{2(1-\alpha)}}, \tag{4.14}$$

which identifies the key radial length scale in this problem[12] with the boundary layer equations being those noted in the PTT high Weissenberg limit for small κ in [HR97]. We also note agreement with the analysis of viscometric behaviour from section 2.3.1, which as seen in table 2.2 predicts $T_{12} = O(\kappa^{-1/2})$ in an intermediate boundary layer between the two extremes of UCM and PTT $\kappa = O(1)$ viscometric boundary layers. The analysis of this section gives the scaling $T_{12} = \epsilon^{\alpha-1}\bar{T}_{12} = \kappa^{-1/2}\bar{T}_{12}$ confirming this.

We are now able to build the asymptotic structure shown in figure 4-1, where we obtain the PTT $\kappa = O(1)$ problem on smaller length scales and the UCM $\kappa = 0$ problem on larger length scales. Our intention is to identify the scalings for these asymptotic regions and the leading order equations arising within them. As such, we consider the governing equations in Cartesian form and avoid the use of natural stress variables (although brief analysis in the natural stress variables will be considered later in section 4.1.4). Also, without loss of generality we consider the upstream boundary layers, where similar structures are assumed to occur at the downstream wall.

4.1.3 The asymptotic regions

The exterior regions $\kappa^{\frac{1}{2(1-\alpha)}} \ll r \ll 1$

These are the length scales on which we obtain the UCM problem. We label the 'outer' region away from the walls as core region 1 and the inner regions at the walls as boundary layer 1 (which occur upstream and downstream). The scalings for core

[12] We now have $\kappa\epsilon^{2\alpha-q} = \kappa^{\frac{2-q}{2(1-\alpha)}}$ and the second condition in (4.5) holds provided the first one does.

region 1 are

$$r = \hat{\epsilon}\hat{R}^*, \quad x = \hat{\epsilon}\hat{X}^*, \quad y = \hat{\epsilon}\hat{Y}^*,$$
$$\psi = \hat{\epsilon}^{(3-\alpha)\alpha}\hat{\Psi}^*, \quad \mathbf{v} = \hat{\epsilon}^{(3-\alpha)\alpha-1}\hat{\mathbf{v}}^*, \quad \mathbf{T} = \hat{\epsilon}^{2(\alpha-1)}\hat{\mathbf{T}}^*, \quad p = \hat{\epsilon}^{2(\alpha-1)}\hat{p}^*, \tag{4.15}$$

where we use the gauge $\hat{\epsilon}$ for our exterior region length scale and satisfies $\epsilon \ll \hat{\epsilon} \ll 1$. The governing equations are

$$0 = -\hat{\nabla}^*\hat{p}^* + \hat{\nabla}^*.\hat{\mathbf{T}}^*, \tag{4.16}$$

$$\hat{\epsilon}^{(2-\alpha)(1-\alpha)}\hat{\mathbf{T}}^* + \overset{\triangledown}{\hat{\mathbf{T}}}^* + \kappa\hat{\epsilon}^{\alpha(\alpha-1)}(\mathrm{tr}\hat{\mathbf{T}}^*)\hat{\mathbf{T}}^* = 2\hat{\epsilon}^{2(1-\alpha)}\hat{\mathbf{D}}^*. \tag{4.17}$$

The quadratic stress terms are subdominant at leading order since

$$\kappa\hat{\epsilon}^{(\alpha-1)\alpha} = \left(\epsilon^{2-\alpha}\left(\frac{\epsilon}{\hat{\epsilon}}\right)^{\alpha}\right)^{1-\alpha} \ll 1, \tag{4.18}$$

and consequently the upper convected stress derivative dominates in the constitutive equations. The leading order solution in this case is the UCM potential flow and stretching solution of section 3.1.4

$$\hat{\Psi}^* = \frac{\hat{C}_0}{\alpha^{n_1}}\hat{R}^{*\alpha n_1}\sin^{n_1}(\alpha\theta), \quad \hat{\mathbf{T}}^* = \hat{\lambda}^*(\hat{\Psi}^*)\hat{\mathbf{v}}^*\hat{\mathbf{v}}^{*T}, \quad \hat{p}^* = \frac{\hat{p}_0}{\hat{R}^{*2(1-\alpha)}}, \tag{4.19}$$

with

$$\hat{\lambda}^*(\hat{\Psi}^*) = \frac{2\hat{p}_0}{n_1^2\hat{C}_0^2}\left(\frac{\hat{\Psi}^*}{\hat{C}_0}\right)^{\frac{2(1-n_1)}{n_1}}, \qquad \text{and} \qquad n_1 = 3-\alpha. \tag{4.20}$$

The constants $\hat{C}_0$, $\hat{p}_0$ are set from incoming flow from outside this region.

The scalings for boundary layer 1 are

$$\hat{X}^* = \hat{X}, \quad \hat{Y}^* = \hat{\epsilon}^{1-\alpha}\hat{Y}, \quad \hat{\Psi}^* = \hat{\epsilon}^{(1-\alpha)(3-\alpha)}\hat{\Psi},$$
$$\hat{p}^* = \hat{p}, \quad \hat{T}_{11}^* = \hat{T}_{11}, \quad \hat{T}_{12}^* = \hat{\epsilon}^{1-\alpha}\hat{T}_{12}, \quad \hat{T}_{22}^* = \hat{\epsilon}^{2(1-\alpha)}\hat{T}_{22}, \tag{4.21}$$

the governing equations being

$$0 = -\frac{\partial\hat{p}}{\partial\hat{X}} + \frac{\partial\hat{T}_{11}}{\partial\hat{X}} + \frac{\partial\hat{T}_{12}}{\partial\hat{Y}}, \quad 0 = -\frac{\partial\hat{p}}{\partial\hat{Y}} + \hat{\epsilon}^{2(1-\alpha)}\left(\frac{\partial\hat{T}_{12}}{\partial\hat{X}} + \frac{\partial\hat{T}_{22}}{\partial\hat{Y}}\right),$$
$$\hat{\mathbf{T}} + \overset{\triangledown}{\hat{\mathbf{T}}} + \left(\frac{\epsilon}{\hat{\epsilon}}\right)^{2(1-\alpha)}(\mathrm{tr}\hat{\mathbf{T}})\hat{\mathbf{T}} = 2\hat{\mathbf{D}}, \tag{4.22}$$

where

$$(\mathrm{tr}\hat{\mathbf{T}}) = \hat{T}_{11} + \hat{\epsilon}^{2(1-\alpha)}\hat{T}_{22}, \qquad \hat{D}_{11} = 2\hat{\epsilon}^{2(1-\alpha)}\frac{\partial^2\hat{\Psi}}{\partial\hat{X}\partial\hat{Y}},$$
$$\hat{D}_{12} = \frac{\partial^2\hat{\Psi}}{\partial\hat{Y}^2} - \hat{\epsilon}^{2(1-\alpha)}\frac{\partial^2\hat{\Psi}}{\partial\hat{X}^2}, \qquad \hat{D}_{22} = -2\frac{\partial^2\hat{\Psi}}{\partial\hat{X}\partial\hat{Y}}. \tag{4.23}$$

At leading order we obtain the UCM boundary layer equations

$$0 = -\frac{d\hat{p}}{d\hat{X}} + \frac{\partial\hat{T}_{11}}{\partial\hat{X}} + \frac{\partial\hat{T}_{12}}{\partial\hat{Y}} \tag{4.24}$$

$$\hat{T}_{11} + \left(\frac{\partial\hat{\Psi}}{\partial\hat{Y}}\frac{\partial\hat{T}_{11}}{\partial\hat{X}} - \frac{\partial\hat{\Psi}}{\partial\hat{X}}\frac{\partial\hat{T}_{11}}{\partial\hat{Y}} - 2\frac{\partial^2\hat{\Psi}}{\partial\hat{Y}^2}\hat{T}_{12} - 2\frac{\partial^2\hat{\Psi}}{\partial\hat{X}\partial\hat{Y}}\hat{T}_{11}\right) = 0, \tag{4.25}$$

$$\hat{T}_{22} + \left(\frac{\partial\hat{\Psi}}{\partial\hat{Y}}\frac{\partial\hat{T}_{22}}{\partial\hat{X}} - \frac{\partial\hat{\Psi}}{\partial\hat{X}}\frac{\partial\hat{T}_{22}}{\partial\hat{Y}} + 2\frac{\partial^2\hat{\Psi}}{\partial\hat{X}^2}\hat{T}_{12} + 2\frac{\partial^2\hat{\Psi}}{\partial\hat{X}\partial\hat{Y}}\hat{T}_{22}\right) = -2\frac{\partial^2\hat{\Psi}}{\partial\hat{X}\partial\hat{Y}}, \tag{4.26}$$

$$\hat{T}_{12} + \left(\frac{\partial\hat{\Psi}}{\partial\hat{Y}}\frac{\partial\hat{T}_{12}}{\partial\hat{X}} - \frac{\partial\hat{\Psi}}{\partial\hat{X}}\frac{\partial\hat{T}_{12}}{\partial\hat{Y}} + \frac{\partial^2\hat{\Psi}}{\partial\hat{X}^2}\hat{T}_{11} - \frac{\partial^2\hat{\Psi}}{\partial\hat{Y}^2}\hat{T}_{22}\right) = \frac{\partial^2\hat{\Psi}}{\partial\hat{Y}^2}, \tag{4.27}$$

subject to the core 1 matching conditions

$$\text{as } \hat{Y}\to\infty, \qquad \hat{\Psi} \sim \hat{C}_0\hat{X}^{n_1(\alpha-1)}\hat{Y}^{n_1}, \quad \hat{p} = \hat{p}_0\hat{X}^{2\alpha-2}, \quad \hat{T}_{11} \sim 2\hat{p}_0\hat{X}^{(2\alpha-2)},$$
$$\hat{T}_{12} \sim 2\hat{p}_0(1-\alpha)\hat{X}^{(2\alpha-3)}\hat{Y}, \quad \hat{T}_{22} \sim 2\hat{p}_0(1-\alpha)^2\hat{X}^{(2\alpha-4)}\hat{Y}^2, \tag{4.28}$$

with no-slip at the wall. Details of solutions for these core and boundary layer equations are given in [Eva08a] and [Eva08b].

The interior regions $r \ll \kappa^{\frac{1}{2(1-\alpha)}}$

These are the length scales on which we obtain the PTT $\kappa = O(1)$ problem. We label the outer region away from the walls as core region 3 and the inner regions at the walls as boundary layer 3. The scalings for core region 3 are

$$r = \tilde{\epsilon}\tilde{R}^*, \quad x = \tilde{\epsilon}\tilde{X}^*, \quad y = \tilde{\epsilon}\tilde{Y}^*,$$
$$\psi = \kappa\tilde{\epsilon}^{(1+\alpha)\alpha}\tilde{\Psi}^*, \quad \mathbf{v} = \kappa\tilde{\epsilon}^{(1+\alpha)\alpha-1}\tilde{\mathbf{v}}^*, \quad \mathbf{T} = \tilde{\epsilon}^{2(\alpha-1)}\tilde{\mathbf{T}}^*, \quad p = \tilde{\epsilon}^{2(\alpha-1)}\tilde{p}^*, \tag{4.29}$$

where we use the gauge $\tilde{\epsilon}$ for our interior region length scale and satisfies $\tilde{\epsilon} \ll \epsilon \ll 1$. The governing equations are

$$0 = -\tilde{\nabla}^* \tilde{p}^* + \tilde{\nabla}^* . \tilde{\mathbf{T}}^*, \tag{4.30}$$

$$\frac{\tilde{\epsilon}^{(2+\alpha)(1-\alpha)}}{\kappa} \tilde{\mathbf{T}}^* + \overset{\triangledown}{\tilde{\mathbf{T}}}^* + \tilde{\epsilon}^{\alpha(1-\alpha)} (\mathrm{tr}\tilde{\mathbf{T}}^*) \tilde{\mathbf{T}}^* = 2\tilde{\epsilon}^{2(1-\alpha)} \tilde{\mathbf{D}}^*. \tag{4.31}$$

The linear stress terms are subdominant at leading order since

$$\frac{\tilde{\epsilon}^{(2+\alpha)(1-\alpha)}}{\kappa} = \left(\frac{\tilde{\epsilon}}{\epsilon}\right)^{2(1-\alpha)} \tilde{\epsilon}^{\alpha(1-\alpha)} \ll 1, \tag{4.32}$$

and consequently the upper convected stress derivative dominates at leading order in the constitutive equations. The leading order solution in this case is the PTT potential flow and stretching solution (3.27)–(3.30), thus

$$\tilde{\Psi}^* = \frac{\tilde{C}_0}{\alpha^{n_3}} \tilde{R}^{*\alpha n_3} \sin^{n_3}(\alpha\theta), \quad \tilde{\mathbf{T}}^* = \tilde{\lambda}^*(\tilde{\Psi}^*) \tilde{\mathbf{v}}^* \tilde{\mathbf{v}}^{*T}, \quad \tilde{p}^* = \frac{\tilde{p}_0}{\tilde{R}^{*2(1-\alpha)}}, \tag{4.33}$$

with

$$\tilde{\lambda}^*(\tilde{\Psi}^*) = \frac{2\tilde{p}_0}{n_3^2 \tilde{C}_0^2} \left(\frac{\tilde{\Psi}^*}{\tilde{C}_0}\right)^{\frac{2(1-n_3)}{n_3}}, \qquad \text{and} \qquad n_3 = 1 + \alpha. \tag{4.34}$$

The constants $\tilde{C}_0$, $\tilde{p}_0$ are set from incoming flow from outside this region, namely the intermediate regions which we will consider next.

The scalings for boundary layer 3 are

$$\begin{gathered} \tilde{X}^* = \tilde{X}, \quad \tilde{Y}^* = \tilde{\epsilon}^{1-\alpha} \tilde{Y}, \quad \tilde{\Psi}^* = \tilde{\epsilon}^{1-\alpha^2} \tilde{\Psi}, \\ \tilde{p}^* = \tilde{p}, \quad \tilde{T}_{11}^* = \tilde{T}_{11}, \quad \tilde{T}_{12}^* = \tilde{\epsilon}^{1-\alpha} \tilde{T}_{12}, \quad \tilde{T}_{22}^* = \tilde{\epsilon}^{2(1-\alpha)} \tilde{T}_{22}, \end{gathered} \tag{4.35}$$

the governing equations being

$$\begin{gathered} 0 = -\frac{\partial \tilde{p}}{\partial \tilde{X}} + \frac{\partial \tilde{T}_{11}}{\partial \tilde{X}} + \frac{\partial \tilde{T}_{12}}{\partial \tilde{Y}}, \quad 0 = -\frac{\partial \tilde{p}}{\partial \tilde{Y}} + \tilde{\epsilon}^{2(1-\alpha)} \left(\frac{\partial \tilde{T}_{12}}{\partial \tilde{X}} + \frac{\partial \tilde{T}_{22}}{\partial \tilde{Y}}\right), \\ \left(\frac{\tilde{\epsilon}}{\epsilon}\right)^{2(1-\alpha)} \tilde{\mathbf{T}} + \overset{\triangledown}{\tilde{\mathbf{T}}} + (\mathrm{tr}\tilde{\mathbf{T}}) \tilde{\mathbf{T}} = 2\tilde{\mathbf{D}}, \end{gathered} \tag{4.36}$$

where

$$(\mathrm{tr}\tilde{\mathbf{T}}) = \tilde{T}_{11} + \tilde{\epsilon}^{2(1-\alpha)}\tilde{T}_{22}, \qquad \tilde{D}_{11} = 2\tilde{\epsilon}^{2(1-\alpha)}\frac{\partial^2\tilde{\Psi}}{\partial\tilde{X}\partial\tilde{Y}},$$
$$\tilde{D}_{12} = \frac{\partial^2\tilde{\Psi}}{\partial\tilde{Y}^2} - \tilde{\epsilon}^{2(1-\alpha)}\frac{\partial^2\tilde{\Psi}}{\partial\tilde{X}^2}, \qquad \tilde{D}_{22} = -2\frac{\partial^2\tilde{\Psi}}{\partial\tilde{X}\partial\tilde{Y}}. \tag{4.37}$$

At leading order we obtain the PTT $\kappa = 1$ boundary layer equations

$$0 = -\frac{d\tilde{p}}{d\tilde{X}} + \frac{\partial\tilde{T}_{11}}{\partial\tilde{X}} + \frac{\partial\tilde{T}_{12}}{\partial\tilde{Y}} \tag{4.38}$$

$$\left(\frac{\partial\tilde{\Psi}}{\partial\tilde{Y}}\frac{\partial\tilde{T}_{11}}{\partial\tilde{X}} - \frac{\partial\tilde{\Psi}}{\partial\tilde{X}}\frac{\partial\tilde{T}_{11}}{\partial\tilde{Y}} - 2\frac{\partial^2\tilde{\Psi}}{\partial\tilde{Y}^2}\tilde{T}_{12} - 2\frac{\partial^2\tilde{\Psi}}{\partial\tilde{X}\partial\tilde{Y}}\tilde{T}_{11}\right) + \tilde{T}_{11}^2 = 0, \tag{4.39}$$

$$\left(\frac{\partial\tilde{\Psi}}{\partial\tilde{Y}}\frac{\partial\tilde{T}_{22}}{\partial\tilde{X}} - \frac{\partial\tilde{\Psi}}{\partial\tilde{X}}\frac{\partial\tilde{T}_{22}}{\partial\tilde{Y}} + 2\frac{\partial^2\tilde{\Psi}}{\partial\tilde{X}^2}\tilde{T}_{12} + 2\frac{\partial^2\tilde{\Psi}}{\partial\tilde{X}\partial\tilde{Y}}\tilde{T}_{22}\right) + \tilde{T}_{11}\tilde{T}_{22} = -2\frac{\partial^2\tilde{\Psi}}{\partial\tilde{X}\partial\tilde{Y}}, \tag{4.40}$$

$$\left(\frac{\partial\tilde{\Psi}}{\partial\tilde{Y}}\frac{\partial\tilde{T}_{12}}{\partial\tilde{X}} - \frac{\partial\tilde{\Psi}}{\partial\tilde{X}}\frac{\partial\tilde{T}_{12}}{\partial\tilde{Y}} + \frac{\partial^2\tilde{\Psi}}{\partial\tilde{X}^2}\tilde{T}_{11} - \frac{\partial^2\tilde{\Psi}}{\partial\tilde{Y}^2}\tilde{T}_{22}\right) + \tilde{T}_{11}\tilde{T}_{12} = \frac{\partial^2\tilde{\Psi}}{\partial\tilde{Y}^2}, \tag{4.41}$$

subject to the core 3 matching conditions

$$\text{as } \tilde{Y}\to\infty, \qquad \tilde{\Psi} \sim \tilde{C}_0\tilde{X}^{n_3(\alpha-1)}\tilde{Y}^{n_3}, \quad \tilde{p} \sim \tilde{p}_0\tilde{X}^{2\alpha-2}, \quad \tilde{T}_{11} \sim 2\tilde{p}_0\tilde{X}^{(2\alpha-2)},$$
$$\tilde{T}_{12} \sim 2\tilde{p}_0(1-\alpha)\tilde{X}^{(2\alpha-3)}\tilde{Y}, \quad \tilde{T}_{22} \sim 2\tilde{p}_0(1-\alpha)^2\tilde{X}^{(2\alpha-4)}\tilde{Y}^2, \tag{4.42}$$

and no-slip at the wall.

We refer to chapter 3 for details of the solution for these core and boundary layer regions, where we note that construction of a self-similar solution is currently restricted to the corner angle range $2/3 < \alpha < 1$.

The intermediate regions $r = O(\kappa^{\frac{1}{2(1-\alpha)}})$

The scalings for the regions on this length scale have been identified in section 4.1.2. In core region 2 (the outer region away from the walls) we have at leading order

$$0 = -\nabla^* p^* + \nabla^*.\mathbf{T}^*, \qquad \overset{\triangledown}{\mathbf{T}}{}^* = 0. \tag{4.43}$$

These equations have been shown in [Ren97c], and also here in section 3.1.4 to be equivalent to the compressible Euler equations, the solution in this region belonging to the general solution class for such equations. The incompressible potential flow solutions appear only relevant in the radial limits as core regions 1 and 3 are approached.

Specifically, for matching we have

$$\text{as } R^* \to \infty, \qquad \Psi^* = h(\hat{\psi}) = \hat{C}_0 \left(\frac{\hat{\psi}}{(2\hat{p}_0)^{1/2}} \right)^{n_1}, \quad \mathbf{T}^* = \lambda^*(\Psi^*)\mathbf{v}^*\mathbf{v}^{*T},$$
$$p^* = \frac{1}{2}\lambda^*(\Psi^*)\mathbf{v}^{*2} = \frac{\hat{p}_0}{R^{*2(1-\alpha)}}, \qquad (4.44)$$

where

$$\lambda^* = \left(\frac{dh}{d\hat{\psi}} \right)^{-2}, \qquad \hat{\psi} = \frac{(2\hat{p}_0)^{1/2}}{\alpha} R^{*\alpha} \sin(\alpha\theta), \qquad (4.45)$$

where equation (3.32) has been utilised to find these behaviours, and we also have the analogous behaviour

$$\text{as } R^* \to 0, \qquad \Psi^* = h(\tilde{\psi}) = \tilde{C}_0 \left(\frac{\tilde{\psi}}{(2\tilde{p}_0)^{1/2}} \right)^{n_3}, \quad \mathbf{T}^* = \lambda^*(\Psi^*)\mathbf{v}^*\mathbf{v}^{*T},$$
$$p^* = \frac{1}{2}\lambda^*(\Psi^*)\mathbf{v}^{*2} = \frac{\tilde{p}_0}{R^{*2(1-\alpha)}}, \qquad (4.46)$$

where

$$\lambda^* = \left(\frac{dh}{d\tilde{\psi}} \right)^{-2}, \qquad \tilde{\psi} = \frac{(2\tilde{p}_0)^{1/2}}{\alpha} R^{*\alpha} \sin(\alpha\theta). \qquad (4.47)$$

Here the function h takes power law form and the stream functions $\hat{\psi}$ and $\tilde{\psi}$ are associated with the velocity field $\lambda^{1/2}\mathbf{v}$ (see section 3.1.4). The separable potential solution that vanishes on the walls $\theta = 0$ and $\theta = \pi/\alpha$ has been taken for the associated stream functions, with the arbitrary multiplicative constant chosen to give the appropriate pressure coefficient (see (3.32) as mentioned). For $R^* = O(1)$, it appears that there is no such behaviour of this form even for a more general function h which is consistent with these two limiting radial behaviours and the requirement of matching to the wall boundary layers. A more general solution within the compressible Euler class appears necessary, this solution only being self-similar (separable) in the extreme radial limits. Work performed to search for more general solutions is given in appendix D.

The solution behaviour (4.44) now matches with (4.19) of core region 1 provided $q = n_1\alpha = (3-\alpha)\alpha$ in this large R^* limit, whilst (4.46) matches with (4.33) if $q = n_3\alpha + 2(1-\alpha)$ in the small R^* limit. For intermediate R^* we anticipate the value of q to lie in between as given in (4.6), its variability a consequence of the solution not being a simple power of the radial variable.

We may write the core 2 solution wall behaviour in the form

$$\begin{aligned} \text{as } Y^* \to 0, \qquad & \Psi^* \sim a_0(X^*, Y^*), \quad p^* \sim b_0(X^*), \quad T^*_{11} \sim a_{11}(X^*), \\ & T^*_{12} \sim a_{12}(X^*)Y^*, \quad T^*_{22} \sim a_{22}(X^*)Y^{*2}, \end{aligned} \tag{4.48}$$

where a_0, b_0, a_{ij} are functions determined by boundary layer 2, the form of the extra-stresses being deducible from the scalings (4.7). If the stream function is to vanish on the walls then $a_0(X^*, 0) = 0$ and further we expect (4.48) to have the limiting behaviours

$$\begin{aligned} \text{as } X^* \to \infty, \qquad & a_0(X^*, Y^*) \sim \hat{C}_0 X^{*n_1(\alpha-1)} Y^{*n_1}, \\ & b_0 \sim \hat{p}_0 X^{*2\alpha-2}, \quad a_{11} \sim 2\hat{p}_0 X^{*(2\alpha-2)}, \\ & a_{12} \sim 2\hat{p}_0(1-\alpha) X^{*(2\alpha-3)}, \quad a_{22} \sim 2\hat{p}_0(1-\alpha)^2 X^{*(2\alpha-4)}, \end{aligned} \tag{4.49}$$

and

$$\begin{aligned} \text{as } X^* \to 0, \qquad & a_0(X^*, Y^*) \sim \tilde{C}_0 X^{*n_3(\alpha-1)} Y^{*n_3}, \\ & b_0 \sim \tilde{p}_0 X^{*2\alpha-2}, \quad a_{11} \sim 2\tilde{p}_0 X^{*(2\alpha-2)}, \\ & a_{12} \sim 2\tilde{p}_0(1-\alpha) X^{*(2\alpha-3)}, \quad a_{22} \sim 2\tilde{p}_0(1-\alpha)^2 X^{*(2\alpha-4)}, \end{aligned} \tag{4.50}$$

for consistency with (4.44) and (4.46).

The boundary layer 2 equations are

$$0 = -\frac{d\bar{p}}{d\bar{X}} + \frac{\partial \bar{T}_{11}}{\partial \bar{X}} + \frac{\partial \bar{T}_{12}}{\partial \bar{Y}} \tag{4.51}$$

$$\bar{T}_{11} + \left(\frac{\partial \bar{\Psi}}{\partial \bar{Y}} \frac{\partial \bar{T}_{11}}{\partial \bar{X}} - \frac{\partial \bar{\Psi}}{\partial \bar{X}} \frac{\partial \bar{T}_{11}}{\partial \bar{Y}} - 2\frac{\partial^2 \bar{\Psi}}{\partial \bar{Y}^2} \bar{T}_{12} - 2\frac{\partial^2 \bar{\Psi}}{\partial \bar{X} \partial \bar{Y}} \bar{T}_{11} \right) + \bar{T}_{11}^2 = 0, \tag{4.52}$$

$$\bar{T}_{22} + \left(\frac{\partial \bar{\Psi}}{\partial \bar{Y}} \frac{\partial \bar{T}_{22}}{\partial \bar{X}} - \frac{\partial \bar{\Psi}}{\partial \bar{X}} \frac{\partial \bar{T}_{22}}{\partial \bar{Y}} + 2\frac{\partial^2 \bar{\Psi}}{\partial \bar{X}^2} \bar{T}_{12} + 2\frac{\partial^2 \bar{\Psi}}{\partial \bar{X} \partial \bar{Y}} \bar{T}_{22} \right) + \bar{T}_{11}\bar{T}_{22} = -2\frac{\partial^2 \bar{\Psi}}{\partial \bar{X} \partial \bar{Y}}, \tag{4.53}$$

$$\bar{T}_{12} + \left(\frac{\partial \bar{\Psi}}{\partial \bar{Y}} \frac{\partial \bar{T}_{12}}{\partial \bar{X}} - \frac{\partial \bar{\Psi}}{\partial \bar{X}} \frac{\partial \bar{T}_{12}}{\partial \bar{Y}} + \frac{\partial^2 \bar{\Psi}}{\partial \bar{X}^2} \bar{T}_{11} - \frac{\partial^2 \bar{\Psi}}{\partial \bar{Y}^2} \bar{T}_{22} \right) + \bar{T}_{11}\bar{T}_{12} = \frac{\partial^2 \bar{\Psi}}{\partial \bar{Y}^2}. \tag{4.54}$$

which are subject to no-slip on the wall and the matching conditions with core region 2 behaviour (4.48), namely

$$\begin{aligned} \text{as } \bar{Y} \to \infty, \qquad & \bar{\Psi} \sim \bar{a}_0(\bar{X}, \bar{Y}), \quad \bar{p} \sim b_0(\bar{X}), \quad \bar{T}_{11} \sim a_{11}(\bar{X}), \\ & \bar{T}_{12} \sim a_{12}(\bar{X})\bar{Y}, \quad \bar{T}_{22} \sim a_{22}(\bar{X})\bar{Y}^2. \end{aligned} \tag{4.55}$$

Here we have introduced the function $\bar{a}_0$, defined by

$$\frac{a_0(\bar{X}, \epsilon^{1-\alpha}\bar{Y})}{\epsilon^{3-\alpha-q}} = \bar{a}_0(\bar{X}, \bar{Y}) = O(1), \tag{4.56}$$

which is required to hold if the stream functions in core 2 and boundary layer 2 regions are to match. Using (4.49) and (4.50), we note that this expression holds in the large and small $\bar{X}$ limits where

$$\bar{a}_0(\bar{X}, \bar{Y}) = \begin{cases} \hat{C}_0 \bar{X}^{n_1(\alpha-1)} \bar{Y}^{n_1} & \text{as } \bar{X} \to \infty, \quad q = n_1\alpha, \\ \tilde{C}_0 \bar{X}^{n_3(\alpha-1)} \bar{Y}^{n_3} & \text{as } \bar{X} \to 0, \quad q = n_3\alpha + 2(1-\alpha). \end{cases} \tag{4.57}$$

There is no straightforward self-similar solution[13] to the these boundary layer equations, the solution to which (as well as the core 2 equations) needs to be determined numerically.

For completeness, we explain how matching proceeds between the boundary layer equations of this region and those of the exterior and interior regions. We recover boundary layer 1 equations (4.24)-(4.27) from (4.51)-(4.54) through the scalings

$$\bar{X} = \frac{\hat{\epsilon}}{\epsilon}\hat{X}, \quad \bar{Y} = \left(\frac{\hat{\epsilon}}{\epsilon}\right)^{2-\alpha} \hat{Y}, \quad \bar{\Psi} = \left(\frac{\hat{\epsilon}}{\epsilon}\right)^{n_1} \hat{\Psi},$$
$$\bar{p} = \left(\frac{\hat{\epsilon}}{\epsilon}\right)^{2(\alpha-1)} \hat{p}, \quad \bar{T}_{11} = \left(\frac{\hat{\epsilon}}{\epsilon}\right)^{2(\alpha-1)} \hat{T}_{11}, \quad \bar{T}_{12} = \left(\frac{\hat{\epsilon}}{\epsilon}\right)^{\alpha-1} \hat{T}_{12}, \quad \bar{T}_{22} = \hat{T}_{22}, \tag{4.59}$$

the quadratic stress terms being subdominant to the linear stress terms at leading order since $\epsilon \ll \hat{\epsilon}$. In a similar manner we obtain boundary layer 3 equations (4.38)-(4.41) from (4.51)-(4.54) using these same scalings (except with hats replaced with tildes and n_1 replaced with n_3). The linear stress terms are now subdominant to the quadratic stress terms at leading order since $\tilde{\epsilon} \ll \epsilon$.

4.1.4 The $\kappa = o(1)$ limit using the natural stress basis

We add to the small κ limit analysis using the Cartesian stress basis of the previous section by considering the limit using the natural stress variables, with the governing equations in the natural stress are given in (2.37)–(2.42). This is an important consideration because as we have seen, the natural stress formulation allows the solution to be completed at the downstream wall.

[13]It is worth mentioning that these boundary layer equations possess the similarity solution

$$\xi = \frac{\bar{Y}}{\bar{X}^2} \quad \bar{\Psi} = \bar{X}^2 f(\xi), \quad \bar{T}_{11} = t_{11}(\xi), \quad \bar{T}_{12} = t_{12}(\xi), \quad \bar{T}_{22} = t_{22}(\xi), \tag{4.58}$$

although this does not appear to play any role for the situation under consideration.

The analysis is very similar to the Cartesian basis of the previous section, and thus only the interesting points (which occur in the intermediate region) will be mentioned.

The main length scale $r = O(\kappa^{\frac{1}{2(1-\alpha)}})$

In the core region, the balance $\overset{\triangledown}{\mathbf{T}} = 0$ may be converted to natural stress variables using (2.32) becoming

$$\begin{aligned} (\mathbf{v}.\nabla)\lambda + 2\mu\nabla.\mathbf{w} + \frac{2}{|\mathbf{v}|^4}\mathbf{v}^T\left(\nabla\mathbf{v}\right)\mathbf{v} = 0, \\ (\mathbf{v}.\nabla)\mu + \nu\nabla.\mathbf{w} - |\mathbf{v}|^2\nabla.\mathbf{w} = 0, \qquad (\mathbf{v}.\nabla)\nu - 2\mathbf{v}^T\left(\nabla\mathbf{v}\right)\mathbf{v} = 0, \end{aligned} \tag{4.60}$$

which can be be more conveniently written as

$$\begin{aligned} (\mathbf{v}.\nabla)\left(\lambda - \frac{1}{|\mathbf{v}|^2}\right) + 2\mu\nabla.\mathbf{w} = 0, \\ (\mathbf{v}.\nabla)\mu + \left(\nu - |\mathbf{v}|^2\right)\nabla.\mathbf{w} = 0, \quad (\mathbf{v}.\nabla)\left(\nu - |\mathbf{v}|^2\right) = 0. \end{aligned} \tag{4.61}$$

We expect, however, that the balance to hold in the core will be

$$(\mathbf{v}.\nabla)\lambda + 2\mu\nabla.\mathbf{w} = 0, \quad (\mathbf{v}.\nabla)\mu + \nu\nabla.\mathbf{w} = 0, \quad (\mathbf{v}.\nabla)\nu = 0, \tag{4.62}$$

since requiring the fullest balance would in fact be equating terms which are the same size as the terms from $2\mathbf{D}$, giving a different core balance. Hence we can now determine the scalings for the core region.

To begin, we confirm the length scale which will give fullest balance in the constitutive equations, thus we consider distances $O(\epsilon)$ from the corner, where $\epsilon(\kappa)$ is a small parameter whose dependency on κ is to be found. We consider the scalings (found from balancing terms in (4.62)) of

$$\begin{aligned} r = \epsilon R^*, \quad x = \epsilon X^*, \quad y = \epsilon Y^*, \quad \psi = \epsilon^q \Psi^*, \\ \mathbf{v} = \epsilon^{q-1}\mathbf{v}^*, \quad \mathbf{w} = \epsilon^{1-q}\mathbf{w}^*, \quad \lambda = \epsilon^{\chi-4q+4}\lambda^*, \\ \mu = \epsilon^{\chi-2q+2}\mu^*, \quad \nu = \epsilon^{\chi}\nu^*, \quad \mathbf{T} = \epsilon^{\chi-2q+2}\mathbf{T}^*, \quad p = \epsilon^{\chi-2q+2}p^*, \end{aligned} \tag{4.63}$$

which give the leading order momentum equations in outer variables as

$$\begin{aligned} 0 = -\frac{\partial p^*}{\partial X^*} + (\mathbf{v}^*.\nabla^*)(\lambda^* u^*) + \nabla^*.(\mu^* u^* \mathbf{w}^* + \mu^* \mathbf{v}^* w_1^*) + \nabla^*.\left(\nu^* \mathbf{w}^* w_1^*\right), \\ 0 = -\frac{\partial p^*}{\partial Y^*} + (\mathbf{v}^*.\nabla^*)(\lambda^* v^*) + \nabla^*.(\mu^* v^* \mathbf{w}^* + \mu^* \mathbf{v}^* w_2^*) + \nabla^*.\left(\nu^* \mathbf{w}^* w_2^*\right), \end{aligned} \tag{4.64}$$

and the constitutive equations in outer variables, from (2.37)-(2.39), are

$$\begin{aligned}
&(\mathbf{v}^*.\nabla^*)\lambda^* + \epsilon^{2-q}\lambda^* + 2\mu^*\nabla^*.\mathbf{w}^* + \kappa\mathrm{tr}(\mathbf{T}^*)\left(\lambda^* - \epsilon^{2q-2-\chi}\frac{1}{|\mathbf{v}^*|^2}\right) = \epsilon^{q-\chi}\frac{1}{|\mathbf{v}^*|^2},\\
&(\mathbf{v}^*.\nabla^*)\mu^* + \epsilon^{2-q}\mu^* + \nu^*\nabla^*.\mathbf{w}^* + \kappa\mathrm{tr}(\mathrm{T}^*)\mu^* = 0,\\
&(\mathbf{v}^*.\nabla^*)\nu^* + \epsilon^{2-q}\nu^* + \kappa\mathrm{tr}(\mathrm{T}^*)\left(\nu^* - \epsilon^{2q-2-\chi}|\mathbf{v}^*|^2\right) = \epsilon^{q-\chi}|\mathbf{v}^*|^2,
\end{aligned} \tag{4.65}$$

where

$$\mathrm{tr}(\mathrm{T}^*) = \left(\epsilon^{\chi-3q+4}\lambda^*|\mathbf{v}^*|^2 - 2\epsilon^{2-q} + \epsilon^{\chi-3q+4}\frac{\nu^*}{|\mathbf{v}^*|^2}\right). \tag{4.66}$$

We also have

$$\mathbf{T}^* = -\epsilon^{2q-2-\chi}\mathbf{I} + \lambda\mathbf{v}^*\mathbf{v}^{*T} + \mu^*(\mathbf{v}^*\mathbf{w}^{*T} + \mathbf{w}^*\mathbf{v}^{*T}) + \nu^*\mathbf{w}^*\mathbf{w}^{*T}. \tag{4.67}$$

Assuming that

$$\kappa\epsilon^{\chi-3q+4} \ll 1, \text{ and } 2 > q > \chi, \tag{4.68}$$

which may be verified as we can determine that $\chi = 2q + 2\alpha - 4$ by using the $\mathbf{T}$ scaling of $\mathbf{T} = \epsilon^{2(\alpha-1)}\mathbf{T}^*$ in equation (4.2), and that q is in the range given in (4.6), then at leading order in the constitutive equations we have

$$(\mathbf{v}^*.\nabla^*)\,\lambda^* + 2\mu^*\nabla^*.\mathbf{w}^* = 0, \quad (\mathbf{v}^*.\nabla^*)\,\mu^* + \nu^*\nabla^*.\mathbf{w}^* = 0, \quad (\mathbf{v}^*.\nabla^*)\,\nu^* = 0. \tag{4.69}$$

To scale into the boundary layer we use

$$\begin{aligned}
X^* = \bar{X}, \quad Y^* = \delta\bar{Y}, \quad \Psi^* = \delta^{q_1}\bar{\Psi}, \quad u^* = \delta^{q_1-1}\bar{u},\\
v^* = \delta^{q_1}\bar{v}, \quad |\mathbf{v}^*|^2 = \delta^{2q_1-2}|\bar{\mathbf{v}}|^2, \quad w_1^* = \delta^{2-q_1}\bar{w}_1, \quad w_2^* = \delta^{1-q_1}\bar{w}_2,\\
\lambda^* = \delta^{\chi_1-4q_1+2}\bar{\lambda}, \quad \mu^* = \delta^{\chi_1-2q_1+1}\bar{\mu}, \quad \nu^* = \delta^{\chi_1}\bar{\nu}, \quad p^* = \delta^{p_1}\bar{p},
\end{aligned} \tag{4.70}$$

where

$$\bar{u} = \frac{\partial\bar{\Psi}}{\partial\bar{Y}}, \quad \bar{v} = -\frac{\partial\bar{\Psi}}{\partial\bar{X}}, \quad |\bar{\mathbf{v}}|^2 = \bar{u}^2 + \delta^2\bar{v}^2, \quad \bar{w}_1 = -\frac{\bar{v}}{|\bar{\mathbf{v}}|^2}, \quad \text{and} \quad \bar{w}_2 = \frac{\bar{u}}{|\bar{\mathbf{v}}|^2}.$$

The momentum equations become

$$0 = -\delta^{p_1+2q_1-\chi_1}\frac{\partial \bar{p}}{\partial \bar{X}} + (\bar{\mathbf{v}}.\bar{\nabla})(\bar{\lambda}\bar{u}) + \delta^2\frac{\partial}{\partial \bar{X}}(2\bar{\mu}\bar{u}\bar{w}_1 + \delta^2\bar{\nu}\bar{w}_1^2) + \frac{\partial}{\partial \bar{Y}}(\bar{\mu}\bar{u}\bar{w}_2 + \delta^2\bar{\mu}\bar{v}\bar{w}_1 + \delta^2\bar{\nu}\bar{w}_1\bar{w}_2), \tag{4.71}$$

$$0 = -\delta^{p_1+2q_1-\chi_1}\frac{\partial \bar{p}}{\partial \bar{Y}} + \delta^2(\bar{\mathbf{v}}.\bar{\nabla})(\bar{\lambda}\bar{v}) + \delta^2\frac{\partial}{\partial \bar{X}}(\delta^2\bar{\mu}\bar{v}\bar{w}_1 + \bar{\mu}\bar{u}\bar{w}_2 + \delta^2\bar{\nu}\bar{w}_1\bar{w}_2) + \delta^2\frac{\partial}{\partial \bar{Y}}(2\bar{\mu}\bar{v}\bar{w}_2 + \bar{\nu}\bar{w}_2^2), \tag{4.72}$$

and the constitutive equations in inner variables become

$$(\bar{\mathbf{v}}.\bar{\nabla})\bar{\lambda} + \delta^{1-q_1}\epsilon^{2-q}\bar{\lambda} + 2\bar{\mu}\bar{\nabla}.\bar{\mathbf{w}} + \kappa\mathrm{tr}(\bar{\mathrm{T}})\left(\bar{\lambda} - \delta^{2q_1-\chi_1}\epsilon^{2q-2-\chi}\frac{1}{|\bar{\mathbf{v}}|^2}\right) = \delta^{1+q_1-\chi_1}\epsilon^{q-\chi}\frac{1}{|\bar{\mathbf{v}}|^2}, \tag{4.73}$$

$$(\bar{\mathbf{v}}.\bar{\nabla})\bar{\mu} + \delta^{1-q_1}\epsilon^{2-q}\bar{\mu} + \bar{\nu}\bar{\nabla}.\bar{\mathbf{w}} + \kappa\mathrm{tr}(\bar{\mathrm{T}})\bar{\mu} = 0, \tag{4.74}$$

$$(\bar{\mathbf{v}}.\bar{\nabla})\bar{\nu} + \delta^{1-q_1}\epsilon^{2-q}\bar{\nu} + \kappa\mathrm{tr}(\bar{\mathrm{T}})\left(\bar{\nu} - \delta^{2q_1-2-\chi_1}\epsilon^{2q-2-\chi}|\bar{\mathbf{v}}|^2\right) = \delta^{q_1-1-\chi_1}\epsilon^{q-\chi}|\bar{\mathbf{v}}|^2, \tag{4.75}$$

where

$$\mathrm{tr}(\bar{\mathrm{T}}) = \left(\delta^{\chi_1-3q_1+1}\epsilon^{\chi-3q+4}\bar{\lambda}|\bar{\mathbf{v}}|^2 - 2\delta^{1-q_1}\epsilon^{2-q} + \delta^{\chi_1-3q_1+3}\epsilon^{\chi-3q+4}\frac{\bar{\nu}}{|\bar{\mathbf{v}}|^2}\right), \tag{4.76}$$

and

$$\bar{\nabla}\cdot\bar{\mathbf{w}} = \frac{\partial}{\partial \bar{Y}}\left(\frac{\bar{u}}{\bar{u}^2+\delta^2\bar{v}^2}\right) - \delta^2\frac{\partial}{\partial \bar{X}}\left(\frac{\bar{v}}{\bar{u}^2+\delta^2\bar{v}^2}\right).$$

We obtain fullest balance when

$$\delta^{p_1+2q_1-\chi_1} = 1, \quad \delta^{1-q_1}\epsilon^{2-q} = 1, \quad \delta^{q_1-1-\chi_1}\epsilon^{q-\chi} = 1, \quad \kappa\delta^{\chi_1-3q_1+1}\epsilon^{\chi-3q+4} = 1 \tag{4.77}$$

which give

$$p_1 = \chi_1 - 2q_1, \qquad \kappa = \delta^2, \qquad \delta = \epsilon^{\frac{q-2}{1-q_1}}, \qquad (2-\chi)(1-q_1) + (2-q)\chi_1 = 0. \tag{4.78}$$

Using the known values of $\chi = 2q + 2\alpha - 4$ and $\delta = \epsilon^{1-\alpha}$ from the Cartesian analysis we can thus find

$$\kappa = \epsilon^{2(1-\alpha)}, \qquad q_1 = \frac{3-\alpha-q}{1-\alpha}, \qquad \chi_1 = \frac{2(3-\alpha-q)}{1-\alpha}, \qquad p_1 = 0, \tag{4.79}$$

thus at leading order

$$0 = -\frac{d\bar{p}}{d\bar{X}} + (\bar{\mathbf{v}}.\bar{\nabla})(\bar{\lambda}\bar{u}) + \frac{\partial\bar{\mu}}{\partial\bar{Y}}, \tag{4.80}$$

$$(\bar{\mathbf{v}}.\bar{\nabla})\bar{\lambda} + \bar{\lambda} - \frac{2\bar{\mu}}{\bar{u}^2}\frac{\partial\bar{u}}{\partial\bar{Y}} + \bar{\lambda}^2\bar{u}^2 = 0, \tag{4.81}$$

$$(\bar{\mathbf{v}}.\bar{\nabla})\bar{\mu} + \bar{\mu} - \frac{\bar{\nu}}{\bar{u}^2}\frac{\partial\bar{u}}{\partial\bar{Y}} + \bar{\lambda}\bar{\mu}\bar{u}^2 = 0, \tag{4.82}$$

$$(\bar{\mathbf{v}}.\bar{\nabla})\bar{\nu} + \bar{\nu} + \bar{\lambda}\bar{u}^2\left(\bar{\nu} - \bar{u}^2\right) = \bar{u}^2. \tag{4.83}$$

To make any further progress, a solution to the core solution (4.69) would need to be found, to then be able to write matching conditions. Otherwise we can merely say that

$$\begin{aligned} \text{as } Y^* \to 0, \qquad & \Psi^* \sim a_0(X^*, Y^*), \quad p^* \sim b_0(X^*), \quad \lambda^* \sim b_1(X^*, Y^*), \\ & \mu^* \sim b_2(X^*, Y^*), \quad \nu^* \sim b_3(X^*, Y^*), \end{aligned} \tag{4.84}$$

where

$$\begin{aligned} \text{as } X^* \to \infty \qquad & a_0(X^*, Y^*) \sim \hat{C}_0\hat{X}^{*n_1(\alpha-1)}\hat{Y}^{*n_1}, \quad b_0 \sim \hat{p}_0\hat{X}^{*2\alpha-2}, \\ & b_1(X^*, Y^*) \sim \frac{2\hat{p}_0}{n_1^2\hat{C}_0^2}\hat{X}^{*2(n_1-1)(1-\alpha)}\hat{Y}^{*2(1-n_1)}, \\ & b_2(X^*, Y^*) \sim \hat{d}_2\hat{X}^{*(2-n_1)(\alpha-1)}\hat{Y}^{*2-n_1}, \\ & b_3(X^*, Y^*) \sim \hat{d}_3\hat{X}^{*2(\alpha-1)}\hat{Y}^{*2}, \end{aligned} \tag{4.85}$$

with $n_1 = 3 - \alpha$, and

$$\begin{aligned} \text{as } X^* \to 0 \qquad & a_0(X^*, Y^*) \sim \tilde{C}_0\tilde{X}^{*n_3(\alpha-1)}\tilde{Y}^{*n_3}, \quad b_0 \sim \tilde{p}_0\tilde{X}^{*2\alpha-2}, \\ & b_1(X^*, Y^*) \sim \frac{2\tilde{p}_0}{n_3^2\tilde{C}_0^2}\tilde{X}^{*2(n_3-1)(1-\alpha)}\tilde{Y}^{*2(1-n_3)}, \\ & b_2(X^*, Y^*) \sim \tilde{d}_2\tilde{X}^{*(\alpha-1)^2}\tilde{Y}^{*\alpha-1}, \\ & b_3(X^*, Y^*) \sim \tilde{d}_3\tilde{X}^{*2(2\alpha-1)(\alpha-1)}\tilde{Y}^{*2(2\alpha-1)}, \end{aligned} \tag{4.86}$$

with $n_3 = 1 + \alpha$ (holding when $2/3 < \alpha < 1$) to match to the UCM and PTT $\kappa = O(1)$ situations.

4.1.5 Summary

Nine asymptotic regions local to the re-entrant corner, have been identified for the planar flow of a Phan-Thien-Tanner fluid in the limit of small model parameter κ. These regions are summarised in figure 4-1 and hold for the case of no solvent viscosity. The

scalings and matching between the various regions have been explained, where the key radial length scale on which the fullest balance in the boundary layer equations occurs when $r = O\left(\kappa^{\frac{1}{2(1-\alpha)}}\right)$. This distance gives the regions at the heart of the structure, the solutions in which need to be determined numerically since analytical progress from the original PDEs appears limited, unlike in the UCM and PTT $\kappa = O(1)$ regions. The Weissenberg number has been taken as unity and we expect such a structure to hold for Weissenberg order 1.

4.2 The Newtonian limit of the PTT equations, $\kappa = O(1)$, $\mathrm{We} \to 0$

We consider here the analysis of the Newtonian limit, $\mathrm{We} \to 0$, of the PTT model equations with the parameter $\kappa = O(1)$. The analysis of the small Weissenberg number limit follows a similar approach to the previous section, 4.1, where the small κ limit was investigated. The analysis will differ in structure slightly from the UCM small Weissenberg number limit of [Eva06], although the results will be clear for comparison between the UCM and PTT models, indeed showing a high degree of similarity.

To begin, we naively set $\mathrm{We} = 0$ in the governing equations (1.32)–(1.34). This then gives the balance $\mathbf{T} \sim 2\mathbf{D}$ from the constitutive equation, which along with the unchanged momentum and continuity equations form the Newtonian governing equations. The Newtonian solution is explained in detail in the following chapter, in section 5.1, and as such the analysis of this section will refer to there where relevant.

The Newtonian solution behaviour will be expected to persist until the point at which the small parameter We interacts with the length scale away from the corner in a similar way to the small κ limit. This interaction will yield three sets of core and boundary layer regions, the exterior containing the Newtonian solution as explained, the interior closest to the corner recapturing $\mathrm{We} = O(1)$ behaviour, and an intermediate region where a fuller balance of terms is expected.

Figure 4-2 shows the main asymptotic regions in the small Weissenberg number limit of the PTT equations (1.32)–(1.34). Included are the important results of the stream function and stress orders of magnitude, boundary layer thicknesses and leading order balances holding in each of the regions. As in previous analysis we consider complete flow around the corner, thus excluding the possibility of reverse flow regions at either upstream or downstream wall.

The intermediate regions and the main length scale, $r = O\left(\mathrm{We}^{\frac{1}{1-\lambda_0}}\right)$

To begin, we determine the length scale at which the Newtonian solution no longer persists, and the fullest balance in the constitutive equations is obtained. Considering distances from the corner of $O(\epsilon)$, with the gauge $\epsilon(\mathrm{We})$ being a small parameter whose dependency on We is to be found, then an outer region away from the walls is found via the scalings

$$r = \epsilon R^*, \quad x = \epsilon X^*, \quad y = \epsilon Y^*, \quad \psi = \epsilon^q \Psi^*, \quad \mathbf{v} = \epsilon^{q-1}\mathbf{v}^*, \quad \mathbf{T} = \epsilon^w \mathbf{T}^*, \quad p = \epsilon^w p^*, \tag{4.87}$$

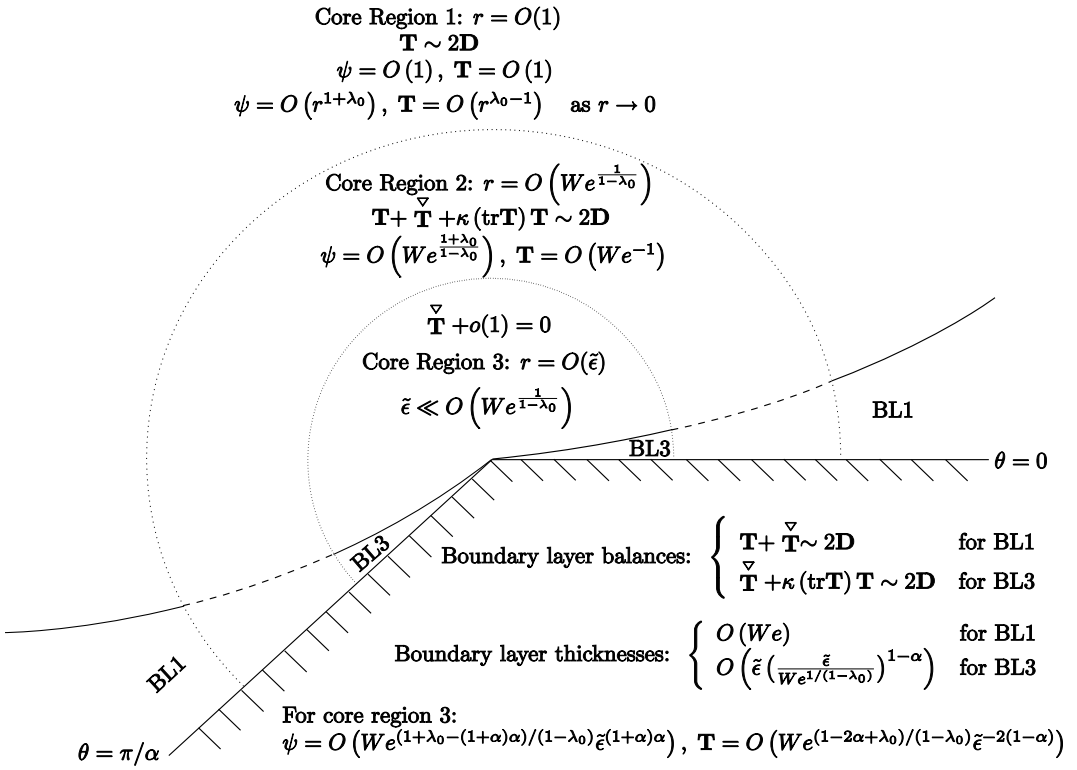

Figure 4-2: Schematic illustration of the main asymptotic regions local to the re-entrant corner in the limit We $\to$ 0. The dominant balances are shown in all three core regions and the two boundary layer regions upstream (and repeated in the downstream boundary layers as the structure is assumed to be symmetric). Core region 2 applies uniformly up to the walls and thus there is no need to consider an intermediate boundary layer in region 2. The core and boundary layer regions 3 are in fact artificial as they depend upon the artificial parameter $\hat{\epsilon}$, with the only restriction $\hat{\epsilon} \ll We^{1/(1-\lambda_0)}$.

where the velocity and stress scalings are left arbitrary through the unknown exponents q and w to be found, and this intermediate core region holds for $R^* = O(1)$. The pressure scaling is determined to be equal to the stress scaling to achieve balance in the momentum equations. The constitutive equations (from (1.34)) in this region are thus

$$\frac{\epsilon^{2-q}}{\mathrm{We}}\mathbf{T}^* + \overset{\triangledown}{\mathbf{T}}^* + \epsilon^{w+2-q}\kappa(\mathrm{tr}\mathbf{T}^*)\mathbf{T}^* = 2\frac{1}{\epsilon^w \mathrm{We}}\mathbf{D}^*. \tag{4.88}$$

The three critical length scales are now apparent:

- $r = O\left(\mathrm{We}^{1/(2-q)}\right)$: The fullest balance is able to retain all terms, and determines $w = q - 2$ and $\mathrm{We} = \epsilon^{2-q}$.
- $r \gg O\left(\mathrm{We}^{1/(2-q)}\right)$: Here the linear stress terms dominate over the upper con-

vected derivative, and the Newtonian balance is recovered. This region holds up to $r = O(1)$.

- $r \ll O\left(\mathrm{We}^{1/(2-q)}\right)$: The upper convected stress derivative now dominates over the linear stress terms, and the $\mathrm{We} = O(1)$ PTT balance is recovered.

In this intermediate region then, $r = O\left(\mathrm{We}^{1/(2-q)}\right)$, $w = q-2$ and $\mathrm{We} = \epsilon^{2-q}$, implying that $\epsilon = \mathrm{We}^{1/(2-q)}$. The constitutive and momentum equations are thus

$$\mathbf{T}^* + \overset{\triangledown}{\mathbf{T}}^* + \kappa(\mathrm{tr}\mathbf{T}^*)\mathbf{T}^* = 2\mathbf{D}^*, \qquad \epsilon^q \mathrm{Re}\ (\mathbf{v}^*.\nabla^*)\mathbf{v}^* = -\nabla^* p^* + \nabla^*.\mathbf{T}^*, \tag{4.89}$$

implying that $q > 0$, or equivalently $\epsilon^2 \mathrm{We}^{-1} \ll 1$ for the inertia terms to be negligible. To match the Newtonian stream function behaviour of the exterior regions we require $q = 1 + \lambda_0$ (see equation (5.2)), and this determines the key radial length scale

$$\epsilon = \mathrm{We}^{\frac{1}{1-\lambda_0}}. \tag{4.90}$$

Although explicit solutions to the leading order equations cannot be obtained, to match into the interior core region, where we expect the PTT $\mathrm{We} = O(1)$ problem to be recovered we note that

$$\text{as } R^* \to 0, \qquad \Psi^* \sim \tilde{c}_0 R^{*n\alpha} \sin^n(\alpha\theta), \quad \mathbf{T}^* \sim g(\Psi^*)\mathbf{v}^*\mathbf{v}^{*T} \tag{4.91}$$

where $g(\Psi^*) = \tilde{c}_1 \Psi^{*(2/n)(1-n)}$, $\tilde{c}_0$, $\tilde{c}_1$ are arbitrary constants, and n is an as yet unknown exponent, but which will be found to be $n = 1+\alpha$ when we consider these inner regions.

The scalings for this intermediate region were for the core, away from the walls. Given that all terms in the constitutive equations have been retained, there is no need for a boundary layer. To confirm the viscometric behaviour as $y \to 0$ however, we create an artificial boundary layer via the scalings

$$\begin{gathered} X^* = \bar{X}, \quad Y^* = \delta^* \bar{Y}, \quad \Psi^* = \delta^{*2}\bar{\Psi}, \quad p^* = \bar{p} \\ T^*_{11} = \bar{T}_{11}, \quad T^*_{12} = \bar{T}_{12}, \quad T^*_{22} = \delta^* \bar{T}_{22}, \end{gathered} \tag{4.92}$$

where δ^* is an artificial small gauge. At leading order the constitutive equations are then

$$\bar{T}_{11} + \kappa \bar{T}_{11}^2 = 2\frac{\partial^2 \bar{\Psi}}{\partial \bar{Y}^2}\bar{T}_{12}, \quad \bar{T}_{12} + \kappa \bar{T}_{11}\bar{T}_{12} = \frac{\partial^2 \bar{\Psi}}{\partial \bar{Y}^2}, \quad \bar{T}_{22} + \kappa \bar{T}_{11}\bar{T}_{22} = -2\frac{\partial^2 \bar{\Psi}}{\partial \bar{X}\partial \bar{Y}}. \tag{4.93}$$

Comparing this to the viscometric behaviour given in table 2.2 we can see that all the necessary terms are retained. Also, we can confirm the size of T_{12}. Here $T_{12} = O(\epsilon^{q-2}) = O(\mathrm{We}^{-1})$, which again is as expected in section 2.3.1, table 2.2.

The exterior regions, $r \gg \mathrm{We}^{\frac{1}{1-\lambda_0}}$

Discussed in the introduction of the problem, the exterior regions at leading order recover the Newtonian governing equations. This holds even for the radial distance $r = O(1)$. As we are interested in the behaviour near the corner, we consider the behaviour as $r \to 0$, but still with $r \gg \mathrm{We}^{\frac{1}{1-\lambda_0}}$. The leading order momentum and constitutive equations are given in equation (5.1), and the solution of these equations is explained in detail throughout section 5.1 with the important results

$$\text{as } r \to 0, \qquad \psi \sim c_0 r^{1+\lambda_0} f_0(\theta), \qquad \mathbf{T} \sim 2\mathbf{D}, \tag{4.94}$$

where the exponent λ_0 satisfies equation (5.14) (the numerical solution given in figure 5-1), and the function $f_0(\theta)$ is found in (5.17). Finally, the solution for the pressure is given in equation (5.21). Critically, for re-entrant corner flow $\lambda_0 < 1$, and from these solutions we may obtain the order of magnitude estimates for the exterior core region as

$$\begin{aligned} \text{for } r = O(1): &\quad \psi = O(1), &&\mathbf{T} = O(1), \\ \text{as } r \to 0: &\quad \psi = O(r^{1+\lambda_0}), &&\mathbf{T} = O(r^{-1+\lambda_0}). \end{aligned} \tag{4.95}$$

The behaviour of the Newtonian solution variables as $\theta \to 0$ is given in (5.33) and is not consistent with PTT viscometric behaviour, thus demonstrating the need for a boundary layer. These $\theta \to 0$ behaviours determine the boundary layer scalings as

$$\begin{aligned} x = \hat{X}, \quad y = \mathrm{We}\hat{Y}, \quad \psi = \mathrm{We}^2\hat{\Psi}, \quad p = \hat{p}_0(\hat{X}) + \mathrm{We}\hat{p}, \\ T_{11} = \mathrm{We}\hat{T}_{11}, \quad T_{12} = \hat{T}_{12}, \quad T_{22} = \mathrm{We}\hat{T}_{22}, \end{aligned} \tag{4.96}$$

where the scaling for y is determined through the only possible balance of $\hat{T}_{11} = O\left(\frac{\partial^2\hat{\Psi}}{\partial\hat{Y}^2}\hat{T}_{12}\right)$ in the $\hat{T}_{11}$ equation (if the y scaling is left general, all other possible balances of terms result in a large y scaling signifying a wide, and thus unphysical,

boundary layer thickness). The momentum equations become

$$\mathrm{We}^3\mathrm{Re}\left(\frac{\partial\hat{\Psi}}{\partial\hat{Y}}\frac{\partial^2\hat{\Psi}}{\partial\hat{X}\partial\hat{Y}}-\frac{\partial\hat{\Psi}}{\partial\hat{X}}\frac{\partial^2\hat{\Psi}}{\partial\hat{Y}^2}\right)=-\mathrm{We}\frac{\partial\hat{p}_0}{\partial\hat{X}}+\mathrm{We}^2\left(-\frac{\partial\hat{p}}{\partial\hat{X}}+\frac{\partial\hat{T}_{11}}{\partial\hat{X}}\right)+\frac{\partial\hat{T}_{12}}{\partial\hat{Y}}, \tag{4.97}$$

$$\mathrm{We}^3\mathrm{Re}\left(-\frac{\partial\hat{\Psi}}{\partial\hat{Y}}\frac{\partial^2\hat{\Psi}}{\partial\hat{X}^2}+\frac{\partial\hat{\Psi}}{\partial\hat{X}}\frac{\partial^2\hat{\Psi}}{\partial\hat{X}\partial\hat{Y}}\right)=-\frac{\partial\hat{p}}{\partial\hat{Y}}+\frac{\partial\hat{T}_{12}}{\partial\hat{X}}+\frac{\partial\hat{T}_{22}}{\partial\hat{Y}}, \tag{4.98}$$

with the constitutive equations

$$\begin{aligned}\hat{T}_{11}+\mathrm{We}^2\Bigg(&\frac{\partial\hat{\Psi}}{\partial\hat{Y}}\frac{\partial\hat{T}_{11}}{\partial\hat{X}}-\frac{\partial\hat{\Psi}}{\partial\hat{X}}\frac{\partial\hat{T}_{11}}{\partial\hat{Y}}\\&-\frac{2}{\mathrm{We}^2}\frac{\partial^2\hat{\Psi}}{\partial\hat{Y}^2}\hat{T}_{12}-2\frac{\partial^2\hat{\Psi}}{\partial\hat{X}\partial\hat{Y}}\hat{T}_{11}+\kappa\left(\hat{T}_{11}+\hat{T}_{22}\right)\hat{T}_{11}\Bigg)=2\frac{\partial^2\hat{\Psi}}{\partial\hat{X}\partial\hat{Y}},\end{aligned} \tag{4.99}$$

$$\begin{aligned}\hat{T}_{22}+\mathrm{We}^2\Bigg(&\frac{\partial\hat{\Psi}}{\partial\hat{Y}}\frac{\partial\hat{T}_{22}}{\partial\hat{X}}-\frac{\partial\hat{\Psi}}{\partial\hat{X}}\frac{\partial\hat{T}_{22}}{\partial\hat{Y}}\\&+2\frac{\partial^2\hat{\Psi}}{\partial\hat{X}^2}\hat{T}_{12}+2\frac{\partial^2\hat{\Psi}}{\partial\hat{X}\partial\hat{Y}}\hat{T}_{22}+\kappa\left(\hat{T}_{11}+\hat{T}_{22}\right)\hat{T}_{22}\Bigg)=-2\frac{\partial^2\hat{\Psi}}{\partial\hat{X}\partial\hat{Y}},\end{aligned} \tag{4.100}$$

$$\begin{aligned}\hat{T}_{12}+\mathrm{We}^2\Bigg(&\frac{\partial\hat{\Psi}}{\partial\hat{Y}}\frac{\partial\hat{T}_{12}}{\partial\hat{X}}-\frac{\partial\hat{\Psi}}{\partial\hat{X}}\frac{\partial\hat{T}_{12}}{\partial\hat{Y}}\\&+\mathrm{We}^2\frac{\partial^2\hat{\Psi}}{\partial\hat{X}^2}\hat{T}_{11}-\frac{\partial^2\hat{\Psi}}{\partial\hat{Y}^2}\hat{T}_{22}+\kappa\left(\hat{T}_{11}+\hat{T}_{22}\right)\hat{T}_{12}\Bigg)=\frac{\partial^2\hat{\Psi}}{\partial\hat{Y}^2}-\mathrm{We}^2\frac{\partial^2\hat{\Psi}}{\partial\hat{X}^2}.\end{aligned} \tag{4.101}$$

At leading order in We we thus obtain

$$\hat{T}_{11}-2\frac{\partial^2\hat{\Psi}}{\partial\hat{Y}^2}\hat{T}_{12}=2\frac{\partial^2\hat{\Psi}}{\partial\hat{X}\partial\hat{Y}},\quad \hat{T}_{22}=-2\frac{\partial^2\hat{\Psi}}{\partial\hat{X}\partial\hat{Y}},\quad \hat{T}_{12}=\frac{\partial^2\hat{\Psi}}{\partial\hat{Y}^2}, \tag{4.102}$$

$$0=\frac{\partial\hat{T}_{12}}{\partial\hat{Y}},\quad 0=-\frac{\partial\hat{p}}{\partial\hat{Y}}+\frac{\partial\hat{T}_{12}}{\partial\hat{X}}+\frac{\partial\hat{T}_{22}}{\partial\hat{Y}}, \tag{4.103}$$

which have the exact solution

$$\begin{aligned}\hat{\Psi}=\frac{1}{2}c_0f_0''(0)\hat{X}^{\lambda_0-1}\hat{Y}^2,\qquad \hat{T}_{11}&=2\left((\lambda_0-1)c_0f_0''(0)\hat{X}^{\lambda_0-2}\hat{Y}+(c_0f_0''(0))^2\hat{X}^{2(\lambda_0-1)}\right),\\ \hat{T}_{12}=c_0f_0''(0)\hat{X}^{\lambda_0-1},\qquad \hat{T}_{22}&=-2(\lambda_0-1)c_0f_0''(0)\hat{X}^{\lambda_0-2}\hat{Y},\\ \hat{p}&=-(\lambda_0-1)c_0f_0''(0)\hat{X}^{\lambda_0-2}\hat{Y}+p_0\hat{X}^{\lambda_0-1},\end{aligned} \tag{4.104}$$

after matching to the small θ core behaviour (5.33), and satisfying the low shear rate PTT viscometric behaviour of (2.54) as $\hat{Y} \to 0$, where $\dot{\gamma} = c_0 f_0''(0) \bar{X}^{\lambda_0 - 1}$ to agree. The solution to these boundary layer equations is described in more detail in the salient corner flow problem of section 5.2 as the same leading order boundary layer equations are relevant.

The interior regions, $r \ll \mathrm{We}^{\frac{1}{1-\lambda_0}}$

The final regions to consider are the interior regions closest to the corner, where we expect to recover the PTT $\mathrm{We} = O(1)$ problem. We introduce the rescaled variables

$$\begin{gathered} r = \tilde{\epsilon}\tilde{R}^*, \quad x = \tilde{\epsilon}\tilde{X}^*, \quad y = \tilde{\epsilon}\tilde{Y}^*, \quad \psi = \epsilon^{q-n\alpha}\tilde{\epsilon}^{n\alpha}\tilde{\Psi}^*, \\ \mathbf{v} = \epsilon^{q-n\alpha}\tilde{\epsilon}^{n\alpha-1}\tilde{\mathbf{v}}^*, \quad \mathbf{T} = \epsilon^{q-2\alpha}\tilde{\epsilon}^{-2(1-\alpha)}\tilde{\mathbf{T}}^*, \quad p = \epsilon^{q-2\alpha}\ \tilde{\epsilon}^{-2(1-\alpha)}\tilde{p}^*, \end{gathered} \tag{4.105}$$

which have been obtained from using the limiting solution approaching this region from core region 2 given in equation (4.91) and the scalings (4.87). The small parameter $\tilde{\epsilon}$ satisfies $\tilde{\epsilon} \ll \epsilon$ and thus $\left(\frac{\tilde{\epsilon}}{\epsilon}\right) \ll 1$. The constitutive equations in this region are then

$$\left(\frac{\tilde{\epsilon}}{\epsilon}\right)^{2-n\alpha} \tilde{\mathbf{T}}^* + \overset{\triangledown}{\mathbf{T}}^* + \left(\frac{\tilde{\epsilon}}{\epsilon}\right)^{(2-n)\alpha} \kappa(\mathrm{tr}\tilde{\mathbf{T}}^*)\tilde{\mathbf{T}}^* = 2\left(\frac{\tilde{\epsilon}}{\epsilon}\right)^{2(1-\alpha)} \tilde{\mathbf{D}}^*, \tag{4.106}$$

which confirms that the upper convected stress derivative dominates, with the core balance being

$$\overset{\triangledown}{\mathbf{T}}^* + o(1) = 0. \tag{4.107}$$

The momentum equations become

$$\epsilon^q \left(\frac{\tilde{\epsilon}}{\epsilon}\right)^{2\alpha(n-1)} \mathrm{Re}\ (\tilde{\mathbf{v}}^*.\tilde{\nabla}^*)\tilde{\mathbf{v}}^* = -\tilde{\nabla}^*\tilde{p}^* + \tilde{\nabla}^*.\tilde{\mathbf{T}}^*, \tag{4.108}$$

with the inertia terms negligible provided $n > 1$.

These core region 3 equations at leading order are the same as the $\mathrm{We} = O(1)$ problem, and thus the results of section 3.2.1 hold (or indeed the results of core region 3 in the small κ analysis). Specifically, we have the matching behaviour

$$\begin{aligned} \text{as } \tilde{Y}^* \to 0, \qquad & \tilde{\Psi}^* \sim \tilde{C}_0 \tilde{X}^{*n(\alpha-1)} \tilde{Y}^{*n}, \quad \tilde{p}^* \sim \tilde{p}_0 \tilde{X}^{*2\alpha-2}, \quad \tilde{T}_{11}^* \sim 2\tilde{p}_0 \tilde{X}^{*(2\alpha-2)}, \\ & \tilde{T}_{12}^* \sim 2\tilde{p}_0(1-\alpha)\tilde{X}^{*(2\alpha-3)}\tilde{Y}^*, \quad \tilde{T}_{22}^* \sim 2\tilde{p}_0(1-\alpha)^2 \tilde{X}^{*(2\alpha-4)}\tilde{Y}^{*2}, \end{aligned} \tag{4.109}$$

which motivates the boundary layer scalings

$$\tilde{X}^* = \tilde{X}, \quad \tilde{Y}^* = \left(\frac{\tilde{\epsilon}}{\epsilon}\right)^{1-\alpha} \tilde{Y}, \quad \tilde{\Psi}^* = \left(\frac{\tilde{\epsilon}}{\epsilon}\right)^{n(1-\alpha)} \tilde{\Psi},$$
$$\tilde{p}^* = \tilde{p}, \quad \tilde{T}_{11}^* = \tilde{T}_{11}, \quad \tilde{T}_{12}^* = \left(\frac{\tilde{\epsilon}}{\epsilon}\right)^{1-\alpha} \tilde{T}_{12}, \quad \tilde{T}_{22}^* = \left(\frac{\tilde{\epsilon}}{\epsilon}\right)^{2(1-\alpha)} \tilde{T}_{22}, \tag{4.110}$$

with the governing equations becoming

$$\begin{aligned}
&\text{Re } \epsilon^q \left(\frac{\tilde{\epsilon}}{\epsilon}\right)^{2(n-1)} \left(\frac{\partial\bar{\Psi}}{\partial\bar{Y}}\frac{\partial^2\bar{\Psi}}{\partial\bar{X}\partial\bar{Y}} - \frac{\partial\bar{\Psi}}{\partial\bar{X}}\frac{\partial^2\bar{\Psi}}{\partial\bar{Y}^2}\right) = -\frac{\partial\bar{p}}{\partial\bar{X}} + \frac{\partial\bar{T}_{11}}{\partial\bar{X}} + \frac{\partial\bar{T}_{12}}{\partial\bar{Y}}, \\
&\text{Re } \epsilon^q \left(\frac{\tilde{\epsilon}}{\epsilon}\right)^{2(n-\alpha)} \left(-\frac{\partial\bar{\Psi}}{\partial\bar{Y}}\frac{\partial^2\bar{\Psi}}{\partial\bar{X}^2} + \frac{\partial\bar{\Psi}}{\partial\bar{X}}\frac{\partial^2\bar{\Psi}}{\partial\bar{X}\partial\bar{Y}}\right) \\
&\qquad\qquad = -\frac{\partial\bar{p}}{\partial\bar{Y}} + \tilde{\epsilon}^{2(1-\alpha)} \left(\frac{\partial\bar{T}_{12}}{\partial\bar{X}} + \frac{\partial\bar{T}_{22}}{\partial\bar{Y}}\right),
\end{aligned} \tag{4.111}$$

and

$$\left(\frac{\tilde{\epsilon}}{\epsilon}\right)^{3-\alpha-n} \tilde{\mathbf{T}} + \overset{\triangledown}{\tilde{\mathbf{T}}} + \left(\frac{\tilde{\epsilon}}{\epsilon}\right)^{1+\alpha-n} \kappa(\text{tr}\tilde{\mathbf{T}})\tilde{\mathbf{T}} = 2\tilde{\mathbf{D}}, \tag{4.112}$$

where

$$\begin{aligned}
(\text{tr}\tilde{\mathbf{T}}) = \tilde{T}_{11} + \left(\frac{\tilde{\epsilon}}{\epsilon}\right)^{2(1-\alpha)} \tilde{T}_{22}, \qquad \tilde{D}_{11} = 2\left(\frac{\tilde{\epsilon}}{\epsilon}\right)\frac{\partial^2\tilde{\Psi}}{\partial\tilde{X}\partial\tilde{Y}}, \\
\tilde{D}_{12} = \frac{\partial^2\tilde{\Psi}}{\partial\tilde{Y}^2} - \left(\frac{\tilde{\epsilon}}{\epsilon}\right)^{2(1-\alpha)} \frac{\partial^2\tilde{\Psi}}{\partial\tilde{X}^2}, \qquad \tilde{D}_{22} = -2\frac{\partial^2\tilde{\Psi}}{\partial\tilde{X}\partial\tilde{Y}}.
\end{aligned} \tag{4.113}$$

This confirms that $n = 1 + \alpha$, and then at leading order we obtain the PTT with $\text{We} = O(1)$ boundary layer equations

$$0 = -\frac{d\tilde{p}}{d\tilde{X}} + \frac{\partial\tilde{T}_{11}}{\partial\tilde{X}} + \frac{\partial\tilde{T}_{12}}{\partial\tilde{Y}} \tag{4.114}$$

$$\left(\frac{\partial\tilde{\Psi}}{\partial\tilde{Y}}\frac{\partial\tilde{T}_{11}}{\partial\tilde{X}} - \frac{\partial\tilde{\Psi}}{\partial\tilde{X}}\frac{\partial\tilde{T}_{11}}{\partial\tilde{Y}} - 2\frac{\partial^2\tilde{\Psi}}{\partial\tilde{Y}^2}\tilde{T}_{12} - 2\frac{\partial^2\tilde{\Psi}}{\partial\tilde{X}\partial\tilde{Y}}\tilde{T}_{11}\right) + \tilde{T}_{11}^2 = 0, \tag{4.115}$$

$$\left(\frac{\partial\tilde{\Psi}}{\partial\tilde{Y}}\frac{\partial\tilde{T}_{22}}{\partial\tilde{X}} - \frac{\partial\tilde{\Psi}}{\partial\tilde{X}}\frac{\partial\tilde{T}_{22}}{\partial\tilde{Y}} + 2\frac{\partial^2\tilde{\Psi}}{\partial\tilde{X}^2}\tilde{T}_{12} + 2\frac{\partial^2\tilde{\Psi}}{\partial\tilde{X}\partial\tilde{Y}}\tilde{T}_{22}\right) + \tilde{T}_{11}\tilde{T}_{22} = -2\frac{\partial^2\tilde{\Psi}}{\partial\tilde{X}\partial\tilde{Y}}, \tag{4.116}$$

$$\left(\frac{\partial\tilde{\Psi}}{\partial\tilde{Y}}\frac{\partial\tilde{T}_{12}}{\partial\tilde{X}} - \frac{\partial\tilde{\Psi}}{\partial\tilde{X}}\frac{\partial\tilde{T}_{12}}{\partial\tilde{Y}} + \frac{\partial^2\tilde{\Psi}}{\partial\tilde{X}^2}\tilde{T}_{11} - \frac{\partial^2\tilde{\Psi}}{\partial\tilde{Y}^2}\tilde{T}_{22}\right) + \tilde{T}_{11}\tilde{T}_{12} = \frac{\partial^2\tilde{\Psi}}{\partial\tilde{Y}^2}, \tag{4.117}$$

subject to the core 3 matching conditions

$$\text{as } \tilde{Y} \to \infty, \qquad \tilde{\Psi} \sim \tilde{C}_0 \tilde{X}^{n(\alpha-1)} \tilde{Y}^n, \quad \tilde{p} \sim \tilde{p}_0 \tilde{X}^{2\alpha-2}, \quad \tilde{T}_{11} \sim 2\tilde{p}_0 \tilde{X}^{(2\alpha-2)},$$
$$\tilde{T}_{12} \sim 2\tilde{p}_0(1-\alpha)\tilde{X}^{(2\alpha-3)}\tilde{Y}, \quad \tilde{T}_{22} \sim 2\tilde{p}_0(1-\alpha)^2\tilde{X}^{(2\alpha-4)}\tilde{Y}^2, \quad (4.118)$$

and no-slip at the wall.

We refer to chapter 3 for details of the solution for these core and boundary layer regions, where we again note that construction of a self-similar solution is currently restricted to the corner angle range $2/3 < \alpha < 1$.

Summary

A complex seven region structure has been identified local to the re-entrant corner for the planar flow of the Phan-Thien-Tanner fluid in the small Weissenberg number limit. These regions are summarised in figure 4-2 and hold for the case of no solvent viscosity.

The analysis has been performed in the Cartesian stress basis to allow the determination of the important length scales, and to identify the asymptotic structure. As has been seen in the $\kappa \to 0$ limit of the PTT equations, the analysis in the natural stress basis is likely to follow similarly, and has thus been omitted here, although would need to be performed for a complete description of the problem.

The structure has been found to be very similar to the UCM low Weissenberg case, in particular the length scales at which each region exists, boundary layer thicknesses and the stress singularity sizes all agree. Core and boundary layer regions 1, where Newtonian flow dominates, agree for both UCM and PTT fluids. The quadratic stress terms of the PTT equations play a role in core region 2, however the stream function and stresses are of the same orders of magnitude. The differences only manifest in core and boundary layer regions 3, where the We $= O(1)$ problem is recaptured for both UCM and PTT, and hence the stream function vanishes at a slower rate for PTT, as found in chapter 3.

4.3 The high Weissenberg number limit, $\kappa = O(1)$, We $\to \infty$

The high Weissenberg limiting behaviour of the PTT equations again mirrors that of the UCM analysis [Eva06] closely, however there are subtle differences in all regions. The asymptotic structure is shown in figure 4-3.

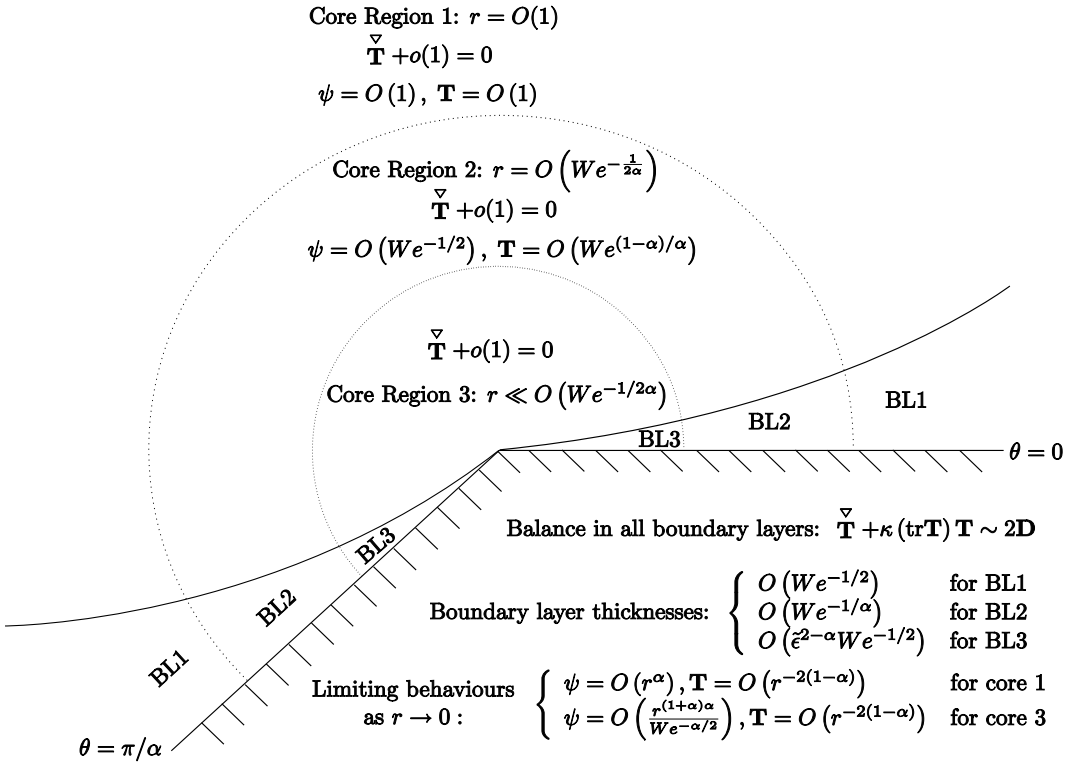

Figure 4-3: Schematic illustration of the main asymptotic regions local to the re-entrant corner in the limit We $\to \infty$. The dominant balances are shown in all three core regions and upstream boundary layers (and repeated in the downstream boundary layers as the structure is assumed to be symmetric).

The exterior: core and boundary layer 1

Away from the boundaries we expect the upper convected stress derivative terms to dominate, however we check that this is the case by letting We $\to \infty$ in the constitutive equations and observing that the balance of

$$\overset{\triangledown}{\mathbf{T}} + o(1) = 0, \tag{4.119}$$

holds as in the $\mathrm{We} = O(1)$ case. The solution to this balance is given in (3.27)–(3.28), and thus we consider the form

$$\mathbf{T} = \lambda(\psi)\mathbf{v}\mathbf{v}^T, \quad \psi = \frac{\hat{C}_0}{\alpha^{n_1}} r^{n_1\alpha} \sin^{n_1}(\alpha\theta), \quad \lambda(\psi) = \frac{2\hat{p}_0}{n_1^2 \hat{C}_0^2} \left(\frac{\psi}{\hat{C}_0}\right)^{\frac{2(1-n_1)}{n_1}}, \tag{4.120}$$

which has the limiting behaviour

$$\begin{aligned} \text{as } y \to 0, \qquad & \psi \sim \hat{C}_0 x^{n_1(\alpha-1)} y^{n_1}, && T_{11} \sim 2\hat{p}_0 x^{2\alpha-2}, \\ & T_{12} \sim 2\hat{p}_0(1-\alpha) x^{2\alpha-3} y, && T_{22} \sim 2\hat{p}_0(1-\alpha)^2 x^{2\alpha-4} y^2. \end{aligned} \tag{4.121}$$

The solution above does not capture viscometric behaviour, which may be recovered in a boundary layer using the scalings

$$\begin{aligned} x = \hat{X}, \quad y = \frac{\hat{Y}}{\mathrm{We}^{1/2}}, \quad \psi = \frac{\hat{\Psi}}{\mathrm{We}^{1/2}}, \quad & T_{11} = \hat{T}_{11}, \\ & T_{12} = \frac{\hat{T}_{12}}{\mathrm{We}^{1/2}}, \quad T_{22} = \frac{\hat{T}_{22}}{\mathrm{We}}, \quad p = \hat{p}, \end{aligned} \tag{4.122}$$

with matching to core region 1 determining $n_1 = 1$. This boundary layer is of thickness $O(\mathrm{We}^{-1/2})$, and occurs at distances $r = O(1)$ from the corner. The leading order boundary layer equations are

$$0 = -\frac{d\hat{p}}{d\hat{X}} + \frac{\partial \hat{T}_{11}}{\partial \hat{X}} + \frac{\partial \hat{T}_{12}}{\partial \hat{Y}} \tag{4.123}$$

$$\left(\frac{\partial \hat{\Psi}}{\partial \hat{Y}}\frac{\partial \hat{T}_{11}}{\partial \hat{X}} - \frac{\partial \hat{\Psi}}{\partial \hat{X}}\frac{\partial \hat{T}_{11}}{\partial \hat{Y}} - 2\frac{\partial^2 \hat{\Psi}}{\partial \hat{X}\partial \hat{Y}}\hat{T}_{11} - 2\frac{\partial^2 \hat{\Psi}}{\partial \hat{Y}^2}\hat{T}_{12}\right) + \kappa \hat{T}_{11}^2 = 0, \tag{4.124}$$

$$\left(\frac{\partial \hat{\Psi}}{\partial \hat{Y}}\frac{\partial \hat{T}_{22}}{\partial \hat{X}} - \frac{\partial \hat{\Psi}}{\partial \hat{X}}\frac{\partial \hat{T}_{22}}{\partial \hat{Y}} + 2\frac{\partial^2 \hat{\Psi}}{\partial \hat{X}\partial \hat{Y}}\hat{T}_{22} + 2\frac{\partial^2 \hat{\Psi}}{\partial \hat{X}^2}\hat{T}_{12}\right) + \kappa \hat{T}_{11}\hat{T}_{22} = -2\frac{\partial^2 \hat{\Psi}}{\partial \hat{X}\partial \hat{Y}}, \tag{4.125}$$

$$\left(\frac{\partial \hat{\Psi}}{\partial \hat{Y}}\frac{\partial \hat{T}_{12}}{\partial \hat{X}} - \frac{\partial \hat{\Psi}}{\partial \hat{X}}\frac{\partial \hat{T}_{12}}{\partial \hat{Y}} + \frac{\partial^2 \hat{\Psi}}{\partial \hat{X}^2}\hat{T}_{11} - \frac{\partial^2 \hat{\Psi}}{\partial \hat{Y}^2}\hat{T}_{22}\right) + \kappa \hat{T}_{11}\hat{T}_{12} = \frac{\partial^2 \hat{\Psi}}{\partial \hat{Y}^2}, \tag{4.126}$$

subject to the matching conditions

$$\begin{aligned} \text{as } \hat{Y} \to \infty, \qquad & \hat{\Psi} \sim \hat{C}_0 \hat{X}^{-(1-\alpha)} \hat{Y}, && \hat{T}_{11} \sim 2\hat{p}_0 \hat{X}^{(2\alpha-2)}, \\ & \hat{T}_{12} \sim 2\hat{p}_0(1-\alpha)\hat{X}^{(2\alpha-3)}\hat{Y}, && \hat{T}_{22} \sim 2\hat{p}_0(1-\alpha)^2 \hat{X}^{(2\alpha-4)}\hat{Y}^2, \end{aligned} \tag{4.127}$$

with $\hat{p} = \hat{p}_0 \hat{X}^{2(\alpha-1)}$and the usual wall conditions

$$\text{on } Y = 0, \qquad \hat{\Psi} = \frac{\partial \hat{\Psi}}{\partial \hat{Y}} = 0. \tag{4.128}$$

The intermediate layer: core and boundary layer 2

To consider a region closer to the corner than that of $r = O(1)$ in core region 1, we re-scale r so that

$$r = \epsilon R^*, \quad x = \epsilon X^*, \quad y = \epsilon Y^*, \tag{4.129}$$

where $\epsilon = \epsilon(\text{We}) \ll 1$ is to be determined. Matching to core region 1 determines

$$\psi = \epsilon^{\alpha} \Psi^*, \quad \mathbf{T} = \epsilon^{-2(1-\alpha)} \mathbf{T}^*, \quad p = \epsilon^{-2(1-\alpha)} p^*, \tag{4.130}$$

and thus the constitutive equations become

$$\epsilon^{2-\alpha} \mathbf{T}^* + \text{We} \left(\overset{\triangledown}{\mathbf{T}}{}^* + \kappa \epsilon^{\alpha} (\text{tr } \mathbf{T}^*) \mathbf{T}^* \right) = 2\epsilon^{2(1-\alpha)} \mathbf{D}^*, \tag{4.131}$$

with $\overset{\triangledown}{\mathbf{T}}{}^*$ dominating. Again, we need to recover viscometric behaviour in a boundary layer via the scalings

$$\begin{gathered} x = \epsilon \bar{X}, \quad y = \frac{\epsilon^{2-\alpha}}{\text{We}^{1/2}} \bar{Y}, \quad \psi = \frac{\epsilon^{1+\alpha}}{\text{We}^{1/2}} \bar{\Psi}, \\ T_{11} = \epsilon^{2(\alpha-1)} \bar{T}_{11}, \quad T_{12} = \frac{\epsilon^{\alpha-1}}{\text{We}^{1/2}} \bar{T}_{12}, \quad T_{22} = \frac{1}{\text{We}} \bar{T}_{22}, \quad p = \epsilon^{-2(1-\alpha)} \bar{p}, \end{gathered} \tag{4.132}$$

which give the same boundary layer equations as in boundary layer region 1 with hats replaced with bars. These are then subject to the matching conditions

$$\begin{aligned} \text{as } \bar{Y} \to \infty, \qquad & \bar{\Psi} \sim \bar{c}_0(\bar{X}) \bar{Y}^{n_2}, && \bar{T}_{11} \sim \bar{c}_{11}(\bar{X}), \\ & \bar{T}_{12} \sim \bar{c}_{12}(\bar{X}) \bar{Y}, && \bar{T}_{22} \sim \bar{c}_{22}(\bar{X}) \bar{Y}^2, \end{aligned} \tag{4.133}$$

with $n_2 = 1 + \alpha$ (determined by matching to the core and boundary layer regions 3). Considering the core to boundary layer scalings of $Y^* = \frac{\epsilon^{1-\alpha}}{\text{We}^{1/2}} \bar{Y}$ and $\Psi^* = \frac{\epsilon}{\text{We}^{1/2}} \bar{\Psi}$ then we can determine that

$$\left(\frac{\epsilon^{1-\alpha}}{\text{We}^{1/2}} \right)^{n_2} = \frac{\epsilon}{\text{We}^{1/2}}, \tag{4.134}$$

which implies $\epsilon^{2(n_2-1-n_2\alpha)} = \mathrm{We}^{n_2-1}$. With $n_2 = 1+\alpha$ we can also determine ϵ as

$$\epsilon = \mathrm{We}^{-1/2\alpha}. \tag{4.135}$$

Core and boundary layer regions 3

Finally we consider the inner regions. To consider core region 3 we introduce

$$r = \tilde{\epsilon}\tilde{R}, \quad x = \tilde{\epsilon}\tilde{X}, \quad y = \tilde{\epsilon}\tilde{Y}, \tag{4.136}$$

for some gauge $\tilde{\epsilon} \ll \epsilon$. In this core region, we once again obtain the balance (4.119). In this region we take the self similar solution

$$\psi = \tilde{\delta}_0 \frac{\tilde{C}_0}{\alpha^{n_3}} \tilde{R}^{n_3\alpha} \sin^{n_3}(\alpha\theta), \qquad \mathbf{T} = \tilde{\delta}_1 \tilde{\delta}_0^{-(2/n_3)} \tilde{\lambda}(\psi)\mathbf{v}\mathbf{v}^T, \tag{4.137}$$

where $\tilde{\lambda}(\psi) = \frac{2\tilde{p}_0}{n_3^2 \tilde{C}_0^2}\left(\frac{\psi}{\tilde{C}_0}\right)^{\frac{2(1-n_3)}{n_3}}$ and $n_3 = 1+\alpha$ as in this region we expect to recover the $\mathrm{We} = O(1)$ PTT problem. Matching these to the equivalent solution in core region 2 determines

$$\tilde{\delta}_0 = \epsilon^{(1-n_3)\alpha}\tilde{\epsilon}^{n_3\alpha} = \epsilon^{-\alpha^2}\tilde{\epsilon}^{(1+\alpha)\alpha}, \qquad \tilde{\delta}_1 = \tilde{\epsilon}^{2\alpha}. \tag{4.138}$$

Viscometric behaviour is given by boundary layer region 3, defined by the scalings

$$\begin{aligned} x = \tilde{\epsilon}\tilde{X}, \quad y = \frac{\delta}{\mathrm{We}^{1/2}}\tilde{Y}, \quad \psi = \frac{\tilde{\epsilon}^{n_3(\alpha-1)}\delta^{n_3}}{\mathrm{We}^{1/2}}\tilde{\Psi}, \\ T_{11} = \tilde{\epsilon}^{2(\alpha-1)}\tilde{T}_{11}, \quad T_{12} = \frac{\tilde{\epsilon}^{2\alpha-3}\delta}{\mathrm{We}^{1/2}}\tilde{T}_{12}, \quad T_{22} = \frac{\tilde{\epsilon}^{2\alpha-4}\delta^2}{\mathrm{We}}\tilde{T}_{22}, \quad p = \tilde{\epsilon}^{-2(1-\alpha)}\tilde{p}, \end{aligned} \tag{4.139}$$

where the fullest balance of the upper convected derivative terms with the strain terms determines $\delta = \tilde{\epsilon}^{2-\alpha}$. The leading order boundary layer equations in boundary layer region 3 are once again the same as in boundary layer region 1, but with hats replaced with tildes. These are then subject to the usual wall conditions and the matching conditions

$$\begin{aligned} \text{as } \tilde{Y} \to \infty, \qquad & \tilde{\Psi} \sim \tilde{C}_0 \tilde{X}^{-n_3(1-\alpha)}\tilde{Y}^{n_3}, && \tilde{T}_{11} \sim 2\tilde{p}_0\tilde{X}^{(2\alpha-2)}, \\ & \tilde{T}_{12} \sim 2\tilde{p}_0(1-\alpha)\tilde{X}^{(2\alpha-3)}\tilde{Y}, && \tilde{T}_{22} \sim 2\tilde{p}_0(1-\alpha)^2\tilde{X}^{(2\alpha-4)}\tilde{Y}^2, \end{aligned} \tag{4.140}$$

with $\hat{p} = \hat{p}_0\hat{X}^{2(\alpha-1)}$, where $n_3 = 1+\alpha$.

Summary

Nine asymptotic regions local to the re-entrant corner, have been identified for the planar flow of a Phan-Thien-Tanner fluid in the limit of the high Weissenberg number. These regions are summarised in figure 4-3 and hold for the case of no solvent viscosity.

The structure has been found to be very similar to the UCM high Weissenberg case, in particular the same length scales at which each region exists and the same boundary layer thicknesses are found. The only significant difference is the stream function vanishes at a slower rate as $r \to 0$ in all core regions, UCM has $\psi = O(r^{3\alpha})$, $\psi = O(\mathrm{We}^{-3/2})$ and $\psi = O(\mathrm{We}^{-\alpha/2} r^{(3-\alpha)\alpha})$ in core regions 1-3 respectively, compared to the PTT results of $\psi = O(r^{\alpha})$, $\psi = O(\mathrm{We}^{-1/2})$ and $\psi = O(\mathrm{We}^{\alpha/2} r^{(1+\alpha)\alpha})$. This, as in the $\mathrm{We} = O(1)$ problem may be attributed to the shear thinning behaviour of the PTT fluid.

4.4 Discussion

For the re-entrant corner geometry, we have considered three physically relevant limits of the PTT equations, those of small κ with $\mathrm{We} = O(1)$, and small and high We with $\kappa = O(1)$. The double limits involving both κ and We are expected to form an even more complicated structure with additional regions needing to be included. The structures of this chapter are likely to be present as part of these more complex structures however.

Whilst the natural stress formulation has not been utilised in either Weissenberg number limit, it is not expected to provide any further information. All asymptotic regions and variable behaviours have been able to be identified through the use of the simpler Cartesian formulation.

It would be of interest to see if the three structures here can be validated through full numerical simulation of the equations. Unlike for the UCM equations, full numerical work for the particular PTT equations considered here (affine and without solvent viscosity) is less prevalent. In particular, validation of the radial behaviours of the stress and stream function and also identification of the balances proposed here in the constitutive equations for the respective regions would be of interest.

Finally, it should be noted that the $\kappa = O(1)$, $\mathrm{We} = O(1)$ problem is recovered closest to the corner for all three structures found here. This implies that the same issue of finding complete flow only for $2/3 < \alpha < 1$ occurs in this region. A possibility is that this could determine the size of an upstream (or downstream) lip vortex in both small κ and small We limits as complete flow is still able to be achieved through core and boundary layer regions 1 (where UCM and Newtonian flow occurs respectively). This

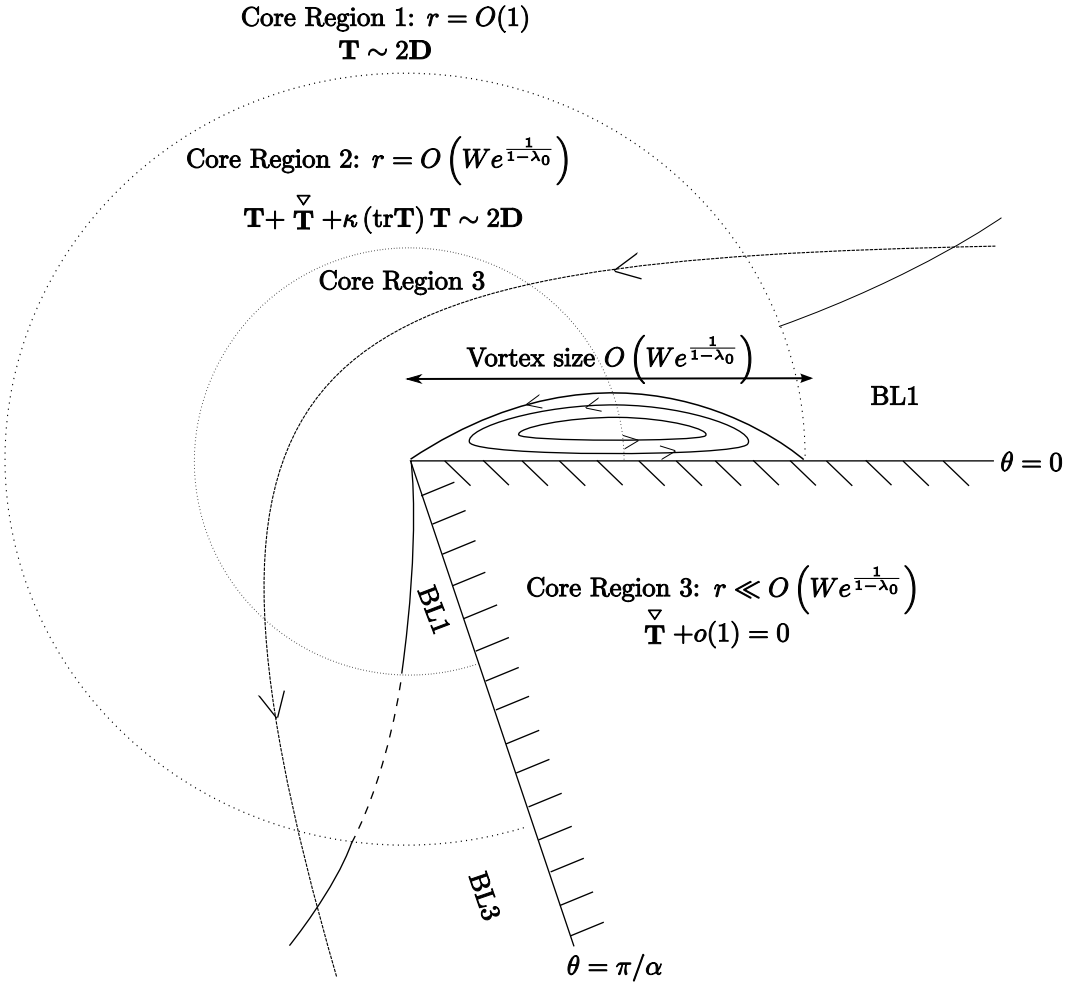

Figure 4-4: A possible flow scenario around a re-entrant corner with an upstream vortex in the limit We $\to 0$. Further analytical and numerical work to understand lip vortices is required, here we have speculated that the results of section 4.2 imply a lip vortex of size $O(\mathrm{We}^{1/1-\lambda_0})$. The situation could instead have a downstream lip vortex of the same size. Finally, similar speculation suggests a lip vortex of size $O(\kappa^{1/2(1-\alpha)})$ when We $= O(1)$ and $\kappa \to 0$.

situation is shown for the We $\to 0$ structure in figure 4-4. If this hypothesis is correct, full numerical results should be able to determine lip vortex size of $O(\kappa^{1/2(1-\alpha)})$ for small κ, and $O(\mathrm{We}^{1/1-\lambda_0})$ for small Weissenberg number flow, and would be particularly useful to motivate work on reverse flow and separating streamlines.

Chapter 5

Salient corner flow

In this chapter we will consider the salient corner flow of the PTT fluid. The salient corner analysis is given in section 5.2, preceded by a full description of corner flow (both re-entrant and salient) for the Newtonian fluid in section 5.1. The Newtonian analysis has direct application to the salient flow of PTT (and other viscoelastic) fluids so is appropriate to include this here. A discussion will then be given, including brief consideration of the high and low Weissenberg limits.

5.1 Newtonian flow

Before considering the salient corner flow it is important to understand the Newtonian solution. This is because the Newtonian solution will dominate in the core region away from the walls. As seen in previously, it is also useful in other situations such as low Weissenberg number flow.

The analysis here is based upon that of Dean and Montagnon [DM49] and Moffatt [Mof64], and will build on their work where appropriate for use in other problems of this thesis. [Mof64] contains other more complex flow scenarios around the corner including symmetrical flows and flows with eddies. Whilst we will not discuss these here, such situations could be interesting to consider for viscoelastic fluids.

The governing equations for Newtonian flow are

$$\mathrm{Re}(\mathbf{v}.\nabla)\mathbf{v} = -\nabla p + \nabla.\mathbf{T}, \qquad \nabla.\mathbf{v} = 0, \qquad \mathbf{T} = 2\mathbf{D}, \tag{5.1}$$

with the equations written in the same form as the viscoelastic fluids to allow for easy comparison. Noting that since the distance to the corner whilst small ($r \ll 1$) is not prescribed, there is no length scale and thus upon introducing the usual stream function ψ in polar coordinates, $v_r = \frac{1}{r}\frac{\partial \psi}{\partial \theta}$ and $v_\theta = -\frac{\partial \psi}{\partial r}$, we see it can be expressed in the

separable form

$$\psi = c_0 r^{1+\lambda_0} f_0(\theta), \tag{5.2}$$

where c_0 is a constant.

From the stream function behaviour we can determine the order of magnitude estimates

$$\psi = O(r^{1+\lambda_0}), \quad \mathbf{v} = O(r^{\lambda_0}), \quad \mathbf{D} = \frac{1}{2}\left(\nabla\mathbf{v} + (\nabla\mathbf{v})^T\right) = O(r^{-1+\lambda_0}),$$
$$\mathbf{T} = O(r^{-1+\lambda_0}), \quad \nabla.\mathbf{T} = O(r^{-2+\lambda_0}), \quad \nabla p = O(r^{-2+\lambda_0}), \quad (\mathbf{v}.\nabla)\mathbf{v} = O(r^{-1+2\lambda_0}), \tag{5.3}$$

and hence the inertia terms are negligible in the momentum equation when $1+\lambda_0 > 0$, which is true since we expect the stream function behaviour in (5.2) to vanish as $r \to 0$.

At leading order then, after simplification we have

$$\nabla p = \nabla.\left(\nabla\mathbf{v} + (\nabla\mathbf{v})^T\right), \tag{5.4}$$

implying that

$$\nabla p = \nabla^2\mathbf{v}, \tag{5.5}$$

seen by expanding the right hand side of (5.4) and using incompressibility, $\nabla.\mathbf{v} = 0$. This can then be reduced to the biharmonic equation

$$\nabla^4\psi = 0, \qquad \text{where} \qquad \nabla^2 = \frac{\partial^2}{\partial r^2} + \frac{1}{r}\frac{\partial}{\partial r} + \frac{1}{r^2}\frac{\partial^2}{\partial\theta^2}, \tag{5.6}$$

after introducing the stream function, differentiating the two equations by the appropriate independent variables and combining them. This is more straightforward in Cartesian components, but may be also proven in polar coordinates noting that the Laplacian operator acting on a vector in polar coordinates is

$$\nabla^2\mathbf{A} = \left(\nabla^2 A_r - \frac{A_r}{r^2} - \frac{2}{r^2}\frac{\partial A_\theta}{\partial\theta}\right)\mathbf{e}_r + \left(\nabla^2 A_\theta - \frac{A_\theta}{r^2} + \frac{2}{r^2}\frac{\partial A_r}{\partial\theta}\right)\mathbf{e}_\theta. \tag{5.7}$$

Substituting behaviour (5.2) into equation (5.6) yields the nonlinear eigenvalue problem

$$f_0'''' + 2(\lambda_0^2+1)f_0'' + (\lambda_0^2-1)^2 f_0 = 0, \tag{5.8}$$

and we also have to satisfy no-slip and no normal velocity at the walls, hence require

the boundary conditions

$$f_0(0) = f_0'(0) = f_0(\pi/\alpha) = f_0'(\pi/\alpha) = 0. \tag{5.9}$$

The simplest general solution to (5.8) is

$$\begin{aligned} f_{0s} = C_{1s}\sin\left((\lambda_0-1)\theta\right) + C_{2s}\cos\left((\lambda_0-1)\theta\right) + C_{3s}\sin\left((\lambda_0+1)\theta\right) \\ + C_{4s}\cos\left((\lambda_0+1)\theta\right), \end{aligned} \tag{5.10}$$

but can instead be written

$$\begin{aligned} f_0 =& C_1\sin\left((\lambda_0-1)\left(\theta-\frac{\pi}{2\alpha}\right)\right) + C_2\cos\left((\lambda_0-1)\left(\theta-\frac{\pi}{2\alpha}\right)\right) \\ &+ C_3\sin\left((\lambda_0+1)\left(\theta-\frac{\pi}{2\alpha}\right)\right) + C_4\cos\left((\lambda_0+1)\left(\theta-\frac{\pi}{2\alpha}\right)\right), \end{aligned} \tag{5.11}$$

allowing simple use of the fact that the solution is required to be symmetric about $\theta+\frac{\pi}{2\alpha}$, and hence $C_1 = C_3 = 0$. The boundary conditions at $f_0(0) = f_0'(0) = f_0(\pi/\alpha) = f_0'(\pi/\alpha) = 0$ imply the two equations

$$C_2\cos\left((\lambda_0-1)\left(\frac{\pi}{2\alpha}\right)\right) + C_4\cos\left((\lambda_0+1)\left(\frac{\pi}{2\alpha}\right)\right) = 0, \tag{5.12}$$

$$C_2(\lambda_0-1)\sin\left((\lambda_0-1)\left(\frac{\pi}{2\alpha}\right)\right) + C_4(\lambda_0+1)\sin\left((\lambda_0+1)\left(\frac{\pi}{2\alpha}\right)\right) = 0, \tag{5.13}$$

hence combining these and using double angle formulae leaves

$$\sin\left(\frac{\lambda_0\pi}{\alpha}\right) = -\lambda_0\sin\left(\frac{\pi}{\alpha}\right), \tag{5.14}$$

to be solved numerically to determine λ_0. Equation (5.12) can now be used to determine C_4 in terms of C_2 to find f_0 as

$$f_0 = C_2\left(\frac{\cos\left((\lambda_0-1)\left(\theta-\frac{\pi}{2\alpha}\right)\right)}{\cos\left((\lambda_0-1)\left(\frac{\pi}{2\alpha}\right)\right)} - \frac{\cos\left((\lambda_0+1)\left(\theta-\frac{\pi}{2\alpha}\right)\right)}{\cos\left((\lambda_0+1)\left(\frac{\pi}{2\alpha}\right)\right)}\right)\cos\left((\lambda_0-1)\left(\frac{\pi}{2\alpha}\right)\right), \tag{5.15}$$

and it is also possible to determine that

$$f_0''(0) = 4\lambda_0 C_2\cos\left((\lambda_0-1)\left(\frac{\pi}{2\alpha}\right)\right), \tag{5.16}$$

hence

$$f_0 = \frac{f_0''(0)}{4\lambda_0}\left(\frac{\cos\left((\lambda_0-1)\left(\theta-\frac{\pi}{2\alpha}\right)\right)}{\cos\left((\lambda_0-1)\left(\frac{\pi}{2\alpha}\right)\right)} - \frac{\cos\left((\lambda_0+1)\left(\theta-\frac{\pi}{2\alpha}\right)\right)}{\cos\left((\lambda_0+1)\left(\frac{\pi}{2\alpha}\right)\right)}\right). \tag{5.17}$$

Finally, the pressure may now be determined from (5.5). Using $\nabla = \mathbf{e}_r\frac{\partial}{\partial r} + \mathbf{e}_\theta\frac{1}{r}\frac{\partial}{\partial\theta}$, and the vector Laplacian operator from (5.7) then

$$\frac{\partial p}{\partial r} = \frac{1}{r^2}\frac{\partial^2\psi}{\partial r\partial\theta} + \frac{1}{r}\frac{\partial^3\psi}{\partial r^2\partial\theta} + \frac{1}{r^3}\frac{\partial^3\psi}{\partial\theta^3}, \tag{5.18}$$

$$\frac{\partial p}{\partial\theta} = -r\frac{\partial^3\psi}{\partial r^3} - \frac{\partial^2\psi}{\partial r^2} - \frac{1}{r}\frac{\partial^3\psi}{\partial r\partial\theta^2} + \frac{1}{r}\frac{\partial\psi}{\partial r} + \frac{2}{r^2}\frac{\partial^2\psi}{\partial\theta^2}. \tag{5.19}$$

Now using the ψ behaviour from (5.2) these become

$$\frac{\partial p}{\partial r} = c_0 r^{\lambda_0-2}\left(f_0''' + (1+\lambda_0)^2 f_0'\right), \qquad \frac{\partial p}{\partial\theta} = -c_0(\lambda_0-1)r^{\lambda_0-1}\left(f_0'' + (1+\lambda_0)^2 f_0\right). \tag{5.20}$$

Equation (5.8) can be determined from here by differentiating these equations by θ and r respectively and combining them, however we instead may determine p to be

$$p = \frac{c_0}{\lambda_0-1}r^{\lambda_0-1}\left(f_0''' + (1+\lambda_0)^2 f_0'\right) = c_0 f_0''(0) r^{\lambda_0-1}\frac{\sin\left((1-\lambda_0)\left(\theta-\frac{\pi}{2\alpha}\right)\right)}{\cos\left((1-\lambda_0)\left(\frac{\pi}{2\alpha}\right)\right)}, \tag{5.21}$$

having also used the solution for f_0 from (5.17).

In summary the solution to the Newtonian flow around a corner is defined by the form of the stream function in (5.2), where the exponent λ_0 must satisfy (5.14) and the function $f_0(\theta)$ is found in (5.17). The pressure is found above in equation (5.21), and finally the stress components are

$$\begin{aligned} T_{rr} &= 2\frac{\partial v_r}{\partial r} = 2c_0\lambda_0 r^{\lambda_0-1} f_0', \\ T_{r\theta} &= \frac{\partial v_\theta}{\partial r} + \frac{1}{r}\frac{\partial v_r}{\partial\theta} - \frac{v_\theta}{r} = c_0 r^{\lambda_0-1}\left(f_0'' + (1-\lambda_0^2)f_0\right), \\ T_{\theta\theta} &= 2\left(\frac{v_r}{r} + \frac{1}{r}\frac{\partial v_\theta}{\partial\theta}\right) = -2c_0\lambda_0 r^{\lambda_0-1} f_0', \end{aligned} \tag{5.22}$$

where these forms for the stress components can be found from writing $\mathbf{T} = 2\mathbf{D}$ in polar coordinates (see for example the appendix A4 of [Tan00]).

The transcendental equation (5.14) must be solved numerically. For re-entrant corners and large angled salient corners, i.e. corners with angles greater than about 146.3^o, (5.14) may be solved relatively simply by searching for the smallest positive

root λ_0 of the equation. For corner angles smaller than this, the root λ_0 is complex and thus requires some analysis first. We write

$$\lambda_0 = x_{\lambda 0} + i y_{\lambda 0}, \tag{5.23}$$

where both $x_{\lambda 0}$ and $y_{\lambda 0}$ are real. Substituting this into (5.14), using double angle formulae and the exponential forms of cos, sin, cosh and sinh, leads to the two equations

$$\text{Real part:} \qquad \sin\left(\frac{x_{\lambda 0}\pi}{\alpha}\right)\cosh\left(\frac{y_{\lambda 0}\pi}{\alpha}\right) = -x_{\lambda 0}\sin\left(\frac{\pi}{\alpha}\right), \tag{5.24}$$

$$\text{Imaginary part:} \qquad \cos\left(\frac{x_{\lambda 0}\pi}{\alpha}\right)\sinh\left(\frac{y_{\lambda 0}\pi}{\alpha}\right) = -y_{\lambda 0}\sin\left(\frac{\pi}{\alpha}\right). \tag{5.25}$$

The roots $x_{\lambda 0}$ and $y_{\lambda 0}$ can be found simultaneously using MATLAB's 'fminsearch' routine. Inputted are initial guesses for $x_{\lambda 0}$ and $y_{\lambda 0}$ and the routine searches for the local minimiser for the function

$$\left|\sin\left(\frac{x_{\lambda 0}\pi}{\alpha}\right)\cosh\left(\frac{y_{\lambda 0}\pi}{\alpha}\right) + x_{\lambda 0}\sin\left(\frac{\pi}{\alpha}\right)\right| + \left|\cos\left(\frac{x_{\lambda 0}\pi}{\alpha}\right)\sinh\left(\frac{y_{\lambda 0}\pi}{\alpha}\right) + y_{\lambda 0}\sin\left(\frac{\pi}{\alpha}\right)\right|. \tag{5.26}$$

Initially, we start from a small α (large corner angle) where we already know $y_{\lambda 0} = 0$, and to form a guess for $x_{\lambda 0}$ we note that $\cosh(\theta^*) > 0$ always, and $\sinh(\theta^*) > 0$ for $\theta^* > 0$. In our case we have $\theta^* = \frac{y_{\lambda 0}\pi}{\alpha}$. Mapping $y_{\lambda 0} \mapsto -y_{\lambda 0}$ leaves the equations invariant, so we may take $y_{\lambda 0} > 0$ without loss of generality, hence $\sinh\left(\frac{y_{\lambda 0}\pi}{\alpha}\right) > 0$. Finally, we must require $x_{\lambda 0} > 0$ to have the correct ψ behaviour vanishing as $r \to 0$. All of this implies that

$$\sin\left(\frac{x_{\lambda 0}\pi}{\alpha}\right) < 0 \quad \text{and} \quad \cos\left(\frac{x_{\lambda 0}\pi}{\alpha}\right) < 0, \tag{5.27}$$

(with $x_{\lambda 0} > 0$). For these to be true then

$$\alpha(1 + 2n_{\lambda 0}) < x_{\lambda 0} < \alpha\left(\frac{3}{2} + 2n_{\lambda 0}\right), \tag{5.28}$$

where $n_{\lambda 0} \in \mathbb{Z}$. The smallest positive root will lie in the interval of $n_{\lambda 0} = 0$, and hence a sensible guess for $x_{\lambda 0}$ lies in the range

$$\alpha < x_{\lambda 0} < \frac{3\alpha}{2}. \tag{5.29}$$

Figure 5-1 shows the values of λ_0 (when not complex), $x_{\lambda 0}$ and $y_{\lambda 0}$ over a range of α, showing in particular that $1/2 \leq \lambda_0 < 1$ for re-entrant corners where $1/2 \leq \alpha < 1$, and that $\Re(\lambda_0) > 1$ for salient corners where α lies in the range $(1, \infty)$. Also shown is

the value of the minimiser of (5.26) confirming that the solutions are genuine roots of (5.14).

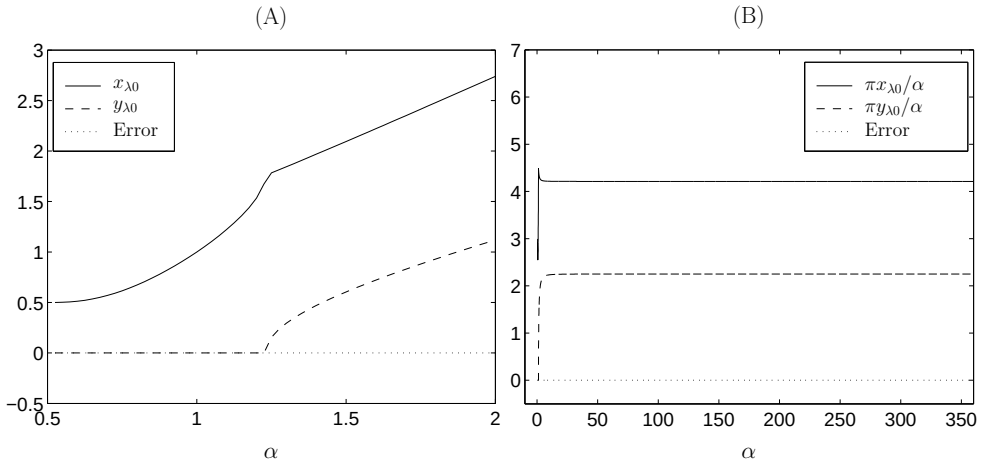

Figure 5-1: Plots of $x_{\lambda 0}$ and $y_{\lambda 0}$, the real and imaginary parts of λ_0 as defined in (5.23). (A) shows the small α behaviour, with the corner angle shown from 360^o to 90^o.(B) shows the larger α behaviour, up to $\alpha = 360$ (a corner angle of 0.5^o). Shown is that $\frac{\pi x_{\lambda 0}}{\alpha}$ and $\frac{\pi y_{\lambda 0}}{\alpha}$ both tend to constants as α increases. There is agreement with Table 1 of [Mof64], for example at $\alpha = 18$ ($\theta = 10^o$), $\frac{\pi x_{\lambda 0}}{\alpha} = 4.213$ and $\frac{\pi y_{\lambda 0}}{\alpha} = 2.245$, and at $\alpha = 2$ ($\theta = 90^o$), $\frac{\pi x_{\lambda 0}}{\alpha} = 4.303$ and $\frac{\pi y_{\lambda 0}}{\alpha} = 1.758$.

To show that there is no need for boundary layers in this Newtonian case, we consider the limit $\theta \to 0$ and verify that the wall behaviour satisfies simple shear. To find the matching behaviour of all the variables, we need the limiting behaviour of f_0, f_0', and obviously $f_0'' \to f_0''(0)$ as $\theta \to 0$.

It is possible through double angle formulae and use of the λ_0 equation (5.14) to determine

$$f_0 \sim \frac{1}{2} f_0''(0)\theta^2, \quad f_0' \sim f_0''(0)\theta, \quad \text{and} \quad p \sim p_0 r^{\lambda_0 - 1} + c_0 f_0''(0) r^{\lambda_0 - 1}(1-\lambda_0)\theta, \quad (5.30)$$

where $p_0 = -c_0 f_0''(0) \tan\left(\frac{(1-\lambda_0)\pi}{2\alpha}\right)$.

For use in later sections, this will be more convenient in Cartesian and hence we consider how to convert from the polar coordinate form. We have that $\hat{\mathbf{r}} = \cos(\theta)\mathbf{i} + \sin(\theta)\mathbf{j}$ and $\hat{\theta} = -\sin(\theta)\mathbf{i} + \cos(\theta)\mathbf{j}$, so

$$\begin{aligned} \mathbf{T} &= T_{11}\mathbf{i}\mathbf{i}^T + T_{12}\mathbf{i}\mathbf{j}^T + T_{12}\mathbf{j}\mathbf{i}^T + T_{22}\mathbf{j}\mathbf{j}^T \\ &= T_{rr}\hat{\mathbf{r}}\hat{\mathbf{r}}^T + T_{r\theta}\hat{\mathbf{r}}\hat{\theta}^T + T_{r\theta}\hat{\theta}\hat{\mathbf{r}}^T + T_{\theta\theta}\hat{\theta}\hat{\theta}^T, \end{aligned} \quad (5.31)$$

and thus the conversion is

$$\begin{aligned} T_{11} &= \cos^2\theta T_{rr} - 2\sin\theta\cos\theta T_{r\theta} + \sin^2\theta T_{\theta\theta}, \\ T_{12} &= \sin\theta\cos\theta T_{rr} + (\cos^2\theta - \sin^2\theta) T_{r\theta} - \sin\theta\cos\theta T_{\theta\theta}, \\ T_{22} &= \sin^2\theta T_{rr} + 2\sin\theta\cos\theta T_{r\theta} + \cos^2\theta T_{\theta\theta}. \end{aligned} \tag{5.32}$$

All variable limits can now be approximated in the $\theta \to 0$ limit as previously in footnote 9, and in particular in (3.62) and (3.63).

This produces the behaviours

$$\begin{aligned} \psi \sim \frac{1}{2} c_0 f_0''(0) x^{\lambda_0 - 1} y^2, \quad p \sim p_0 x^{\lambda_0 - 1} + (1-\lambda_0) c_0 f_0''(0) x^{\lambda_0 - 2} y, \\ T_{11} \sim 2(\lambda_0 - 1) c_0 f_0''(0) x^{\lambda_0 - 2} y, \quad T_{12} \sim c_0 f_0''(0) x^{\lambda_0 - 1}, \\ T_{22} \sim -2(\lambda_0 - 1) c_0 f_0''(0) x^{\lambda_0 - 2} y, \quad \text{as } y \to 0, \end{aligned} \tag{5.33}$$

confirming that steady shear flow (where we require $\psi \sim \frac{1}{2}\dot{\gamma} y^2$, $T_{11} = T_{22} = 0$, $T_{12} \sim \dot{\gamma}$) is achieved near the walls, and thus there is no need for boundary layers.

5.2 Salient corner flow of the PTT fluid, $\kappa = O(1)$, We $= O(1)$

We consider now the salient corner flow of the PTT fluid (1.32)–(1.34). The geometry to consider is shown in figure 5-2. In this geometry, it is expected that the velocity gradient

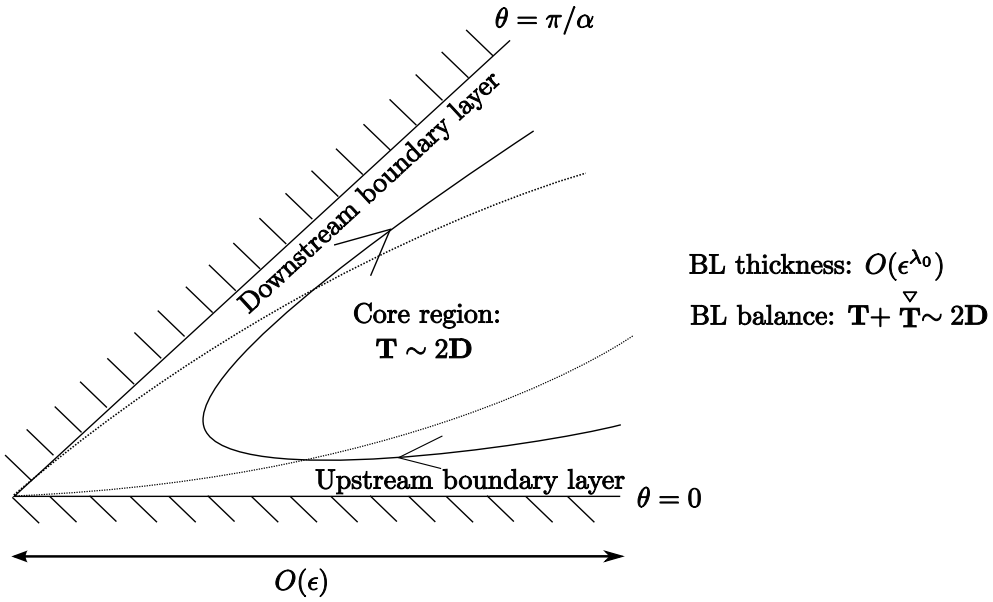

Figure 5-2: Salient corner geometry, with the main asymptotic regions and dominant balances shown. Distances to the corner are of $O(\epsilon)$, and are assumed to be small. This geometry differs from the re-entrant corner as here the corner angle depends upon α in the range $\alpha \in (1, \infty)$.

and viscous stresses are zero (for example section 4 of [Ren00a]) which correspond to the zero Weissenberg number limit, the dominant behaviour being described by the Stokes equation. As such, we assume the balance in the core flow away from the walls to satisfy

$$\mathbf{T} + o(1) = 2\mathbf{D}. \tag{5.34}$$

This means that the analysis of the previous section all applies, the only thing to note is for salient corners we have α in the range $\alpha \in (1, \infty)$, and thus the critical stream function exponent λ_0 satisfies $\Re(\lambda_0) > 1$. We note here that for corners with angles less than about 146.3^o λ_0 is complex and may give rise to eddies near the corner (as suggested by Moffatt, [Mof64]). The presence of these eddies may require a change to our asymptotic structure and thus this salient corner analysis is only guaranteed to hold for corner angles $\theta \in (146.3^o, 180^o)$.

Using the wall behaviour as $y \to 0$ from (5.33) we may see that although it satisfies the simple shear of Newtonian flow, it does not satisfy PTT viscometric behaviour, either with large shear rate (2.53) or low shear rate (2.54). Low shear rate would be expected in salient corner flow in comparison to the high shear rate of re-entrant corner flow due to the comparative motion of the fluid being trapped in the corner.

As viscometric behaviour is not satisfied, we require wall boundary layers, and can use the behaviours (5.33) to suggest the scalings

$$\begin{aligned} x = \epsilon\bar{X}, \quad y = \delta\bar{Y}, \quad \psi = \epsilon^{\lambda_0-1}\delta^2\bar{\Psi}, \quad p = \epsilon^{\lambda_0-1}\bar{p}_0(X) + \epsilon^{\lambda_0-2}\delta\bar{p}, \\ T_{11} = \epsilon^{\lambda_0-2}\delta\bar{T}_{11}, \quad T_{12} = \epsilon^{\lambda_0-1}\bar{T}_{12}, \quad T_{22} = \epsilon^{\lambda_0-2}\delta\bar{T}_{22}, \end{aligned} \tag{5.35}$$

and then the constitutive equations become

$$\begin{aligned} &\bar{T}_{11} + \left(\epsilon^{\lambda_0-2}\delta\left(\frac{\partial\bar{\Psi}}{\partial\bar{Y}}\frac{\partial\bar{T}_{11}}{\partial\bar{X}} - \frac{\partial\bar{\Psi}}{\partial\bar{X}}\frac{\partial\bar{T}_{11}}{\partial\bar{Y}} - 2\frac{\partial^2\bar{\Psi}}{\partial\bar{X}\partial\bar{Y}}\bar{T}_{11}\right) - 2\epsilon^{\lambda_0}\delta^{-1}\frac{\partial^2\bar{\Psi}}{\partial\bar{Y}^2}\bar{T}_{12}\right) \\ &\quad + \epsilon^{\lambda_0-2}\delta\kappa(\bar{T}_{11}+\bar{T}_{22})\bar{T}_{11} = 2\frac{\partial^2\bar{\Psi}}{\partial\bar{X}\partial\bar{Y}}, \end{aligned} \tag{5.36}$$

$$\begin{aligned} &\bar{T}_{22} + \epsilon^{\lambda_0-2}\delta\left(\frac{\partial\bar{\Psi}}{\partial\bar{Y}}\frac{\partial\bar{T}_{22}}{\partial\bar{X}} - \frac{\partial\bar{\Psi}}{\partial\bar{X}}\frac{\partial\bar{T}_{22}}{\partial\bar{Y}} + 2\frac{\partial^2\bar{\Psi}}{\partial\bar{X}^2}\bar{T}_{12} + 2\frac{\partial^2\bar{\Psi}}{\partial\bar{X}\partial\bar{Y}}\bar{T}_{22}\right) \\ &\quad + \epsilon^{\lambda_0-2}\delta\kappa(\bar{T}_{11}+\bar{T}_{22})\bar{T}_{22} = -2\frac{\partial^2\bar{\Psi}}{\partial\bar{X}\partial\bar{Y}}, \end{aligned} \tag{5.37}$$

$$\begin{aligned} &\bar{T}_{12} + \left(\epsilon^{\lambda_0-2}\delta\left(\frac{\partial\bar{\Psi}}{\partial\bar{Y}}\frac{\partial\bar{T}_{12}}{\partial\bar{X}} - \frac{\partial\bar{\Psi}}{\partial\bar{X}}\frac{\partial\bar{T}_{12}}{\partial\bar{Y}} - \frac{\partial^2\bar{\Psi}}{\partial\bar{Y}^2}\bar{T}_{22}\right) + \epsilon^{\lambda_0-4}\delta^3\frac{\partial^2\bar{\Psi}}{\partial\bar{X}^2}\bar{T}_{11}\right) \\ &\quad + \epsilon^{\lambda_0-2}\delta\kappa(\bar{T}_{11}+\bar{T}_{22})\bar{T}_{12} = \frac{\partial^2\bar{\Psi}}{\partial\bar{Y}^2} - \left(\frac{\delta}{\epsilon}\right)^2\frac{\partial^2\bar{\Psi}}{\partial\bar{X}^2}, \end{aligned} \tag{5.38}$$

with the momentum equations

$$\begin{aligned} &\mathrm{Re}\ \epsilon^{\lambda_0-2}\delta^3\left(\frac{\partial\bar{\Psi}}{\partial\bar{Y}}\frac{\partial^2\bar{\Psi}}{\partial\bar{X}\partial\bar{Y}} - \frac{\partial\bar{\Psi}}{\partial\bar{X}}\frac{\partial^2\bar{\Psi}}{\partial\bar{Y}^2}\right) \\ &\qquad = -\left(\left(\frac{\delta}{\epsilon}\right)\frac{\partial\bar{p}_0}{\partial\bar{X}} + \left(\frac{\delta}{\epsilon}\right)^2\frac{\partial\bar{p}}{\partial\bar{X}}\right) + \left(\frac{\delta}{\epsilon}\right)^2\frac{\partial\bar{T}_{11}}{\partial\bar{X}} + \frac{\partial\bar{T}_{12}}{\partial\bar{Y}} \end{aligned} \tag{5.39}$$

$$\mathrm{Re}\ \epsilon^{\lambda_0-2}\delta^3\left(-\frac{\partial\bar{\Psi}}{\partial\bar{Y}}\frac{\partial^2\bar{\Psi}}{\partial\bar{X}^2} + \frac{\partial\bar{\Psi}}{\partial\bar{X}}\frac{\partial^2\bar{\Psi}}{\partial\bar{X}\partial\bar{Y}}\right) = -\frac{\partial\bar{p}}{\partial\bar{Y}} + \frac{\partial\bar{T}_{12}}{\partial\bar{X}} + \frac{\partial\bar{T}_{22}}{\partial\bar{Y}}. \tag{5.40}$$

The only possible balance which allows a thin boundary layer (where $\delta \ll \epsilon$), is that of

$\delta = \epsilon^{\lambda_0}$, leaving

$$\bar{T}_{11} + \left(\epsilon^{2(\lambda_0-1)}\left(\frac{\partial\bar{\Psi}}{\partial\bar{Y}}\frac{\partial\bar{T}_{11}}{\partial\bar{X}} - \frac{\partial\bar{\Psi}}{\partial\bar{X}}\frac{\partial\bar{T}_{11}}{\partial\bar{Y}} - 2\frac{\partial^2\bar{\Psi}}{\partial\bar{X}\partial\bar{Y}}\bar{T}_{11}\right) - 2\frac{\partial^2\bar{\Psi}}{\partial\bar{Y}^2}\bar{T}_{12}\right) + \epsilon^{2(\lambda_0-1)}\kappa(\bar{T}_{11}+\bar{T}_{22})\bar{T}_{11} = 2\frac{\partial^2\bar{\Psi}}{\partial\bar{X}\partial\bar{Y}}, \tag{5.41}$$

$$\bar{T}_{22} + \epsilon^{2(\lambda_0-1)}\left(\frac{\partial\bar{\Psi}}{\partial\bar{Y}}\frac{\partial\bar{T}_{22}}{\partial\bar{X}} - \frac{\partial\bar{\Psi}}{\partial\bar{X}}\frac{\partial\bar{T}_{22}}{\partial\bar{Y}} + 2\frac{\partial^2\bar{\Psi}}{\partial\bar{X}^2}\bar{T}_{12} + 2\frac{\partial^2\bar{\Psi}}{\partial\bar{X}\partial\bar{Y}}\bar{T}_{22}\right) + \epsilon^{2(\lambda_0-1)}\kappa(\bar{T}_{11}+\bar{T}_{22})\bar{T}_{22} = -2\frac{\partial^2\bar{\Psi}}{\partial\bar{X}\partial\bar{Y}}, \tag{5.42}$$

$$\bar{T}_{12} + \left(\epsilon^{2(\lambda_0-1)}\left(\frac{\partial\bar{\Psi}}{\partial\bar{Y}}\frac{\partial\bar{T}_{12}}{\partial\bar{X}} - \frac{\partial\bar{\Psi}}{\partial\bar{X}}\frac{\partial\bar{T}_{12}}{\partial\bar{Y}} - \frac{\partial^2\bar{\Psi}}{\partial\bar{Y}^2}\bar{T}_{22}\right) + \epsilon^{4(\lambda_0-1)}\frac{\partial^2\bar{\Psi}}{\partial\bar{X}^2}\bar{T}_{11}\right) + \epsilon^{2(\lambda_0-1)}\kappa(\bar{T}_{11}+\bar{T}_{22})\bar{T}_{12} = \frac{\partial^2\bar{\Psi}}{\partial\bar{Y}^2} - \epsilon^{2(\lambda_0-1)}\frac{\partial^2\bar{\Psi}}{\partial\bar{X}^2}, \tag{5.43}$$

and

$$\text{Re }\epsilon^{2(2\lambda_0-1)}\left(\frac{\partial\bar{\Psi}}{\partial\bar{Y}}\frac{\partial^2\bar{\Psi}}{\partial\bar{X}\partial\bar{Y}} - \frac{\partial\bar{\Psi}}{\partial\bar{X}}\frac{\partial^2\bar{\Psi}}{\partial\bar{Y}^2}\right) = -\left(\epsilon^{\lambda_0-1}\frac{\partial\bar{p}_0}{\partial\bar{X}} + \epsilon^{2(\lambda_0-1)}\frac{\partial\bar{p}}{\partial\bar{X}}\right) + \epsilon^{2(\lambda_0-1)}\frac{\partial\bar{T}_{11}}{\partial\bar{X}} + \frac{\partial\bar{T}_{12}}{\partial\bar{Y}} \tag{5.44}$$

$$\text{Re }\epsilon^{2(2\lambda_0-1)}\left(-\frac{\partial\bar{\Psi}}{\partial\bar{Y}}\frac{\partial^2\bar{\Psi}}{\partial\bar{X}^2} + \frac{\partial\bar{\Psi}}{\partial\bar{X}}\frac{\partial^2\bar{\Psi}}{\partial\bar{X}\partial\bar{Y}}\right) = -\frac{\partial\bar{p}}{\partial\bar{Y}} + \frac{\partial\bar{T}_{12}}{\partial\bar{X}} + \frac{\partial\bar{T}_{22}}{\partial\bar{Y}}. \tag{5.45}$$

At leading order we thus obtain

$$\bar{T}_{11} - 2\frac{\partial^2\bar{\Psi}}{\partial\bar{Y}^2}\bar{T}_{12} = 2\frac{\partial^2\bar{\Psi}}{\partial\bar{X}\partial\bar{Y}}, \quad \bar{T}_{22} = -2\frac{\partial^2\bar{\Psi}}{\partial\bar{X}\partial\bar{Y}}, \quad \bar{T}_{12} = \frac{\partial^2\bar{\Psi}}{\partial\bar{Y}^2}, \tag{5.46}$$

$$0 = \frac{\partial\bar{T}_{12}}{\partial\bar{Y}}, \quad 0 = -\frac{\partial\bar{p}}{\partial\bar{Y}} + \frac{\partial\bar{T}_{12}}{\partial\bar{X}} + \frac{\partial\bar{T}_{22}}{\partial\bar{Y}}, \tag{5.47}$$

and as such, contains no contribution from the quadratic stress terms of the PTT equations. This indicates that the analysis would be identical to that of UCM salient corner flow.

From the leading order boundary layer equations $0 = \frac{\partial\bar{T}_{12}}{\partial\bar{Y}}$ and $\bar{T}_{12} = \frac{\partial^2\bar{\Psi}}{\partial\bar{Y}^2}$ imply that $\frac{\partial^3\bar{\Psi}}{\partial\bar{Y}^3} = 0$, and thus

$$\bar{\Psi} = \frac{1}{2}\bar{a}(\bar{X})\bar{Y}^2 + \bar{b}(\bar{X})\bar{Y} + \bar{c}(\bar{X}). \tag{5.48}$$

The no-slip and no normal velocity conditions on the wall imply that $\bar{\Psi} = \frac{\partial\bar{\Psi}}{\partial\bar{Y}} = 0$ on

$\bar{Y} = 0$, forcing $\bar{b}(\bar{X}) = \bar{c}(\bar{X}) = 0$ and leaving

$$\bar{\Psi} = \frac{1}{2}\bar{a}(\bar{X})\bar{Y}^2. \tag{5.49}$$

The other boundary layer equations may then be used to find

$$\bar{T}_{11} = 2\left(\bar{a}'(\bar{X})\bar{Y} + \bar{a}(\bar{X})^2\right), \qquad \bar{T}_{12} = \bar{a}(\bar{X}), \qquad \bar{T}_{22} = -2\bar{a}'(\bar{X})\bar{Y},$$
$$\bar{p} = -\bar{a}'(\bar{X})\bar{Y} + \bar{p}^*(\bar{X}), \tag{5.50}$$

which is an explicit solution to the boundary layer equations in terms of the arbitrary functions $\bar{a}(\bar{X})$ and $\bar{p}^*(\bar{X})$. The far-field behaviour as $\bar{Y} \to \infty$ can be obtained from (5.33) as

$$\bar{\Psi} \sim \frac{1}{2}c_0 f_0''(0)\bar{X}^{\lambda_0 - 1}\bar{Y}^2, \quad \bar{p} \sim p_0\bar{X}^{\lambda_0 - 1} + (1-\lambda_0)c_0 f_0''(0)\bar{X}^{\lambda_0 - 2}\bar{Y},$$
$$\bar{T}_{11} \sim 2(\lambda_0 - 1)c_0 f_0''(0)\bar{X}^{\lambda_0 - 2}\bar{Y}, \quad \bar{T}_{12} \sim c_0 f_0''(0)\bar{X}^{\lambda_0 - 1},$$
$$\bar{T}_{22} \sim -2(\lambda_0 - 1)c_0 f_0''(0)\bar{X}^{\lambda_0 - 2}\bar{Y}, \quad \text{as } \bar{Y} \to \infty, \tag{5.51}$$

and thus we may determine the functions $\bar{a} = c_0 f_0''(0)\bar{X}^{\lambda_0 - 1}$ and $\bar{p}^* = p_0\bar{X}^{\lambda_0 - 1}$. To summarise, the leading order boundary equations have the solution

$$\bar{\Psi} = \frac{1}{2}c_0 f_0''(0)\bar{X}^{\lambda_0 - 1}\bar{Y}^2, \qquad \bar{T}_{11} = 2\left((\lambda_0 - 1)c_0 f_0''(0)\bar{X}^{\lambda_0 - 2}\bar{Y} + (c_0 f_0''(0))^2\bar{X}^{2(\lambda_0 - 1)}\right),$$
$$\bar{T}_{12} = c_0 f_0''(0)\bar{X}^{\lambda_0 - 1}, \qquad \bar{T}_{22} = -2(\lambda_0 - 1)c_0 f_0''(0)\bar{X}^{\lambda_0 - 2}\bar{Y},$$
$$\bar{p} = -(\lambda_0 - 1)c_0 f_0''(0)\bar{X}^{\lambda_0 - 2}\bar{Y} + p_0\bar{X}^{\lambda_0 - 1}, \tag{5.52}$$

which matches to the far-field behaviour, and satisfies the low shear rate PTT viscometric behaviour of (2.54) as $\bar{Y} \to 0$, which is also UCM viscometric behaviour. To agree with (2.54), We $= 1$ as it has been scaled out of the problem, and $\dot{\gamma} = c_0 f_0''(0)\bar{X}^{\lambda_0 - 1}$.

5.3 Discussion

The salient corner flow of the PTT fluid has now been found. The flow, dominated by Newtonian behaviour, has zero velocity gradient and viscous stresses at the corner in comparison to the singular behaviour of these in re-entrant corner flow. These features allow the analysis to be far more straightforward, indeed as far as to have an analytical solution in the core and boundary layer regions. The quadratic stress terms of the PTT model are subdominant in both core and boundary layer regions and as such

the analysis of the UCM fluid will follow as above (the UCM fluid having not been considered in the literature, presumably due to its simplicity when compared to the re-entrant corner problem). This solution is only guaranteed to hold for corner angles $\theta \in (146.3^o, 180^o)$ due to the complex nature of the Newtonian eigenvalue λ_0 for smaller corner angles. Further work to understand eddy formation for UCM or PTT fluids (as in [Mof64] for Newtonian flow) is required.

We conclude by making remarks on the continuity of the salient and re-entrant corner solution behaviours and then discuss the salient corner flow in the various parameter limits as considered for the re-entrant corner.

5.3.1 Continuity between salient and re-entrant flow

It is of interest to consider the limit $\alpha \to 1$ in both the salient ($\alpha \to 1^+$) and re-entrant ($\alpha \to 1^-$) corner flows, to see if they agree. It should be mentioned that the analysis breaks down in these limits, and as such this is only a brief exploration of the continuity between the two flows.

The stream function in the core flow of the salient corner is $\psi = c_0 r^{\lambda_0+1} f_0(\theta)$ from (5.2), and f_0 is given in (5.17). In the limit $\alpha \to 1^+$, the plot in figure 5-1 shows that $\lambda_0 \to 1^+$, or indeed directly from equation (5.14) it can be calculated that $\lambda_0 = 1$ when $\alpha = 1$.

Setting $\alpha = \lambda_0 = 1$ gives

$$f_0 = \frac{f_0''(0)}{4}\left(1 - \cos^2(\theta) + \sin^2(\theta)\right) = \frac{f_0''(0)}{2}\sin^2(\theta),$$

$$\text{thus} \quad \psi \to c_0 \frac{f_0''(0)}{2} r^2 \sin^2(\theta) \quad \text{as} \quad \alpha \to 1^+. \tag{5.53}$$

Considering now the stream function for the core flow of the re-entrant corner, we have that $\psi = c_0 r^{n\alpha} \sin^n(\alpha\theta)$, where $n = 1 + \alpha$, from (3.27). Thus

$$\psi \to c_0 r^2 \sin^2(\theta) \quad \text{as} \quad \alpha \to 1^-. \tag{5.54}$$

This simple analysis would thus suggest the unknown and arbitrary constant $f_0''(0)$ be fixed as $f_0''(0) = 2$.

The stresses are not as simple to compare, and the boundary layer behaviour may not be expected to be continuous as the viscometric behaviour for the two situations is different for the PTT model (see section 2.3.1). In the limit $\alpha \to 1$ the higher order (in ϵ) terms in the boundary layer equations for both corner situations may become important at leading order, and would be of interest for future work - although the simpler case of the UCM fluid may be easier to approach initially.

5.3.2 Low Weissenberg number limit

As for the re-entrant corner, it is of interest to consider the limits of the parameter κ and the Weissenberg number. Given that the quadratic stress terms play no role in the $\mathrm{We} = O(1)$ problem, and hence the PTT and UCM models behave identically at leading order for salient corner flow, the small κ limit is irrelevant.

The limit of low Weissenberg number (with $\kappa = O(1)$) is straightforward, and is summarised in figure 5-3.

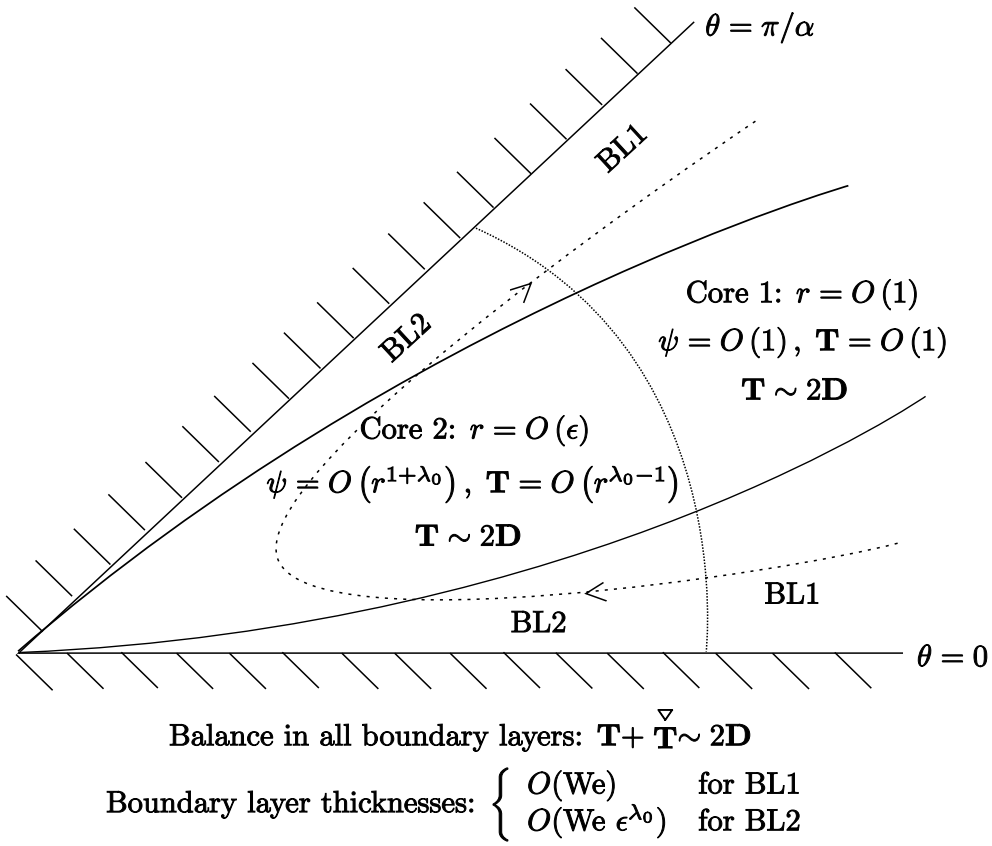

Figure 5-3: Salient corner geometry in the limit of low Weissenberg number, with the main asymptotic regions and dominant balances shown. Core and boundary layer regions 2 are artificial, the same leading order equations, stream function and stress behaviours occur in the low Weissenberg limit as for $\mathrm{We} = O(1)$, with the behaviours now extending to $r = O(1)$.

At leading order in the outer core (core region 1) the behaviour $\mathbf{T} \sim 2\mathbf{D}$ from (5.34) still applies, and so then does $\psi \sim r^{1+\lambda_0} f(\theta)$, although now these behaviours hold for

$r = O(1)$. The boundary layer scalings

$$x = \hat{X}, \quad y = \mathrm{We}\hat{Y}, \quad \psi = \mathrm{We}^2\hat{\Psi}, \quad p = \hat{p}_0(\hat{X}) + \mathrm{We}\hat{p},$$
$$T_{11} = \mathrm{We}\hat{T}_{11}, \quad T_{12} = \hat{T}_{12}, \quad T_{22} = \mathrm{We}\hat{T}_{22}, \tag{5.55}$$

recover the leading order boundary layer equations (5.46)–(5.47) with the same solution (5.52), all with bars replaced with hats. Moving closer to the corner, we use the scalings

$$r = \epsilon R^*, \quad x = \epsilon X^*, \quad y = \epsilon Y^*, \quad \psi = \epsilon^{1+\lambda_0}\Psi^*, \quad p = \epsilon^{\lambda_0 - 1}p^*, \quad \mathbf{T} = \epsilon^{\lambda_0-1}\mathbf{T}^* \tag{5.56}$$

to match to the behaviour of core region 1. The constitutive and momentum equations are thus

$$\mathbf{T}^* + \mathrm{We}\ \epsilon^{\lambda_0-1}\left(\overset{\triangledown}{\mathbf{T}}^* + \kappa(\mathrm{tr}\mathbf{T}^*)\mathbf{T}^*\right) = 2\mathbf{D}^*, \quad \mathrm{Re}\ \epsilon^{\lambda_0+1}(\mathbf{v}^*.\nabla^*)\mathbf{v}^* = -\nabla^* p^* + \nabla^*.\mathbf{T}^*, \tag{5.57}$$

and the same Newtonian balance dominates at leading order. The boundary layer scalings motivated by the Newtonian matching behaviour (5.33) are then

$$X^* = \bar{X}, \quad Y^* = \delta\bar{Y}, \quad \Psi^* = \delta^2\bar{\Psi}, \quad p^* = \bar{p}_0(X) + \delta\bar{p},$$
$$T^*_{11} = \delta\bar{T}_{11}, \quad T^*_{12} = \bar{T}_{12}, \quad T^*_{22} = \delta\bar{T}_{22}, \tag{5.58}$$

and then the constitutive equations become

$$\bar{T}_{11} + \mathrm{We}\ \epsilon^{\lambda_0-1}\left(\delta\left(\frac{\partial\bar{\Psi}}{\partial\bar{Y}}\frac{\partial\bar{T}_{11}}{\partial\bar{X}} - \frac{\partial\bar{\Psi}}{\partial\bar{X}}\frac{\partial\bar{T}_{11}}{\partial\bar{Y}} - 2\frac{\partial^2\bar{\Psi}}{\partial\bar{X}\partial\bar{Y}}\bar{T}_{11}\right) - 2\delta^{-1}\frac{\partial^2\bar{\Psi}}{\partial\bar{Y}^2}\bar{T}_{12}\right.$$
$$\left.+\delta\kappa(\bar{T}_{11} + \bar{T}_{22})\bar{T}_{11}\right) = 2\frac{\partial^2\bar{\Psi}}{\partial\bar{X}\partial\bar{Y}}, \tag{5.59}$$
$$\bar{T}_{22} + \mathrm{We}\ \epsilon^{\lambda_0-1}\delta\left(\frac{\partial\bar{\Psi}}{\partial\bar{Y}}\frac{\partial\bar{T}_{22}}{\partial\bar{X}} - \frac{\partial\bar{\Psi}}{\partial\bar{X}}\frac{\partial\bar{T}_{22}}{\partial\bar{Y}} + 2\frac{\partial^2\bar{\Psi}}{\partial\bar{X}^2}\bar{T}_{12} + 2\frac{\partial^2\bar{\Psi}}{\partial\bar{X}\partial\bar{Y}}\bar{T}_{22}\right.$$
$$\left.+\epsilon^{\lambda_0-2}\delta\kappa(\bar{T}_{11} + \bar{T}_{22})\bar{T}_{22}\right) = -2\frac{\partial^2\bar{\Psi}}{\partial\bar{X}\partial\bar{Y}}, \tag{5.60}$$
$$\bar{T}_{12} + \mathrm{We}\ \epsilon^{\lambda_0-1}\left(\delta\left(\frac{\partial\bar{\Psi}}{\partial\bar{Y}}\frac{\partial\bar{T}_{12}}{\partial\bar{X}} - \frac{\partial\bar{\Psi}}{\partial\bar{X}}\frac{\partial\bar{T}_{12}}{\partial\bar{Y}} - \frac{\partial^2\bar{\Psi}}{\partial\bar{Y}^2}\bar{T}_{22}\right) + \delta^3\frac{\partial^2\bar{\Psi}}{\partial\bar{X}^2}\bar{T}_{11}\right.$$
$$\left.+\epsilon^{\lambda_0-2}\delta\kappa(\bar{T}_{11} + \bar{T}_{22})\bar{T}_{12}\right) = \frac{\partial^2\bar{\Psi}}{\partial\bar{Y}^2} - \delta^2\frac{\partial^2\bar{\Psi}}{\partial\bar{X}^2}, \tag{5.61}$$

determining $\delta = \mathrm{We}\,\epsilon^{\lambda_0 - 1}$. The momentum equations are then

$$\mathrm{Re}\,\epsilon^{2(2\lambda_0-1)}\mathrm{We}^3\left(\frac{\partial\bar{\Psi}}{\partial\bar{Y}}\frac{\partial^2\bar{\Psi}}{\partial\bar{X}\partial\bar{Y}} - \frac{\partial\bar{\Psi}}{\partial\bar{X}}\frac{\partial^2\bar{\Psi}}{\partial\bar{Y}^2}\right)$$
$$= -\left(\mathrm{We}\,\epsilon^{\lambda_0-1}\frac{\partial\bar{p}_0}{\partial\bar{X}} + \mathrm{We}^2\epsilon^{2(\lambda_0-1)}\frac{\partial\bar{p}}{\partial\bar{X}}\right) + \mathrm{We}^2\epsilon^{2(\lambda_0-1)}\frac{\partial\bar{T}_{11}}{\partial\bar{X}} + \frac{\partial\bar{T}_{12}}{\partial\bar{Y}} \tag{5.62}$$

$$\mathrm{Re}\,\epsilon^{2(2\lambda_0-1)}\mathrm{We}^3\left(-\frac{\partial\bar{\Psi}}{\partial\bar{Y}}\frac{\partial^2\bar{\Psi}}{\partial\bar{X}^2} + \frac{\partial\bar{\Psi}}{\partial\bar{X}}\frac{\partial^2\bar{\Psi}}{\partial\bar{X}\partial\bar{Y}}\right) = -\frac{\partial\bar{p}}{\partial\bar{Y}} + \frac{\partial\bar{T}_{12}}{\partial\bar{X}} + \frac{\partial\bar{T}_{22}}{\partial\bar{Y}}. \tag{5.63}$$

Once again the leading order boundary layer equations are (5.46)–(5.47) with the same solution (5.52). This determines that core and boundary layer regions 2 are artificial, having the same behaviour as core and boundary layer regions 1, but on length scales near to the corner. This can be instead thought of as the low Weissenberg number limit of the salient corner flow being the same as the flow with $\mathrm{We} = O(1)$ but with the behaviour extending to radial distances of $r = O(1)$, rather than being restricted to regions near to the corner.

Other parameter limits

The other possible parameter limits of $\mathrm{We} \to \infty$ with $\kappa = O(1)$ and $(\mathrm{We}, \kappa) \to (\infty, 0)$ are left as open problems. The salient corner flow with $\mathrm{We} \to \infty$ and $\kappa = O(1)$ is likely to have a very similar structure to the low Weissenberg re-entrant corner flow (with $\kappa = O(1)$) but with the dominant behaviours reversed - it would be expected that the behaviours are PTT $\mathrm{We} = O(1)$, an intermediate region and then Newtonian behaviour closest to the corner.

Chapter 6

Discussion

The asymptotic structure local to both re-entrant and salient corners has been described for a class of self-similar solutions of the PTT equations in applicable parameter regimes. Discussions of the results of each problem are given at the end of the relevant chapters. Here we discuss the achievements and limitations of the work presented, along with future work to be pursued.

Prior to the work of this thesis the re-entrant corner problem was well understood for the UCM fluid, with the salient corner assumed trivial due to the Newtonian flow field dominating. Analysis using the more complex PTT model was limited, with only the work of Renardy [Ren97b] and an incorrect Newtonian flow assumption available.

Whilst the main parameter limits (for both salient and re-entrant corners) have been investigated, some are left as open problems. The regions in the parameter limits of chapter 4 and the end of chapter 5 will likely form part of a larger and more complex structure in the multiple limits of both the PTT model parameter κ and the Weissenberg number. The particular limit of $(\kappa, \mathrm{We}) \to (0, \infty)$ is of interest for all geometries of the PTT fluid as many fluids of interest have $\kappa = o(1)$ as described in the introduction (in section 1.2). Numerical schemes have trouble converging with increasing Weissenberg number (although cope more easily with low Weissenberg number due to the Newtonian flow behaviour which dominates), and as such this limit is of use to aid in the understanding of this high Weissenberg number problem. It is noteworthy that the best source of numerical results for the flow of the PTT fluid, in [AOP03], actually apply to the PTT model with solvent viscosity considered in appendix A here. Their results, in particular Fig. 12 of [AOP03], confirm the behaviours found in (A.23) for the PTT model with solvent viscosity. It would therefore be of particular interest to see similar results using the PTT model considered here.

This thesis has improved the understanding of the PTT corner problem and un-

covered some interesting features of the model. Whilst all of the work presented has assumed complete flow around the corner (both re-entrant and salient), the analysis has indicated that this class of solutions may only hold for corner angles $(180^o, 270^o)$. Suggestions have been made in figures 3-11 and 4-4 that reverse flow situations arise to allow the analysis to hold for any corner angle. It would be of great interest to see if these hypotheses can be investigated in full numerical simulations. There has been some work by Evans in [Eva05a] and comment in the paper by Rallison and Hinch [RH04] about the problem of reverse flow (for the UCM and Oldroyd-B fluids). A suggestion common to both is the possibility of a wide region of recirculation (i.e. not restricted to a thin boundary layer), with results of chapter 3 applicable in the rest of the flow. In this case, the limit of zero shear rate ($a \to 0$) may be relevant, being applicable on the separating streamline. This limit was not fully understood here in section 3.2.3 for the PTT fluid, in comparison to the UCM case which had a well defined and understood zero shear rate case. One issue raised in section 3.2.3 was that the wall behaviour in the $a \to 0$ limit appeared relevant only to the upstream boundary layer. In this context of reverse flow this may be justified by the observation that lip vortices are found to occur at the upstream rather than the downstream wall (see the discussion on reverse flow in section 3.4). Whilst many of these suggestions are speculative it appears that the PTT model may support the physically important situations of reverse flow and lip vortices more readily than apparent with the UCM model. The problem, however, is a long way from being fully understood for the viscoelastic fluids mentioned, and is an open problem for which insight is needed.

Another extension to the work here is to consider the flows of the other viscoelastic fluids mentioned in the introduction. The Giesekus model, for example, appears to be very similar to the PTT model. The Giesekus equations in contrast do not admit boundary layer structures for the balances considered in chapter 3 and as such the re-entrant corner flow remains an open question. As more complex models such as FENE-P and Rollie-Poly become more widely used in numerical simulations the need to understand the asymptotic behaviours near singularities (to benchmark the numerical algorithms) also increases. It is clear that the need to understand simpler models is important before tackling these problems however - the analysis of the PTT equations here would not have been possible without the understanding of the UCM model first.

Finally we mention other geometries and flows of interest. Here the case of anti-symmetrical flow around a corner has been pursued, being of relevance to contraction and expansion flows. For the Newtonian fluid Moffatt has also considered symmetrical flow in [Mof64], a situation which may be of interest to analyse for the viscoelastic models discussed. There is also more detail in [Mof64] about the situation when the

stream function exponent for Newtonian flow, λ_0, becomes complex (a situation relevant to the salient corner flow of section 5.2). Moffatt relates this to a series of eddies induced near the corner. Further analysis (using the UCM model) to understand the presence of these eddies, indeed a comparison to the Newtonian flow results to ascertain any differences, would be interesting to pursue. Sink wedge flow is understood for the UCM and Oldroyd-B models (see [EH08]), however following the same process for the PTT fluid fails, detailed in appendix C. Once the flow into the wedge is understood, the problem of a wedge with a line source is then of interest. Other flows to consider are stick-slip flow and flows with separation points, although these would need to be investigated initially with the simpler UCM equations.

Appendix A

PTT model with solvent viscosity

As mentioned in the introduction (section 1.2), the PTT model can also be considered with a solvent viscosity, being formed analogously as the Oldroyd-B model from the UCM model i.e. by considering the superposition of the Newtonian solvent stresses with the PTT stresses. The (non-dimensional) governing equations of this model are

$$\nabla.\mathbf{v} = 0, \qquad \text{Re}\ (\mathbf{v}.\nabla)\mathbf{v} = -\nabla p + \nabla.\mathbf{T}, \tag{A.1}$$

$$\mathbf{T} = \mathbf{T}^s + \mathbf{T}^p, \qquad \mathbf{T}^s = 2\beta\mathbf{D}, \tag{A.2}$$

$$\mathbf{T}^p + \overset{\triangledown}{\mathbf{T}}^p + \kappa\,(\text{tr}\mathbf{T}^p)\,\mathbf{T}^p = 2(1-\beta)\mathbf{D}, \tag{A.3}$$

where the Weissenberg number has been scaled out in the usual way. To analyse which terms will dominate in the core, we set $\psi = O(r^k)$, $\mathbf{T}^p = O(r^{-p})$ and $\mathbf{T} = O(r^{-m})$ for unknown k, p, and m, with $p > 0$ due to the assumed stress singularity at the corner. The solvent stress behaviour can be determined as $\mathbf{T}^s = O(r^{k-2})$. It is also noteworthy that either $m = p$, $m = 2 - k$, or indeed $m = p = 2 - k$. The terms in the governing equation (A.3) are then

$$\mathbf{T}^p = O(r^{-p}), \quad \overset{\triangledown}{\mathbf{T}}{}^p = O(r^{k-2-p}), \quad (\text{tr}\mathbf{T}^p)\,\mathbf{T}^p = O(r^{-2p}), \quad \mathbf{D} = O(r^{k-2}), \tag{A.4}$$

showing that the two largest terms are $\overset{\triangledown}{\mathbf{T}}{}^p$ and $(\text{tr}\mathbf{T}^p)\,\mathbf{T}^p$. The expected dominant balance is that the upper convected stress derivative dominates (as in the other cases of Oldroyd-B, UCM and PTT without solvent viscosity) and hence $-p > k - 2$. This condition thus means that the solvent stress dominates the polymer stress in the core

region. In summary in the core at leading order

$$\mathbf{T}^s \gg \mathbf{T}^p \gg 1, \qquad \mathbf{T} \sim \mathbf{T}^s = 2\beta\mathbf{D}, \qquad 0 = -\nabla p + \nabla.\mathbf{T}, \qquad \overset{\triangledown}{\mathbf{T}}^p = 0, \tag{A.5}$$

the inertia terms also being negligible in the momentum equations provided $k > 0$. With the Newtonian solvent stress dominating in the core, the velocity field may be assumed to be the Newtonian solution (described in section 5.1).

Crucially with the Newtonian velocity field being present in the core, this shows that the results of Renardy's PTT re-entrant corner paper [Ren97b] should in fact provide results for the case with a solvent viscosity. The analysis of this case has been performed by Evans (in submission, [Eva09]), following similar techniques to the analysis in chapter 3. It was found that the problem was in fact simpler than the PTT without solvent viscosity problem due to the decoupling of the polymer stress and flow fields, with the integration of the stresses in the known flow field far simpler.

As [Ren97b] was the only corner analysis for the PTT fluid at the commencement of this thesis, it is worthwhile to explain its analysis, and compare the results to that of [Eva09].

The key results of [Ren97b] are of finding the boundary layer thickness and the (polymer) stress singularity. These are found through an elegant argument comparing the expected behaviour of the variables in the core and boundary layer regions, a modified version is explained below.

The PTT corner analysis of Renardy

Beginning at the wall, viscometric behaviour is expected, as given in (2.58). The stream function in Newtonian flow (see section 5.1, specifically equation (5.2) for more details) is

$$\psi = c_0 r^{\lambda_0+1} f(\theta) \sim \frac{1}{2}\dot{\gamma} y^2 \sim \frac{1}{2}\dot{\gamma}\,(r\theta)^2\,, \tag{A.6}$$

with the latter results coming from the viscometric behaviour of the stream function. Thus

$$f \sim \theta^2, \qquad \dot{\gamma} \sim r^{\lambda_0 - 1}. \tag{A.7}$$

The viscometric stresses satisfy

$$T^p_{rr} \sim \dot{\gamma}^{2/3}, \qquad T^p_{r\theta} \sim \dot{\gamma}^{1/3}, \qquad T^p_{\theta\theta} \sim \dot{\gamma}^{1/3}\theta, \tag{A.8}$$

with the dominant stress component thus being T^p_{11}.[14]

The viscometric behaviour comes from the boundary layer equations of

$$\overset{\triangledown}{\mathbf{T}}^p + \kappa \left(\mathrm{tr}\mathbf{T}^p\right) \mathbf{T}^p = 2\mathbf{D}, \tag{A.10}$$

and thus the behaviour persists until terms become of the same magnitude, before further from the walls the upper convected stress derivative dominates. The sizes of these terms for the dominant stress component are

$$\overset{\triangledown}{T^p}_{rr} \sim r^{\frac{5}{3}(\lambda_0 - 1)}\theta, \qquad \left(\mathrm{tr}\mathbf{T}^p\right) T^p_{rr} \sim r^{\frac{4}{3}(\lambda_0-1)}, \qquad 2\mathbf{D}_{rr} = 2\frac{\partial v_r}{\partial r} \sim r^{\lambda_0 - 1}\theta, \tag{A.11}$$

with the largest two terms $\overset{\triangledown}{T^p}_{rr}$ and $\left(\mathrm{tr}\mathbf{T}^p\right) T^p_{rr}$ balancing when

$$\theta \sim r^{\frac{1-\lambda_0}{3}}, \tag{A.12}$$

which is small as $\lambda_0 < 1$ for re-entrant corners (again see the analysis of section 5.1). At values of θ greater than this, the core region starts and the upper convected stress derivative dominates.

At the transition between boundary layer and core then we have

$$\theta \sim r^{\frac{1-\lambda_0}{3}}, \qquad T^p_{rr} \sim r^{\frac{2(\lambda_0-1)}{3}}, \qquad \psi \sim r^{1+\lambda_0}\theta^2, \tag{A.13}$$

allowing the determination (for later use) of

$$v_r \sim r^{\lambda_0}\theta \sim \left(\frac{\psi}{\theta}\right)^{\frac{\lambda_0}{1+\lambda_0}} \theta = \psi^{\frac{\lambda_0}{1+\lambda_0}} \theta^{\frac{1-\lambda_0}{1+\lambda_0}}. \tag{A.14}$$

Combining the above we also can find

$$\psi \sim r^{\frac{5+\lambda_0}{3}}, \qquad T^p_{rr} \sim \psi^{\frac{2(\lambda_0-1)}{5+\lambda_0}}. \tag{A.15}$$

Now, the core region begins at

$$\theta = \theta_0 = r^{\frac{1-\lambda_0}{3}} \sim \psi^{\frac{1-\lambda_0}{5+\lambda_0}}, \tag{A.16}$$

[14] These may be derived from $\hat{\mathbf{r}} = \cos(\theta)\mathbf{i} + \sin(\theta)\mathbf{j}$ and $\hat{\theta} = -\sin(\theta)\mathbf{i} + \cos(\theta)\mathbf{j}$ and the comparison of the stress tensor written in both Cartesian and polar coordinates, giving the small θ conversion of

$$T_{rr} \sim T_{11}, \qquad T_{r\theta} \sim T_{12}, \qquad T_{\theta\theta} \sim T_{22} - 2\theta T_{12}. \tag{A.9}$$

A more detailed discussion of this conversion is given in the Newtonian analysis section, equations (5.31)-(5.32).

and in the core $\mathbf{T}^p = g(\psi)\mathbf{v}\mathbf{v}^T$. From (A.14) we can find that

$$\left(\mathbf{v}\mathbf{v}^T\right)_{rr} = v_r^2 \sim \psi^{\frac{2\lambda_0}{1+\lambda_0}}\theta^{\frac{2(1-\lambda_0)}{1+\lambda_0}}. \tag{A.17}$$

From the beginning of the core region, at $\theta = \theta_0$, if we proceed along a streamline (so that ψ is constant) until $\theta = O(1)$ then the stress goes from $T_{rr}^p \sim g(\psi)\psi^{\frac{2\lambda_0}{1+\lambda_0}}\theta_0^{\frac{2(1-\lambda_0)}{1+\lambda_0}}$ to $T_{rr}^p \sim g(\psi)\psi^{\frac{2\lambda_0}{1+\lambda_0}}$, thus the stress has been magnified by an amplitude

$$\theta_0^{\frac{2(\lambda_0-1)}{1+\lambda_0}} = \psi^{\frac{-2(1-\lambda_0)^2}{(1+\lambda_0)(5+\lambda_0)}}. \tag{A.18}$$

Multiplying this by the known value of the stress at the transition from equation (A.15), we find the stress singularity of

$$T_{rr}^p \sim \psi^{\frac{4(\lambda_0-1)}{(1+\lambda_0)(5+\lambda_0)}} \sim r^{\frac{4(\lambda_0-1)}{5+\lambda_0}}, \tag{A.19}$$

since $\psi \sim r^{1+\lambda_0}$ when $\theta = O(1)$. This analysis has thus provided us the two important results that the boundary layer thickness (from (A.12)) is

$$\theta \sim r^{\frac{1-\lambda_0}{3}}, \quad \text{thus} \quad y \sim r^{\frac{4-\lambda_0}{3}}, \tag{A.20}$$

and the stress singularity in the core region (when $\theta = O(1)$) is

$$T_{11}^p \sim T_{rr}^p \sim r^{\frac{-4(1-\lambda_0)}{5+\lambda_0}}. \tag{A.21}$$

The PTT with solvent viscosity analysis

As mentioned, the full analysis of the re-entrant corner problem has been completed by Evans [Eva09], using similar methods to the work in this thesis for the PTT without solvent viscosity and Newtonian models. This analysis provides the two results of the Renardy analysis, the boundary layer thickness (in A.20) and stress singularities (in A.21) both arising from their respective boundary layer scalings. The analysis of [Eva09] finds that y scales like $\epsilon\delta$ into the boundary layer, where $\delta = \epsilon^{(1-\lambda_0)/3}$, and the polymer stresses scale with $\epsilon^{2\lambda_0+n_1(\lambda_0+1)}$ in the core region. Both δ and $n_1 = -\frac{2(\lambda_0+2)}{\lambda_0+5}$ are found after correctly balancing the terms in the boundary layer equations analogously to (3.88) here.

It is interesting to note the comparisons between the PTT with and without the solvent viscosity, and with the UCM model. We summarise the stream function, stress,

polymer stress and boundary layer thicknesses here as

$$\psi \sim \begin{cases} r^{1+\lambda_0} & \text{for PTT with } \eta_s \neq 0 \\ r^{(1+\alpha)\alpha} & \text{for PTT with } \eta_s = 0 \\ r^{(3-\alpha)\alpha} & \text{for UCM} \end{cases} \quad \mathbf{T} \sim \begin{cases} r^{-(1-\lambda_0)} & \text{for PTT with } \eta_s \neq 0 \\ r^{-2(1-\alpha)} & \text{for PTT with } \eta_s = 0 \\ r^{-2(1-\alpha)} & \text{for UCM} \end{cases}$$

$$\mathbf{T}^p \sim \begin{cases} r^{-4\frac{1-\lambda_0}{5+\lambda_0}} & \text{for PTT with } \eta_s \neq 0 \\ r^{-2(1-\alpha)} & \text{for PTT with } \eta_s = 0 \\ r^{-2(1-\alpha)} & \text{for UCM} \end{cases} \quad \theta \sim \begin{cases} r^{(1-\lambda_0)/3} & \text{for PTT with } \eta_s \neq 0 \\ r^{1-\alpha} & \text{for PTT with } \eta_s = 0 \\ r^{1-\alpha} & \text{for UCM} \end{cases} \tag{A.22}$$

and remark that for $\alpha = 2/3$, a corner angle of 270^o, these have values

$$\psi \sim \begin{cases} r^{1.54} & \text{for PTT with } \eta_s \neq 0 \\ r^{10/9} \approx r^{1.11} & \text{for PTT with } \eta_s = 0 \\ r^{14/9} \approx r^{1.56} & \text{for UCM} \end{cases} \quad \mathbf{T} \sim \begin{cases} r^{-0.456} & \text{for PTT with } \eta_s \neq 0 \\ r^{-2/3} & \text{for PTT with } \eta_s = 0 \\ r^{-2/3} & \text{for UCM} \end{cases}$$

$$\mathbf{T}^p \sim \begin{cases} r^{-0.329} & \text{for PTT with } \eta_s \neq 0 \\ r^{-2/3} & \text{for PTT with } \eta_s = 0 \\ r^{-2/3} & \text{for UCM} \end{cases} \quad \theta \sim \begin{cases} r^{0.152} & \text{for PTT with } \eta_s \neq 0 \\ r^{1/3} & \text{for PTT with } \eta_s = 0 \\ r^{1/3} & \text{for UCM} \end{cases} \tag{A.23}$$

and so we may conclude that the stream function vanishes faster for both UCM and PTT with a solvent viscosity at similar rates than PTT with $\eta_s = 0$, however the dominant stresses are more singular for UCM and PTT with $\eta_s = 0$ than for the PTT model with $\eta_s \neq 0$. Finally, we can see that the boundary layer thickness of the UCM and PTT with $\eta_s = 0$ are the same size and thinner than the PTT with a solvent viscosity boundary layer. This may explain why the PTT with solvent viscosity model has been found to be simpler to implement numerically than either PTT with $\eta_s = 0$ or the UCM model.

Appendix B

Determinant relationship

A determinant relationship is given in section 2.2, specifically in equation (2.29). If the analysis of chapter 3 proceeded first using the Cartesian stress basis, then this relationship could be used to determine the core scalings of the natural stress variables μ and ν (although only for the case $2/3 < \alpha < 1$ as we will see). Instead, these scalings have been left unknown and determined by matching to the self-similar boundary layer equations, however in this appendix we show how the determinant relationship may be used, and verify the scalings found in chapter 3.

First, we record our determinant relationship in core variables. Equation (2.29) becomes

$$\begin{aligned}(\mathbf{v}^*.\nabla^*)\det(\mathbf{T}^* + \epsilon^{2(1-\alpha)}\mathbf{I}) = \\ \left(\kappa\epsilon^{2-\alpha n}\mathrm{tr}(\mathbf{T}^*) + \epsilon^{4-\alpha(n+2)}\right)\left(\mathrm{tr}(\mathbf{T}^* + \epsilon^{2(1-\alpha)}\mathbf{I}) - 2\epsilon^{2(\alpha-1)}\det(\mathbf{T}^* + \epsilon^{2(1-\alpha)}\mathbf{I})\right),\end{aligned} \tag{B.1}$$

and hence to leading order we have

$$(\mathbf{v}^*.\nabla^*)\det(\mathbf{T}^* + \epsilon^{2(1-\alpha)}\mathbf{I}) = 0. \tag{B.2}$$

This suggests that $\det(\mathbf{T}^* + \epsilon^{2(1-\alpha)}\mathbf{I})$ is constant along streamlines, and we make the assumption that it takes the form

$$\det(\mathbf{T}^* + \epsilon^{2(1-\alpha)}\mathbf{I}) = \epsilon^{m_1}\Delta_0\left(\frac{\Psi^*}{C_0}\right)^{m_2}, \tag{B.3}$$

for some constants m_1, m_2 to be determined next.

Now, scaling our determinant relationship into the boundary layer and using the

similarity scalings gives

$$\epsilon^{2(1-\alpha)}\bar{X}^{2(\alpha-1)}\left(t_{11}(t_{22}+1)-t_{12}^2\right)=\epsilon^{m_1+m_2n(1-\alpha)}\bar{X}^{m_2(1+\alpha)}\Delta_0\left(\frac{f}{C_0}\right)^{m_2}. \tag{B.4}$$

Equating powers of $\bar{X}$ and ϵ determines m_1 and m_2 as

$$m_1=2(1-\alpha)(2-\alpha), \qquad m_2=\frac{2(\alpha-1)}{n}, \tag{B.5}$$

so in the boundary layer

$$t_{11}(t_{22}+1)-t_{12}^2=\Delta_0\left(\frac{f}{C_0}\right)^{\frac{2(\alpha-1)}{n}}. \tag{B.6}$$

We finally then have the condition

$$\det(\mathbf{T}+\mathbf{I})=\Delta_0\left(\frac{\psi}{C_0}\right)^{\frac{2(\alpha-1)}{n}}, \tag{B.7}$$

holding in the core region.

We can verify the values of θ_2 and θ_3 by using a relationship between the two bases involving the determinant. From (2.36) we had that

$$\det(\mathbf{T}+\mathbf{I})=\lambda\nu-\mu^2, \tag{B.8}$$

and with our determinant relationship (B.7) we can now verify the scalings for μ and ν. We had the scalings

$$\psi=\epsilon^{n\alpha}\Psi^*, \quad \lambda=\epsilon^{2\alpha(1-n)}\lambda^*, \quad \mu=\theta_2\mu^*, \quad \nu=\theta_3\nu^*, \tag{B.9}$$

and we can now consider the scaling for $\det(\mathbf{T}+\mathbf{I})$ into the core, which is

$$(\epsilon^{n\alpha})^{\frac{2(\alpha-1)}{n}}=\epsilon^{2\alpha(\alpha-1)}. \tag{B.10}$$

We can finally balance this with the other terms in equation (B.8) to find that

$$\theta_2=\epsilon^{\alpha(\alpha-1)}, \quad \text{and} \quad \theta_3=\epsilon^{2\alpha(\alpha+n-2)}. \tag{B.11}$$

which agrees with (3.117). This result only holds for the $2/3<\alpha<1$ region, which can be seen by instead carefully performing the scalings in the natural stress basis. The term $\kappa\lambda^{*(0)}\left|\mathbf{v}^{*(0)}\right|^4$ once again intrudes when $1/2\leq\alpha\leq 2/3$, but in the (B.8) equation.

Finally, we use the complete description of the far-field and consider our determinant relationship. Using the far-field behaviour for $f(\xi)$ in equation (B.6) we find at leading order

$$t_{11}(t_{22}+1) - t_{12}^2 \sim \Delta_0 \xi^{-2+2\alpha}, \qquad \text{as } \xi \to \infty. \tag{B.12}$$

Using our full far-field expansions, we can verify that this is satisfied for $\alpha > 2/3$, with the constant

$$\Delta_0 = \frac{C_1^2(2-\alpha)^2}{\alpha(1+\alpha)(3\alpha^2-10\alpha+6)}\left(2(2\alpha-3)C_5 + \frac{(1-2\alpha)(3\alpha^6-22\alpha^5+54\alpha^4-30\alpha^3-45\alpha^2+48\alpha-12)C_4^2}{(1+\alpha)(\alpha^2-5\alpha+2)^2}\right), \tag{B.13}$$

however in the cases $\alpha = 2/3$ and $\alpha < 2/3$, a forcing term intrudes and the leading order term of $t_{11}(t_{22}+1) - t_{12}^2$ is at $O(\log(\xi)\xi^{-2/3})$ and $O(\xi^{-\alpha})$ respectively. Thus confirms that this determinant relationship holds only for $\alpha \in (\frac{2}{3}, 1)$.

It can be verified when $2/3 < \alpha < 1$ that these satisfy

$$\tilde{\lambda}\tilde{\nu} - \tilde{\mu}^2 \sim \Delta_0 \xi^{-2+2\alpha}, \qquad \text{as } \xi \to \infty, \tag{B.14}$$

with Δ_0 as given in (B.13), showing consistency with (B.7). The forcing term in ν intrudes for the other ranges causing the breakdown of this determinant relationship analysis, and again displays that it holds only when $2/3 < \alpha < 1$.

Appendix C

Wedge sink flow using the PTT equations

We here provide a brief initial investigation of the flow of the PTT fluid into a wedge - wedge sink flow. The analysis here attempts a similar analysis to that of the UCM and Oldroyd-B models in this geometry by Evans and Hagen in [EH08], but matching the core solution to a viscometric boundary layer fails. The geometry in question is shown in figure C-1.

C.1 The core solution

The scalings in the core are motivated by assuming that away from the walls the component of the velocity in the θ direction is zero, i.e. the stream function away from the walls will be a function of θ only. Thus $\psi = \psi(\theta)$ in the core, and $\theta = O(1)$. These motivate the order of magnitude estimates

$$r = O(\epsilon), \quad \psi = O(1), \quad \mathbf{v} = O(\epsilon^{-1}), \quad \mathbf{T} = O(\epsilon^{-q}), \quad p = O(\epsilon^{-p_*}). \tag{C.1}$$

The terms in the governing equations (1.32)–(1.34) are then of the sizes

$$\begin{gathered}\text{Re } (\mathbf{v}.\nabla)\,\mathbf{v} = O(\epsilon^{-3}), \quad -\nabla p = O(\epsilon^{-p_*-1}), \quad \nabla.\mathbf{T} = O(\epsilon^{-q-1}), \\ \mathbf{T} = O(\epsilon^{-q}), \quad \overset{\triangledown}{\mathbf{T}} = O(\epsilon^{-2-q}), \quad \kappa\,(\text{tr } \mathbf{T})\,\mathbf{T} = O(\epsilon^{-2q}), \quad 2\mathbf{D} = O(\epsilon^{-2}).\end{gathered} \tag{C.2}$$

The fullest balance, which retains the inertia terms in the momentum, occurs when $q = p_* = 2$ and gives the leading order core equations of

$$\text{Balance 1:} \qquad \text{Re } (\mathbf{v}.\nabla)\,\mathbf{v} = -\nabla p + \nabla.\mathbf{T}, \qquad \overset{\triangledown}{\mathbf{T}} + \kappa\,(\text{tr } \mathbf{T})\,\mathbf{T} = 0. \tag{C.3}$$

There are two other possibilities not considered here of

$$\begin{aligned} &\text{Balance 2:} \quad p_* = 2, \quad q < 2 \quad \text{Re } (\mathbf{v}.\nabla)\,\mathbf{v} = -\nabla p \quad \overset{\triangledown}{\mathbf{T}} = 0, \\ &\text{Balance 3:} \quad p_* = q, \quad q > 2 \quad \nabla p = \nabla.\mathbf{T}, \qquad\qquad (\text{tr } \mathbf{T})\,\mathbf{T} = 0. \end{aligned} \tag{C.4}$$

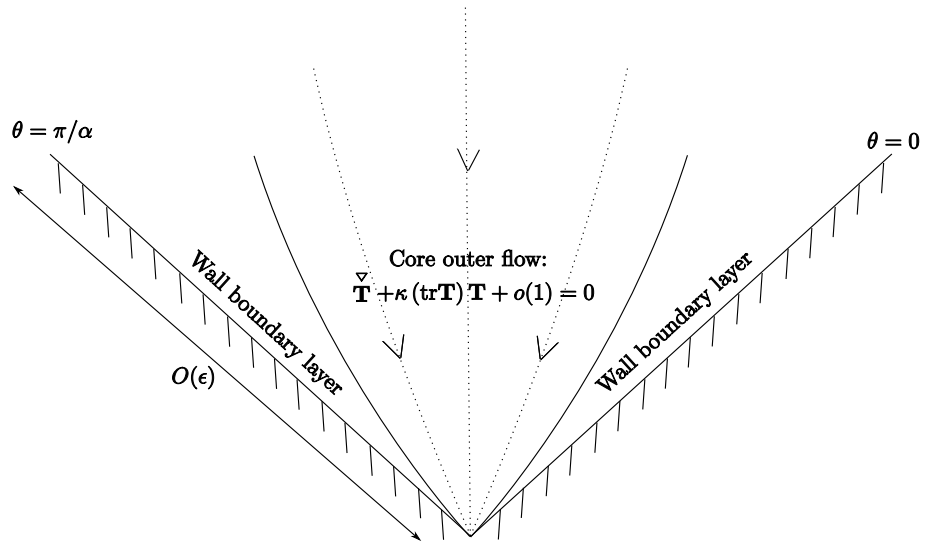

Figure C-1: Schematic of the wedge sink flow geometry, symmetric about $\theta = \pi/2\alpha$. Shown are the likely asymptotic regions of the core flow and boundary layers using the PTT equations. The boundary layer thicknesses and boundary layer balances are unknown as matching the core solution to wall boundary layers has been unsuccessful.

In the core region we seek a solution to balance 1. The following calculations are performed in polar coordinates. Assuming

$$\mathbf{T} = \frac{1}{r^2}\begin{pmatrix} g_{rr}(\theta) & g_{r\theta}(\theta) \\ g_{r\theta}(\theta) & g_{\theta\theta}(\theta) \end{pmatrix}, \qquad \text{and} \qquad \psi = g(\theta), \tag{C.5}$$

then substituting into balance 1 gives

$$-2g''g_{r\theta} + \kappa g_{rr}(g_{rr} + g_{\theta\theta}) = 0 \tag{C.6}$$

$$g_{\theta\theta}(-4g' + \kappa(g_{rr} + g_{\theta\theta})) = 0 \tag{C.7}$$

$$-2g'g_{r\theta} - g''g_{\theta\theta} + \kappa g_{r\theta}(g_{rr} + g_{\theta\theta}) = 0, \tag{C.8}$$

giving two possible solutions where $g_{\theta\theta} = 0$ and $g_{\theta\theta} \neq 0$ in (C.7). The first solution has $g_{\theta\theta} = 0$ to satisfy (C.7), causing $g_{rr} = \frac{2g'}{\kappa}$ (ignoring the trivial solution) and $g_{r\theta} = \frac{2g'^2}{\kappa g''}$. Solution 2 has $g_{\theta\theta} = \frac{16g'^3}{\kappa(g''^2+4g'^2)}$ to solve (C.7), causing $g_{rr} = \frac{4g'g''^2}{\kappa(g''^2+4g'^2)}$ and $g_{r\theta} = \frac{8g'^2g''}{\kappa(g''^2+4g'^2)}$. A third solution comes from considering the form of the UCM solution, and instead taking $T_{r\theta} = T_{\theta\theta} = 0$. This automatically solves two of the constitutive equations, and the third gives

$$rg'\frac{\partial T_{rr}}{\partial r} + 2g'T_{rr} + \kappa T_{rr}^2 r^2 = 0 \tag{C.9}$$

which has the general solution

$$T_{rr} = \frac{g'}{r^2(\kappa \log(r) + A(\theta)g')}, \qquad \text{where } A(\theta) \text{ is an arbitrary function of } \theta. \tag{C.10}$$

Solution 1

Using the solution

$$T_{rr} = \frac{2g'}{\kappa r^2}, \qquad T_{r\theta} = \frac{2g'^2}{\kappa g'' r^2}, \qquad T_{\theta\theta} = 0, \tag{C.11}$$

we find the momentum equations implying $p = p(r)$, and

$$-2g'^2g''' - g''^2\left(-Reg'^2\kappa + \frac{dp}{dr}r^3\kappa - 2g'\right) = 0, \tag{C.12}$$

with solution

$$p(r) = \frac{1}{r^2}\left(\frac{g'^2g'''}{\kappa g''^2} - \frac{Reg'^2}{2} - \frac{g'}{\kappa}\right) + C_p = \frac{p_0}{r^2} + C_p. \tag{C.13}$$

Solution 2

This is the solution

$$T_{rr} = \frac{4g'g''^2}{\kappa(g''^2 + 4g'^2)r^2}, \qquad T_{r\theta} = \frac{8g'^2g''}{\kappa(g''^2 + 4g'^2)r^2}, \qquad T_{\theta\theta} = \frac{16g'^3}{\kappa(g''^2 + 4g'^2)r^2}, \tag{C.14}$$

however, when substituted into the momentum equations this solution form does not give the desired effect of forcing $p = p(r)$.

Solution 3

The solution

$$T_{rr} = \frac{g'}{r^2(\kappa \log(r) + A(\theta)g')}, \qquad T_{r\theta} = T_{\theta\theta} = 0, \tag{C.15}$$

where $A(\theta)$ is an arbitrary function of θ in the momentum equations gives $p = p(r)$ and

$$\frac{dp}{dr} = \frac{\left(ReA(\theta)^2 g'^3 + 2Re\kappa \log(r) A(\theta) g'^2 + (Re\kappa^2 \log(r)^2 - A(\theta))g' - \kappa - \kappa \log(r)\right) g'}{r^3(\kappa \log(r) + A(\theta)g')^2}, \tag{C.16}$$

provided $\kappa \log(r) + A(\theta)g' \neq 0$, which has no easy solution for p. This form of the stresses would motivate boundary layer scalings containing logarithmic terms, consequently preventing a simple balance to obtain viscometric behaviour.

C.2 The matching behaviour of solution 1

Continuing with solution 1, to find boundary layer scalings we require the behaviour as $\theta \to 0$. In Cartesian coordinates, solution 1 is (without approximation)

$$\begin{aligned}
T_{11} &= \cos^2\theta \frac{2g'}{\kappa r^2} - 2\sin\theta\cos\theta \frac{2g'^2}{\kappa g'' r^2} = \frac{2g'}{\kappa r^2}\cos\theta\left(\cos\theta - 2\sin\theta\frac{g'}{g''}\right), \\
T_{12} &= \sin\theta\cos\theta\frac{2g'}{\kappa r^2} + (\cos^2\theta - \sin^2\theta)\frac{2g'^2}{\kappa g'' r^2} = \frac{2g'}{\kappa r^2}\left(\sin\theta\cos\theta + (\cos^2\theta - \sin^2\theta)\frac{g'}{g''}\right), \\
T_{22} &= \sin^2\theta\frac{2g'}{\kappa r^2} + 2\sin\theta\cos\theta\frac{2g'^2}{\kappa g'' r^2} = \frac{2g'}{\kappa r^2}\sin\theta\left(\sin\theta + 2\cos\theta\frac{g'}{g''}\right),
\end{aligned} \tag{C.17}$$

which as $\theta \to 0$ implies

$$\begin{aligned}
T_{11} &\sim \frac{2g'}{\kappa r^2}\cos\theta\,(\cos\theta) \sim \frac{2g'}{\kappa r^2}, \\
T_{12} &\sim \frac{2g'}{\kappa r^2}\cos\theta\left(\sin\theta + \cos\theta\frac{g'}{g''}\right) \sim \frac{2g'}{\kappa r^2}\left(\theta + \frac{g'}{g''}\right), \\
T_{22} &\sim \frac{2g'}{\kappa r^2}\sin\theta\left(\sin\theta + 2\cos\theta\frac{g'}{g''}\right) \sim \frac{2g'}{\kappa r^2}\theta\left(\theta + 2\frac{g'}{g''}\right).
\end{aligned} \tag{C.18}$$

Making the power law assumption that

$$g \sim C_0\theta^n + C_1\theta^{n+1} + ... \qquad \text{as} \qquad \theta \to 0, \tag{C.19}$$

motivates the boundary layer scalings

$$x = \epsilon\bar{X}, \quad y = \delta\bar{Y}, \quad \psi = \left(\frac{\delta}{\epsilon}\right)^n \bar{\Psi},$$
$$p = \epsilon^2\bar{p}, \quad T_{11} = \frac{\delta^{n-1}}{\epsilon^{n+1}}\bar{T}_{11}, \quad T_{12} = \frac{\delta^n}{\epsilon^{n+2}}\bar{T}_{12}, \quad T_{22} = \frac{\delta^{n+1}}{\epsilon^{n+3}}\bar{T}_{22}, \tag{C.20}$$

provided $n \neq 1$. If $n = 1$ the scalings change and correct terms to achieve viscometric behaviour are unable to be retained, unfortunately however, when using the scalings from (C.20) then to obtain the correct terms in the boundary layer equations for viscometric behaviour forces $n = 1$. This result (that $n = 1$) is as expected when performing the analysis as in [EH08]. This is seen as in the UCM and Oldroyd-B cases it was found that sink wedge flow had the same results as for the upstream boundary layer re-entrant corner flow but with $\alpha = 0$. PTT re-entrant corner flow has the stream function vanishing as $O(r^{n\alpha})$ with $n = 1 + \alpha$, compared to $n = 3 - \alpha$ for both UCM and Oldroyd-B. It is this result that now prevents the same analysis holding for the PTT flow in the sink wedge geometry.

We note briefly that modifications to (C.19) including $g \sim C_0\theta + C_1\theta^2\log(\theta)$, $g \sim C_0\theta\log(\theta) + C_1\theta$ and $g \sim C_0\theta\log(\theta)^2 + C_1\theta$ are unable to match the core solution into a viscometric boundary layer.

The solution for sink wedge flow of the PTT fluid remains an outstanding problem.

Appendix D

A generalised core solution

In section 3.1.4, a derivation of the core solution relevant to the situation when the upper convected derivative dominates was given. There is an assumption made to equation (3.19) that the forcing term f must be zero, with brief discussion made. Here we relax this assumption, and attempt to find a more general core solution relevant to the corner flows we have been considering. Unfortunately none of the solutions found are able to both determine the correct core balance and match into viscometric boundary layers. We record the analysis here as the solutions may be of relevance for other problems or situations.

D.1 The particular solution with a constant forcing term

Poisson's equation in two-dimensional polar coordinates is

$$\frac{1}{r}\frac{\partial}{\partial r}\left(r\frac{\partial\tilde{\psi}}{\partial r}\right)+\frac{1}{r^2}\frac{\partial^2\tilde{\psi}}{\partial\theta^2}=k, \tag{D.1}$$

where the arbitrary forcing term function f has been assumed to be a constant $f(\tilde{\psi})=k$. We now take the form

$$\tilde{\psi}=A_1r^{m_1}g_1(\theta)+A_2r^{m_2}g_2(\theta), \tag{D.2}$$

and derive the equation

$$A_1{m_1}^2r^{m_1}g_1+A_2{m_2}^2r^{m_2}g_2+A_1r^{m_1}\frac{d^2g_1}{d\theta^2}+A_2r^{m_2}\frac{d^2g_2}{d\theta^2}=kr^2. \tag{D.3}$$

There is a choice of balances, but since $m_1<m_2$, then clearly we must have $m_1=2$. The homogeneous option here would give the solution of section 3.1.4. At leading order

then, we have the equation

$$4A_1 g_1 + A_1 \frac{d^2 g_1}{d\theta^2} = k. \tag{D.4}$$

This equation in g_1 is a second order, constant coefficient ODE, and hence can be easily solved as $g_1 = C_1 \cos(2\theta) + C_2 \sin(2\theta) + \frac{k}{4A_1}$. Combining this with the no-slip conditions at the walls, of $g(0) = g(\pi/\alpha) = 0$, the solution becomes

$$\tilde{\psi} = \frac{k}{4} r^2 \left(1 - \cos(2\theta) + \frac{\cos(\frac{2\pi}{\alpha}) - 1}{\sin(\frac{2\pi}{\alpha})} \sin(2\theta) \right), \tag{D.5}$$

and thus as $\theta \to 0$,

$$\tilde{\psi} \sim \frac{k}{2} r^2 \theta \left(\frac{\cos(\frac{2\pi}{\alpha}) - 1}{\sin(\frac{2\pi}{\alpha})} \right). \tag{D.6}$$

The resulting matching conditions and scalings

Having found the behaviour of $\tilde{\psi}$, we now want to find the matching conditions for ψ and its derivatives to determine this solutions suitability. From above we have

$$\tilde{\psi} \sim \frac{k}{2} r^2 \theta \left(\frac{\cos(\frac{2\pi}{\alpha}) - 1}{\sin(\frac{2\pi}{\alpha})} \right), \tag{D.7}$$

and then we convert this into our stream function ψ using (3.24), (3.62), and (3.63). This means that

$$\psi \sim c_1 \left(\frac{k}{2} \left(\frac{\cos(\frac{2\pi}{\alpha}) - 1}{\sin(\frac{2\pi}{\alpha})} \right) \right)^n r^{2n} \theta^n. \tag{D.8}$$

The core scalings we obtain from this, along with our knowledge that $\mathbf{T} = \lambda(\psi)\mathbf{v}\mathbf{v}^T$ and $\lambda = c_1 \psi^{\frac{2(1-n)}{n}}$ allows us to find the core scalings

$$r = \epsilon R^*, \quad x = \epsilon X^*, \quad y = \epsilon Y^*, \quad \psi = \epsilon^{2n} R^*, \quad \mathbf{v} = \epsilon^{2n-1} \mathbf{v}^*, \quad \mathbf{T} = \epsilon^2 \mathbf{T}^*, \quad p = \epsilon^2 p^*. \tag{D.9}$$

The governing equations thus become

$$\begin{aligned} \mathrm{Re}\, \epsilon^{4n-4} (\mathbf{v}^*.\nabla^*)\mathbf{v}^* &= -\nabla^* p^* + \nabla^*.\mathbf{T}^*, \qquad \nabla^*.\mathbf{v}^* = 0, \\ \epsilon^{2-2n}\mathbf{T}^* + \left(\overset{\triangledown}{\mathbf{T}}{}^* + \kappa \epsilon^{4-2n} (\mathrm{tr}\ \mathbf{T}^*)\mathbf{T}^* \right) &= \epsilon^{-2} 2\mathbf{D}^*. \end{aligned} \tag{D.10}$$

Unfortunately these scalings show that $\overset{\triangledown}{\mathbf{T}}^*$ does not dominate in the core region for any choice of n, and hence this form for the stream function does not work. We can achieve the Newtonian balance of $\mathbf{T}^* = 2\mathbf{D}^*$ if we choose $n = 2$, although this is not of interest here.

D.2 The particular solution with a power law forcing term

The Poisson equation in two-dimensional polar coordinates that we are interested in is

$$\frac{1}{r}\frac{\partial}{\partial r}\left(r\frac{\partial\tilde{\psi}}{\partial r}\right) + \frac{1}{r^2}\frac{\partial^2\tilde{\psi}}{\partial\theta^2} = f(\tilde{\psi}). \tag{D.11}$$

We assume the arbitrary function f takes a power law form $f(\tilde{\psi}) = k\tilde{\psi}^{-q}$. To make progress, we take the form

$$\tilde{\psi} = A_1 r^{m_1} g_1(\theta) + A_2 r^{m_2} g_2(\theta), \tag{D.12}$$

and derive the equation

$$\begin{aligned} A_1 g_1 m_1^2 r^{m_1-2} + A_2 g_2 m_2^2 r^{m_2-2} + A_1 r^{m_1-2} g_1'' + A_2 r^{m_2-2} g_2'' \\ = k\left(A_1 r^{m_1} g_1 + A_2 r^{m_2} g_2\right)^{-q}, \end{aligned} \tag{D.13}$$

which after expanding and truncating the right hand side is

$$\begin{aligned} A_1 g_1 m_1^2 r^{m_1-2} + A_2 g_2 m_2^2 r^{m_2-2} + A_1 r^{m_1-2} g_1'' + A_2 r^{m_2-2} g_2'' \\ = k\left(A_1^{-q} r^{-qm_1} g_1^{-q} - qA_1^{-q-1} A_2 r^{m_2-m_1(q+1)} g_1^{-q-1} g_2\right). \end{aligned} \tag{D.14}$$

At leading order, this equation becomes

$$A_1 g_1 m_1^2 r^{m_1-2} + A_1 r^{m_1-2} g_1'' = kA_1^{-q} r^{-qm_1} g_1^{-q}. \tag{D.15}$$

D.2.1 Case 1, $q \neq 1$

In this case, we can balance the r powers (choosing not to gives Hinch's core solution), and find that $m_1 = \frac{2}{1+q}$, provided $q \neq -1$. We are then left with the equation

$$4A_1^{1+q} g_1^{1+q} + (1+q)^2 A_1^{1+q} g_1'' g_1^q = (1+q)^2 k, \tag{D.16}$$

and to make further progress we make the substitution

$$g_1 = B_1\theta^{p_1} + B_2\theta^{p_2}. \tag{D.17}$$

The resulting balances give two options.

Case 1(a), $q < 1$

By making this choice, the leading order balance gives $p_1 = 1$ and then $p_2 = 2 - q$. It is possible to determine B_2 in terms of the other variables, requiring $q \neq 1, 2$, but as $q < 1$, this does not pose any further restrictions. Here then the form for $\tilde{\psi}$ is

$$\tilde{\psi} \sim A_1 r^{\frac{2}{1+q}} \left(B_1\theta + B_2\theta^{2-q}\right). \tag{D.18}$$

Converting this, we see

$$\begin{aligned}
\psi &\sim c_1 A_1^n r^{\frac{2n}{1+q}} \left(B_1\theta + B_2\theta^{2-q}\right)^n, \\
&\sim c_1 A_1^n r^{\frac{2n}{1+q}} \left(B_1^n\theta^n + nB_1^{n-1}B_2\theta^{n+1-q}\right), \\
&\sim C_0 r^{\frac{2n}{1+q}} \left(\theta^n + C_1\theta^{n+1-q}\right),
\end{aligned} \tag{D.19}$$

allowing us to find the core scalings

$$\begin{gathered}
r = \epsilon R^*, \quad x = \epsilon X^*, \quad y = \epsilon Y^*, \\
\psi = \epsilon^{\frac{2n}{1+q}} R^*, \quad \mathbf{v} = \epsilon^{\frac{2n}{1+q}-1}\mathbf{v}^*, \quad \mathbf{T} = \epsilon^{\frac{4}{1+q}-2}\mathbf{T}^*, \quad p = \epsilon^{\frac{4}{1+q}-2}p^*.
\end{gathered} \tag{D.20}$$

This is true provided $n \neq 0$. The governing equations thus become

$$\begin{gathered}
\mathrm{Re}\,\epsilon^{\frac{4n-4}{1+q}}(\mathbf{v}^*.\nabla^*)\mathbf{v}^* = -\nabla^* p^* + \nabla^*.\mathbf{T}^*, \qquad \nabla^*.\mathbf{v}^* = 0, \\
\epsilon^{2-\frac{2n}{1+q}}\mathbf{T}^* + \left(\overset{\triangledown}{\mathbf{T}}^* + \kappa\epsilon^{\frac{4-2n}{1+q}}(\mathrm{tr}\ \mathbf{T}^*)\mathbf{T}^*\right) = \epsilon^{2-\frac{4}{1+q}} 2\mathbf{D}^*.
\end{gathered} \tag{D.21}$$

So here we have the correct balances providing (in the case of $q > -1$): $n > 1$, $n < 1+q$, $n < 2$, $q > 1$. So here there is a contradiction, and $\mathbf{D}^*$ dominates. In the case of $q < -1$, all of these conditions swap their inequalities, and so we require $n < 1$, $1+q < n$, $2 < n$, $q < 1$, and the contradiction comes from stating that $n < 1$, but also $n > 2$.

Case 1(b), $q > 1$

By making this choice, the leading order balance gives $p_1 = \frac{2}{1+q}$ and then $p_2 = \frac{2q}{1+q}$. It is possible to determine B_1 in terms of the other variables and actually take out A_1 too,

with the requirement $q \neq 1$, but as $q > 1$, this does not pose any further restrictions. Here then the form for $\tilde{\psi}$ is

$$\begin{aligned}\tilde{\psi} &\sim A_0 r^{\frac{2}{1+q}} \left(\theta^{\frac{2}{1+q}} + B_2 \theta^{\frac{2q}{1+q}}\right), \\ &\sim A_0 (r\theta)^{\frac{2}{1+q}} \left(1 + B_2 \theta^{\frac{2q-2}{1+q}}\right). \end{aligned} \tag{D.22}$$

Converting this, we see

$$\begin{aligned}\psi &\sim c_1 A_0^n (r\theta)^{\frac{2n}{1+q}} \left(1 + B_2 \theta^{\frac{2q-2}{1+q}}\right)^n, \\ &\sim c_1 A_0^n (r\theta)^{\frac{2n}{1+q}} \left(1 + nB_2 \theta^{\frac{2q-2}{1+q}}\right), \\ &\sim C_0 (r\theta)^{\frac{2n}{1+q}} \left(1 + C_1 \theta^{\frac{2q-2}{1+q}}\right), \end{aligned} \tag{D.23}$$

allowing us to find the core scalings

$$\begin{aligned} r = \epsilon R^*, \quad x = \epsilon X^*, \quad y = \epsilon Y^*, \\ \psi = \epsilon^{\frac{2n}{1+q}} R^*, \quad \mathbf{v} = \epsilon^{\frac{2n}{1+q}-1} \mathbf{v}^*, \quad \mathbf{T} = \epsilon^{\frac{4}{1+q}-2} \mathbf{T}^*, \quad p = \epsilon^{\frac{4}{1+q}-2} p^*. \end{aligned} \tag{D.24}$$

This is true provided $n \neq 0$. The governing equations thus become

$$\begin{aligned} \mathrm{Re}\, \epsilon^{\frac{4n-4}{1+q}} (\mathbf{v}^*.\nabla^*)\mathbf{v}^* = -\nabla^* p^* + \nabla^*.\mathbf{T}^*, \qquad \nabla^*.\mathbf{v}^* = 0, \\ \epsilon^{2-\frac{2n}{1+q}} \mathbf{T}^* + \left(\overset{\triangledown}{\mathbf{T}}{}^* + \kappa \epsilon^{\frac{4-2n}{1+q}} (\mathrm{tr}\ \mathbf{T}^*)\mathbf{T}^*\right) = \epsilon^{2-\frac{4}{1+q}} 2\mathbf{D}^*. \end{aligned} \tag{D.25}$$

So here we have the correct balances providing $n > 1$, $1 + q > n$, $2 > n$, $q > 1$. Summarising, we need $1 < n < 2$, with all other conditions satisfied due to the $q > 1$ range already imposed. In this case we have the correct core balance and continue to make progress into the boundary layer.

We had the stream function as

$$\psi \sim C_0 (r\theta)^{\frac{2n}{1+q}} \left(1 + C_1 \theta^{\frac{2q-2}{1+q}}\right), \tag{D.26}$$

and at leading order we know $r \sim x$, $\theta \sim \frac{y}{x}$ as $\theta \to 0$. Thus

$$\begin{aligned} \psi &\sim C_0 y^{\frac{2n}{1+q}} \left(1 + C_1 \left(\frac{y}{x}\right)^{\frac{2q-2}{1+q}}\right), \\ \frac{\partial \psi}{\partial x} &\sim C_0 y^{\frac{2n+2q-2}{1+q}} \left(C_1 \left(\frac{2-2q}{1+q}\right) x^{\frac{1-3q}{1+q}}\right), \\ \frac{\partial \psi}{\partial y} &\sim C_0 \left(\frac{2n}{1+q}\right) y^{\frac{2n-1-q}{1+q}}. \end{aligned} \tag{D.27}$$

Unfortunately, the scalings for the T_{ij}'s require $\frac{\partial \psi}{\partial x}/\frac{\partial \psi}{\partial y} \sim F(x)y$ to balance the terms within the upper convected stress derivative, yet here $\frac{\partial \psi}{\partial x}/\frac{\partial \psi}{\partial y} \sim F(x)y^{\frac{3q-1}{1+q}}$, thus requiring $q = 1$, which is outside our current range $q > 1$.

D.2.2 Case 2, $q = 1$

Here we discuss the degenerate case of $q = 1$, and the leading order equations then force a balance of $m_1 = 1$. The equation for g_1 becomes

$$A_1^2 g_1 (g_1 + g_1'') = k. \tag{D.28}$$

There is a possible solution g_1=Const, so we perform an eigenmode analysis about $g_1 = C_0$. Linearising so that $g_1 = C_{0g} + \delta g_2$, and taking terms of $O(\delta)$ gives a solvable ODE in g_2, with solution

$$g_2 = C_{1g} \sin(\sqrt{2}\theta) + C_{2g} \cos(\sqrt{2}\theta). \tag{D.29}$$

This implies looking for the type of form as has been considered previously. Considering the θ powers, the options for p_1 at leading order are $p_1 = 1$ to balance, or $p_1 = 0$ in the homogeneous case. As would be expected from Case 1, the choice of $p_1 = 1$ causes a contradiction in the size of p_2 relative to p_1 at the following order (this situation would be Case 1 with $q = 1$ so was likely to have issues), and thus the remaining option to consider $p_1 = 0$. So, in this case $\tilde{\psi} \sim A_1 r + \ldots$, which clearly cannot satisfy the boundary condition that $\tilde{\psi} \to 0$ as $\theta \to 0$.

There is an alternative form for g_1 which we could also consider

$$g_1 = C_0 \theta^n \log(\theta)^m. \tag{D.30}$$

We then have the equation

$$C_0^2 A_1^2 \theta^{2n-2} m(m-1)\log(\theta)^{2m-2} + 2m\left(n-\frac{1}{2}\right)\theta^{2n-2} C_0^2 A_1^2 \log(\theta)^{2m-1} + C_0^2 A_1^2 n \log(\theta)^{2m}(n-1)\theta^{2n-2} = k, \tag{D.31}$$

and thus we must balance $n = 1$ leaving

$$C_0^2 A_1^2 m(m-1)\log(\theta)^{2m-2} + m C_0^2 A_1^2 \log(\theta)^{2m-1} = k, \tag{D.32}$$

forcing $m = 1/2$. Thus at leading order, we have the stream function

$$\psi = A_1 C_0 r\theta\sqrt{\log(\theta)}. \tag{D.33}$$

For small θ this then gives the unrealistic result of complex stream function behaviour.

D.2.3 Case 3, $q = -1$

Here assuming the form of ψ as $\psi = A_1 r^{m_1} g_1$ gives the equation

$$\left(m_1^2 g_1 + g_1''\right) r^{m_1-1} = k r^{m_1+1} g_1. \tag{D.34}$$

Clearly it is impossible to balance the r powers, and thus the leading order must be the homogeneous equation $m_1^2 g_1 + g_1'' = 0$, providing us with Hinch's core solution previously studied.

D.3 A $\log(r)$ form for ψ, with $q = 1$

It is possible to assume a leading order form for ψ of

$$\tilde{\psi} \sim A_1 r^{m_1}\left(\log(r)^{m_2} g_1(\theta) + A_2 g_2(\theta)\right), \tag{D.35}$$

and at leading order in the Poisson equation, balancing forces $m_1 = 1$. To balance the leading order with the forcing term gives $m_2 = 0$, which would remove the logarithmic behaviour, so the next possibility of those terms being homogeneous, and the next terms balancing gives then the requirement that $A_2 = 0$, $m_2 = 1/2$, and $g_1 + g_1'' = 0$. This final ODE has the general solution $g_1 = C_1\sin(\theta) + C_2\cos(\theta)$. At leading order, the only thing left is to require $A_1^2 g_1^2 = k$. We thus have

$$\tilde{\psi} \sim A_1 r\sqrt{\log(r)}\left(C_1\sin(\theta) + C_2\cos(\theta)\right). \tag{D.36}$$

Requiring $A_1^2 g_1^2 = k$ unfortunately requires $C_2 = \frac{\sqrt{k}}{A_1}$ when $\theta = 0$, and thus we do not have $\tilde{\psi} \to 0$ as $\theta \to 0$.

D.4 A different forcing term in Poisson's equation

A recap of the Poisson equation in two-dimensional polar coordinates that we are interested in is

$$\frac{1}{r}\frac{\partial}{\partial r}\left(r\frac{\partial \tilde{\psi}}{\partial r}\right) + \frac{1}{r^2}\frac{\partial^2 \tilde{\psi}}{\partial \theta^2} = f(\tilde{\psi}). \tag{D.37}$$

We can instead now assume the arbitrary function f has a log form $f(\tilde{\psi}) = k\tilde{\psi}^{-1}\log\psi$, where we are trying to find an analogue of the $q = 1$ case before, but hopefully the log term prevents the degeneracy. Assuming the form

$$\tilde{\psi} = A_1 r^{m_1}\theta^{p_1}\left(\log(\theta)^{p_2} + A_2\right), \tag{D.38}$$

and balancing we find that $A_1 = \sqrt{k}$, $m_1 = p_1 = p_2 = 1$, and A_2 is arbitrary. Thus

$$\tilde{\psi} \sim \sqrt{k} r\theta\left(\log(\theta) + A_2\right), \tag{D.39}$$

which then gives

$$\tilde{\psi} \sim \sqrt{k} y\left(\log(y/x) + A_2\right), \quad \frac{\partial \tilde{\psi}}{\partial x} \sim -\sqrt{k}\left(y/x\right), \quad \frac{\partial \tilde{\psi}}{\partial y} \sim \sqrt{k}\left(\log(y/x) + A_2 + 1\right). \tag{D.40}$$

The scalings resulting from this behaviour would involve logarithmic terms and not allow the correct balances to be obtained.

Appendix E

Re-entrant corner flow in the $\frac{1}{2} \leq \alpha \leq \frac{2}{3}$ case

Revisiting the core region analysis, but with the knowledge that the $\nu^{*(0)}$ core balance is that of (3.120) for the case $\frac{1}{2} \leq \alpha \leq \frac{2}{3}$ (which corresponds to corners $270^o \leq \theta \leq 360^o$), the leading order equations are

$$\begin{gathered} 0 = \nabla^* p^{*(0)} + (\mathbf{v}^{*(0)}.\nabla^*)(\lambda^{*(0)}\mathbf{v}^{*(0)}), \\ (\mathbf{v}^{*(0)}.\nabla^*)\lambda^{*(0)} = 0, \quad (\mathbf{v}^{*(0)}.\nabla^*)\mu^{*(0)} = 0, \quad \left(\mathbf{v}^{*(0)}.\nabla^*\right)\nu^{*(0)} = \kappa\lambda^{*(0)}\left|\mathbf{v}^{*(0)}\right|^4, \end{gathered} \tag{E.1}$$

with $\mathbf{T}^{*(0)} = \lambda^{*(0)}\mathbf{v}^{*(0)}\mathbf{v}^{*(0)T}$. The general solution to these equations is then

$$\begin{gathered} \Psi^{*(0)} = \frac{C_0}{\alpha^n} R^{*n\alpha}\sin^n(\alpha\theta), \quad p^{*(0)} = p_0 R^{*-2(1-\alpha)}, \\ \lambda^{*(0)} = \frac{2p_0}{n^2 C_0^2}\left(\frac{\Psi^{*(0)}}{C_0}\right)^{\frac{2(1-n)}{n}}, \quad \mu^{*(0)} = d_2\left(\frac{\Psi^{*(0)}}{C_0}\right)^{n_2}, \end{gathered} \tag{E.2}$$

with the solution for $\nu^{*(0)}$ considered next.

The simplest way to investigate the solution to (3.120) is to consider it in polar coordinates and convert it into an ODE with respect to the polar angle θ along streamlines. Following [Ren97b], we have

$$\left(\mathbf{v}^{*(0)}.\nabla^*\right) = v_r\frac{\partial}{\partial R^*} + \frac{v_\theta}{R^*}\frac{\partial}{\partial\theta}, \tag{E.3}$$

and $\frac{v_r}{v_\theta} = \frac{1}{R^*}\frac{dR^*}{d\theta}$, where $v_r = \frac{1}{R^*}\frac{\partial \Psi^{*(0)}}{\partial \theta}$, $v_\theta = -\frac{\partial \Psi^{*(0)}}{\partial R^*}$. From (E.3) then

$$\left(\mathbf{v}^{*(0)}.\nabla^*\right) = \frac{v_\theta}{R^*}\frac{dR^*}{d\theta}\frac{\partial}{\partial R^*} + \frac{v_\theta}{R^*}\frac{\partial}{\partial \theta} = \frac{v_\theta}{R^*}\left(\frac{dR^*}{d\theta}\frac{\partial}{\partial R^*} + \frac{\partial}{\partial \theta}\right) = \frac{v_\theta}{R^*}\frac{d}{d\theta}. \tag{E.4}$$

The core balance (3.120) now becomes

$$\frac{v_\theta}{R^*}\frac{d\nu^{*(0)}}{d\theta} = \kappa\lambda^{*(0)}\left|\mathbf{v}^{*(0)}\right|^4, \tag{E.5}$$

which upon using the general solutions (E.2) gives

$$\frac{d\nu^{*(0)}}{d\theta} = -2p_0\kappa C_0 n\alpha^{\frac{3\alpha-2}{\alpha}}\left(\frac{\Psi^{*(0)}}{C_0}\right)^{1+\frac{2\alpha-2}{n\alpha}}\sin^{\frac{2-4\alpha}{\alpha}}(\alpha\theta), \tag{E.6}$$

with solution

$$\nu^{*(0)} = \begin{cases} -2p_0\kappa C_0 n\left(\frac{\Psi^{*(0)}}{C_0}\right)^{\frac{n-1}{n}}\left(-\log\delta + \int_{s=\pi/2\alpha}^{s=\theta}\frac{1}{\sin(\alpha s)}ds \right. \\ \qquad\qquad \left. -\frac{1}{2n}\log\left(\frac{\Psi^{*(0)}}{C_0}\right)\right), \quad \text{for } \alpha = \frac{2}{3}, \\ \\ -2p_0\kappa C_0 n\alpha^{\frac{3\alpha-2}{\alpha}}\left(\frac{\Psi^{*(0)}}{C_0}\right)^{1+\frac{2\alpha-2}{n\alpha}}\int_{s=0}^{s=\theta}(\sin(\alpha s))^{\frac{2-4\alpha}{\alpha}}ds, \qquad \text{for } \frac{1}{2} \leq \alpha < \frac{2}{3}. \end{cases} \tag{E.7}$$

This solution omits the additive homogeneous solutions (i.e. the arbitrary functions of $\Psi^{*(0)}$). Such terms match into higher order boundary layer terms and play no role in the main analysis. Further, the integral limits follow only after matching with the upstream boundary layer (which have been pre-empted here for conciseness, but will be derived later in this appendix). In the $\alpha = 2/3$ case the quadrature has the explicit evaluation

$$\int_{s=\pi/2\alpha}^{s=\theta}\frac{1}{\sin(\alpha s)}ds = \frac{1}{\alpha}\log\left(\frac{\sin(\alpha\theta)}{1+\cos(\alpha\theta)}\right). \tag{E.8}$$

For matching purposes, the upstream wall behaviour as $\theta \to 0$ is then

$$\text{as } Y^* \to 0, \quad \Psi^{*(0)} \sim C_0 X^{*n(\alpha-1)}Y^{*n}, \quad p^{*(0)} \sim p_0 X^{*2(\alpha-1)},$$
$$\lambda^{*(0)} \sim \frac{2p_0}{n^2 C_0^2}X^{*2(\alpha-1)(1-n)}Y^{*2(1-n)}, \quad \mu^{*(0)} \sim d_2 X^{*n(\alpha-1)n_2}Y^{*nn_2},$$
$$\nu^{*(0)} \sim \begin{cases} -2p_0\kappa C_0 n X^{*(1-n)/3}Y^{*n-1}\left(-\log\delta + \log\left(\frac{Y^*}{X^{*4/3}}\right)\right), & \text{for } \alpha = \frac{2}{3}, \\ -\frac{2p_0\kappa C_0 n}{2-3\alpha}X^{*1+(n+2)(\alpha-1)}Y^{*n-1}, & \text{for } \frac{1}{2} \leq \alpha < \frac{2}{3}. \end{cases} \tag{E.9}$$

The boundary layer

The scalings from (3.72) continue to hold with this different core balance for $\nu^{*(0)}$. The only difference lies in the scaling $\nu^* = \delta^{nn_3}\bar{\nu}$, where (E.9) would suggest $n_3 = (n-1)/n$ in contrast to the other range $2/3 < \alpha < 1$ where $n_3 = 2(2\alpha - 1)/n$. The scaling exponent n_3 here will be left general as (E.9) has only been stated but not proven from the previous section.

As the scalings have not been altered, the analysis of the boundary layer equations follows as in section 3.2.2. The same leading order boundary layer equations are found (as in (3.101), or (3.109) in terms of the stream function), with the dominant balance giving the same results as in (3.90). In particular, this gives $\theta_3\delta^{nn_3} = \epsilon^{2(2\alpha-1)}$ but also from the core balance for this range $1/2 \leq \alpha \leq 2/3$ we have in (3.119) that $\theta_3 = \epsilon^{\alpha^2+3\alpha-2}$. These pieces of information allow the determination of n_3 as

$$n_3 = \frac{\alpha}{1+\alpha}. \tag{E.10}$$

The matching conditions in (3.113) hold for this range $1/2 \leq \alpha \leq 2/3$, except for $\bar{\nu}$. We thus seek to find the form for the $\bar{\nu}$ matching condition, and confirm the results of equations (E.7) and (E.9). The core balance (3.120) scaled into the boundary layer is

$$\delta^{n-1+nn_3}\left(\bar{\Psi}_{\bar{Y}}\bar{\nu}_{\bar{X}} - \bar{\Psi}_{\bar{X}}\bar{\nu}_{\bar{Y}}\right) = \kappa\frac{C_1}{n^2C_0^{2/n}}\bar{\Psi}^{\frac{2(1-n)}{n}}\delta^{2(1-n)}\left(\delta^{2(n-1)}\bar{\Psi}_{\bar{Y}}^2 + \delta^{2n}\bar{\Psi}_{\bar{X}}^2\right)^2, \tag{E.11}$$

which at leading order (having used n_3 from (E.10)) this says

$$\bar{\Psi}_{\bar{Y}}\bar{\nu}_{\bar{X}} - \bar{\Psi}_{\bar{X}}\bar{\nu}_{\bar{Y}} = \kappa\frac{C_1}{n^2C_0^{2/n}}\bar{\Psi}^{\frac{2(1-n)}{n}}\bar{\Psi}_{\bar{Y}}^4. \tag{E.12}$$

Making the assumption that the $\bar{\nu}$ matching condition is of the form

$$\bar{\nu} \sim E\bar{X}^{m_1}\bar{Y}^{m_2} \tag{E.13}$$

for unknown constants E, m_1 and m_2, then (E.12) with the applicable results of (3.113) give

$$\begin{aligned} E\left(m_1 + m_2(1-\alpha)\right)\bar{X}^{n(\alpha-1)+m_1-1}\bar{Y}^{n-1+m_2} \\ \sim \kappa\frac{C_1}{n^2C_0^{2/n}}C_0^{\frac{2(1-n)}{n}+3}n^3\bar{X}^{2(\alpha-1)(1+n)}\bar{Y}^{2(n-1)}. \end{aligned} \tag{E.14}$$

Equating coefficients gives

$$m_1 = (\alpha - 1)(2 + n) + 1 = \alpha^2 + 2\alpha - 2, \qquad m_2 = \alpha, \qquad E = -\frac{\kappa C_0 C_1 n}{2 - 3\alpha}, \tag{E.15}$$

or E in terms of d_1 or p_0 equivalently

$$E = -\frac{\kappa d_1 C_0^3 n^3}{2 - 3\alpha} = -\frac{2p_0\kappa(1 + \alpha)C_0}{2 - 3\alpha}. \tag{E.16}$$

The coefficient E has a singularity when $\alpha = 2/3$, indicating the assumed form in (E.13) has to be modified for this value of α, and will be considered next. To conclude, there are three cases to consider in the natural stress basis: $1/2 \leq \alpha < 2/3$, $\alpha = 2/3$, and $2/3 < \alpha < 1$, and in the $\frac{1}{2} \leq \alpha < \frac{2}{3}$ case the ν matching condition is

$$\text{as } \bar{Y} \to \infty, \qquad \bar{\nu} \sim -\frac{2p_0\kappa(1 + \alpha)C_0}{2 - 3\alpha} \bar{X}^{\alpha^2 + 2\alpha - 2} \bar{Y}^{\alpha}. \tag{E.17}$$

It can also be noted that this is invariant under the scaling group (3.115), and thus the same similarity solution will occur for both cases $\frac{1}{2} < \alpha < \frac{2}{3}$ and $\frac{2}{3} < \alpha < 1$.

The case $\alpha = \frac{2}{3}$

The two cases $\frac{1}{2} < \alpha < \frac{2}{3}$ and $\frac{2}{3} < \alpha < 1$ now need to be joined by a third case at the point $\alpha = \frac{2}{3}$. As well as being of mathematical interest, this corresponds to the 270^o angle that occurs in a contraction flow, mentioned at the start of chapter 3 and shown in figure 3-1. The leading order boundary layer equation for the $\bar{\nu}$ matching condition is given in (E.12), and the assumption (E.13) needs to be altered to take into account the singularity in E occurring at $\alpha = 2/3$. Considering

$$\bar{\nu} = E_0 \bar{X}^{m_1} \bar{Y}^{m_2} \left(L_1 \log(\bar{X}) + L_2 \log(\bar{Y}) \right), \tag{E.18}$$

with unknown constants E_0, L_1 and L_2, where $m_1 = -\frac{2}{9}$, $m_2 = \frac{2}{3}$ as $\alpha = 2/3$ in this case, leads to

$$\frac{5}{9} E_0 C_0 \left(3L_1 + L_2\right) \bar{X}^{-\frac{16}{9}} \bar{Y}^{\frac{4}{3}} \sim \left(\frac{5}{3}\right)^2 \kappa C_1 C_0^2 \bar{X}^{-\frac{16}{9}} \bar{Y}^{\frac{4}{3}}, \tag{E.19}$$

after using (E.12) and the known matching conditions as $\bar{Y} \to \infty$. The $\bar{X}$ and $\bar{Y}$ powers agree, leaving only to equate

$$E_0 = \frac{5\kappa C_0 C_1}{3L_1 + L_2} = \frac{10\kappa p_0 C_0}{3L_1 + L_2}, \tag{E.20}$$

and hence

$$\text{as } \bar{Y} \to \infty, \qquad \bar{\nu} \sim \frac{10\kappa p_0 C_0}{3L_1 + L_2} \bar{X}^{-\frac{2}{9}} \bar{Y}^{\frac{2}{3}} \left(L_1 \log(\bar{X}) + L_2 \log(\bar{Y}) \right), \tag{E.21}$$

where L_1 and L_2 are still arbitrary. For the scaling group (3.115) to leave this matching condition invariant, we require $L_2 = -\frac{3}{4} L_1$, which simplifies the matching condition to

$$\text{as } \bar{Y} \to \infty, \qquad \bar{\nu} \sim -\frac{10}{3} \kappa p_0 C_0 \bar{X}^{-\frac{2}{9}} \bar{Y}^{\frac{2}{3}} \log \left(\frac{\bar{Y}}{\bar{X}^{4/3}} \right). \tag{E.22}$$

Appendix F

Full far-field expansions

We record here the full far-field expansions relevant to section 3.2.4. The expressions found are significantly larger than the UCM equivalent, and thus many of the coefficients are recorded separately, with the superscripts of these coefficients indicating the free constants for which the forcing term is associated (e.g. $F^{(23)}$ is a forcing term associated with C_2 and C_3). Additionally, there are two expansions given - one for $\alpha \neq 2/3$ and one for $\alpha = 2/3$ due to the singular coefficients at this specific (and important) α value.

Similar to UCM in [Eva08a], it is found that the forcing terms associated with C_2 increase in number as $\alpha \to \infty$. All terms involving C_2 which are larger than $O(\xi^{-4+2\alpha})$ (the size of the last eigenmode) are given for the range $1/2 \leq \alpha \leq 2/3$, with more terms intruding (but not given) as α increases. All terms involving the other constants are included irrespective of the value of α.

The order of the terms in the series varies with α, and so the terms are ordered in the case when $\alpha < 2/3$ (in the $\alpha \neq 2/3$ expansion). We thus have the $\alpha \neq 2/3$ farfield expansion as

$$
\begin{aligned}
f(\xi) \sim \frac{C_0}{\kappa}\xi^{1+\alpha}\Bigg(1 &+ \frac{\kappa C_1(2\alpha-1)}{\alpha(3\alpha-2)(1-\alpha)C_0}\xi^{-\alpha} + C_2\xi^{-2+2\alpha} + C_3\xi^{-1} + F_2\xi^{-2\alpha} \\
&+ C_4\xi^{-2+\alpha} + \frac{\kappa C_1 C_3(2\alpha-1)}{C_0\alpha(3\alpha-2)(1-\alpha)(1+\alpha)}\xi^{-1-\alpha} + F_3\xi^{-3\alpha} + F_1^{(2)}\xi^{-4+4\alpha} + F_1^{(23)}\xi^{2\alpha-3} \\
&+ \left(F_2^{(2)} + F_1^{(3)} + F_1^{(4)}\right)\xi^{-2} + F_2^{(3)}\xi^{-1-2\alpha} + F_4\xi^{-4\alpha} + \left(F_1^{(24)} + F_3^{(2)}\right)\xi^{3\alpha-4} \\
&+ \frac{C_3C_4(2\alpha-1)}{1+\alpha}\xi^{\alpha-3} + \left(F_4^{(2)} + F_2^{(4)} + \frac{\kappa(3\alpha+2)(\alpha-1)}{6C_0\alpha(1+\alpha)(3\alpha-2)(2+\alpha)}\right)\xi^{-2-\alpha} \\
&+ F_3^{(3)}\xi^{-1-3\alpha} + F_5\xi^{-5\alpha} + F_5^{(2)}\xi^{6\alpha-6} + F_2^{(23)}\xi^{-5+4\alpha} + C_5\xi^{-4+2\alpha} \\
&+ \left(F_6^{(2)} + F_2^{(24)}\right)\xi^{-6+5\alpha} + F_7^{(2)}\xi^{-8+8\alpha}\Bigg),
\end{aligned}
\tag{F.1}
$$

$$
\begin{aligned}
t_{11}(\xi) \sim C_1 \Bigg(& 1 + \frac{\kappa C_1}{C_0(1+\alpha)(3\alpha-2)}\xi^{-\alpha} + \frac{2(2\alpha-1)C_2}{1+\alpha}\xi^{-2+2\alpha} + A_2\xi^{-2\alpha} \\
& + \left(\frac{2(1-\alpha)(2\alpha-1)(2-\alpha)C_4}{(1+\alpha)(\alpha^2-5\alpha+2)} + A_1^{(2)}\right)\xi^{-2+\alpha} + A_1^{(3)}\xi^{-1-\alpha} + A_3\xi^{-3\alpha} \\
& + \frac{4{C_2}^2(2\alpha-1)(\alpha-1)}{(1+\alpha)^2}\xi^{-4+4\alpha} + \frac{4(\alpha-1)(2\alpha-1)C_3C_2}{(1+\alpha)^2}\xi^{2\alpha-3} \\
& + \left(A_2^{(2)} + A_1^{(4)}\right)\xi^{-2} + A_2^{(3)}\xi^{-1-2\alpha} + A_4\xi^{-4\alpha} \\
& + \left(A_1^{(24)} + A_3^{(2)}\right)\xi^{3\alpha-4} + \left(A_1^{(23)} + A_1^{(34)}\right)\xi^{\alpha-3} \\
& + \left(\frac{\kappa}{3C_0\alpha(3\alpha-2)(1+\alpha)} + A_2^{(4)} + \frac{\alpha\kappa C_1C_3^2}{2C_0(3\alpha-2)(1+\alpha)^2} + A_4^{(2)}\right)\xi^{-2-\alpha} \\
& + A_3^{(3)}\xi^{-1-3\alpha} + A_5\xi^{-5\alpha} + A_5^{(2)}\xi^{6\alpha-6} + \frac{16(2\alpha-1)(1-\alpha)^2C_2^2C_3}{(1+\alpha)^3}\xi^{-5+4\alpha} \\
& + \left(A_6^{(2)} + A_2^{(24)} + A_2^{(23)} + A_3^{(4)} + \frac{6(2\alpha-3)(1-\alpha)(2-\alpha)C_5}{(1+\alpha)(3\alpha^2-10\alpha+6)}\right)\xi^{-4+2\alpha} \\
& + \left(A_3^{(24)} + A_7^{(2)}\right)\xi^{-6+5\alpha} + A_8^{(2)}\xi^{-8+8\alpha}\Bigg),
\end{aligned} \tag{F.2}
$$

$$
\begin{aligned}
t_{12}(\xi) \sim C_1(1-\alpha)\xi \Bigg(& 1 + \frac{\kappa C_1(\alpha^2-4\alpha+2)}{C_0(1+\alpha)(3\alpha-2)(1-\alpha)^2}\xi^{-\alpha} \\
& - \frac{4(1-\alpha)C_2}{1+\alpha}\xi^{-2+2\alpha} - \frac{C_3}{(1-\alpha)(1+\alpha)}\xi^{-1} \\
& + B_2\xi^{-2\alpha} + \left(\frac{2(\alpha^2-2\alpha+2)(2\alpha-1)(2-\alpha)C_4}{(1+\alpha)(\alpha^2-5\alpha+2)(1-\alpha)} + B_1^{(2)}\right)\xi^{-2+\alpha} \\
& + B_1^{(3)}\xi^{-1-\alpha} + B_3\xi^{-3\alpha} + B_2^{(2)}\xi^{-4+4\alpha} + B_1^{(23)}\xi^{2\alpha-3} \\
& + \left(B_3^{(2)} + B_1^{(4)}\right)\xi^{-2} + B_2^{(3)}\xi^{-1-2\alpha} + B_4\xi^{-4\alpha} + \left(B_1^{(24)} + B_4^{(2)}\right)\xi^{3\alpha-4} \\
& + \left(B_2^{(23)} + B_1^{(34)}\right)\xi^{\alpha-3} \\
& + \left(B_5^{(2)} + B_3^{(3)} + B_2^{(4)} + \frac{(\alpha^2-2\alpha-2)\kappa}{3C_0\alpha(3\alpha-2)(1+\alpha)^2(\alpha-1)}\right)\xi^{-2-\alpha} \\
& + B_4^{(3)}\xi^{-1-3\alpha} + B_5\xi^{-5\alpha} + B_6^{(2)}\xi^{6\alpha-6} + B_3^{(23)}\xi^{-5+4\alpha} \\
& + \left(\frac{12(\alpha^2-3\alpha+3)(-2+\alpha)C_5}{(1+\alpha)(3\alpha^2-10\alpha+6)} + B_3^{(4)} + B_2^{(24)} + B_4^{(23)} + B_7^{(2)}\right)\xi^{-4+2\alpha} \\
& + \left(B_8^{(2)} + B_3^{(24)}\right)\xi^{-6+5\alpha} + B_9^{(2)}\xi^{-8+8\alpha}\Bigg),
\end{aligned} \tag{F.3}
$$

$$
\begin{aligned}
t_{22}(\xi) \sim\, & C_1(1-\alpha)^2\xi^2\left(1+\frac{(\alpha^2-6\alpha+3)\kappa C_1}{(1+\alpha)(3\alpha-2)(1-\alpha)^2C_0}\xi^{-\alpha}+\frac{2(2\alpha-3)C_2}{1+\alpha}\xi^{-2+2\alpha}\right.\\
& -\frac{2C_3}{(1-\alpha)(1+\alpha)}\xi^{-1}+D_2\xi^{-2\alpha}+\left(\frac{2C_4(2-\alpha)(2\alpha-1)(\alpha^2-2\alpha+3)}{(1-\alpha)(1+\alpha)(\alpha^2-5\alpha+2)}+D_1^{(2)}\right)\xi^{-2+\alpha}\\
& +D_1^{(3)}\xi^{-1-\alpha}+D_3\xi^{-3\alpha}+\frac{4C_2^2(2\alpha-3)(4\alpha^2-9\alpha+4)}{(4\alpha-3)(1+\alpha)^2}\xi^{-4+4\alpha}\\
& +\frac{4C_2C_3(2\alpha^2-5\alpha+4)}{(1+\alpha)^2}\xi^{2\alpha-3}\\
& +\left(D_1^{(4)}+D_2^{(2)}+\frac{C_3^2}{(1-\alpha)^2(1+\alpha)^2}-\frac{1}{C_1(1-\alpha)^2}\right)\xi^{-2}\\
& +D_2^{(3)}\xi^{-1-2\alpha}+D_4\xi^{-4\alpha}+\left(D_1^{(24)}+D_3^{(2)}\right)\xi^{3\alpha-4}+\left(D_1^{(23)}+D_1^{(34)}\right)\xi^{\alpha-3}\\
& +\left(D_4^{(2)}+D_3^{(3)}+D_2^{(4)}+\frac{\kappa(\alpha^3-2\alpha^2+4\alpha+3)}{3C_0\alpha(1+\alpha)^2(1-\alpha)^2(3\alpha-2)}\right)\xi^{-2-\alpha}\\
& +D_4^{(3)}\xi^{-1-3\alpha}+D_5\xi^{-5\alpha}+D_5^{(2)}\xi^{6\alpha-6}+D_2^{(23)}\xi^{-5+4\alpha}\\
& +\left(\frac{2C_5(-2+\alpha)(6\alpha^5-33\alpha^4+75\alpha^3-73\alpha^2+20\alpha+6)}{\alpha(1+\alpha)(1-\alpha)^2(3\alpha^2-10\alpha+6)}\right.\\
& \left.+D_3^{(4)}+D_2^{(24)}+D_3^{(23)}+D_6^{(2)}\right)\xi^{-4+2\alpha}\\
& \left.+\left(D_3^{(24)}+D_7^{(2)}\right)\xi^{-6+5\alpha},+D_8^{(2)}\xi^{-8+8\alpha}\right). \qquad \text{(F.4)}
\end{aligned}
$$

and the $\alpha = 2/3$ expansion as

$$
\begin{aligned}
f(\xi) \sim \frac{C_0}{\kappa}\xi^{5/3}\Bigg\{1 &- \left[\frac{3\kappa C_1 \ln(\xi)}{2C_0} - C_2\right]\xi^{-2/3} + C_3\xi^{-1} \\
&+ \left[\frac{63\kappa^2 {C_1}^2 (\ln(\xi))^2}{40{C_0}^2} + \frac{3\kappa C_1(-56C_0C_2 + 351\kappa C_1)\ln(\xi)}{80{C_0}^2} + C_4\right]\xi^{-4/3} \\
&- \left[\frac{9C_3\kappa C_1 \ln(\xi)}{10C_0} + \frac{3C_3(3\kappa C_1 - 2C_0C_2)}{10C_0}\right]\xi^{-5/3} - \Bigg[\frac{207\kappa^3 {C_1}^3 (\ln(\xi))^3}{400{C_0}^3} \\
&+ \frac{9\kappa^2 {C_1}^2 (1417\kappa C_1 - 184C_0C_2)(\ln(\xi))^2}{1600{C_0}^3} \\
&+ \frac{\kappa C_1\left(893187\kappa^2 {C_1}^2 - 304200\kappa C_1C_2C_0 + 18208{C_0}^2{C_2}^2 + 11840{C_0}^2C_4\right)\ln(\xi)}{38400{C_0}^3} \\
&- \frac{F_{log}}{460800{C_0}^3}\Bigg]\xi^{-2} \\
&+ \Bigg[\frac{63\kappa^2 {C_1}^2 C_3 (\ln(\xi))^2}{200{C_0}^2} + \frac{3\kappa C_1C_3(603\kappa C_1 - 56C_0C_2)\ln(\xi)}{400{C_0}^2} \\
&+ \frac{C_3\left(80{C_0}^2C_4 + 3159\kappa^2 {C_1}^2 - 504\kappa C_1C_2C_0\right)}{400{C_0}^2}\Bigg]\xi^{-7/3} \\
&+ \Bigg[\frac{567\kappa^4 {C_1}^4 (\ln(\xi))^4}{16000{C_0}^4} + \frac{27\kappa^3 {C_1}^3 (3021\kappa C_1 - 112C_0C_2)(\ln(\xi))^3}{32000{C_0}^4} \\
&+ \frac{3\kappa^2 {C_1}^2\left(3089367\kappa^2 {C_1}^2 - 420930\kappa C_1C_2C_0 + 280{C_0}^2{C_2}^2 + 14000{C_0}^2C_4\right)(\ln(\xi))^2}{320000{C_0}^4} \\
&+ \frac{1}{25600000{C_0}^4}\Bigg(2060800\left(\frac{150}{161} + \left({C_2}^2 - \frac{50}{23}C_4\right)C_2C_1\right)\kappa {C_0}^3 \\
&+ 995520{C_1}^2\left({C_2}^2 + \frac{69490}{1037}C_4\right)\kappa^2 {C_0}^2 \\
&- 403213680\kappa^3 {C_1}^3 C_2C_0 + 1736030961\kappa^4 {C_1}^4\Bigg)\ln(\xi) + C_5\Bigg]\xi^{-8/3}\Bigg\},
\end{aligned}
\tag{F.5}
$$

$$
\begin{aligned}
t_{11}(\xi) \sim C_1 \Bigg\{ & 1 - \left[\frac{3\kappa C_1 \ln(\xi)}{5C_0} + \frac{27\kappa C_1 - 4C_0 C_2}{10C_0} \right] \xi^{-2/3} \\
& - \left[\frac{9\kappa^2 {C_1}^2 (\ln(\xi))^2}{25{C_0}^2} + \frac{3\kappa C_1 (-16C_0 C_2 + 63\kappa C_1) \ln(\xi)}{100{C_0}^2} + \frac{C_4}{5} \right. \\
& \left. + \frac{32{C_0}^2 {C_2}^2 + 792\kappa C_1 C_2 C_0 - 11421\kappa^2 {C_1}^2}{1600{C_0}^2} \right] \xi^{-4/3} \\
& + \left[\frac{6C_3 \kappa C_1 \ln(\xi)}{25C_0} + \frac{2C_3 (-2C_0 C_2 + 9\kappa C_1)}{25C_0} \right] \xi^{-5/3} + \left[\frac{9639\kappa^3 {C_1}^3 (\ln(\xi))^2}{4000{C_0}^3} \right. \\
& \left. + \frac{3\kappa C_1 \left(223317\kappa^2 {C_1}^2 - 37080\kappa C_1 C_2 C_0 + 224{C_0}^2 {C_2}^2 - 320{C_0}^2 C_4\right) \ln(\xi)}{32000{C_0}^3} \right. \\
& \left. + \frac{T_{11log}}{128000{C_0}^3} \right] \xi^{-2} + \left[\frac{36\kappa^2 {C_1}^2 C_3 (\ln(\xi))^2}{125{C_0}^2} + \frac{3C_3 \kappa C_1 (45\kappa C_1 - 16C_0 C_2) \ln(\xi)}{125{C_0}^2} \right. \\
& \left. + \frac{32C_3 \left(10C_4 + {C_2}^2\right) {C_0}^2 + 1368C_0 C_2 C_3 C_1 \kappa - 13689\kappa^2 {C_1}^2 C_3}{2000{C_0}^2} \right] \xi^{-7/3} \\
& + \left[\frac{27\kappa^4 {C_1}^4 (\ln(\xi))^4}{125{C_0}^4} + \frac{9\kappa^3 {C_1}^3 (11463\kappa C_1 - 1280C_0 C_2) (\ln(\xi))^3}{20000{C_0}^4} \right. \\
& \left. + \frac{\kappa^2 {C_1}^2 \left(118240{C_2}^2 + 94400C_4\right) {C_0}^2 - 2472984\kappa^3 {C_1}^3 C_2 C_0 + 7039953\kappa^4 {C_1}^4}{320000{C_0}^4} (\ln(\xi))^2 \right. \\
& \left. + \frac{1}{960000{C_0}^4} \left(18560 \left(-\frac{450}{29} - \left(\frac{590}{29} C_2 C_4 + \frac{180}{29} {C_3}^2 - {C_2}^3 \right) C_1 \right) \kappa {C_0}^3 \right. \right. \\
& \left. \left. + 940608 {C_1}^2 \kappa^2 \left({C_2}^2 + \frac{5825}{1633} C_4 \right) {C_0}^2 + 1282068\kappa^3 {C_1}^3 C_2 C_0 \right. \right. \\
& \left. \left. - 77896971\kappa^4 {C_1}^4 \right) \ln(\xi) + \frac{1}{2304000000{C_0}^4} \left(\left(-9216000000 C_5 + 921600000 {C_4}^2 \right. \right. \right. \\
& \left. \left. \left. + 26624000 {C_2}^4 - 450560000 {C_2}^2 C_4 + 184320000 {C_3}^2 C_2 \right) {C_0}^4 \right. \right. \\
& \left. \left. + 529689600 \left(-\frac{75}{209} + \left(-\frac{22590}{2299} C_2 C_4 - \frac{720}{121} {C_3}^2 + {C_2}^3 \right) C_1 \right) \kappa {C_0}^3 \right. \right. \\
& \left. \left. + 7877027520 {C_1}^2 \kappa^2 \left(\frac{2752510}{911693} C_4 + {C_2}^2 \right) {C_0}^2 - 83327978880\kappa^3 {C_1}^3 C_2 C_0 \right. \right. \\
& \left. \left. + 436053477951\kappa^4 {C_1}^4 \right) \right] \xi^{-8/3} \Bigg\}, \qquad \text{(F.6)}
\end{aligned}
$$

$$
\begin{aligned}
t_{12}(\xi) \sim \frac{1}{3}C_1\xi\Bigg\{1 &+ \left[\frac{6\kappa C_1\ln(\xi)}{5C_0} - \frac{27\kappa C_1 + 4C_0C_2}{5C_0}\right]\xi^{-2/3} - \frac{9C_3}{5}\xi^{-1} \\
&- \Bigg[\frac{18\kappa^2{C_1}^2\left(\ln(\xi)\right)^2}{5{C_0}^2} + \frac{3\kappa C_1\left(-80C_0C_2 + 531\kappa C_1\right)\ln(\xi)}{50{C_0}^2} \\
&+ 2C_4 + \frac{-2952\kappa C_1C_2C_0 + 160{C_0}^2{C_2}^2 + 1215\kappa^2{C_1}^2}{800{C_0}^2}\Bigg]\xi^{-4/3} \\
&+ \left[\frac{42C_3\kappa C_1\ln(\xi)}{25C_0} + \frac{C_3\left(153\kappa C_1 - 28C_0C_2\right)}{25C_0}\right]\xi^{-5/3} + \Bigg[\frac{28917\kappa^3{C_1}^3\left(\ln(\xi)\right)^2}{2000{C_0}^3} \\
&+ \frac{9\kappa C_1\left(240453\kappa^2{C_1}^2 - 37080\kappa C_1C_2C_0 + 224{C_0}^2{C_2}^2 - 320{C_0}^2C_4\right)\ln(\xi)}{16000{C_0}^3} \\
&+ \frac{T_{12log}^{(1)}}{64000{C_0}^3}\Bigg]\xi^{-2} + \Bigg[\frac{198\kappa^2{C_1}^2C_3\left(\ln(\xi)\right)^2}{125{C_0}^2} + \frac{3C_3\kappa C_1\left(549\kappa C_1 - 176C_0C_2\right)\ln(\xi)}{250{C_0}^2} \\
&+ \frac{352C_3\left(10C_4 + {C_2}^2\right){C_0}^2 + 13320C_0C_2C_3C_1\kappa - 143775\kappa^2{C_1}^2C_3}{4000{C_0}^2}\Bigg]\xi^{-7/3} \\
&+ \Bigg[\frac{702\kappa^4{C_1}^4\left(\ln(\xi)\right)^4}{625{C_0}^4} + \frac{9\kappa^3{C_1}^3\left(30495\kappa C_1 - 3328C_0C_2\right)\left(\ln(\xi)\right)^3}{10000{C_0}^4} \\
&+ \frac{\left(T_{12log}^{(2)}\right)\left(\ln(\xi)\right)^2}{800000{C_0}^4} + \frac{1}{12000000{C_0}^4}\Bigg(1206400\left(-\frac{450}{29} + \left(-\frac{590}{29}C_2C_4\right.\right. \\
&\left.\left. - \frac{180}{29}{C_3}^2 + {C_2}^3\right)C_1\right)\kappa{C_0}^3 + 67524480{C_1}^2\kappa^2\left(C_2{}^2 + \frac{77495}{23446}C_4\right){C_0}^2 \\
&- 68122620\kappa^3{C_1}^3C_2C_0 - 4506576021\kappa^4{C_1}^4\Bigg)\ln(\xi) \\
&+ \frac{1}{1152000000{C_0}^4}\Bigg(\left(-1171456000{C_2}^2C_4 + 479232000{C_3}^2C_2\right. \\
&\left. - 23961600000C_5 + 69222400{C_2}^4 + 2396160000{C_4}^2\right){C_0}^4 + 1393228800\kappa\left(-\frac{3225}{6047}\right. \\
&\left. + \left(-\frac{60150}{6047}C_2C_4 + {C_2}^3 - \frac{36000}{6047}{C_3}^2\right)C_1\right){C_0}^3 \\
&+ 21660730560\left(\frac{7526030}{2507029}C_4 + {C_2}^2\right){C_1}^2\kappa^2{C_0}^2 \\
&- 224268963840\kappa^3{C_1}^3C_2C_0 + 1098503540343\kappa^4{C_1}^4\Bigg)\Bigg]\xi^{-8/3}\Bigg\}, \qquad \text{(F.7)}
\end{aligned}
$$

$$
\begin{aligned}
t_{22}(\xi) \sim \frac{1}{9}C_1\xi^2 \Bigg\{ 1 + \Bigg[\frac{3\kappa C_1 \ln(\xi)}{C_0} - \frac{81\kappa C_1 + 20C_0C_2}{10C_0} \Bigg] \xi^{-2/3} - \frac{18C_3}{5}\xi^{-1} \\
+ \Bigg[\frac{18\kappa^2 {C_1}^2 (\ln(\xi))^2}{5{C_0}^2} + \frac{3\kappa C_1 (-32C_0C_2 + 477\kappa C_1)\ln(\xi)}{20{C_0}^2} \\
+ \frac{19}{5}C_4 + \frac{-1696{C_0}^2{C_2}^2 - 22968\kappa C_1C_2C_0 + 4617\kappa^2{C_1}^2}{1600{C_0}^2} \Bigg] \xi^{-4/3} - \Bigg[\frac{84C_3\kappa C_1 \ln(\xi)}{25C_0} \\
- \frac{C_3(56C_0C_2 + 531\kappa C_1)}{25C_0} \Bigg] \xi^{-5/3} \\
+ \Bigg[- \frac{243\kappa^3{C_1}^3(\ln(\xi))^3}{25{C_0}^3} - \frac{81\kappa^2{C_1}^2(3011\kappa C_1 - 960C_0C_2)(\ln(\xi))^2}{4000{C_0}^3} \\
+ \frac{3\kappa C_1\left(3822687\kappa^2{C_1}^2 + 229752\kappa C_1C_2C_0 - 87392{C_0}^2{C_2}^2 - 72640{C_0}^2C_4\right)\ln(\xi)}{32000{C_0}^3} \\
+ \frac{-1152000{C_0}^3 + 414720C_1{C_3}^2{C_0}^3 + 581120C_1C_2C_4{C_0}^3}{128000C_1{C_0}^3} + \frac{T_{22log}^{(1)}}{128000C_1{C_0}^3} \Bigg] \xi^{-2} \\
+ \Bigg[\frac{396\kappa^2{C_1}^2C_3(\ln(\xi))^2}{25{C_0}^2} + \frac{33C_3\kappa C_1(909\kappa C_1 - 160C_0C_2)\ln(\xi)}{250{C_0}^2} \\
+ \frac{C_3\left({C_0}^2\left(5536{C_2}^2 + 32320C_4\right) - 147177\kappa^2{C_1}^2 - 36360\kappa C_1C_2C_0\right)}{4000{C_0}^2} \Bigg] \xi^{-7/3} \\
+ \Bigg[\frac{4914\kappa^4{C_1}^4(\ln(\xi))^4}{625{C_0}^4} + \frac{9\kappa^3{C_1}^3(469347\kappa C_1 - 46592C_0C_2)(\ln(\xi))^3}{20000{C_0}^4} \\
+ \frac{\kappa^2{C_1}^2\left(T_{22log}^{(2)}\right)(\ln(\xi))^2}{1600000{C_0}^4} + \frac{1}{6000000{C_0}^4}\Big(\big(\kappa\left(3768800{C_2}^3 - 85256000C_2C_4\right. \\
\left. - 26208000{C_3}^2\right)C_1 - 49320000\kappa\big){C_0}^3 + 362366280\left({C_2}^2 + \frac{2298260}{1006573}C_4\right){C_1}^2\kappa^2{C_0}^2 \\
- 3318326595\kappa^3{C_1}^3C_2C_0 + 248634279\kappa^4{C_1}^4\Big)\ln(\xi) \\
+ \frac{1}{2304000000{C_0}^4}\Big(\big(-12032000000{C_2}^2C_4 + 6709248000{C_3}^2C_2 - 252518400000C_5 \\
+ 582041600{C_2}^4 + 26910720000{C_4}^2\big){C_0}^4 - 14867942400\left(\frac{13425}{64531} - \left(-\frac{773490}{64531}C_2C_4\right.\right. \\
\left.\left. + {C_2}^3 - \frac{431640}{64531}{C_3}^2\right)C_1\right)\kappa{C_0}^3 + 320208050880{C_1}^2\kappa^2\left(\frac{107208790}{37061117}C_4 + {C_2}^2\right){C_0}^2 \\
- 3351648352320\kappa^3{C_1}^3C_2C_0 + 14078177461539\kappa^4{C_1}^4\Big)\Bigg]\xi^{-8/3}\Bigg\}, \qquad \text{(F.8)}
\end{aligned}
$$

where

$$
\begin{aligned}
F_{log} &= 94720C_2C_4{C_0}^3 + 92160{C_3}^2{C_0}^3 + 4352{C_2}^3{C_0}^3 - 19683567\kappa^3{C_1}^3 \\
&\quad + 9141984C_2C_0{C_1}^2\kappa^2 - 960480C_1\kappa{C_0}^2{C_2}^2 + 227520C_1\kappa{C_0}^2C_4, \\
T_{11log} &= 1476225\kappa^3{C_1}^3 - 1205280C_2C_0{C_1}^2\kappa^2 + 2560C_2C_4{C_0}^3 \\
&\quad - 1792{C_2}^3{C_0}^3 + 113184C_1\kappa{C_0}^2{C_2}^2 + 66240C_1\kappa{C_0}^2C_4, \\
T^{(1)}_{12log} &= 3\left(2575125\kappa^3{C_1}^3 - 1353600C_2C_0{C_1}^2\kappa^2 + 114080C_1\kappa{C_0}^2{C_2}^2\right. \\
&\quad \left. +64960C_1\kappa{C_0}^2C_4 + 2560C_2C_4{C_0}^3 - 1792{C_2}^3{C_0}^3\right), \\
T^{(2)}_{12log} &= \kappa^2{C_1}^2\left(1537120{C_2}^2 + 1227200C_4\right){C_0}^2 \\
&\quad - 33144120\kappa^3{C_1}^3C_2C_0 + 101328813\kappa^4{C_1}^4, \\
T^{(1)}_{22log} &= 37928331\kappa^3{C_1}^4 - 13404960C_0\kappa^2{C_1}^3C_2 + 260448{C_1}^2\kappa{C_0}^2{C_2}^2 \\
&\quad + 1957440{C_1}^2\kappa{C_0}^2C_4 - 38144C_1{C_2}^3{C_0}^3, \\
T^{(2)}_{22log} &= 2115705987\kappa^2{C_1}^2 - 526235400\kappa C_1C_2C_0 \\
&\quad + 21610400{C_0}^2{C_2}^2 + 17051200{C_0}^2C_4.
\end{aligned}
$$

The coefficients in the $\alpha \neq 2/3$ expansions are

$$F_2 = -\frac{C_1^2\kappa^2\left(8\alpha^4-39\alpha^3+47\alpha^2-21\alpha+3\right)}{4\alpha C_0^2(1+\alpha)(1-\alpha)^2(2\alpha-1)^2(3\alpha-2)^2},$$

$$F_3 = -\frac{\kappa^3 C_1^3\left(120\alpha^6-439\alpha^5+436\alpha^4-71\alpha^3-102\alpha^2+50\alpha-6\right)}{6\alpha^2 C_0^3(3\alpha-1)(2\alpha-1)(5\alpha-2)(\alpha-1)^2(1+\alpha)^2(3\alpha-2)^3},$$

$$F_4 = \frac{\begin{array}{c}(34560\alpha^{12}-184288\alpha^{11}+378928\alpha^{10}-349905\alpha^9+55207\alpha^8+191663\alpha^7\\ -196009\alpha^6+83387\alpha^5-10803\alpha^4-4779\alpha^3+2337\alpha^2-394\alpha+24)\kappa^4 C_1^4\end{array}}{32\alpha^3 C_0^4(4\alpha-1)(3\alpha-1)(5\alpha-2)(1-\alpha)^3(1+\alpha)^3(2\alpha-1)^4(3\alpha-2)^4},$$

$$F_5 = \begin{pmatrix} (1075200\alpha^{14}-5198216\alpha^{13}+9006495\alpha^{12}-4648586\alpha^{11}-5731564\alpha^{10}\\ +10310478\alpha^9-5922050\alpha^8+345887\alpha^7\\ \dfrac{+1365070\alpha^6-755590\alpha^5+152789\alpha^4+5415\alpha^3-8028\alpha^2+1332\alpha-72)C_1^5\kappa^5}{\begin{array}{c}60\alpha^4 C_0^5(1-4\alpha)(3\alpha-1)(7\alpha-2)(5\alpha-2)\\ \cdot(5\alpha-1)(2\alpha-1)^2(\alpha-1)^4(1+\alpha)^4(3\alpha-2)^5\end{array}} \end{pmatrix}.$$

$$F_1^{(2)} = \frac{C_2^2(8\alpha-3)(\alpha-1)}{2(1+\alpha)(4\alpha-3)},$$

$$F_2^{(2)} = -\frac{\begin{array}{c}(112\alpha^{10}-728\alpha^9+2152\alpha^8-3261\alpha^7\\ +1705\alpha^6+1692\alpha^5-3204\alpha^4+2131\alpha^3-721\alpha^2+122\alpha-8)C_1^2C_2\kappa^2\end{array}}{4\alpha^2C_0^2(\alpha^2-5\alpha+2)(\alpha-1)^2(2\alpha-1)^2(3\alpha-2)^2(1+\alpha)^2},$$

$$F_3^{(2)} = \frac{4C_1C_2^2\kappa(2\alpha-1)^2(53\alpha^6-225\alpha^5+340\alpha^4-258\alpha^3+151\alpha^2-75\alpha+18)}{3C_0\alpha(1-\alpha)(-2+\alpha)(3\alpha-4)(3\alpha-2)(4\alpha-3)(\alpha^2-5\alpha+2)(1+\alpha)^2},$$

$$F_4^{(2)} = \frac{\begin{array}{c}C_1^3C_2\kappa^3(420\alpha^9-2408\alpha^8+4287\alpha^7-798\alpha^6\\ -3155\alpha^5+1850\alpha^4+542\alpha^3-724\alpha^2+200\alpha-16)\end{array}}{3\alpha^3C_0^3(1+\alpha)^4(3\alpha-2)^3(\alpha^2-5\alpha+2)(2+\alpha)(5\alpha-2)},$$

$$F_5^{(2)} = \frac{C_2^3(\alpha-1)(144\alpha^3-338\alpha^2+225\alpha-45)}{6(4\alpha-3)(6\alpha-5)(1+\alpha)^2},$$

$$F_6^{(2)} = \frac{\begin{array}{c}16(2\alpha-1)^2(1089\alpha^8-7008\alpha^7+18388\alpha^6-25941\alpha^5\\ +22586\alpha^4-14145\alpha^3+7208\alpha^2-2625\alpha+450)\kappa C_1C_2^3\\ \hline 15(1+\alpha)^3(\alpha^2-5\alpha+2)(6\alpha-5)\\ \cdot(3\alpha-2)(3\alpha-4)(6-5\alpha)(-2+\alpha)(\alpha-1)\alpha C_0\end{array}},$$

$$F_7^{(2)} = \frac{\begin{array}{c}C_2^4(\alpha-1)(6144\alpha^6-32960\alpha^5+70256\alpha^4\\-76150\alpha^3+44377\alpha^2-13218\alpha+1575)\end{array}}{8(6\alpha-5)(8\alpha-7)(4\alpha-3)^2(1+\alpha)^3}.$$

$$F_1^{(23)} = \frac{C_2C_3(3\alpha-1)}{1+\alpha}, \qquad F_2^{(23)} = \frac{C_2^2C_3(\alpha-1)(5\alpha-3)(8\alpha-3)}{2(4\alpha-3)(1+\alpha)^2}.$$

$$F_1^{(3)} = \frac{\alpha C_3^2}{2(1+\alpha)}, \qquad F_2^{(3)} = \frac{C_1^2C_3\kappa^2(8\alpha^4-39\alpha^3+47\alpha^2-21\alpha+3)}{4\alpha C_0^2(\alpha-1)(2\alpha-1)^2(3\alpha-2)^2(1+\alpha)^2},$$
$$F_3^{(3)} = \frac{\kappa^3C_1^3C_3(120\alpha^6-439\alpha^5+436\alpha^4-71\alpha^3-102\alpha^2+50\alpha-6)}{6\alpha^2C_0^3(3\alpha-1)\left(5\alpha-2\right)\left(\alpha-1\right)^2\left(1+\alpha\right)^3\left(3\alpha-2\right)^3}.$$

$$F_1^{(4)} = \frac{\kappa C_1C_4(2-\alpha)(\alpha^4+2\alpha^3+30\alpha^2-34\alpha+9)}{4C_0(1+\alpha)(3\alpha-2)(\alpha-1)(\alpha^2-5\alpha+2)},$$
$$F_2^{(4)} = \frac{\kappa^2C_1^2C_4(\alpha-1)(12\alpha^7-100\alpha^6+557\alpha^5-521\alpha^4-46\alpha^3+238\alpha^2-88\alpha+8)}{6\alpha^2C_0^2(1+\alpha)^3(3\alpha-2)^2(\alpha^2-5\alpha+2)(2+\alpha)(2\alpha-1)}.$$

$$F_1^{(24)} = \frac{2C_2C_4(5\alpha^3+10\alpha^2-31\alpha+12)(1-2\alpha)}{3(1+\alpha)(\alpha^2-5\alpha+2)(3\alpha-4)},$$
$$F_2^{(24)} = \frac{\begin{array}{c}2C_2^2C_4(1383\alpha^6-3518\alpha^5\\-2197\alpha^4+15388\alpha^3-18570\alpha^2+9126\alpha-1620)(2\alpha-1)\end{array}}{15(1+\alpha)^2(\alpha^2-5\alpha+2)(3\alpha-4)(4\alpha-3)(6-5\alpha)}.$$

$$A_2 = \frac{C_1^2\kappa^2(8\alpha^3-5\alpha^2-3\alpha+2)}{2\alpha(3\alpha-2)^2(1+\alpha)^2C_0^2(2\alpha-1)(\alpha-1)},$$
$$A_3 = \frac{\kappa^3{C_1}^3\left(120\alpha^6-115\alpha^5-80\alpha^4+118\alpha^3-22\alpha^2-13\alpha+4\right)}{4\left(\alpha-1\right)^2\left(2\alpha-1\right)^2\left(3\alpha-2\right)^2\left(1+\alpha\right)^3{C_0}^3\alpha^2\left(5\alpha-2\right)},$$
$$A_4 = \frac{\begin{array}{c}\kappa^4{C_1}^4(15360\alpha^{11}-39176\alpha^{10}+16975\alpha^9+42297\alpha^8\\-56710\alpha^7+18215\alpha^6+10862\alpha^5-10316\alpha^4+2521\alpha^3+212\alpha^2-192\alpha+24)\end{array}}{12(3\alpha-1)\left(5\alpha-2\right)\left(2\alpha-1\right)^3\left(\alpha-1\right)^3\left(1+\alpha\right)^4\left(3\alpha-2\right)^4{C_0}^4\alpha^3},$$
$$A_5 = \begin{pmatrix}(16800000\alpha^{16}-61746272\alpha^{15}+63298920\alpha^{14}+48264601\alpha^{13}-164903817\alpha^{12}\\+133113062\alpha^{11}-3168672\alpha^{10}-68802120\alpha^9+49756418\alpha^8-10949986\alpha^7\\\frac{-4337136\alpha^6+3501931\alpha^5-876981\alpha^4+36368\alpha^3+27844\alpha^2-5904\alpha+384){C_1}^5\kappa^5}{96(4\alpha-1)(3\alpha-1)}\\\cdot(5\alpha-2)(2\alpha-1)^4(\alpha-1)^4(1+\alpha)^5(3\alpha-2)^5(7\alpha-2){C_0}^5\alpha^4\end{pmatrix}.$$

$$A_1^{(2)} = \frac{\kappa C_1C_2(\alpha-1)(17\alpha^3-9\alpha^2-8\alpha+4)}{C_0\alpha\left(3\alpha-2\right)\left(\alpha^2-5\alpha+2\right)\left(1+\alpha\right)^2},$$
$$A_2^{(2)} = \frac{{C_1}^2\kappa^2\left(2\alpha-1\right)\left(7\alpha^4-2\alpha^3+17\alpha^2-24\alpha+8\right)C_2}{{C_0}^2\alpha^2\left(\alpha^2-5\alpha+2\right)\left(3\alpha-2\right)^2\left(1+\alpha\right)^3},$$

$$A_3^{(2)} = \frac{\begin{array}{c}\kappa {C_1} {C_2}^2 (512\alpha^7 - 1553\alpha^6 \\ +1479\alpha^5 - 1495\alpha^4 + 2765\alpha^3 - 2752\alpha^2 + 1204\alpha - 192)\end{array}}{2C_0\alpha\left(4\alpha-3\right)\left(3\alpha-2\right)\left(\alpha^2-5\alpha+2\right)\left(1+\alpha\right)^3\left(2-\alpha\right)},$$

$$A_4^{(2)} = \frac{\begin{array}{c}(5040\alpha^{14} - 41496\alpha^{13} + 197832\alpha^{12} - 538427\alpha^{11} + 927557\alpha^{10} - 1070645\alpha^9 + 773999\alpha^8 \\ -176831\alpha^7 - 317497\alpha^6 + 440649\alpha^5 - 292775\alpha^4 + 118358\alpha^3 - 29484\alpha^2 + 4168\alpha - 256)\kappa^3 {C_1}^3 C_2\end{array}}{12\alpha^3 {C_0}^3 (3\alpha-1)(5\alpha-2)(\alpha^2-5\alpha+2)(2\alpha-1)^2(\alpha-1)^2(1+\alpha)^4(3\alpha-2)^3},$$

$$A_5^{(2)} = \frac{4{C_2}^3\left(\alpha-1\right)\left(2\alpha-1\right)\left(2\alpha-3\right)\left(3\alpha-2\right)}{\left(4\alpha-3\right)\left(1+\alpha\right)^3},$$

$$A_6^{(2)} = \left(\begin{array}{c}\begin{array}{c}(24192\alpha^{15} - 312480\alpha^{14} + 1757520\alpha^{13} - 5967664\alpha^{12} + 13979363\alpha^{11} \\ -23774018\alpha^{10} + 29480427\alpha^9 - 26421228\alpha^8 + 17607647\alpha^7 - 10310216\alpha^6 + 6898447\alpha^5 \\ -4766162\alpha^4 + 2493156\alpha^3 - 833112\alpha^2 + 156864\alpha - 12672)(2\alpha-3)\kappa^2 C_1^2 C_2^2\end{array} \\ \hline \begin{array}{c}12 C_0^2 \alpha^2 (1-\alpha)(2-\alpha)(3\alpha-4)(4\alpha-3) \\ \cdot(3\alpha^2-10\alpha+6)(\alpha^2-5\alpha+2)(2\alpha-1)^2(3\alpha-2)^2(1+\alpha)^4\end{array}\end{array}\right),$$

$$A_7^{(2)} = \frac{\begin{array}{c}(164352\alpha^{10} - 1114330\alpha^9 + 3170123\alpha^8 - 5087920\alpha^7 \\ +5504508\alpha^6 - 4913864\alpha^5 + 4056421\alpha^4 - 2733766\alpha^3 + 1237444\alpha^2 - 317592\alpha + 34560)\kappa C_1 C_2^3\end{array}}{6\alpha C_0(2-\alpha)(3\alpha-4)(3\alpha-2)(4\alpha-3)(6\alpha-5)(\alpha^2-5\alpha+2)(1+\alpha)^4},$$

$$A_8^{(2)} = \frac{16C_2^4(\alpha-1)(2\alpha-1)(2\alpha-3)(18\alpha^3-56\alpha^2+52\alpha-15)}{3(4\alpha-3)(1+\alpha)^4(6\alpha-5)}.$$

$$A_1^{(3)} = \frac{\kappa C_1 C_3 \alpha}{C_0\left(2-3\alpha\right)\left(1+\alpha\right)^2}, \qquad A_2^{(3)} = \frac{{C_1}^2\kappa^2(8\alpha^3-5\alpha^2-3\alpha+2)C_3}{\left(1-\alpha\right)\left(2\alpha-1\right)\left(3\alpha-2\right)^2\left(1+\alpha\right)^3 {C_0}^2},$$

$$A_3^{(3)} = \frac{3\kappa^3 C_1^3 C_3(120\alpha^6 - 115\alpha^5 - 80\alpha^4 + 118\alpha^3 - 22\alpha^2 - 13\alpha + 4)}{4\left(2-5\alpha\right)\left(\alpha-1\right)^2\left(2\alpha-1\right)^2\left(3\alpha-2\right)^2\left(1+\alpha\right)^4 {C_0}^3\alpha}.$$

$$A_1^{(23)} = \frac{\kappa C_1 C_2 C_3(2-\alpha)(1-\alpha)(17\alpha^3-9\alpha^2-8\alpha+4)}{\left(3\alpha-2\right)\left(\alpha^2-5\alpha+2\right)\left(1+\alpha\right)^3\alpha C_0},$$

$$A_2^{(23)} = \frac{C_2 C_3^2\alpha(1-\alpha)(15\alpha^2-35\alpha+16)(2\alpha-3)}{(3\alpha^2-10\alpha+6)(1+\alpha)^3}.$$

$$A_1^{(4)} = \frac{\kappa C_1 C_4\left(\alpha-1\right)\left(\alpha^3+21\alpha^2-26\alpha+8\right)}{2C_0\alpha\left(3\alpha-2\right)\left(\alpha^2-5\alpha+2\right)\left(1+\alpha\right)^2},$$

$$A_2^{(4)} = \frac{\begin{array}{c}(6\alpha^9 - 9\alpha^8 + 235\alpha^7 - 510\alpha^6 + 802\alpha^5 - 1387\alpha^4 \\ +1753\alpha^3 - 1258\alpha^2 + 456\alpha - 64)\kappa^2 {C_1}^2 C_4\end{array}}{12{C_0}^2\alpha^2\left(3\alpha-2\right)^2\left(1+\alpha\right)^3\left(\alpha-1\right)\left(2\alpha-1\right)\left(\alpha^2-5\alpha+2\right)},$$

$$A_3^{(4)} = \frac{C_4^2(1-\alpha)(2-\alpha)(2\alpha-1)(3\alpha^2-\alpha+2)(2\alpha-3)}{(1+\alpha)^2(\alpha^2-5\alpha+2)(3\alpha^2-10\alpha+6)}.$$

$$A_1^{(24)} = \frac{2C_2C_4(1-\alpha)\left(2\alpha-1\right)\left(\alpha^2+11\alpha-8\right)}{\left(1+\alpha\right)^2\left(\alpha^2-5\alpha+2\right)},$$

$$A_2^{(24)} = \frac{\begin{array}{c}(2\alpha-3)(27\alpha^9-99\alpha^8+882\alpha^7\\ -5684\alpha^6+14181\alpha^5-14313\alpha^4+1870\alpha^3+7056\alpha^2-4848\alpha+960)\kappa C_1C_2C_4\end{array}}{6\alpha C_0\left(1+\alpha\right)^3\left(3\alpha-2\right)\left(\alpha^2-5\alpha+2\right)\left(3\alpha^2-10\alpha+6\right)\left(3\alpha-4\right)},$$

$$A_3^{(24)} = \frac{C_2^2C_4(1-\alpha)(2\alpha-1)(824\alpha^5-729\alpha^4-4866\alpha^3+10349\alpha^2-7290\alpha+1728)}{3(1+\alpha)^3(\alpha^2-5\alpha+2)(4\alpha-3)(3\alpha-4)}.$$

$$A_1^{(34)} = \frac{2C_3C_4(2-\alpha)^2\left(\alpha-1\right)\left(2\alpha-1\right)}{\left(1+\alpha\right)^2\left(\alpha^2-5\alpha+2\right)}.$$

$$B_2 = \frac{C_1^2\kappa^2(8\alpha^3-5\alpha^2-3\alpha+2)(\alpha^2-3\alpha+1)}{C_0^2\alpha(1+\alpha)^2(3\alpha-2)^2(2\alpha-1)^2(1-\alpha)^2},$$

$$B_3 = \frac{C_1^3\kappa^3(120\alpha^6-115\alpha^5-80\alpha^4+118\alpha^3-22\alpha^2-13\alpha+4)(3\alpha^2-8\alpha+2)}{4C_0^3\alpha^2(\alpha-1)^3(2\alpha-1)^2(3\alpha-2)^2(1+\alpha)^3(5\alpha-2)(3\alpha-1)},$$

$$B_4 = \frac{\begin{array}{c}C_1^4\kappa^4(15360\alpha^{11}-39176\alpha^{10}+16975\alpha^9+42297\alpha^8-56710\alpha^7\\ +18215\alpha^6+10862\alpha^5-10316\alpha^4+2521\alpha^3+212\alpha^2-192\alpha+24)(2\alpha^2-5\alpha+1)\end{array}}{6(4\alpha-1)(3\alpha-1)(5\alpha-2)(2\alpha-1)^3(1-\alpha)^4(1+\alpha)^4(3\alpha-2)^4\alpha^3C_0^4},$$

$$B_5 = \left(\begin{array}{c}\begin{array}{c}(16800000\alpha^{16}-61746272\alpha^{15}+63298920\alpha^{14}+48264601\alpha^{13}-164903817\alpha^{12}\\ +133113062\alpha^{11}-3168672\alpha^{10}-68802120\alpha^9\\ +49756418\alpha^8-10949986\alpha^7-4337136\alpha^6+3501931\alpha^5-876981\alpha^4\\ +36368\alpha^3+27844\alpha^2-5904\alpha+384)\kappa^5C_1^5(5\alpha^2-12\alpha+2)\end{array}\\ \hline \begin{array}{c}96C_0^5\alpha^4(4\alpha-1)\\ \cdot(3\alpha-1)(5\alpha-2)(2\alpha-1)^4(\alpha-1)^5(1+\alpha)^5(3\alpha-2)^5(7\alpha-2)(5\alpha-1)\end{array}\end{array}\right).$$

$$B_1^{(2)} = \frac{\kappa C_1C_2(\alpha^2-2\alpha+2)(17\alpha^3-9\alpha^2-8\alpha+4)}{C_0\alpha(\alpha-1)(3\alpha-2)(\alpha^2-5\alpha+2)(1+\alpha)^2},$$

$$B_2^{(2)} = \frac{8C_2^2\left(\alpha-1\right)\left(2\alpha-3\right)\left(2\alpha-1\right)}{\left(4\alpha-3\right)\left(1+\alpha\right)^2},$$

$$B_3^{(2)} = \frac{2\kappa^2C_1^2C_2(2\alpha-1)(7\alpha^4-2\alpha^3+17\alpha^2-24\alpha+8)}{C_0^2\alpha^2(1-\alpha)(\alpha^2-5\alpha+2)\left(3\alpha-2\right)^2\left(1+\alpha\right)^3},$$

$$B_4^{(2)} = \frac{\begin{array}{c}\kappa C_1C_2^2(512\alpha^7-1553\alpha^6+1479\alpha^5\\ -1495\alpha^4+2765\alpha^3-2752\alpha^2+1204\alpha-192)(3\alpha^2-8\alpha+6)\end{array}}{6C_0\alpha(4\alpha-3)(3\alpha-2)(\alpha^2-5\alpha+2)(1+\alpha)^3(2-\alpha)(1-\alpha)^2},$$

$$B_5^{(2)} = \frac{\begin{array}{c}\kappa^3C_1^3C_2(5040\alpha^{14}-41496\alpha^{13}+197832\alpha^{12}-538427\alpha^{11}+927557\alpha^{10}-1070645\alpha^9+773999\alpha^8\\ -176831\alpha^7-317497\alpha^6+440649\alpha^5-292775\alpha^4+118358\alpha^3-29484\alpha^2+4168\alpha-256)(\alpha^2-2\alpha-2)\end{array}}{12\alpha^3C_0^3(3\alpha-1)(5\alpha-2)(\alpha^2-5\alpha+2)(2\alpha-1)^2(\alpha-1)^3(1+\alpha)^5(3\alpha-2)^3},$$

$$B_6^{(2)} = \frac{8\left(\alpha-1\right)\left(3\alpha-5\right)\left(3\alpha-2\right)\left(2\alpha-3\right)\left(2\alpha-1\right){C_2}^3}{\left(6\alpha-5\right)\left(4\alpha-3\right)\left(1+\alpha\right)^3},$$

$$B_7^{(2)} = \left(\begin{array}{c} (\alpha^2-3\alpha+3)(24192\alpha^{15}-312480\alpha^{14}+1757520\alpha^{13}-5967664\alpha^{12} \\ +13979363\alpha^{11}-23774018\alpha^{10}+29480427\alpha^9-26421228\alpha^8 \\ +17607647\alpha^7-10310216\alpha^6+6898447\alpha^5 \\ \frac{-4766162\alpha^4+2493156\alpha^3-833112\alpha^2+156864\alpha-12672)\kappa^2 C_1^2 C_2^2}{6\alpha^2(1-\alpha)^2(-2+\alpha)} \\ \cdot(3\alpha-4)(4\alpha-3)(3\alpha^2-10\alpha+6)(\alpha^2-5\alpha+2)(2\alpha-1)^2(3\alpha-2)^2(1+\alpha)^4 C_0^2 \end{array} \right),$$

$$B_8^{(2)} = \left(\begin{array}{c} \kappa C_1 C_2^3(164352\alpha^{10}-1114330\alpha^9+3170123\alpha^8 \\ -5087920\alpha^7+5504508\alpha^6-4913864\alpha^5+4056421\alpha^4 \\ \frac{-2733766\alpha^3+1237444\alpha^2-317592\alpha+34560)(5\alpha^2-14\alpha+10)}{30C_0\alpha(2-\alpha)(3\alpha-4)} \\ \cdot(3\alpha-2)(4\alpha-3)(6\alpha-5)(\alpha^2-5\alpha+2)(1+\alpha)^4(1-\alpha)^2 \end{array} \right),$$

$$B_9^{(2)} = \frac{32C_2^4(1-\alpha)(2\alpha-1)(2\alpha-3)(18\alpha^3-56\alpha^2+52\alpha-15)(7-4\alpha)}{3(4\alpha-3)(1+\alpha)^4(6\alpha-5)(8\alpha-7)}.$$

$$B_1^{(3)} = \frac{\kappa C_1 C_3 \alpha(3-\alpha)}{C_0(3\alpha-2)\left(1+\alpha\right)^2(\alpha-1)}, \quad B_2^{(3)} = \frac{(8\alpha^3-5\alpha^2-3\alpha+2)(5-2\alpha)\kappa^2 C_1^2 C_3}{2(2\alpha-1)(1-\alpha)^2(3\alpha-2)^2(1+\alpha)^3 C_0^2},$$

$$B_3^{(3)} = \frac{\kappa C_1 C_3^2 \alpha(\alpha^2-2\alpha-2)}{2C_0(3\alpha-2)(1+\alpha)^3(\alpha-1)},$$

$$B_4^{(3)} = \frac{\kappa^3 C_1^3 C_3(120\alpha^6-115\alpha^5-80\alpha^4+118\alpha^3-22\alpha^2-13\alpha+4)(7-3\alpha)}{4\alpha\left(5\alpha-2\right)\left(\alpha-1\right)^3\left(2\alpha-1\right)^2\left(3\alpha-2\right)^2\left(1+\alpha\right)^4 {C_0}^3}.$$

$$B_1^{(23)} = \frac{2C_2C_3(2\alpha^2-5\alpha+4)(2\alpha-1)}{(\alpha-1)(1+\alpha)^2},$$

$$B_2^{(23)} = \frac{(\alpha^2-3\alpha+4)(17\alpha^3-9\alpha^2-8\alpha+4)\kappa C_1 C_2 C_3}{\left(3\alpha-2\right)\left(\alpha^2-5\alpha+2\right)\left(1+\alpha\right)^3\alpha C_0},$$

$$B_3^{(23)} = \frac{4C_2^2C_3(4\alpha^2-11\alpha+8)(2\alpha-1)}{(1+\alpha)^3},$$

$$B_4^{(23)} = \frac{2\alpha(\alpha^2-3\alpha+3)(-15\alpha^2+35\alpha-16)C_2C_3^2}{(1+\alpha)^3(3\alpha^2-10\alpha+6)}.$$

$$B_1^{(4)} = \frac{(\alpha^3+21\alpha^2-26\alpha+8)\kappa C_1 C_4}{\alpha C_0\left(1+\alpha\right)^2\left(2-3\alpha\right)\left(\alpha^2-5\alpha+2\right)},$$

$$B_2^{(4)} = \frac{\begin{array}{c}(6\alpha^9-9\alpha^8+235\alpha^7-510\alpha^6+802\alpha^5-1387\alpha^4 \\ +1753\alpha^3-1258\alpha^2+456\alpha-64)(\alpha^2-2\alpha-2)\kappa^2 C_1^2 C_4\end{array}}{12C_0^2\alpha^2(3\alpha-2)^2\left(1+\alpha\right)^4(1-\alpha)^2(2\alpha-1)(\alpha^2-5\alpha+2)},$$

$$B_3^{(4)} = \frac{2C_4^2\left(-2+\alpha\right)\left(2\alpha-1\right)(3\alpha^2-\alpha+2)(\alpha^2-3\alpha+3)}{\left(1+\alpha\right)^2\left(\alpha^2-5\alpha+2\right)(3\alpha^2-10\alpha+6)}.$$

$$B_1^{(24)} = \frac{2C_2C_4(3\alpha^2-8\alpha+6)(2\alpha-1)(\alpha^2+11\alpha-8)}{3(1-\alpha)(1+\alpha)^2(\alpha^2-5\alpha+2)},$$

$$B_2^{(24)} = \frac{\begin{array}{c}(27\alpha^9-99\alpha^8+882\alpha^7-5684\alpha^6+14181\alpha^5\\ -14313\alpha^4+1870\alpha^3+7056\alpha^2-4848\alpha+960)(\alpha^2-3\alpha+3)\kappa C_1C_2C_4\end{array}}{3(3\alpha-2)(\alpha^2-5\alpha+2)\left(1+\alpha\right)^3(3\alpha^2-10\alpha+6)(3\alpha-4)(\alpha-1)\alpha C_0},$$

$$B_3^{(24)} = \frac{\begin{array}{c}C_2^2C_4(5\alpha^2-14\alpha+10)(2\alpha-1)(824\alpha^5-729\alpha^4\\ -4866\alpha^3+10349\alpha^2-7290\alpha+1728)\end{array}}{15(1-\alpha)\left(1+\alpha\right)^3(\alpha^2-5\alpha+2)(4\alpha-3)(3\alpha-4)}.$$

$$B_1^{(34)} = \frac{2(\alpha^2-3\alpha+4)(2\alpha-1)(-2+\alpha)C_3C_4}{(1+\alpha)^2(\alpha^2-5\alpha+2)}.$$

$$D_2 = \frac{{C_1}^2\kappa^2(16\alpha^7-114\alpha^6+275\alpha^5-256\alpha^4+52\alpha^3+60\alpha^2-37\alpha+6)}{2\alpha\left(3\alpha-2\right)^2\left(1+\alpha\right)^2\left(1-\alpha\right)^4\left(2\alpha-1\right)^2{C_0}^2},$$

$$D_3 = \frac{\begin{array}{c}(1080\alpha^{10}-7155\alpha^9+16065\alpha^8-11851\alpha^7-5623\alpha^6\\ +14177\alpha^5-8265\alpha^4+1363\alpha^3+475\alpha^2-218\alpha+24)\kappa^3C_1^3\end{array}}{4{C_0}^3\alpha^2\left(2\alpha-1\right)^2\left(3\alpha-2\right)^3\left(1+\alpha\right)^3\left(1-\alpha\right)^4\left(5\alpha-2\right)\left(3\alpha-1\right)},$$

$$D_4 = \frac{\begin{array}{c}(122880\alpha^{15}-958528\alpha^{14}+2821832\alpha^{13}-3541478\alpha^{12}+323795\alpha^{11}+4567774\alpha^{10}\\ -5786529\alpha^9+2823103\alpha^8+203380\alpha^7-999274\alpha^6+542659\alpha^5-126337\alpha^4\\ +3039\alpha^3+5124\alpha^2-1080\alpha+72){C_1}^4\kappa^4\end{array}}{12\alpha^3\left(3\alpha-1\right)\left(5\alpha-2\right)\left(2\alpha-1\right)^4\left(3\alpha-2\right)^4\left(1+\alpha\right)^4\left(\alpha-1\right)^5\left(4\alpha-1\right){C_0}^4},$$

$$D_5 = \left(\begin{array}{c}\kappa^5C_1^5(84000000\alpha^{19}-695131360\alpha^{18}+2213106856\alpha^{17}\\ -3039970107\alpha^{16}+143228956\alpha^{15}+5512858522\alpha^{14}\\ -7934496954\alpha^{13}+4263700113\alpha^{12}+1059332424\alpha^{11}-3062912192\alpha^{10}\\ +1944015496\alpha^9-451644873\alpha^8-130446584\alpha^7+130753922\alpha^6\\ -42348774\alpha^5+6054483\alpha^4+108500\alpha^3-173916\alpha^2+24240\alpha-1152)\\ \hline 96C_0^5\alpha^4(4\alpha-1)(3\alpha-1)(5\alpha-2)\\ \cdot(2\alpha-1)^4(1+\alpha)^5(3\alpha-2)^5(1-\alpha)^6(5\alpha-1)(7\alpha-2)\end{array}\right).$$

$$D_1^{(2)} = \frac{\kappa C_1C_2(17\alpha^6-60\alpha^5+112\alpha^4-112\alpha^3+11\alpha^2+36\alpha-12)}{C_0\alpha(3\alpha-2)(\alpha^2-5\alpha+2)(1-\alpha)^2(1+\alpha)^2},$$

$$D_2^{(2)} = \frac{\begin{array}{c}\kappa^2C_1^2C_2(56\alpha^{11}-100\alpha^{10}-86\alpha^9+535\alpha^8-1622\alpha^7+3665\alpha^6\\ -5468\alpha^5+5271\alpha^4-3254\alpha^3+1239\alpha^2-264\alpha+24)\end{array}}{C_0^2\alpha^2(-\alpha^2+5\alpha-2)(2\alpha-1)^2(3\alpha-2)^2(1+\alpha)^3(1-\alpha)^4},$$

$$D_3^{(2)} = \frac{\begin{array}{c}\kappa C_1C_2^2(1536\alpha^9-9779\alpha^8+24863\alpha^7-34092\alpha^6\\ +36508\alpha^5-48665\alpha^4+58945\alpha^3-42808\alpha^2+15828\alpha-2304)\end{array}}{6C_0\alpha(4\alpha-3)(3\alpha-2)(\alpha^2-5\alpha+2)(1-\alpha)^2(1+\alpha)^3(2-\alpha)},$$

$$D_4^{(2)} = \frac{\begin{array}{c}\kappa^3C_1^3C_2(5040\alpha^{17}-66696\alpha^{16}+410352\alpha^{15}-1513643\alpha^{14}+3554028\alpha^{13}\\ -5376137\alpha^{12}+5104076\alpha^{11}-2300444\alpha^{10}-1307506\alpha^9+3371424\alpha^8-2988402\alpha^7\\ +1289235\alpha^6+32982\alpha^5-387951\alpha^4+235806\alpha^3-71724\alpha^2+11480\alpha-768)\end{array}}{12C_0^3\alpha^3(3\alpha-1)(5\alpha-2)(\alpha^2-5\alpha+2)(2\alpha-1)^2(3\alpha-2)^3(\alpha-1)^4(1+\alpha)^5},$$

$$D_5^{(2)} = \frac{4(3\alpha-5)(2\alpha-1)(2\alpha-3)(6\alpha^2-15\alpha+8)C_2^3}{(6\alpha-5)(4\alpha-3)(1+\alpha)^3},$$

$$D_6^{(2)} = \left(\begin{array}{c} \kappa^2 C_1^2 C_2^2 (48384\alpha^{19} - 842688\alpha^{18} + 6714432\alpha^{17} \\ -32825264\alpha^{16} + 110314198\alpha^{15} - 269117807\alpha^{14} + 489058280\alpha^{13} \\ -666788284\alpha^{12} + 678137319\alpha^{11} - 515801737\alpha^{10} + 329118060\alpha^9 - 261929520\alpha^8 + 286735673\alpha^7 \\ -277037324\alpha^6 + 190448578\alpha^5 - 88820636\alpha^4 + 27253160\alpha^3 - 5176464\alpha^2 + 532224\alpha - 20736) \\ \hline 12C_0^2\alpha^3(2-\alpha)(3\alpha-4)(4\alpha-3) \\ \cdot(3\alpha^2-10\alpha+6)(\alpha^2-5\alpha+2)(2\alpha-1)^2(3\alpha-2)^2(1-\alpha)^3(1+\alpha)^4 \end{array} \right),$$

$$D_7^{(2)} = \frac{\begin{array}{c}\kappa C_1 C_2^3 (821760\alpha^{12} - 8529986\alpha^{11} + 38854795\alpha^{10} - 102702524\alpha^9 \\ +177237865\alpha^8 - 217902404\alpha^7 + 211353737\alpha^6 - 178609948\alpha^5 \\ +131893863\alpha^4 - 76164602\alpha^3 + 29945756\alpha^2 - 6889320\alpha + 691200)\end{array}}{30C_0\alpha(2-\alpha)(3\alpha-4)(3\alpha-2)(4\alpha-3)(6\alpha-5)(\alpha^2-5\alpha+2)(1-\alpha)^2(1+\alpha)^4},$$

$$D_8^{(2)} = \frac{16C_2^4(2\alpha-1)(2\alpha-3)(4\alpha-7)(8\alpha^2-21\alpha+12)(18\alpha^3-56\alpha^2+52\alpha-15)}{3(6\alpha-5)(4\alpha-3)^2(1+\alpha)^4(8\alpha-7)}.$$

$$D_1^{(3)} = \frac{\kappa C_1 C_3(2-\alpha)(\alpha^3-5\alpha^2+\alpha+1)}{(3\alpha-2)(1+\alpha)^2(\alpha-1)^3 C_0},$$

$$D_2^{(3)} = \frac{(16\alpha^7-98\alpha^6+185\alpha^5-100\alpha^4-16\alpha^3+18\alpha^2+3\alpha-2)\kappa^2 C_1^2 C_3}{\alpha(2\alpha-1)^2(3\alpha-2)^2(1-\alpha)^3(1+\alpha)^3 C_0^2},$$

$$D_3^{(3)} = \frac{\kappa C_1 C_3^2(2-\alpha)(\alpha^3-3\alpha^2-5\alpha+1)}{2C_0(1+\alpha)^3(1-\alpha)^2(2-3\alpha)},$$

$$D_4^{(3)} = \frac{\begin{array}{c}\kappa^3 C_1^3 C_3 (1080\alpha^{10} - 6435\alpha^9 + 12015\alpha^8 - 4791\alpha^7 \\ -7775\alpha^6 + 8781\alpha^5 - 2839\alpha^4 + 15\alpha^3 + 71\alpha^2 + 30\alpha - 8)\end{array}}{4\alpha^2(1-3\alpha)(5\alpha-2)(2\alpha-1)^2(3\alpha-2)^2(\alpha-1)^4(1+\alpha)^4 {C_0}^3}.$$

$$D_1^{(23)} = \frac{\kappa C_1 C_2 C_3(17\alpha^6-77\alpha^5+189\alpha^4-183\alpha^3+92\alpha-32)}{C_0\alpha(1+\alpha)^3(\alpha-1)(3\alpha-2)(\alpha^2-5\alpha+2)},$$

$$D_2^{(23)} = \frac{8(2\alpha-1)(2\alpha-3)(4\alpha^2-11\alpha+8)C_2^2 C_3}{(4\alpha-3)(1+\alpha)^3},$$

$$D_3^{(23)} = \frac{(30\alpha^7-205\alpha^6+587\alpha^5-797\alpha^4+368\alpha^3+162\alpha^2-160\alpha+24){C_2}{C_3}^2}{\alpha(1+\alpha)^3(1-\alpha)(3\alpha^2-10\alpha+6)}.$$

$$D_1^{(4)} = \frac{\kappa C_1 C_4(\alpha^7+21\alpha^6-32\alpha^5-78\alpha^4+225\alpha^3-247\alpha^2+126\alpha-24)}{2C_0\alpha(1-\alpha)^3(1+\alpha)^2(3\alpha-2)(\alpha^2-5\alpha+2)},$$

$$D_2^{(4)} = \frac{\begin{array}{c}\kappa^2 C_1^2 C_4 (6\alpha^{12} - 39\alpha^{11} + 286\alpha^{10} - 1628\alpha^9 + 4184\alpha^8 \\ -5574\alpha^7 + 6184\alpha^6 - 6508\alpha^5 + 4434\alpha^4 - 251\alpha^3 - 1870\alpha^2 + 1112\alpha - 192)\end{array}}{12C_0^2\alpha^2(1+\alpha)^4(\alpha-1)^3(3\alpha-2)^2(2\alpha-1)(\alpha^2-5\alpha+2)},$$

$$D_3^{(4)} = \frac{C_4^2(2-\alpha)(2\alpha-1)(6\alpha^6-29\alpha^5+58\alpha^4-51\alpha^3+48\alpha^2-54\alpha+12)}{\alpha(1+\alpha)^2(1-\alpha)(\alpha^2-5\alpha+2)(3\alpha^2-10\alpha+6)}.$$

$$D_1^{(24)} = \frac{2C_2C_4(2\alpha-1)(3\alpha^4+23\alpha^3-125\alpha^2+191\alpha-96)}{3(1+\alpha)^2(1-\alpha)(\alpha^2-5\alpha+2)},$$

$$D_2^{(24)} = \frac{\begin{array}{c}(54\alpha^{13}-441\alpha^{12}+3087\alpha^{11}-20971\alpha^{10}+92388\alpha^9\\ -244625\alpha^8+380321\alpha^7-291541\alpha^6-38574\alpha^5\\ +303618\alpha^4-282268\alpha^3+120464\alpha^2-22752\alpha+1152)\kappa C_1C_4C_2\end{array}}{6C_0\alpha^2(1+\alpha)^3(1-\alpha)^2(3\alpha-2)(\alpha^2-5\alpha+2)(3\alpha^2-10\alpha+6)(3\alpha-4)},$$

$$D_3^{(24)} = \frac{\begin{array}{c}C_2^2C_4(2\alpha-1)(4120\alpha^7-18477\alpha^6+3552\alpha^5\\ +125318\alpha^4-311122\alpha^3+334855\alpha^2-172854\alpha+34560)\end{array}}{15(1+\alpha)^3(1-\alpha)(\alpha^2-5\alpha+2)(4\alpha-3)(3\alpha-4)}.$$

$$D_1^{(34)} = \frac{2C_3C_4(2-\alpha)(2\alpha-1)(\alpha^4-5\alpha^3+13\alpha^2-15\alpha+8)}{(1-\alpha)^2(1+\alpha)^2(-\alpha^2+5\alpha-2)}.$$

Bibliography

[Ach90] D. J. Acheson. *Elementary Fluid Dynamics*. OUP, 1990.

[AGAK96a] J. Azaiez, R. Guenette, and A. Ait-Kadi. Entry flow calculations using multi-mode models. *Journal of Non-Newtonian Fluid Mechanics*, 66(2-3):271–281, 1996.

[AGAK96b] J. Azaiez, R. Guenette, and A. Ait-Kadi. Numerical simulation of viscoelastic flows through a planar contraction. *Journal of Non-Newtonian Fluid Mechanics*, 62(2-3):253–277, 1996.

[AOP03] Manuel A. Alves, Paulo J. Oliveira, and Fernando T. Pinho. Benchmark solutions for the flow of Oldroyd-B and PTT fluids in planar contractions. *Journal of Non-Newtonian Fluid Mechanics*, 110(1):45–75, 2003.

[Ata08] Kunt Atalik. Group theoretical analysis and similarity solutions for stress boundary layers in viscoelastic flows. *Journal of Non-Newtonian Fluid Mechanics*, 153(1):62–71, 2008.

[BB77] D. V. Boger and R. Binnington. Separation of elastic and shear thinning effects in the capillary rheometer. *Journal of Rheology*, 21(4):515–534, 1977.

[BW93] D. V. Boger and K. Walters. *Rheological Phenomena in Focus*. Elsevier Amsterdam, 1993.

[BW95] R. B. Bird and J. M. Wiest. Constitutive equations for polymeric liquids. *Annual Review of Fluid Mechanics*, 27:169–193, 1995.

[CB00] Regan Crooks and David V. Boger. Influence of fluid elasticity on drops impacting on dry surfaces. *Journal of Rheology*, 44(4):973–996, 2000.

[CR88] M. D. Chilcott and J. M. Rallison. Creeping flow of dilute polymer solutions past cylinders and spheres. *Journal of Non-Newtonian Fluid Mechanics*, 29:381–432, 1988.

[DD93] A. R. Davies and J. Devlin. On corner flows of Oldroyd-B fluids. *Journal of Non-Newtonian Fluid Mechanics*, 60(2–3):173–191, 1993.

[DM49] W. R. Dean and P. E. Montagnon. On the steady motion of viscous liquid in a corner. *Proceeding of the Cambridge Philosophical Society*, 45:389–394, 1949.

[DMC85] S. Dupont, J. M. Marchal, and M. J. Crochet. Finite element simulation of viscoelastic fluids of the integral type. *Journal of Non-Newtonian Fluid Mechanics*, 17(2):157–183, 1985.

[DPT04] Hua-Shu Dou and Nhan Phan-Thien. Criteria of negative wake generation behind a cylinder. *Rheologica Acta*, 43(3):203–209, 2004.

[EH08] Jonathan D. Evans and Thomas Hagen. Viscoelastic sink flow in a wedge for the UCM and Oldroyd-B models. *Journal of Non-Newtonian Fluid Mechanics*, 154(1):39–46, 2008.

[ES08] J. D. Evans and D. N. Sibley. Re-entrant corner flows of PTT fluids in the Cartesian stress basis. *Journal of Non-Newtonian Fluid Mechanics*, 153(1):12–24, 2008.

[ES09] J. D. Evans and D. N. Sibley. Re-entrant corner flow for PTT fluids in the natural stress basis. *Journal of Non-Newtonian Fluid Mechanics*, 157(1-2):79–91, 2009.

[Eva05a] J. D. Evans. Re-entrant corner flows of UCM fluids: the initial formation of lip vortices. *Proceedings of the Royal Society A*, 461(2062):3169–3181, 2005.

[Eva05b] Jonathan D. Evans. Re-entrant corner flows of the upper convected Maxwell fluid. *Proceedings of the Royal Society A*, 461(2053):117–142, 2005.

[Eva06] J. D. Evans. Re-entrant corner flows of upper convected Maxwell fluids: the small and high weissenberg number limits. *Proceedings of the Royal Society A*, 462:3749–3774, 2006.

[Eva08a] J. D. Evans. Re-entrant corner flows of UCM fluids: The Cartesian stress basis. *Journal of Non-Newtonian Fluid Mechanics*, 150(2-3):116–138, 2008.

[Eva08b] J. D. Evans. Re-entrant corner flows of UCM fluids: The natural stress basis. *Journal of Non-Newtonian Fluid Mechanics*, 150(2-3):139–153, 2008.

[Eva09] J. D. Evans. Re-entrant corner flows of the PTT fluid with a solvent viscosity. *Submitted*, 2009.

[Gie82] H. Giesekus. A simple constitutive equation for polymer fluids based on the concept of deformation-dependent tensorial mobility. *Journal of Non-Newtonian Fluid Mechanics*, 11(1-2):69–109, 1982.

[GP01] M. I. Gerritsma and T. N. Phillips. On the use of characteristic variables in viscoelastic flow problems. *IMA Journal of Applied Mathematics*, 66:127–147, 2001.

[GP08] M. I. Gerritsma and T. N. Phillips. On the characteristics and compatibility equations for the UCM model fluid. *ZAMM Zeitschrift fr Angewandte Mathematik und Mechanik*, 88(7):523–539, 2008.

[HHVC97] S. G. Hatzikiriakos, G. Heffner, D. Vlassopoulos, and K. Christodoulou. Rheological characterization of polyethylene terephthalate resins using a multimode Phan-Thien-Tanner constitutive relation. *Rheologica acta*, 43(5):568–578, 1997.

[Hin93] E. J. Hinch. The flow of an Oldroyd fluid around a sharp corner. *Journal of Non-Newtonian Fluid Mechanics*, 50(2-3):161–171, 1993.

[HR97] Thomas Hagen and Michael Renardy. Boundary layer analysis of the Phan-Thien-Tanner and Giesekus model in high Weissenberg number flow. *Journal of Non-Newtonian Fluid Mechanics*, 73(1-2):181–189, 1997.

[Jos90] D. D. Joseph. *Fluid Dynamics of Viscoelastic Liquids*. Springer-Verlag, 1990.

[JRS85] Daniel D. Joseph, Michael Renardy, and Jean-Claude Saut. Hyperbolicity and Change of Type in the Flow of Viscoelastic Fluids. *Arch. Rational Mech. Anal.*, 87:213–251, 1985.

[JS77] M. W. Johnson Jr. and D. Segalman. A model for viscoelastic fluid behavior which allows non-affine deformation. *Journal of Non-Newtonian Fluid Mechanics*, 2(3):255–270, 1977.

[Kei93] R. A. Keiller. Entry-flow calculations for the Oldroyd-B and FENE equations. *Journal of Non-Newtonian Fluid Mechanics*, 46(2–3):143–178, 1993.

[KSI78] Naoichi Kumagai, Sadao Sasajima, and Hidebumi Ito. Long-term creep of rocks: Results with large specimens obtained in about 20 years and those with small specimens in about 3 years. *Journal of the Society of Materials Science (Japan)*, 27(293):155–161, 1978.

[LG03] Alexei E. Likhtman and Richard S. Graham. Simple constitutive equation for linear polymer melts derived from molecular theory: Roliepoly equation. *Journal of Non-Newtonian Fluid Mechanics*, 114(1):1–12, 2003.

[LHJ+98] G. Lielens, P. Halin, I. Jaumain, R. Keunings, and V. Legat. New closure approximations for the kinetic theory of finitely extensible dumbbells. *Journal of Non-Newtonian Fluid Mechanics*, 76(1–3):249–279, 1998.

[Mei75] J. Meissner. Basic parameters, melt rheology, processing and end-use properties of three similar low density polyethylene samples. *Pure and Applied Chemistry*, 42(4):551–612, 1975.

[Mof64] H. K. Moffatt. Viscous and resistive eddies near a sharp corner. *Journal of Fluid Mechanics*, 18:1–18, 1964.

[NB98] Q. D. Nguyen and D. V. Boger. Application of rheology to solving tailings disposal problems. *International Journal of Mineral Processing*, 54(3):217–233, 1998.

[NBFT04] Simin Nasseri, Lynne Bilston, Babatunde Fasheun, and Roger Tanner. Modelling the biaxial elongational deformation of soft solids. *Rheologica Acta*, 43(1):68–79, 2004.

[NW02] V. Ngamaramvaranggul and M. F. Webster. Simulation of pressure-tooling wire-coating flow with Phan-Thien/Tanner models. *International journal for numerical methods in fluids*, 38(7):677–710, 2002.

[OHLM99] John Ockendon, Sam Howison, Andrew Lacey, and Alexander Movchan. *Applied Partial Differential Equations*. OUP, 1999.

[Old50] J. G. Oldroyd. On the Formulation of Rheological Equations of State. *Proceedings of the Royal Society of London. Series A*, 200(1063):523–541, 1950.

[PT78] N. Phan-Thien. A nonlinear network viscoelastic model. *Journal of Rheology*, 22(3):259–283, 1978.

[PT02] Nhan Phan-Thien. *Understanding Viscoelasticity*. Springer-Verlag, 2002.

[PTT77] Nhan Phan Thien and Roger I. Tanner. A new constitutive equation derived from network theory. *Journal of Non-Newtonian Fluid Mechanics*, 2(4):353–365, 1977.

[Ren93] Michael Renardy. The stresses of an upper convected Maxwell fluid in a Newtonian velocity field near a re-entrant corner. *Journal of Non-Newtonian Fluid Mechanics*, 50(2–3):127–134, 1993.

[Ren94] Michael Renardy. How to integrate the upper convected Maxwell (UCM) stresses near a singularity (and maybe elsewhere, too). *Journal of Non-Newtonian Fluid Mechanics*, 52(1):91–95, 1994.

[Ren95] Michael Renardy. A matched solution for corner flow of the upper convected Maxwell fluid. *Journal of Non-Newtonian Fluid Mechanics*, 58(1):83–89, 1995.

[Ren97a] Michael Renardy. High weissenberg number boundary layers for the upper convected Maxwell fluid. *Journal of Non-Newtonian Fluid Mechanics*, 68(1):125–132, 1997.

[Ren97b] Michael Renardy. Re-entrant corner behavior of the PTT fluid. *Journal of Non-Newtonian Fluid Mechanics*, 69(1):99–104, 1997.

[Ren97c] Michael Renardy. The high Weissenberg number limit of the UCM model and the Euler equations. *Journal of Non-Newtonian Fluid Mechanics*, 69(2-3):293–301, 1997.

[Ren00a] Michael Renardy. Current issues in non-Newtonian flows: a mathematical perspective. *Journal of Non-Newtonian Fluid Mechanics*, 90(2–3):243–259, 2000.

[Ren00b] Michael Renardy. *Mathematical Analysis of Viscoelastic Flows*. SIAM, 2000.

[RH04] J. M. Rallison and E. J. Hinch. The flow of an Oldroyd fluid past a reentrant corner: the downstream boundary layer. *Journal of Non-Newtonian Fluid Mechanics*, 116(2-3):141–162, 2004.

[RR04] Michael Renardy and Robert C. Rogers. *An Introduction to Partial Differential Equations*. Springer, second edition edition, 2004.

[SSP+98] Jeroen F. M. Schoonen, Frank H. M. Swartjes, Gerrit W. M. Peters, F. P. T. Baaijens, and Han E. H. Meijer. A 3D numerical/experimental

study on a stagnation flow of a polyisobutylene solution. *Journal of Non-Newtonian Fluid Mechanics*, 79(2-3):529–561, 1998.

[Tan00] Roger I. Tanner. *Engineering Rheology*. Oxford University Press, second edition, 2000.

[TN65] C. Truesdell and W. Noll. *The Non-Linear Field Theories of Mechanics*. Springer-Verlag, 1965.

[WB91] L. T. Wardhaugh and D. V. Boger. Flow characteristics of waxy crude oils: Application to pipeline design. *American Institute of Chemical Engineers*, 37(6):871–885, 1991.

[WW99] D. A. Wilkie and A. M Willis. Viscoelastic materials in veterinary ophthalmology. *Veterinary Ophthalmology*, 2(3):147–153, 1999.